ABSTRACT

CHRISTENSEN, SARA IRENE. The Role of Temperature in Cloud Droplet Activation. (Under the direction of Markus Petters.)

Aerosols in the atmosphere are composed of a wide variety of organic species, reflecting the multitude of sources and growth processes of these particles. Especially challenging is predicting how these particles may act as cloud condensation nuclei (CCN). Here, we use classic Köhler theory to relate a particle's dry diameter to its critical supersaturation. Inclusion of a hygroscopicity parameter, kappa (κ), parameterizes this relationship in terms of the particle's chemical composition. Previous studies have characterized κ-values for pure and mixed compounds at laboratory temperatures, but did not account for a potential dependence of the relationship between critical supersaturation and particle dry diameter on temperature. Here we characterize the temperature dependence of κ derived from CCN measurements for a variety of organic compounds. Single component organic aerosol and secondary organic aerosol from the reaction of α-pinene and O_3 were generated in the laboratory and activation properties were analyzed using size-resolved CCN analysis. The CCN instrument was placed inside a temperature-controlled enclosure. During the experiment the temperature inside the enclosure was ramped down from approximately 40˚ to 0˚C over a period of approximately six hours. Activation data were collected by alternating diameter scans between organic aerosol and ammonium sulfate aerosol for calibration. We establish distinct κ definitions based on calculation method, i.e. κ based on physical observations or κ based on chemical properties, and distinguish these κ-values as standard state or temperature dependent. The results can be explained by a weak dependence

of water activity on temperature, a moderate dependence of solubility in water on temperature, and a strong dependence of surface tension on temperature. Including the hygroscopicity-temperature relationship into climate models may have a large impact on the estimated aerosol radiative forcing. We anticipate that these observations will help to guide input and parameterization choices in global circulation models and regional models that rely on theory to extrapolate laboratory and ambient data to temperatures outside of those during data collection.

The Role of Temperature in Cloud Droplet Activation

by
Sara Irene Christensen

A thesis submitted to the Graduate Faculty of
North Carolina State University
in partial fulfillment of the
requirements for the Degree of
Master of Science

Marine, Earth and Atmospheric Sciences

Raleigh, North Carolina

2012

APPROVED BY:

Sukanta Basu	Yang Zhang

Markus Petters
Chair of Advisory Committee

DEDICATION

To Mom and Hart & Dad and Sue.

BIOGRAPHY

Sara was born in Bettendorf, Iowa and graduated from Pleasant Valley Community High School in Pleasant Valley, Iowa in 2006. She attended Valparaiso University in Valparaiso, Indiana and interned at the National Weather Service and Colorado State University before graduating with a Bachelor of Science degree in Meteorology in 2010.

ACKNOWLEDGMENTS

I would like to thank my graduate advisor Dr. Markus Petters for providing me direction, encouragement, and patience during the entire process of this thesis work. I would also like to thank Drs. Sonia M. Kreidenweis and Paul J. Ziemann for their guidance and for providing their insightful expertise. Thanks also to Drs. Yang Zhang and Sukanta Basu, my graduate committee members, for their support and for taking the time to help me complete this work. Lastly, I thank my research group members Sarah Suda and Tim Wright for their advice, input and collaboration throughout the course of this research.

This research was funded by the Office of Science (BER), US Department of Energy, under DE-FG02-05ER63984.

TABLE OF CONTENTS

LIST OF TABLES

LIST OF FIGURES

1. Introduction

1.1 Background

Earth's atmosphere is a chemically diverse and dynamic region composed of a wide variety of gaseous compounds as well as liquid and solid aerosol particles. The makeup of these particles (varying fractions of inorganic and organic constituents) represents the complexity of their sources and the aging processes they undergo in the atmosphere. This suspended particulate matter has far-reaching and important influences on weather and climate – namely, the amount of radiation the earth receives and the amount re-emitted back to space (Charlson et al., 1992; Haywood and Boucher, 2000). This is regulated through multiple processes known as the direct (Ångström, 1929) and indirect effects (Twomey, 1974; Albrecht, 1989; Lohmann and Feichter, 2005). The aerosol direct effect relates to the amount of radiation the particle itself absorbs and/or scatters into the atmosphere due to optical properties, while indirect effects relate to the modification of cloud properties by the particles.

For example, cloud condensation nuclei (CCN) are hygroscopic particles that provide a surface for water vapor to condense onto in order to form cloud droplets. They determine, in part, the cloud droplet number concentration (e.g. Fitzgerald and Spyers-Duran, 1973; Andreae and Rosenfeld, 2008). Increasing the number of these CCN can then alter cloud characteristics such as albedo (Twomey, 1974) and cloud lifetime (Albrecht, 1989). Because of this relationship, changes in particle production (i.e. introducing more into the atmosphere

anthropogenically) can produce a change in cloud cover (Twomey et al., 1984), thereby altering the earth's incoming and outgoing solar radiation. The uncertainty surrounding the magnitude of the indirect effect remains the largest in radiative forcing budget estimations (IPCC, 2007). Whether these potential climatic changes are significant – and to what extent – remains an ongoing debate.

With the purpose of investigating the aforementioned aerosols, we look closely at the microphysics behind CCN activity. The ability of an atmospheric particle to serve as a CCN depends on both its physical structure and chemical characteristics – together determining its hygroscopicity, or affinity for water uptake. The hygroscopicities of most inorganics known to be relevant in the atmosphere are well understood (Clegg et al., 1998). Organic compounds are also prevalent in aerosol (Kanakidou et al., 2005; Zhang et al., 2007; Jimenez et al., 2009), but they are relatively less understood due to their variety (Saxena and Hildeman, 1996; Goldstein and Galbally, 2007). Most particles comprise a mixture of both inorganic and organic parts, complicating the theoretical methods by which CCN activity is predicted. Köhler theory is the classic method to determining the relationship between a particle's dry diameter, D_d, and critical supersaturation, s_c (i.e. the saturation at which the CCN undergoes condensational growth). This theory has been widely used in past studies based on a constant temperature and therefore constant surface tension (e.g. Jacobson et al., 1996; Chen et al., 2002; Kreidenweis et al., 2006; Clegg and Seinfeld, 2006; Rosenørn et al., 2006; Rose et al., 2008, 2010; Friese and Ebel, 2010; Snider et al., 2010); however, it does not accurately represent cloud microphysics and likely contributes some errors to closing the gap between observation and theory.

Petters and Kreidenweis (2007) proposed a semi-empirical hygroscopicity parameter, kappa (κ), which subsumes all physicochemical properties (e.g. molecular weight, density, solubility, activity coefficients) and allows for the parameterization of the chemical composition of the particle together with size. It can be calculated both through physical observation and known chemical properties, both of which contain temperature dependent variables. The κ parameter will be utilized in this study to express the CCN activity of laboratory generated organic aerosol particles and to explore the effect of varying temperatures on their hygroscopicity.

1.2 Objectives

This work is motivated by the fact that the relationship between D_d and s_c may be influenced by changes in temperature. Although the temperature range for which cloud droplets activate in a particular cloud is relatively constant, cloud bases exist at many different levels in the atmosphere, thereby providing a large range of possible activation temperatures. The ability to recreate similar conditions in the laboratory is important to accurately explore the aerosol's role in atmospheric processes, especially the organic portion, as substantial uncertainty here calls for more investigation. The purpose of this study was to set forth a catalogue of CCN activity observations of atmospherically relevant organic aerosol proxies. While the CCN measurement techniques used have been previously established, I sought to develop a new approach to measuring CCN efficiency by introducing a method for temperature variance. The main objectives of this work were to

1. Integrate a successful cooling method into the experimental laboratory setup.

2. Characterize the CCN activity of a variety of organic compounds in terms of their physical and chemical properties.
3. Qualitatively assess the influence of temperature on the aforementioned particle properties.

This document will subsequently provide the relevant theoretical methodology and calibration procedures. Additionally, a review of the chemistry and properties of selected aerosol proxies that were used in the laboratory experiments are detailed. A summary of relevant CCN characterization experiments in the literature will also be included to give an overview of the current state of the measurement technique. The penultimate section includes a paper to be submitted for publication in the *Journal of Physical Chemistry A* that delves further into the specific methods and results of the experiments. Lastly, the findings are summarized and we postulate the use of the proposed alternate hygroscopicity parameter to include various temperatures.

1.3 References

Andreae, M. O., and D. Rosenfeld (2008), Aerosol-cloud-precipitation interactions. Part 1. The nature and sources of cloud-active aerosols, Earth-Sci. Rev., 89(1–2), 13–41.

Ångström, A. (1929), On the Atmospheric Transmission of Sun Radiation and on Dust in the Air, Geogr. Ann., 11, 156–166.

Charlson, R. J., and S. E. Schwartz (1992), Climate forcing by anthropogenic aerosols, Science, 255(5043), 423–430.

Chen, C. C., C. J. Tao, and H. C. Cheng (2002), Condensation of Supersaturated Water Vapor on Charged/Neutral Nanoparticles of Glucose and Monosodium Glutamate, J. Colloid Interface Sci., 255, 158–170.

Clegg, S. L., and P. Brimblecombe (1998), Thermodynamic Model of the System H^+-NH_4^+-Na^+-SO_4^{2-}-NO_3^--Cl^--H_2O at 298.15 K, J. Phys. Chem. A, 102, 2155–2171.

Clegg, S. L., and J. H. Seinfeld (2006), Thermodynamic Models of Aqueous Solutions Containing Inorganic Electrolytes and Dicarboxylic Acids at 298.15K 1. The Acids as Nondissociating Components, J. Phys. Chem. A, 110, 5692–5717.

Fitzgerald, J. W., and P. A. Spyers-Duran (1973), Changes in Cloud Nucleus Concentration and Cloud Droplet Distribution Associated with Pollution from St. Louis, J. Appl. Met., 12, 511–516.

Friese, E., and A. Ebel (2010), Temperature Dependent Thermodynamic Model of the System H^+-NH_4^+-Na^+-SO_2—NO_3^--Cl^--H_2O, J. Phys. Chem. A, 114, 11595–11631.

Frosch, M., A. A. Zardini, S. M. Platt, L. Müller, M. C. Reinnig, T. Hoffmann, and M. Bilde (2010), Thermodynamic properties and cloud droplet activation of a series of oxo-acids, Atmos. Chem. Phys., 10, 5873–5890.

Goldstein, A. H., and I. E. Galbally (2007), Known and Unexplored Organic Constituents in the Earth's Atmosphere, Environ. Sci. Technol., 41, 1514–1521.

Haywood, J., and O. Boucher (2000), Estimates of the direct and indirect radiative forcing due to tropospheric aerosols: a review, Rev. Geophys., 38, 513–543.

IPCC, 2007: Climate Change 2007: The Physical Science Basis. Contribution of Working Group I to the Fourth Assessment Report of the Intergovernmental Panel on Climate Change [Solomon, S., D. Qin, M. Manning, Z. Chen, M. Marquis, K.B. Averyt, M.Tignor and H.L. Miller (eds.)]. Cambridge University Press, Cambridge, United Kingdom and New York, NY, USA.

Jacobson, M. Z., A. Tabazadeh, and R. P. Turco (1996), Simulating equilibrium within aerosols and nonequilibrium between gases and aerosols, J. Geophys. Res., 101, 9079–9091.

Jimenez, J. L., M. R. Canagaratna, N. M. Donahue, A. S. H. Prevot, Q. Zhang, J. H. Kroll, P. F. DeCarlo, J. D. Allan, H. Coe, N. L. Ng, A. C. Aiken, K. S. Docherty, I. M. Ulbrich, A. P. Grieshop, A. L. Robinson, J. Duplissy, J. D. Smith, K. R. Wilson, V. A. Lanz, C. Hueglin, Y. L. Sun, J. Tian, A. Laaksonen, T. Raatikainen, J. Rautiainen, P. Vaattovaara, M. Ehn, M. Kulmala, J. M. Tomlinson, D. R. Collins, M. J. Cubison, E. J. Dunlea, J. A. Huffman, T. B. Onasch, M. R. Alfarra, P. I. Williams, K. Bower, Y. Kondo, J. Schneider, F. Drewnick, S. Borrmann, S. Weimer, K. Demerjian, D. Salcedo, L. Cottrell, R. Griffin, A. Takami, T. Miyoshi, S. Hatakeyama, A. Shimono, J. Y Sun, Y. M. Zhang, K. Dzepina, J. R. Kimmel, D. Sueper, J. T. Jayne, S. C.

Herndon, A. M. Trimborn, L. R. Williams, E. C. Wood, A. M. Middlebrook, C. E. Kolb, U. Baltensperger, and D. R. Worsnop (2009), Evolution of Organic Aerosols in the Amtosphere, Science, 326, 1525–1529.

Kanakidou, M., J. H. Seinfeld, S. N. Pandis, I. Barnes, F. J. Dentener, M. C. Facchini, R. Van Dingenen, B. Ervens, A. Nenes, C. J. Nielsen, E. Swietlicki, J. P. Putaud, Y. Balkanski, S. Fuzzi, J. Horth, G. K. Moortgat, R. Winterhalter, C. E. L. Myhre, K. Tsigaridis, E. Vignati, E. G. Stephanou, and J. Wilson (2005), Organic aerosol and global climate modeling: a review, Atmos. Chem. Phys., 5, 1053–123.

Kreidenweis, S. M., M. D. Petters, and P. J. DeMott (2006), Deliquescence-controlled activation of organic aerosols, Geophys. Res. Lett., 33, L06801.

Lohmann, U., and J. Feichter (2005) Global indirect aerosol effects: a review, Atmos. Chem. Phys., 5, 715–737.

Petters, M. D., and S. M. Kreidenweis (2007), A single parameter representation of hygroscopic growth and cloud condensation nucleus activity, Atmos. Chem. Phys., 7, 1961–1971.

Rose, D., S. S. Gunthe, E. Mikhailov, G. P. Frank, U. Dusek, M. O. Andreae, and U. Pöschl (2008), Calibration and measurement uncertainties of a continuous-flow cloud condensation nuclei counter (DMT-CCNC): CCN activation of ammonium sulfate and sodium chloride aerosol particles in theory and experiment, Atmos. Chem. Phys., 8, 1153–1179.

Rose, D., A. Nowak, P. Achtert, A. Wiedensohler, M. Hu, M. Shao, Y. Zhang, M. O. Andreae, and U. Pöschl (2010), Cloud condensation nuclei in polluted air and biomass burning smoke near the mega-city Guangzhou, China – Part 1: Size-resolved measurements and implications for the modeling of aerosol particle hygroscopicity and CCN activity, Atmos. Chem. Phys., 10, 3365–3383.

Rosenørn, T., G. Kiss, and M. Bilde (2006), Cloud droplet activation of saccharides and levoglucosan particles, Atmos. Environ., 40, 1794–1802.

Saxena, P., and L. M. Hildemann (1996), Water-Soluble Organics in Atmospheric Particles: A Critical Review of the Literature and Application of Thermodynamics to Identify Candidate Compounds, J. Atmos. Chem., 24, 57–109.

Snider, J. R., H. Wex, D. Rose, A. Kristensson, F. Stratmann, T. Hennig, S. Henning, A. Kiselev, M. Bilde, M. Burkhart, U. Duse, G. P. Frank, A. Kiendler-Scharr, T. F. Mentel, M. D. Petters, and U. Pöschl (2010), Intercomparison of cloud condensation nuclei andn hygroscopic fraction measurements: Coated soot particles investigated

during the LACIS Experiment in November (LExNo), J. Geophys. Res., 115, D11205.

Twomey, S. A. (1974), Pollution and the planetary albedo, Atmos. Environ., 8(12), 1251–1256.

Twomey, S. A., M. Piepgrass, and T. L. Wolfe (1984), An assessment of the impact of pollution on global cloud albedo, Tellus, 36B, 356–366.

Zhang, Q., J. L. Jimenez, M. R. Canagaratna, J. D. Allan, H. Coe, I. Ulbrich, M. R. Alfarra, A. Takami, A. M. Middlebrook, Y. L. Sun, K. Dzepina, E. Dunlea, K. Docherty, P. F. DeCarlo, D. Salcedo, T. Onasch, J. T. Jayne, T. Miyoshi, A. Shimono, S. Hatakeyama, N. Takegawa, Y. Kondo, J. Schneider, F. Drewnick, S. Borrmann, S. Weimer, K. Demerjian, P. Williams, K. Bower, R. Bahreini, L. Cottrell, R. J. Griffin, J. Rautiainen, J. Y. Sun, Y. M. Zhang, and D. R. Worsnop (2007), Ubiquity and dominance of oxygenated species in organic aerosols in anthropogenically-influenced Northern Hemisphere mid-latitudes, Geophys. Res. Lett., 34, L13801.

2. Methodology

2.1 Kappa-Köhler theory

Each particle emitted into the atmosphere, naturally and anthropogenically, requires a certain ambient supersaturation to trigger condensational growth into a cloud droplet. This relative humidity is the particle's critical supersaturation, s_c; it is determined by the aerosol's dry diameter, D_d, and its chemical composition. Köhler theory (Köhler, 1936) describes this relationship on the basis of thermodynamic equilibrium between the aqueous solution droplet (generally all atmospheric droplets exist as a mixture of liquid water and dissolved compounds) and the ambient water vapor. One form of the Köhler equation (Seinfeld and Pandis, 2006) gives the saturation ratio over an aqueous drop of a given solute concentration (Eqn. 2.1). This is a ratio of the water vapor pressure over the droplet, $p_w(D_p)$, to the water vapor pressure over a flat surface, p^o, at the same temperature:

$$\ln\left(\frac{p_w(D_p)}{p^\circ}\right) = \frac{4M_w\sigma_w}{RT\rho_w D_p} - \frac{6n_s M_w}{\pi\rho_w D_p^3}, \tag{2.1}$$

where M_w is the molecular weight of water, σ_w is the surface tension of water, R is the universal gas constant, T is temperature in Kelvin (typically 298.15K is used), ρ_w is the density of water, D_p is the droplet diameter, and n_s is the moles of solute.

Köhler theory expresses the thermodynamic equilibrium behind cloud droplet activation by accounting for two competing mechanisms, the Kelvin and Raoult terms. The Kelvin term accounts for the effect of curvature on the surface tension of the droplet (Lewis, 2006). From a physical point of view, an increase in particle size decreases the curvature of

the solution/air interface while increasing the surface area. As an aqueous solution drop undergoes condensational growth, the Kelvin effect decreases because the surface tension ceases to dominate on larger scales and the curvature approaches that of a flat surface for larger droplets.

From a molecular point of view, smaller particles contain fewer dissolved molecules, which decreases the attractive forces between water molecules within the droplet – meaning, they are more apt to escape the interface and the droplet will evaporate. In terms of relating this to CCN activity theory, essentially smaller diameter droplets will have a higher equilibrium vapor pressure, and will require higher ambient supersaturations in order for condensation to occur and a cloud droplet to form. The first term in the modified Köhler equation (Eqn. 2.1) represents the Kelvin effect, or "*A*" parameter:

$$A = \frac{4M_w\sigma_w}{RT\rho_w D_p}. \tag{2.2}$$

The Raoult term, conversely, describes the effect of lowering the equilibrium vapor pressure through the presence of surface-tension-depressing organics. It assumes ideality of the solution – that the chemical interactions between any components of the solution are exactly derived from the molecular bonding in each component, and mixing is assumed to be complete. Raoult's law states that the vapor pressure of the solution droplet will be a summation of the individual components' vapor pressures – therefore, adding one or more compounds with relatively lower vapor pressures will lower the equilibrium vapor pressure of the entire solution droplet. In reality, non-ideality describes those solutions whose individual compound volumes or vapor pressures cannot be simply summed to find that of the solution, and those with solubility limitations at certain solute concentrations.

Lowering the equilibrium vapor pressure with the addition of these compounds allows the droplet to grow at lower ambient supersaturations. Atmospheric aerosols are commonly internally mixed or can be influenced by surface-tension-lowering surfactants, highlighting the importance of the Raoult term when considering CCN ability. The second term in the modified Köhler equation (Eqn. 2.1) represents the Raoult term, or "*B*" parameter:

$$B = \frac{6n_s M_w}{\pi \rho_w D_p^3}. \quad (2.3)$$

Theoretically, there are several methods to determining an aerosol's hygroscopicity. Because Raoult's law can be thought of as a water activity effect, the Köhler equation can be re-written as Equation 2.4 below to express saturation ratio, *S*:

$$S = a_w \exp\left(\frac{4\sigma_{s/a} M_w}{RT\rho_w D}\right), \quad (2.4)$$

where a_w is the activity of water in a solution and $\sigma_{s/a}$ is the surface tension at the solution/air interface (assumed to be that of pure water, Equation 2.5).

$$\sigma_{s/a} = 0.0761 - 1.55*10^{-4}\ T\ [°C] \quad (2.5)$$

Petters and Kreidenweis (2007) introduced a hygroscopicity parameter, κ, which includes all physicochemical properties of the droplet and its constituents. Equation 2.6 shows the relationship between κ and a_w.

$$\frac{1}{a_w} = 1 + \kappa \frac{V_s}{V_w}, \quad (2.6)$$

where V_s and V_w are the solute and water volumes, respectively. These volumes are then converted to dry diameter, D_d, and then Eqn. 2.6 can be substituted into Eqn. 2.5 for the definition of "κ-Köhler theory":

$$S(D) = \frac{D^3 - D_d^3}{D^3 - D_d^3(1-\kappa)} \exp\left(\frac{4\sigma_{s/a} M_w}{RT\rho_w D}\right), \quad (2.7)$$

where D is the wet diameter of the particle. Eqn. 2.7 gives a Köhler curve, the maximum of which is the s_c. Equation 2.7 is used as a fit to observed CCN data, which relies on the accuracy of the instrument and subsequent measurement methods. Kappa can be calculated then with any data supplying the D_d and s_c at which the particles activated.

Kappa may also be found through chemical properties of the particle. This method takes into account the number of dissociating ions of the compound (ν) and the osmotic coefficient (ϕ), which describes how much a given solution deviates from an ideal solution; for an ideal solution, $\phi = 1$. The molecular weight and density of the solute and water (denoted by subscripts "*s*" and "*w*") are also necessary inputs and this is expressed in Equation 2.8:

$$\kappa_{sol} = \nu\phi \frac{M_w \rho_s}{M_s \rho_w}. \quad (2.8)$$

For the purposes of this work, when using this equation to explore solubility limitations, we use $\phi = 1$ to represent an ideal aqueous solution droplet; the hygroscopicity in this case is alternately denoted κ_{ideal}.

Because atmospheric aerosols are composed of not single but multiple inorganic and organic compounds, if they are considered at equilibrium with the liquid water in the particle the overall κ of all the components can by found by a mixing rule,

$$\kappa_{ideal} = \sum_i \epsilon_i \kappa_{sol,i} H(x_i), \quad (2.9)$$

where the subscript "*i*" denotes the individual compound properties and ε is the ratio of the individual component volume over the total particle volume, $V_{s,i}/V_s$. $H(x_i)$ is given by

$$H(x_i) = \begin{cases} x_i & x_i < 1 \\ 1 & x_i \geq 1 \end{cases}, \quad (2.10)$$

where x_i is expressed as

$$x_i = (g^3 - 1)C_i/\epsilon_i, \quad (2.11)$$

for which g is the growth factor and C_i is the solubility of the component.

For most CCN in this study we use a solute of one organic compound, the exception being secondary organic aerosol. As detailed in Section 4, adipic acid was the only compound seen to have solubility effects with temperature, and this was modeled using Eqns 2.8 – 2.11 to compare with observed data.

2.2 Calibration techniques

During a typical laboratory experiment ammonium sulfate, $(NH_4)_2SO_4$, aerosol was atomized and measured in between organic scans. The activated fraction (number of CCN out of the total number of particles measured by the condensation particle counter) was then plotted as an activation curve showing diameter (nm) versus the activated fraction, shown in Figure 2.1. The critical diameter is obtained from a fit to the data to find the value where 50% of the particles activated (D_{50}) into cloud droplets in the CCN instrument. The fit line represents a Boltzmann sigmoid curve using Equation 2.12 (Sullivan et al., 2009),

$$\frac{CCN}{CN} = \frac{A_1 - A_2}{1 + e^{(x - x_o)/dx}} + A_2 \quad (2.12)$$

where CCN/CN is the activated fraction, A_1 is the minimum value of that fraction, A_2 is the maximum value, dx is the rate of change of the curve, and x_o is the point between A_1 and A_2 (the diameter at 50% activation, or D_{50}). This exact method is also used to obtain the organic

D_{50} values, which can be found for each experiment in the Appendix.

The Aerosol Inorganics Model, or AIM (Clegg et al., 1998; Friese and Ebel, 2010) was used for CCN instrument calibration with $(NH_4)_2SO_4$. Essentially, the model finds the state of the system at equilibrium in an atmosphere of a particular temperature and relative humidity. The other necessary input is the mole fraction of each ion in the solution. The model then calculates the amount of water (liquid form), dissolved ions, and solid ions in the system.

Water activity, a_w, and corresponding κ from AIM model output were used to find the growth factor (Equation 2.13); this and observed D_{50} critical diameters then give the wet diameters (Equation 2.14).

$$GF = \sqrt[3]{1 + \kappa^* \frac{a_w}{1+a_w}} \tag{2.13}$$

$$D = D_{50} * GF \tag{2.14}$$

The supersaturations are then calculated with this wet diameter, *D*, in Equation 2.7.

2.3 References

Clegg, S. L., P. Brimblecombe, and A. S. Wexler, Thermodynamic Model of the System H+-NH4+-Na+-SO42--NO3--Cl--H2O at 298.15 K. *J. Phys. Chem. A* **1998**, *102,* 2155-2171.

Friese, E., and A. Ebel (2010), Temperature Dependent Thermodynamic Model of the System H^+-NH_4^+-Na^+-SO_4^{2-}-NO_3^--Cl^--H_2O, J. Phys. Chem. A, 114, 11595–11631.

Köhler, H. (1936), The Nucleus in and the Growth of Hygroscopic Droplets, Trans. Farad. Soc., 32, 1152–1161.

Lewis, E. R. (2006), The effect of surface tension (Kelvin effect) on the equilibrium radius of a hygroscopic aqueous aerosol particle, J. Aerosol Sci., 37, 1605–1617.

Petters, M. D., and S. M. Kreidenweis (2007), A single parameter representation of hygroscopic growth and cloud condensation nucleus activity, Atmos. Chem. Phys., 7, 1961–1971.

Seinfeld, J. H., and S. N. Pandis (2006), *Atmospheric chemistry and physics: from air pollution to climate change*, 2nd ed., pp. 770, John Wiley & Sons, Inc., Hoboken, NJ.

Squires, P. (1958), The Microstructure and Colloidal Stability of Warm Clouds. Part II – The Causes of the Variations in Microstructure, Tellus, 10, 262–271.

Sullivan, R. C., M. J. K. Moore, M. D. Petters, S. M. Kreidenweis, G. C. Roberts, and K. A. Prather (2009), Effect of chemical mixing state on the hygroscopicity and cloud nucleation properties of calcium mineral dust particles, Atmos. Chem. Phys., 9, 3303–3316.

2.4 Figures

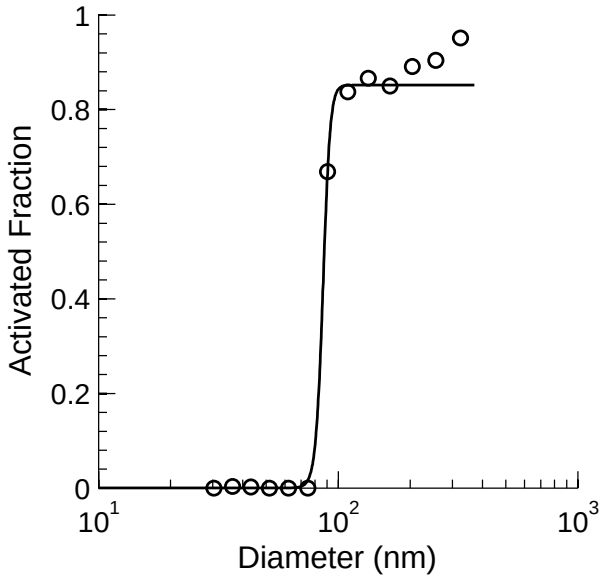

Figure 2.1. Activated fraction versus dry diameter showing a Boltzmann sigmoid curve through the observations. In this case, D_{50} is approximately 86 nm (diameter at which 50% of the particles have activated).

3. Literature Review

3.1 Synopsis of relevant organic aerosol proxies

Specific organic compounds were chosen for this study based on their known existence in ambient aerosol or as proxies based on their chemical structure. We also aimed to observe a wide variety of hygroscopicity trends with temperature. The following sections provide a short background on each compound as they relate to the larger context of atmospheric chemistry and their relevance as CCN.

3.1.1 Marine origin

Methanesulfonic acid (MSA) was used for this work because of its prevalence in the marine environment (Saltzman et al., 1983; Gao et al., 1996; Li et al., 1996; Zorn et al., 2008), ability to act as a CCN (Langley et al., 2010), and subsequent potential impact on climate (Charlson et al., 1987; Quinn et al., 1993). Phytoplankton in ocean water emit dimethyl sulfide (DMS), a volatile reduced sulfur compound, into the marine boundary layer. Here, it undergoes photochemical oxidation with the hydroxyl radical OH during the daytime or NO_3 at nighttime to produce MSA (among other oxidation products).

MSA's presence in the atmosphere as a sulfur compound likely contributes to the scattering of incoming solar radiation, as well as cloud properties such as albedo. This connection between biogenic aerosol and climate change is known as the CLAW hypothesis (Charlson et al., 1987), which essentially proposes that a warming of the ocean due to climate

change would enhance phytoplankton growth, increase DMS – and therefore MSA – production, increase the CCN number concentration, and increase earth's albedo; this is a negative feedback loop for climate change. However, Lovelock (2006) also proposed an "anti-CLAW" hypothesis due to emerging evidence that phytoplankton growth may decline with warming oceans, leading to a decrease in CCN number concentration, and decreased cloud albedo. We anticipate a better understanding of MSA's CCN activity will aid in establishing these ocean-atmosphere mechanisms.

Amines are organic compounds defined by the NH_2 functional group attached to the carbon backbone. Yin et al. (2011) explored the uptake of gaseous amines by sulfuric acid in the laboratory. Amines have been detected in urban and rural ambient aerosol (Neste et al., 1987; Zhang et al., 2002, 2003). Methylamine is a low molecular weight organic compound and the simplest of the amines. For this work, methylamine was mixed with MSA at a 1:1 molar ratio to create methylammonium methylsulfonate aerosol.

3.1.2 Continental origin

Dicarboxylic acids are prevalent in both primary and secondary atmospheric aerosol, and adipic acid is particularly present in SOA (Saxena and Hildemann, 1996). It is classified as a sparingly soluble dicarboxylic compound, or one that may be partially undissolved at equilibrium and whose solubility falls between that of an insoluble and soluble particle. Several studies have attempted to characterize the CCN ability of the acid experimentally with generally no closure or agreement (e.g. Cruz and Pandis, 1997; Prenni et al., 2001; Hori et al., 2003). Proposed reasons for discrepancies between laboratory generated adipic acid

aerosol are the high likelihood of trace contaminants (Hings et al., 2008), differences in the morphology of the particles due to generation method, as non-sphericity would affect measured activation diameters (Cruz and Pandis, 1997), and use of the surface tension of pure water as opposed to that of adipic acid solutions (Bilde and Svenningsson, 2004). Because of the particularly sensitive nature of adipic acid, this compound was chosen to exemplify the hygroscopic behavior of a particle with solubility limitations.

Ketoglutaric acid, also a dicarboxylic acid, is one of two derivatives of glutaric acid. Because of its chemical structure, it is both semi-volatile and water-soluble, and can be found in the gas and condensed phase in the atmosphere due to its vapor pressure (Saxena and Hildemann, 1996; Frosch et al., 2010). Its chemical structure is also comparable to dicarboxylic acids found in secondary organic aerosol (Gao et al., 2004).

Another proxy for dicarboxylic acids is maleic acid. Maleic acid is relevant to atmospheric aerosol in that it is highly soluble and known to react with O_3 to form products such as formic acid and CO_2 (Pope et al., 2010). It has been observed in both rural and urban ambient aerosol (e.g. Kawamura and Kaplan, 1987; Saxena and Hildemann, 1996; Röhrl and Lammel, 2001). Notably, Clegg and Seinfeld (2006) measured the deliquescence relative humidity of several dicarboxylic acids, and found that maleic acid tended to strongly dissociate in an aqueous solution, and this may affect its deliquescence behavior.

Glucose is a monosaccharide identified in both urban (e.g. Nolte et al., 2001) and remote (e.g. Carvalho et al., 2003) ambient air samples. Glucose is a low molecular weight carbohydrate, is water-soluble, has a negligible effect on solution surface tension, and

previously measured κ-values show that it acts essentially as an ideal solution in aqueous droplets (Rosenørn et al., 2006; Petters et al., 2009).

Glutamine is an amino acid that, like glucose, is commonly detected in ambient aerosol (e.g. identified from biomass burning source regions). Its hygroscopicity has been measured in the laboratory (Chan et al., 2005) and ambient atmosphere (e.g. Mandalakis, et al., 2011). Being classified as an amino acid that contains nitrogen, glutamine is an important part of the aerosol water-soluble organic carbon fraction (Saxena and Hildemann, 1996), which may have impacts on climate. Glutamine is also tied in with biosphere nutrient cycling (Zhang et al., 2002) and the formation of new particles (De Haan, 2009).

Polyethylene glycol (PEG) is a high-molecular weight polycarboxylic acid that is infinitely soluble in water (Petters et al., 2006) and represents linear chain polymers of oxyethylene units (Ninni et al., 1999). PEG has been studied for its water activity and other aqueous solution properties although it has not been explored in the literature as it applies to CCN; however PEG resembles humic-like-substances, which are abundant in ambient air samples (Decesari et al., 2001; Brooks et al., 2004; Kalberer et al., 2004).

3.1.3 Secondary organic aerosol

Secondary organic aerosol can be formed from a multitude of chemical reactions occurring in the atmosphere daily. A common reaction is the ozonolysis of volatile organic compounds (VOCs), which produces lower volatility compounds that subsequently condense onto particles. The ozonolysis mechanism is described in detail in Kroll and Seinfeld (2008). To summarize, an alkane (in this case, α-pinene is an endo-cycloalkene) reacts with O_3,

which slices the alkane at the C-C double bond into a carbonyl and a carbonyl oxide, or Criegee intermediate. This Criegee intermediate then decomposes to form OH and an alkyl radical. Following this reaction, various products are formed that make up the SOA system. An OH scavenger is then necessary to isolate the SOA particles and prevent further reactions (Keywood et al., 2004).

For this work, we focused on one such system composed of α-pinene, O_3, and cyclohexane as an OH scavenger. Alpha-pinene is an organic alkene, or monoterpene; it is a common biological emission from vegetation, especially coniferous trees. Its rate of emission is highly dependent on ambient temperature and available sunlight. Alpha-pinene is a reactive hydrocarbon that interacts with O_3, NO_3, and OH to give low-volatility products that easily condense onto particles, thereby providing a mechanism for CCN formation of secondary organic aerosol (vanReken et al., 2005; Prenni et al., 2007).

3.2 Review of CCN characterization experiments

Ambient particulate matter includes a large number of combinations of inorganic and organic fractions. For this reason, isolating particular compounds by generating them in a laboratory setting is essential for a more complete understanding of their behavior. A plethora of experimental studies have taken place to examine various properties of organic CCN, and this section will detail those that either closely resemble or influenced the experimental procedures for this work. A more detailed account of our particular instrumentation and measurement process can be found in Section 4.2.3.

The fundamental particle properties necessary for experimentally validating the accuracy of Köhler theory are the critical supersaturation and dry diameter. With these two pieces of data, information on the particles' hygroscopicity and chemistry can be derived. Differential mobility particle sizer (DMPS) mode is commonly used to analyze polydisperse aerosol populations (Knutson and Whitby, 1975). A polydisperse aerosol travels through a neutralizer, where the particles become either negatively or positively charged in order to create a known charge distribution. The particles then travel through a differential mobility analyzer (DMA) that selects particles based on a certain size (set by the user) based on electrical mobility through the sheath flow inside the column. The resulting monodisperse aerosols are counted by a condensation particle counter (CPC). DMPS mode is frequently used in aerosol measurements and has been proven useful in determining aerosol size distributions (e.g. Hoppel, 1978), especially for particles smaller than 50 nm. For this work, the flow was split between a CPC and a cloud condensation nuclei counter (CCNC, see Section 4.2.3).

One of the first CCN characterization methods akin to this thesis work was set forth by Cruz and Pandis (1997). This consisted of a collision-type atomizer that created a polydisperse aerosol from a solution of approximately 0.1% solute. The wet aerosol traveled through a gel-silica diffusion dryer before it is passed through a neutralizer and a first DMA. The resulting monodisperse aerosol then entered a second DMA (hence the nomenclature "tandem DMA analysis", or HTDMA) before being split between a condensation particle counter (CPC) and a thermal diffusion chamber-type cloud condensation nuclei counter (CCNC).

These types of measurements can be run in two ways – keeping the diameter constant and varying CCNC chamber supersaturation, or vice versa. Cruz and Pandis (1997) validated the accuracy with which this method measured CCN properties, and found that the CCNC could measure the activation diameters of ammonium sulfate within an error of ± 16% when compared to Köhler theory - a nontrivial improvement over previous calculations. This method allows the user to set the particle size, chemical composition, total particle number concentration, and supersaturation in the CCNC while measuring the particle size distribution, total number concentration, and total CCN concentration (Cruz and Pandis, 1997, 1998).

Lammel and Novakov (1995) measured the CCN activity of black carbon and diesel soot in the laboratory (via atomization of suspensions and combustion aerosol) using a DMPS and CCNC system. Likewise, Corrigan and Novakov (1999) measured the activation diameters of several organic compounds via single component aqueous solutions that were atomized and followed the same method of sampling as Cruz and Pandis (1997), with one DMA; both of these studies also operated the instrument with constant supersaturation while varying the particle diameter. Again, the validity of the data was measured using two inorganics – NaCl and $(NH_4)_2SO_4$ and the measured activation diameters showed agreement with theory.

Bilde and Svenningsson (2004) explored the activation of sparingly soluble organics (e.g. adipic acid) with this setup. This study concluded that for compounds such as this, small amounts of inorganic salt and particle phase (i.e. the presence of a solid core) have a significant impact on critical supersaturation; consequently, the disagreement between theory

and observation for these compounds can be accounted for by the likely presence of trace contaminants.

3.3 Cloud microphysics and temperature

Clouds typically form in the earth's lower to middle troposphere where the water vapor content is sufficient. For example, stratus-type clouds usually exist at or below 2000 m, and cumulus cloud bases typically exist at or below 2000 m, but can be higher; in strongly convective cases, cumulus cloud tops can reach greater than 10,000 m into the atmosphere. Depending on the time of year and location, the atmosphere throughout the troposphere ranges from approximately -40° to 40° C. Since the temperature profile typically decreases with height in the troposphere, cloud bases located on different levels in the atmosphere exist due to a certain number of CCN activating at that particular temperature (if the ambient supersaturation is sufficient, among other factors).

The relationship between cloud condensation nuclei concentrations and cloud microphysics has been well documented for several different cloud types known to exist at different atmospheric levels. Twomey and Warner (1967) took sampled ambient CCN around the cloud bases of "small to moderate non-precipitating cumuli, with tops warmer than 0° C" and found in their regression analysis that cloud droplet and cloud nuclei concentrations correlated well. Yum et al., 1998, remarked on the First Aerosol Characterization Experiment (ACE 1) findings within stratocumulus clouds in the Southern Ocean, and re-enforced the general consensus that cloud microphysical properties are strongly influenced by CCN concentrations.

In order for a particle to activate into a cloud droplet in the ambient below-cloud atmosphere, the supersaturation of the air must match that of the particular critical supersaturation (s_c) of the CCN. The supersaturation of the air is dependent on the updraft velocity into the cloud base – this is a major influence on CCN concentration here and subsequently the growth of the cloud (Hudson, 1993; Yum and Hudson, 2002).

Recognizing the correlation between CCN and cloud droplet number concentrations is essential to understanding cloud microphysics. The number of cloud droplets constituting a cloud influences its initial precipitation, growth, and optical properties (Twomey and Warner, 1967).

3.4 References

Bilde, M., and B. Svenningsson (2004), CCN activation of slightly soluble organics: the importance of small amounts of inorganic salt and particle phase, Tellus, 56B, 128–134.

Brooks, S. D., P. J. DeMott, and S. M. Kreidenweis (2004), Water uptake by particles containing humic materials and mixtures of humic materials with ammonium sulfate, Atmos. Environ., 38, 1859–1868.

Chan, M. N., M. Y. Choi, N. L. Ng, and C. K. Chan (2005), Environ. Sci. Technol., 39, 1555–1562.

Charlson, R. J., J. E. Lovelock, M. O. Andreae, and S. G. Warren (1987), Oceanic phytoplankton, atmospheric sulfur, cloud albedo, and climate, Nature, 326, 655–661.

Clegg, S. L., and J. H. Seinfeld (2006), Thermodynamic Models of Aqueous Solutions Containing Inorganic Electrolytes and Dicarboxylic Acids at 298.15K 1. The Acids as Nondissociating Components, J. Phys. Chem. A, 110, 5692–5717.

Corrigan, C. E., and T. Novakov (1999), Cloud condensation nucleus activity of organic compounds: a laboratory study, Atmos. Environ., 33, 2661–2668.

Cruz, C. N., and S. N. Pandis (1997), A study of the ability of pure secondary organic aerosol to act as cloud condensation nuclei, Atmos. Env., 31, 2205–2214.

Cruz, C. N. and S. N. Pandis (1998), The effect of organic coatings on the cloud condensation nuclei activation of inorganic atmospheric aerosol, J. Geophys. Res., 103, 13111–13123.

Decesari, S., M. C. Facchini, E. Matta, F. Lettini, M. Mircea, S. Fuzzi, E. Tagliavini, and J. P. Putaud (2001), Chemical features and seasonal variation of fine aerosol water-soluble organic compounds in the Po Valley, Italy, Atmos. Environ., 35, 3691–3699.

De Haan, D. O., A. L. Corrigan, K. W. Smith, D. R. Stroik, J. J. Turley, F. E. Lee, M A. Tolbert, J . L. Jimenez, K .E. Cordova, and G. R. Ferrell (2009), Secondary Organic Aerosol-Forming Reactions of Glyoxal with Amino Acids, Environ. Sci. Technol., 43, 2818–2824.

Frosch, M., A. A. Zardini, S. M. Platt, L. Müller, M. C. Reinnig, T. Hoffmann, and M. Bilde (2010), Thermodynamic properties and cloud droplet activation of a series of oxo-acids, Atmos. Chem. Phys., 10, 5873–5890.

Gao, Y., R. Arimoto, R. A. Duce, L. Q. Chen, M. Y. Zhou, and D. Y. Gu (1996), Atmospheric non-sea-salt sulfate, nitrate, and methansulfonate over the China sea, J. Geophys. Res., 101, 12601–12611.

Gao, S., Keywood, M., N. Ng, J. Surratt, V. Varutbangkul, R. Bahreini, R. Flagan, and J. H. Seinfeld (2004), Low-Molecular-Weight and Oligomeric Components in Secondary Organic Aerosol from the Ozonolysis of Cycloalkenes and α-Pinene, J. Phys. Chem. A, 108, 10147–10164.

Hings, S. S., W. C. Wrobel, E. S. Cross, D. R. Worsnop, P. Davidovits, and T. B. Onasch (2008), CCN activation experiments with adipic acid: effect of particle phase and adipic acid coatings on soluble and isoluble particles, Atmos. Chem. Phys., 8, 3735–3748.

Hoppel, W. A. (1978), Determination of the aerosol size distribution from the mobility distribution of the charged fraction of aerosols, J. Aerosol Sci., 9, 41–54.

Hori, M., S. Ohta, N. Murao, and S. Yamagata (2003), Activation capability of water soluble organic substances as CCN, J. Aerosol Sci., 34, 419–448.

Hudson, J. G. (1993), Cloud Condensation Nuclei Near Marine Clouds, J. Geophys. Res., 98, 2693–2702.

Kalberer, M., D. Paulsen, M. Sax, M. Steinbacher, J. Dommen, A. S. H. Prevot, R. Fisseha, E. Weingartner, V. Frankevich, R. Zenobi, and U. Baltensperger (2004), Identification of Polymers as Major Components of Atmospheric Organic Aerosols, Science, 303, 1659–1662.

Kawamura, K., and I. R. Kaplan (1987), Motor Exhaust Emissions as a Primary Source for Dicarboxylic Acids in Los Angeles Ambient Air, Environ. Sci. Technol., 21, 105–110.

Keywood, M. D., J. H. Kroll, V. Varutbangkul, R. Bahreini, R. C. Flagan, and J. H. Seinfeld (2004), Secondary Organic Aerosol Formation from Cyclohexene Ozonolysis: Effect of OH Scavenger and the Role of Radical Chemistry, Environ. Sci. Technol., 38, 3343–3350.

Knutson, E. O., and K. T. Whitby (1975), Aerosol classification by electric mobility: apparatus, application, and theory, Aer. Sci., 6, 443–451.

Lammel, G., and T. Novakov (1995), Water nucleation properties of black carbon and diesel soot particles, Atmos. Environ., 29, 813–823.

Langley, L., W. R. Leaitch, U. Lohmann, N. C. Shantz, and D. R. Worsnip (2010), Contributions from DMS and ship emissions to CCN observed over the summertime North Pacific, Atmos. Chem. Phys., 10, 128–1314.

Li, S. M., C. M. Banic, W. R. Leaitch, P. S. K. Liu, G. A. Isaac, X. L. Zhou, and Y. N. Lee (1996), Water-soluble fractions of aerosol and their relations to number size distributions based on aircraft measurements from the North Atlantic Regional Experiment, J. Geophys. Res., 101, 29111–29121.

Lovelock, J. (2006), *The Revenge of Gaia*, Penguin Books Ltd.: New York, New York.

Mandalakis, M., M. Apostolaki, T. Tziaras, P. Polymenakou, E. G. Stephanou (2011), Free and combined amino acids in marine background atmospheric aerosols over the Eastern Mediterranean, Atmos. Environ., 45, 1003–1009.

Van Neste, A., and R. A. Duce (1987), Methylamines in the Marine Atmosphere, Geophys. Res. Lett., 14, 711–714.

Nolte, C. G., J. J. Schauer, G. R. Cass, and B. R. T. Simoneit (2001), Highly Polar Organic Compounds Present in Wood Smoke and in the Ambient Atmosphere, Environ. Sci. Technol., 35, 1912–1919.

Petters, M. D., S. M. Kreidenweis, J. R. Snider, K. A. Koehler, Q. Wang, A. J. Prenni, and P. J. DeMott (2006), Cloud droplet activation of polymerized organic aerosol, Tellus, 58B, 196–205.

Petters, M. D., S. M. Kreidenweis, A. J. Prenni, R. C. Sullivan, C. M. Carrico, K. A. Koehler, and P. J. Ziemann (2009), Role of molecular size in cloud droplet activation, Geophys. Res. Lett., 36, L22801.

Pope, F. D., P. J. Gallimore, S. J. Fuller, R. A. Cox, and M. Kalberer (2010), Ozonolysis of Maleic Acid Aerosols: Effect up on Aerosol Hygroscopicity, Phase and Mass, Environ. Sci. Technol., 44, 6656–6660.

Prenni, A. J., P. J. DeMott, S. M. Kreidenweis, D. E. Sherman, L. M. Russell, and Y. Ming (2001), The Effects of Low Molecular Weight Dicarboxylic Acids on Cloud Formation, J. Phys. Chem. A, 105, 11240–11248.

Prenni, A. J., M. D. Petters, S. M. Kreidenweis, P. J. DeMott, and P. J. Ziemann (2007), Cloud droplet activation of secondary organic aerosol, J. Geophys. Res., 112, D10223.

Quinn, P. K., D. S. Covert, T. S. Bates, V. N. Kapustin, D. C. Ramsey-Bell, and L. M. McInnes (1993), Dimethylsulfide/Cloud Condensation Nuclei/Climate System: Relevant Size-Resolved Measurements of the Chemical and Physical Properties of Atmospheric Aerosol Particles, J. Geophys. Res., 98, 10411–10427.

Röhrl, A., and G. Lammel (2001), Determinatio of malic acid and other C_4 dicarboxylic acids in atmospheric aerosol samples, Chemos., 46, 1195–1199.

Saltzman, E. S., D. L. Savoie, R. G. Zika, and J. M. Prospero (1983), Methane Sulfonic Acid in the Marine Atmosphere, J. Geophys. Res., 88, 10897–10902.

Saxena, P., and L. M. Hildemann (1996), Water-Soluble Organics in Atmospheric Particles: A Critical Review of the Literature and Application of Thermodynamics to Identify Candidate Compounds, J. Atmos. Chem., 24, 57–109.

Twomey, S., and J. Warner (1967), Comparison of Measurements of Cloud Droplets and Cloud Nuclei, J. Atm. Sci., 24, 702–703.

VanReken, T. M., N. L. Ng, R. C. Flagan, and J. H. Seinfeld (2005), Cloud condensation nucleus activation properties of biogenic secondary organic aerosol, J. Geophys. Res., 110, D07206.

Yum, S. S., J. G. Hudson, and Y. Xie, Comparisons of cloud microphysics with cloud condensation nuclei over the summertime Southern Ocean, J. Geophys. Res., 103, 16625–16636.

Zhang, Q. , C. Anastasio, and M. Jimenez-Cruz (2002), Water-soluble organic nitrogen in atmospheric fine-particles ($PM_{2.5}$) from northern California, J. Geophys. Res., 107, D114112.

Zhang, Q., and C. Anastasio (2003), Free and combined amino compounds in atmospheric fine particles ($PM_{2.5}$) and fog waters from Northern California, Atmos. Environ., 37, 2247–2258.

Zorn, S. R., F. Drewnick, M. Schott, T. Hoffmann, and S. Borrmann (2008), Characterization of the South Atlantic marine boundary layer aerosol using an aerodyne aerosol mass spectrometer, Atmos. Chem. Phys., 8, 4711–4728.

4. Journal Submission Paper

The following section contains a paper to be submitted to the *Journal of Physical Chemistry A* for publication. A more detailed description of the instrumentation used and hygroscopicity parameters is included, as well as three case studies exemplifying the results. The complete data analysis for each experimental run can be found in the thesis Appendix.

The role of temperature in cloud droplet activation

S. I. Christensen[1] and M. D. Petters[1*]

[1]Department of Marine, Earth and Atmospheric Sciences, North Carolina State University, Campus Box 8208, Raleigh, NC 27695-8208, USA.

*Corresponding author: Markus D. Petters (markus_petters@ncsu.edu)

Prepared for submission to *Journal of Physical Chemistry A*

Abstract

Aerosols are prevalent in the atmosphere where they can serve as cloud condensation nuclei (CCN). Here we report on new CCN measurements to characterize the temperature dependence of CCN activity for single component organic aerosol and secondary organic aerosol from the reaction of α-pinene and O_3 generated in the laboratory. For compounds with a weak dependence of water activity on temperature, the critical supersaturation of the particles can be well-modeled using temperature dependent surface tension and Köhler theory. We also demonstrate that Köhler theory is valid for sparingly soluble compounds and can quantitatively explain the temperature dependent activation properties of adipic acid aerosol over a broad range of temperatures. Accounting for temperature dependent surface tension strongly affects CCN activity and we anticipate that including this effect in global and regional model simulations may significantly change the estimated aerosol indirect forcing.

4.1. Introduction

Suspended particulate matter in the atmosphere serves as a condensation site for water vapor during the early stages of cloud formation. The number concentration, size, and chemical composition of these particles are important for determining the critical water supersaturation (s_c) that must be achieved to activate them as cloud condensation nuclei (CCN). An increased number of CCN that are active at a given supersaturation generally results in an increased cloud droplet number concentration (Fitzgerald and Spyers-Duran, 1973; Andreae et al., 2008), increased cloud reflectivity (Twomey, 1974), and decreased precipitation efficiency in stratiform (Albrecht, 1989) and cumuliform (Andreae et al., 2004) clouds.

A particle's s_c is in part determined by its dry diameter, D_d. In general, smaller particles require a higher water supersaturation to activate. However, two spherical particles of identical volumes but different chemical compositions also differ in their critical supersaturations. Many studies have characterized the relationship between the aerosol D_d, chemical composition, and s_c for a wide range of individual organic and inorganic compounds found in atmospheric particulate matter (e.g. Cruz and Pandis, 1998; Raymond and Pandis, 2002; Broekhuizen et al., 2004; Petters et al., 2006; Kristensson et al., 2010), as well as for chemically complex proxies such as secondary organic aerosol generated in smog chamber studies (e.g. vanReken et al., 2005; Prenni et al., 2007; King et al., 2007; Duplissy et al., 2009), and ambient aerosol in various environments (Dusek et al., 2006; Gunthe et al., 2008; Rose et al., 2010; Jurányi et al., 2011; Levin et al., 2012). Despite these and other studies, the understanding of the hygroscopic behavior of the organic portion of particulate

matter remains incomplete, especially as it relates to the uncertainty of the Earth's radiation budget (IPCC, 2007).

The relationship between s_c, D_d, and chemical composition can be quantified by assigning each particle type an apparent hygroscopicity, κ (Petters and Kreidenweis, 2007). This κ-value subsumes the physicochemical properties of the aerosol such as compound molecular weight, density, and activity coefficients and ranges from 0 to 1.4 for experiments that have been conducted at room temperature. To the best of our knowledge, all prior published CCN studies have been performed near room temperature and none have systematically explored the dependence of the $s_c - D_d$ relationship or κ on temperature. Nonetheless, some studies have reported the temperature dependence of aerosol water uptake using hygroscopic tandem differential mobility analysis (Gysel et al., 2002) and water activity measurements (Zamora et al., 2011). Thermodynamic models of atmospheric aerosol systems also account for the temperature dependence of a few compounds (e.g. Jacobson et al., 1996; Friese and Ebel, 2010). In general, the experimental studies and modeling results suggest that the temperature dependence of κ is expected to be relatively small, but data particularly for organic compounds that are ubiquitous in the submicron non-refractory aerosol (Jimenez et al., 2009) are not available. Further, the roles of temperature dependence due to surface tension and solubility effects, both relevant for the $s_c - D_d$ relationship, are not accounted for in the water uptake studies (Gysel et al., 2002, Zamora et al., 2011) or the thermodynamic models (Jacobson et al., 1996; Friese and Ebel, 2010).

Here we report data acquired using a new method that involves placing a continuous flow streamwise temperature gradient CCN instrument (Roberts and Nenes,

2005) inside a temperature-controlled enclosure and ramping temperature from approximately 40˚ to 0˚C over a period of approximately six hours. During the temperature ramp the CCN instrument performed diameter scans at a constant streamwise temperature gradient (Petters et al., 2009b) on ammonium sulfate, as a calibration reference, and various organic compounds that were selected as proxies for atmospheric aerosol. We show that after accounting for the temperature dependence of surface tension, and with the exception of sparingly soluble compounds, observed κ-values are only weakly dependent on temperature.

4.2. Methods

4.2.1. Kappa-Köhler framework

According to classic Köhler theory (Köhler, 1936), each particle of a certain dry diameter (D_d) relates to a particular critical supersaturation (s_c) at which it will begin to activate and transition from stable equilibrium into a cloud droplet. Here we use the equations presented by Petters and Kreidenweis (2007, 2008) and Petters et al. (2009a), with the particle's water content expressed as wet diameter (D) and the saturation ratio over the aqueous droplet (S):

$$S(D) = \frac{D^3 - D_d^3}{D^3 - D_d^3(1-\kappa)} \exp\left(\frac{A}{D}\right), \tag{4.1}$$

where

$$A = \frac{4M_w}{R\rho_w}\frac{\sigma_{s/a}}{T} \tag{4.2}$$

and is dependent upon temperature, T, the surface tension of pure water, $\sigma_{s/a}$, the density of water, ρ_w, the molecular weight of water, M_w, and the universal gas constant, R.

Equations 4.1 and 4.2 can be used to compute the relationship between D_d, s_c ($s_c = S_c - 1$, where S_c is the saturation ratio and s_c is usually expressed as a percentage), and κ via an iterative procedure that is described in Petters and Kreidenweis (2008). Kappa can also be approximated from the following analytical solution:

$$\kappa_{app} = \frac{4A^3}{27 D_d^3 \ln^2 S_c}. \quad (4.3)$$

The subscript "*app*" denotes that the κ-value is the apparent value because it reproduces the $s_c - D_d$ observation when applied in Equation 4.1 or 4.3. Higher κ_{app} values correspond to lower s_c for the same D_d.

The "*A*" parameter is generally evaluated using a standard reference state of T = 298.15K and $\sigma_{s/a}$ = 0.072 J m^{-2} (the surface tension of pure water at 298.15K, assuming that the solute does not affect surface tension). The surface tension of pure water increases with decreasing temperature due to greater intermolecular forces between molecules when kinetic energy is lowered. Between 40˚ and 0˚C, which are temperatures relevant to this study, this relationship is linear and is expressed in Equation 4.4 based on empirical fit coefficients described in Pruppacher and Klett (1997):

$$\sigma_{s/a} = 0.0761 - 1.55 \times 10^{-4} T\ [^\circ C]. \quad (4.4)$$

The density of water changes by ~0.8% over the temperature range used in this work and this change is negligible compared to the relative change in surface tension. Therefore for this study, we assume that the density of water is constant in all calculations.

We introduce the superscript "θ" to distinguish between κ evaluated at the reference state (κ_{app}^{θ}) from κ evaluated with an "*A*" parameter that is valid at any temperature

T (κ_{app}). The main advantages for using κ_{app}^{Θ} in previous studies lie in the ability to contrast CCN data irrespective of experimental conditions defined by D_d, s_c, and temperature and to characterize changes in CCN activity that occur during processes such as chemical aging of organic aerosols (e.g. Petters et al., 2006; Jimenez et al., 2009) or the sensitivity of aerosol indirect forcing to changes in κ_{app}^{Θ} (e.g. Liu and Wang, 2010).

Kappa can also be understood in terms of the physicochemical properties of the solute and solvent: solute and water molecular weight (M_s and M_w, respectively), solute and water density (ρ_s and ρ_w), practical osmotic coefficient (ϕ), surface tension ($\sigma_{s/a}$), and solubility in water (C). One commonly used approximation to find κ from modified Raoult's law (Petters et al., 2009a) is

$$\kappa_{sol} = \nu\phi \frac{M_w \rho_s}{M_s \rho_w}, \tag{4.5}$$

where ν is the number of ions the compound dissociates into and the subscript "*sol*" indicates that it was computed from solution theory. For ideal solutions, ϕ = 1 and those κ values will be referred to as κ_{ideal}. For multicomponent mixtures, the overall κ-value is given by the following mixing rule (Petters and Kreidenweis, 2008):

$$\kappa_{theory} = \sum_i \epsilon_i \kappa_{sol,i} H(x_i)$$

$$x_i = (g^3 - 1) C_i / \epsilon_i \tag{4.6}$$

$$H(x_i) = \begin{cases} x_i & x_i < 1 \\ 1 & x_i \geq 1 \end{cases},$$

where ε_i is volume fraction of the i^{th} component in the mixture, $\kappa_{sol,i}$ is the individual component hygroscopicity, C_i is defined as volume of solute per volume of water of a saturated solution, and $g = D / D_d$ is the diameter growth factor. The subscript "*theory*" is

used to indicate that it was computed from κ_{sol} and C of the mixture. The $s_c - D_d$ relationship can be computed via Equation 4.1 from any of the four described κ-values: κ_{app}, κ_{sol}, κ_{ideal}, and κ_{theory}. Each of the κ-values may be evaluated either at their standard state or temperature T. The definitions of these κ-values are summarized in Table 4.1 for reference.

4.2.2. Expected dependencies of CCN activity on temperature

Based on the preceding discussion, the ability of a particle to serve as CCN depends on temperature in various ways. The purpose of the following section is to discuss the expected dependencies based on known behavior of bulk solutions and existing theories. The temperature dependence is explicitly included in the "A" parameter (Eqn. 4.2). CCN activity may also depend on temperature implicitly due to the possible dependence of v, ϕ, $\sigma_{s/a}$, and C on temperature. Each previously defined κ-value in this paper is sensitive to some, but not all, of these parameters. For non-dissociating solutes, κ_{ideal} depends only on the molecular weights and densities and thus is fundamentally independent of temperature. For molecules that dissociate and for which the molecule is only partially dissociated (e.g. an acid in aqueous solution where the pH is near the acid's pKa value), changes in temperature may shift the dissociation equilibrium and this change can be reflected in either κ_{sol} or κ_{ideal}.

In addition to dissociation equilibration, κ_{sol} includes the osmotic coefficient to account for solution nonideal effects on water activity. Jacobson et al. (1996) argue, based on the theory for electrolyte solutions (Harned and Owen, 1958), that the effect of temperature on water activity is expected to be small, especially for dilute solutions that are

most relevant for CCN activation. Thus one would expect that κ_{sol} depends only weakly on temperature. Experimental data relevant to water uptake of some inorganic (Gysel et al., 2002) and organic compounds (Zamora et al., 2011) that are commonly detected in atmospheric aerosols are consistent with a weak or negligible dependence of κ_{sol} on temperature.

Solubility in water together with the water activity of the saturated solution and D_d determines the deliquescence relative humidity (DRH) of a particle. In the context of determining CCN activity, solubility is factored in via κ_{theory} and the role of a compound's solubility can be broadly categorized as follows (Petters and Kreidenweis, 2008): water soluble compounds are those sufficiently soluble to be fully dissolved at typical equilibrium water contents at the point of activation. These compounds are deliquesced, their CCN activity follows from their κ_{sol}, and the actual value of C is inconsequential to the derived s_c. Sparingly soluble compounds are those whose DRH falls into the supersaturated regime. Since deliquescence must precede equilibrium water uptake, the DRH can control the s_c of a particle (Kreidenweis et al., 2006) and the $s_c - D_d$ relationship becomes highly sensitive to small variations in solubility. Water insoluble compounds are those that remain undissolved at water contents relevant for CCN activation. When solubility is expressed as volume of compound per unit volume of water of a saturated solution, the approximate ranges for sufficiently soluble, sparingly soluble, and insoluble are $C > 0.2$, $5*10^{-4} < C < 0.2$, and $C < 5*10^{-4}$, respectively (Petters and Kreidenweis, 2008). Solubility generally decreases with decreasing temperature. If compounds transition from the sufficiently soluble into the sparingly soluble regime a strong decrease in κ_{theory} would be expected.

The equilibrium vapor pressure over a curved surface is greater relative to that of a flat surface, and the magnitude of the increase is determined by the surface tension and the curvature of the droplet. This is the Kelvin effect and it competes against the Raoult effect in Köhler theory. The smaller the molecule, the larger the curvature and surface tension - which results in a higher saturation vapor pressure; therefore increased surface tension raises the s_c that is required to activate the particle into a cloud droplet. Lower temperatures require higher s_c values to activate the particles; consequently, if any κ-value is shown to be approximately constant, κ^{Θ} is expected to decrease with decreasing temperature.

4.2.3. Measurements

Aqueous solutions of ammonium sulfate or organic compounds were prepared in ultrapure deionized water (18.2 MΩ) that consisted of approximately 0.1% mass concentration of the solute. The solutions were atomized (TSI 3076) and passed through two diffusion driers (TSI 3062). Sources and purity of the chemicals are listed in Table 4.2. We selected compounds that are proxies for marine and terrestrial organic aerosols including methanesulfonic acid (e.g. Saltzman et al., 1983; Zorn et al., 2008) and methylammonium methylsulfonate (e.g. Facchini et al., 2008; Yin et al., 2011), carbohydrates (glucose) and organic acids (maleic acid, L-glutamine, α-ketoglutaric acid, and adipic acid), as well as proxies for oligomeric high molecular weight compounds (polyethylene glycol) and multicomponent secondary organic aerosol generated from α-pinene. With the exception of the methanesulfonic acid and methylammonium methylsulfonate, our choice of compounds was also guided by the availability of sometimes-extensive data sets obtained at room

temperature to enable comparison of our data with that of prior studies.

Secondary organic aerosol was generated from the ozonolysis of α-pinene with O_3 in the presence of excess cyclohexane that was added to scavenge hydroxyl radicals that formed from the ozonolysis reaction. Alpha pinene was reacted inside a continuous flow reactor similar to the design described in Petters et al. (2009c). An aliquot of ~25 µl of α-pinene was added into a ¼" Swagelok Union Tee-fitting (SS-400-3) that was capped on two ends and connected to a 10 cm upward pointing ¼" OD stainless steel tube terminating into a second Swagelok Tee-fitting. The Tee-fitting containing α-pinene was immersed into a constant temperature water bath held at 30˚C. The top Tee-fitting was held outside the water bath at room temperature and was constantly flushed with 1 vLpm of zero air (Teledyne 701 outfitted with a high purity hydrocarbon scrubber[1]) to create an α-pinene enriched flow. The α-pinene enriched flow then passed through a third Swagelok Tee fitting (SS-400-3TTF). A syringe pump (Harvard Apparatus 11 Pico Plus Elite) infused 2 µl min^{-1} liquid cyclohexane into a port connector (SS-2-TA-1-2) that was connected to the third Tee fitting. The cyclohexane evaporated and the α-pinene/cyclohexane reactant flow merged with a flow of 1.2 vLpm zero air enriched with 5 ppm of O_3 (Teledyne 703) at the entrance of a laminar flow tube, where O_3 and α-pinene reacted and particles formed via homogeneous nucleation from the reaction products. The flow tube consisted of two 1.45 m long glass-tubes with ~5 cm inner diameter. The stream exiting the flow tube then entered a 10 L mixing chamber also made of glass. At the exit of the reactor a dynamic equilibrium was established and provided

[1] Manufacturer specifications: SO2 < 0.5 ppb, NO < 0.5 ppb, NO2 < 0.5 ppb, O3 < 0.5 ppb, CO < 0.025 ppm, Hydrocarbons < 0.02 ppm

a stable source of polydisperse α-pinene O_3 SOA that had a constant size distribution and number concentration. SOA experiments were performed on two days. Mass concentrations from those two experiments determined from the integration over the size distribution, and assuming a density of 1 g cm^{-3}, were ~950 μg m^{-3} and ~350 μg m^{-3}. Residence time inside the entire continuous flow reactor was ~ 7 min. Figure 4.1 shows a schematic of the measurement setup.

After atomization or ozonolysis, the resulting polydisperse aerosol was charge equilibrated inside a neutralizer (ADI-100 Particle Instruments, LLC) that contained four ^{210}Po charge strips (StaticMaster 2U500, NRD, LLC). Particles were size selected (from approximately 30 to 320 nm) using a long electrostatic classifier column (TSI 3081) whose internal column was charged to result in a negative electric potential using a custom power supply (Spellman, Inc. Model SL10N10). A 9 vLpm recirculating sheath flow was controlled using a diaphragm pump (Gast, DOA-P707-AA) and a precision critical orifice (O'Keefe Controls, CO). The size classified particle flow was then split and fed to a condensation particle counter operating at 1 vLpm (TSI 3771) or a Droplet Measurement Technologies (DMT) continuous-flow streamwise thermal gradient CCN instrument (Robert and Nenes, 2005) operating at 0.5 vLpm. The CCN instrument was enclosed inside an insulated box, whose temperature was controlled using a cryostat interfaced with a heat exchanger. The temperature inside the enclosure was ramped from approximately 40˚ to 0˚C over the course of a 6 – 7 hour experiment.

The CCN instrument actively controls temperature along the sheath and aerosol sample flow paths. Supersaturation is generated by controlling the temperatures $T_1 < T_2 < T_3$

(Figure 4.1), which is done by an internal algorithm based on a user supplied ΔT value. Experiments were typically performed at ΔT = 6K with the exception of experiments involving adipic acid, which required higher supersaturations for activation. The maximum supersaturation is achieved ~1/3 of the distance from the TEC 1 temperature element (Snider et al., 2010), suggesting that the sample experienced some warming before activation. Because we operated the instrument at modest ΔT values, we do not attempt to quantify this warming and temperature values reported here correspond to T_1.

In a typical experiment, the ΔT value was set for the enclosed CCN instrument and the size distribution was scanned in differential mobility particle sizing (DMPS) mode. As the aerosol passed through the column, those particles with a critical supersaturation less than or equal to the set value were activated, counted, and sized by an optical particle counter (Rose et al, 2008). The resulting activation curves were inverted to correct for multiply charged particles and fit to find the diameter where 50% of the particles activated (D_{50}, Petters et al., 2007; Petters et al., 2009b). The instrument supersaturation was found by measuring the activation diameters of ammonium sulfate aerosol. These observed D_{50} values were converted to the corresponding instrument supersaturation using the water activity versus composition relationship obtained from the Aerosol Inorganics Model (AIM) (Clegg et al., 1998) and the temperature dependent surface tension given by Equation 4.4. Figure 4.2 shows how this instrument supersaturation varies with absolute temperature and provides an estimate of the precision of this CCN system. At any given temperature the inferred supersaturation varies ~ ±6% relative to the mean value. The data also show that the instrument supersaturation increases from ~0.25% to 0.5% when the absolute temperature

decreases from ~40˚ to 0˚C. Model simulations presented by Roberts and Nenes (2005) suggest that this behavior is expected based on the design principles of the instrument.

We performed similar simulations to show that there is a semi-quantitative agreement between an instrument model and the calibration for the conditions used in our experiments. Instrument supersaturation versus absolute temperature was modeled by numerically solving the equations for heat and vapor diffusion in 2D axisymmetric cylindrical laminar flow through a pipe. Buoyancy effects that may distort the flow for large temperature gradients (Roberts and Nenes, 2005) are not considered and thus our model is only valid for small to moderate streamwise temperature gradients (< ~8 K m^{-1}). Model boundary conditions prescribe the temperature at the location for TEC 1, TEC 2, and TEC 3 (Figure 4.1) and assume a linear temperature increase at all locations in between. Moisture boundary conditions assume that vapor pressure equals the saturation vapor pressure above pure water at the corresponding wall temperature. Thermal resistance of the walls (Lance et al., 2006, Snider et al., 2006) and lowering of water activity by the substrate (Snider et al., 2006) are not considered. Model inputs are the total volumetric flow rate, absolute pressure, and temperatures T_1, T_2, and T_3. Initial conditions assume that the RH=100% for the sheath flow and the RH=10% for the aerosol flow at the entrance of the chamber. Our instrument model was validated by reproducing Figure 4 of Roberts and Nenes (2005) and has been used previously to model the centerline supersaturation experienced by particles in the CCN instrument (Snider et al., 2010).

Results from our simulations are superimposed in Figure 4.2b. For these calculations we specify T_1 as an absolute temperature and set the first gradient to $T_2 = T_1 +$

3˚C and the second gradient to $T_3 = T_2 + 2.5$˚C, which corresponds to T_2 and T_3 for $\Delta T = 6$˚C. The second gradient is slightly reduced to prevent the formation of a second supersaturation maximum. The resulting model supersaturation was multiplied by the empirical value of 0.80 to achieve approximate agreement between the modeled (nominal) and calibrated (effective) supersaturation at lower temperatures. Discrepancies between nominal and effective instrument supersaturation are well documented for CCN instruments of various designs (Lance et al., 2006; Snider et al., 2006) and the ratio of effective and nominal supersaturation can be as low as 0.6 for static diffusion chambers (Snider et al., 2006). Comparison between our calibration data and the instrument model shows that the data follow a slightly steeper slope, especially at warm temperatures. This discrepancy may be attributable to vapor limitations at very warm temperatures due to the exponential dependence of saturation vapor pressure on temperature or other system non-idealities that are not accounted for in our numerical model of the instrument. We therefore use the ammonium sulfate data to specify the supersaturation in our experiments.

For each studied compound we performed a 6 – 7 hour temperature scan during which the insulated box was first heated to 40˚C followed by cooling at a rate of ~6 ˚C per hour. This cooling rate was implemented in order to avoid cooling the CCN instrument too quickly, which would cause unstable temperatures inside the column. After each diameter scan a computer controlled three-way solenoid valve switched the aerosol source between two atomizers – one that contained the ammonium sulfate solution and the other a solution of the compound to be studied. At the same time, the box was cooled by programming the cryostat temperature. The CCN instrument controls T_1, T_2, and T_3 relative to the inlet

temperature T_{inlet}, which is just above the column, and only adjusts these temperatures if the temperature difference $T_1 - T_{inlet}$ exceeds a threshold value set by the user, typically 2˚ or 3˚C for our experiments. During temperature adjustments in the CCN instrument the supersaturation is unstable. DMPS scans during which the temperature was adjusted were discarded in the post-processing of the data.

4.3. Results

To validate our κ findings, we compared our $\kappa_{app}^{\ominus}$ values to those published previously in literature (see Table 4.2). The three adipic acid runs varied from $\kappa_{app}^{\ominus}$= ~ 0.004 - 0.007, which are consistent with high purity adipic acid experiments reported by Hings et al. (2008). Glucose, polyethylene glycol, and secondary organic aerosol all fell well within the range observed by prior studies. Our ketoglutaric acid $\kappa_{app}^{\ominus}$ tended to be slightly higher than the values reported by Frosch et al. (2010). Literature values for glutamine, maleic acid, methanesulfonic acid, and methylammonium methylsulfonate are not available but are consistent between repeat experimental runs. The observed fit parameters, $\kappa_{app}^{\ominus}$ at 298K, and the literature κ are summarized in Table 4.2. Individual data points are tabulated in Christensen (2012).

4.3.1. Non-dissociating water-soluble species

Figure 4.3a shows the measured activation diameters of glucose and ammonium sulfate aerosol plotted versus temperature obtained from a single experiment. To analyze

these data, we fit the ammonium sulfate and glucose activation data to linear equations. The ammonium sulfate fit line allows us to interpolate the activation diameter that is needed to find the instrument supersaturation at arbitrary temperatures via the ammonium sulfate activation model for the particular experiment (Section 4.2.1). The instrument supersaturation from a calibration scan is then used to find the consecutive organic scan's κ_{app}^{Θ} (Figure 4.3b) and κ_{app} (Figure 4.3c). For glucose, κ_{app} is consistent with the value expected for an ideal solution (κ_{ideal}=0.16) and consistent with activation data obtained at 298K (see Table 4.2, Rosenørn et al., 2006, Petters et al., 2009a). Figure 4.3c suggests that there is a weak decreasing trend of κ_{app} with decreasing temperature. This trend is not statistically significant and does not differ from the null hypothesis that κ_{app} is independent of temperature (p = 0.01). A trend's significance was determined via simulations as described in the Appendix, and is indicated for each experiment in Table 4.2. In brief, we simulate repeats of the experiments using bootstraping with replacement to determine the likelihood that the percent change of κ_{app} between 40° and 0°C is due to random variability given the observed fluctuations in D_d for ammonium sulfate. A statistically significant slope may indicate either that the variability is not fully captured by the simulations or that κ_{app} is indeed temperature dependent. Stronger trends observed over multiple repeats correspond to an increased likelihood that the temperature dependence in κ_{app} exists.

A constant κ_{app} is implied for ideal non-dissociating and sufficiently soluble compounds since for $\nu = 1$, $\phi = 1$ and $C > 0.2$ $\kappa_{app} = \kappa_{ideal}$ must hold, and we assert that the glucose data approximate such an ideal case. Figure 4.3b shows that κ_{app}^{Θ} decreases from

~0.23 to ~0.12 over the studied temperature range. Since κ_{app} is constant, this decrease is solely due to the increasing surface tension with decreasing temperature. We point out that our analysis implicitly assumes that the solute does not affect surface tension as we use that of pure water in the calculations.

Several of the compounds presented here, i.e. maleic acid, glutamine, methane sulfonic acid, and SOA from α-pinene are unremarkable and similar to the glucose data inasmuch as they show κ_{app}~ constant and κ_{app}^{Θ} decreasing with decreasing temperature. A few compounds (adipic acid, methylammonium methylsulfonate, α-ketoglutaric, and polyethylene glycol) showed changes in κ_{app} that were statistically significant. The strongest decrease occurred for adipic acid, which we will show is related to solubility. The trends for methylammonium methylsulfonate and α-ketoglutaric are much weaker and it is likely that the trends are physical and not due to scatter in the data. The large scatter in the polyethylene glycol repeats suggests that the observed trend may be due to experimental variability that is not accounted for in the statistical significance calculations.

4.3.2. Sparingly soluble species

Adipic acid is a sparingly soluble dicarboxylic acid that has been extensively studied by the CCN community (Hori et al., 2003; Bilde and Svenningson, 2004; Hings et al., 2008). Here these experiments were performed in the same manner as glucose, but at ΔT = 8°C and ΔT = 12°C – larger than for all other compounds because a higher supersaturation was required to achieve activation diameters that were smaller than the upper limit of the size

scan (~320 nm). The corresponding s_c and D_d data are summarized in Figure 4.4. These are the same type of activation data as those plotted for glucose in Figure 4.3, but expressed in supersaturation and dry diameter space so as to better highlight solubility effects. For both adipic acid experiments, the supersaturation increased with decreasing temperature as expected from the ammonium sulfate data shown in Figures 4.2 and 4.3a. Additionally, the activation diameters for adipic acid aerosol increased with decreasing temperature. This trend is opposite to that of the glucose data, where activation diameters decreased with decreasing temperature (Figure 4.3a). Superimposed on the data in Figure 4.4 are diagonal solid grey lines that represent lines of constant κ_{app}^{Θ}. The black dashed line represents κ_{ideal} = 0.17 calculated from Equation 4.5 assuming an ideal (ϕ = 1), non-dissociating (ν = 1) aqueous adipic acid solution.

The CCN activity of sparingly soluble compounds is strongly affected by the presence of water-soluble trace contaminants. These trace contaminants turn the atomized particles into a ternary system composed of adipic acid, contaminant, and water. If the contaminant deliquesces and takes up water, some adipic acid may dissolve in the aqueous contaminant solution, thereby leading to a premature deliquescence and activation of the particle. This effect was first described by Hori et al. (2003) and was further explored for adipic acid by Bilde and Svenningsson (2004). Hings et al. (2008) showed that levels of contamination varied between different studies, and that the cleanest studies approximate solubility-limited theory embodied in Equation 4.6. We approximate the purity of our adipic acid particles to be 99.7%, with 0.3% of an unknown contaminant that has an assumed κ_{sol} = 0.2, corresponding to a low molecular weight, water soluble organic compound (Petters et al.,

2009a).

In Figure 4.4 we superimposed the predicted relationship between s_c and D_d using Equations 4.1 – 4.6 assuming that $\kappa_{sol,adipic} = \kappa_{ideal} = 0.17$ and using the solubility values given by Perry (1941) listed in Table 4.2. In our calculations of the theory lines in Figure 4.4, $T = 298.15$ K and $\sigma = 0.072$ J m^{-2} were held constant. A cursory comparison between the data and the theory line shows that the decrease in solubility may be able to quantitatively explain the decrease in activation diameters during our experiment.

To quantify the level of agreement we use the complete CCN model described in Equations 4.1 – 4.6 to infer the effective solubility from the data. In this model we assumed $\varepsilon_{adipic} = 0.997$, $\varepsilon_c = 0.003$, $\kappa_{adipic} = 0.17$, $\kappa_c = 0.2$, $C_c = \infty$, and $\sigma_{s/a}(T)$ as given in Equation 4.4, where the subscript "*c*" denotes the contaminant. We then considered a single observation consisting of D_d and T and iteratively varied C_{adipic} until s_c from the experiment was in agreement with s_c from the model. Agreement was defined as $(s_{c,model} - s_{c,experiment})^2 < 10^{-5}$. This procedure was repeated for each data point shown in Figure 4.4. Conceptually, this model finds the solubility to force agreement with the data given the model assumptions. The resulting values for C_{adipic} are presented in Figure 4.5. They compare reasonably well with the solubility measured by Perry (1941) and Gaivoronskii and Granzhan (2005). The relationship between C_{adipic} and T found from our CCN data can be described by a simple quadratic equation with coefficients provided in the figure.

The C_{adipic} values derived from the CCN data depend moderately on the underlying model assumptions. A specific choice for ε_c and $\kappa_c$will shift the retrieved

C_{adipic} vs. T relationship towards higher or lower values, but does not affect the slope. If one assumes that the surface tension at the point of activation is given by that of the saturated solution (σ = 0.066 J m^{-2}, Raymond and Pandis, 2002) and thus that the surface tension is decreased by ~10% relative to that of water at all temperatures, one will also observe a shift in the C_{adipic} vs. T relationship towards lower C values. Again, the slope is not affected. Thus, this method of inferring solubility from CCN data can only be used to approximate the absolute value of C. Our initial choice of ε_{adipic}, ε_c, κ_{adipic}, κ_c, and C_c is one possibility to match C_{adipic} at T = 24° and 4°C given in Perry (1941). Although we consider our choice reasonable based on prior studies (e.g. Hings et al., 2008), it should be understood that the equations are an underdetermined system that does not allow us to unambiguously deconvolve C_{adipic}, ε_c, κ_c and the impact of adipic acid on $\sigma_{s/a}$.

Our main conclusions from these modeling exercises are: 1) that a single solubility function $C_{adipic}(T)$ can explain the observed activation data reasonably well by a simple quadratic equation, and 2) that the observed solubility temperature dependence is consistent with bulk data. To emphasize the extent of agreement between the model and activation data, we inverted the model and used C_{adipic} = 1.21 – 3.1 x 10^{-3}T + 1.76 x 10$^{-3}T^2$ and $\sigma_{s/a}(T)$ to model the activation diameters of adipic acid. Results from this exercise are shown in Figure 4.6 for the two data sets. The agreement between data and model depends on the $C_{adipic}(T)$ function and 1:1 agreement for all diameters depends on the degree to which the solubility values collapse on a single line for multiple experiments (in Figure 4.5).

4.3.3. Secondary organic aerosol

Results for two experiments with SOA from α-pinene are summarized in Figure 4.7. The observed κ_{app} ~ 0.11 is independent of temperature. The value of $\kappa_{app}^{\ominus}$ (and κ_{app}) at 298.15K is in close agreement with previous measurements of this SOA system (Prenni et al., 2007; King et al., 2007; Duplissy et al., 2009). These results are significant because α-pinene SOA consists of a mixture of many compounds with different underlying κ-values (Suda et al., 2012). Some conceptual models have suggested that the gradual dissolution of sparingly soluble compounds in that mixture (Petters et al., 2009c) can explain an apparent discrepancy between the amount of water uptake and effective CCN activity of α-pinene SOA (Prenni et al., 2007). If sparingly soluble compounds were present in significant amounts, and assuming that the decrease in solubility with decreasing temperature is comparable to that of adipic acid we would expect to observe a decrease in κ_{app} with decreasing temperature. The absence of a temperature dependence in κ_{app} therefore suggests that solubility limitations do not play a role for CCN activation at temperatures greater than 0°C. This finding, however, is limited to this specific system and may not be valid when considering water uptake. Data for other precursor and oxidant combinations are needed before solubility limitations can be ruled out for SOA in general.

4.4. Discussion and Conclusions

Regarding our experimental calibrations, the measured increase in the streamwise gradient CCN instrument supersaturation was slightly stronger but consistent with that

anticipated by our instrument model. The data presented in Figure 4.2 extend the more limited temperature range explored by Rose et al. (2008) who presented calibration data ranging from 22° to 29°C. The change in instrument supersaturation is significant for moderate temperature fluctuations of ~10°C. We briefly tested the sensitivity of this dependence with our model and found that the slope is also quite sensitive to the selected ΔT. We therefore recommend the characterization of adaptive calibrations that account for inlet temperature in measurement environments where temperature cannot be well controlled. If calibration data are not available, a computational model of the instrument supersaturation similar to ours or that of Roberts and Nenes (2005) may be used to compute a first order temperature correction.

From our data we conclude that the influence of temperature dependent surface tension on the $s_c - D_d$ relationship is large, the role of temperature-dependent change in solubility is moderate, and changes in water activity with temperature are weak or negligible. The critical reader might object here, however, that the surface tension argument is circular. Indeed we stipulated its temperature dependence in Eqn 4.4 and used it to determine the supersaturation in the CCN instrument via the Köhler method (Figure 4.2). Do our data independently confirm that the surface tension effect is real? To answer this question one might construct the following experiment that would isolate the surface tension effect. Consider a solute that is non-volatile, forms an ideal solution, does not alter the surface tension of pure water, and that is sufficiently soluble in water. Such a particle's hygroscopicity would reflect $\kappa_{app} = \kappa_{ideal}$ = constant. A properly calibrated CCN instrument thus should measure a constant κ_{app} for such a compound, irrespective of the manner that the

calibration was obtained. Previous measurements have shown that glucose is indistinguishable from that of an ideal solution (Rosenørn, et al., 2006; Petters et al., 2009a). Further, glucose neither dissociates nor does its solubility approach the sparingly soluble regime. Finally, Zamora et al. (2011) show that the water activity vs. composition relationship of glucose is, within experimental uncertainty, indistinguishable between 0° and 30°C. We therefore believe that the observed temperature independent κ_{app} for glucose supports the validity of the instrument calibration and the validity of our theoretical framework to accurately model the role of temperature dependent surface tension on CCN activity.

In order to quantify the importance of accounting for the surface tension effect we consider changes in κ_{app}^{Θ}, which changes approximately by a factor of two over the 0˚ to 40˚C temperature range studied here. A similar change in surface tension would be expected when extending the estimate in the supercooled water droplet regime (-40˚ to 0˚C , Pruppacher and Klett, 1997). For comparison, Liu and Wang (2010) found that changing κ_{app}^{Θ} of secondary organic aerosol from 0.07 to 0.14 in the CAM global climate model led to a change in aerosol indirect forcing (AIF) of 0.2 W m^{-2}, which represented 1/6 of AIF simulated in the control case. During those simulations, surface tension was independent of temperature and held constant (Xiaohong Liu, personal communication). Because temperature dependent surface tension results in changes of κ_{app}^{Θ} that are comparable in magnitude to the perturbation considered by Liu and Wang (2010), we expect that including temperature dependence in regional and global models will have a significant impact on

aerosol radiative forcing calculations. Fortunately, κ_{app} appears to be independent of temperature for many compounds. We thus propose that laboratory derived κ_{app} values can be extrapolated to colder temperatures using Equation 4.1 combined with a temperature dependent "*A*" parameter, and that such an extrapolation will yield realistic values of expected CCN activity.

Sparingly soluble compounds are frequently identified in atmospheric organic aerosols. Because this class of compounds can feature a moderately strong temperature dependence in the temperature range of interest to the troposphere, further studies are needed to establish that laboratory CCN measurements can truly be extrapolated for a wide range of complex organic aerosol mixtures as well as ambient particle compositions. Additionally measurements should be extended into the supercooled water regime where solubility limitations may become more pronounced. Unfortunately, the streamwise temperature gradient continuous flow CCN instrument requires a water-laced boundary to establish the supersaturation and extension of our methodology to sub-zero temperatures in that instrument poses nontrivial experimental problems.

In the atmosphere, there may be other temperature effects on CCN activity that are not accounted for here. For example, co-condensation of organics with water (Topping and McFiggans, 2012) may increase the number of molecules in solution. It is possible that the observed significant trend of decreasing κ_{app} with temperature for methylammonium methylsulfonate could be explained with volatilization of methylamine at warmer temperatures, which would require further experimental confirmation. Colder temperatures may also lead to phase transitions that are not described by classical solubility theory – for

example, organic aerosols may form viscous glasses (Zobrist et al., 2008; Shiraiwa et al., 2011; Koop et al., 2011; Pöschl et al., 2011) that may retard or prevent water uptake. The role of the glass phase transition in droplet activation is not well understood, highlighting the need to for further temperature-dependent studies of this phenomenon.

4.5. Acknowledgements

We thank Sonia Kreidenweis for loaning us the Teledyne 703 O_3 generator. We also thank Sonia Kreidenweis, Yang Zhang, Sukanto Basu, Paul Ziemann, Sarah Suda, and Timothy Wright for their input. This research was funded by the Office of Science (BER), US Department of Energy, under DE-FG02-05ER63984.

4.6. Appendix

In order to classify a compound's κ_{app} trend as temperature dependent or independent, statistical significance was determined using a bootstrap sampling with replacement. The bootstrap algorithm selects random sets of D_{50} and T values from the data for each experiment. Each random set is processed the same way than the original data. The minimum and maximum κ_{app} values were divided by the κ_{app} values at 298.15K to determine the magnitude of the κ_{app} change over the temperature range. Ten thousand sets were selected for each experiment and a histogram of the $\Delta\kappa_{app}\ /\kappa_{app,298}$ statistic was constructed. If more than 99% of the $\Delta\kappa_{app}\ /\kappa_{app,298}$ samples exceed zero, the slope is considered to be statistically significant at the p = 0.01 level.

4.7. References

Albrecht, B. A.; Aerosols, Cloud Microphysics, and Fractional Cloudiness. *Science* **1989**, *245*, 1227-1230.

Andrea, M. O.; Rosenfeld, D.; Artaxo, P.; Costa, A. A.; Frank, G. P.; Longo, K. M.; Silva-Dias, M. A. F. Smoking Rain Clouds over the Amazon. *Science* **2004**, *303*, 1337-1342.

Andreae, M. O.; Rosenfeld, D. Aerosol-cloud-precipitation interactions. Part 1. The nature and sources of cloud-active aerosols. *Earth-Sci. Rev.* **2008**, *89*, 13-41.

Bilde, M.; Svenningsson, B. CCN activation of slightly soluble organics: the importance of small amounts of inorganic salt and particle phase. *Tellus* **2004**, *56B*, 128-134.

Broekhuizen, K.; Kumar, P. P.; Abbatt, J. P. D. Partially soluble organics as cloud condensation nuclei: Role of trace soluble and surface active species. *Geo-phys. Res. Lett.* **2004**, *31*, L01107.

Christensen, S. I. The Role of Temperature in Cloud Drop Activation, M. S. Thesis, North Carolina State University, Raleigh, NC, 2012.

Clegg, S. L.; Brimblecombe, P.; Wexler, A. S. Thermodynamic Model of the System H+-NH4+-Na+-SO42--NO3--Cl--H2O at 298.15 K. *J. Phys. Chem. A* **1998**, *102*, 2155-2171.

Cruz, C. N.; Pandis, S. N. The effect of organic coatings on the cloud condensation nuclei activation of inorganic atmospheric aerosol. *J. Geophys. Res.* **1998**, *103*, 13111-13123.

Duplissy, J.; Gysel, M.; Sjogren, S.; Meyer, N.; Good, N.; Kammermann, L.; Michaud, V.; Weigel, R.; Martins dos Santos, S.; Gruening, C.; Villani, P.; Laj, P.; Sellegri, K.; Metzger, A.; McFiggans, G. B.; Wehrle, G.; Richter, R.; Dommen, J.; Ristovski, Z.; Baltensperger, U.; Weingartner, E. Intercomparison study of six HTDMAs: results and recommendations. *Atmos. Meas. Tech.* **2009**, *2*, 363-378.

Dusek, U.; Frank, G. P.; Hildebrandt, L.; Curtius, J.; Schneider, J.; Walter, S.; Chand, D.; Drewnick, F.; Hings, S.; Jung, D.; Borrmann, S.; Andreae M. O. Size Matters More Than Chemistry for Cloud-Nucleating Ability of Aerosol Particles. *Science* **2006**, *312*, 1375-1378.

Facchini, M. C.; Decesari, S.; Rinaldi, M.; Carbone, C.; Finessi, E.; Mircea, M.; Fuzzi, S.;

Moretti, F.; Tagliavini, E.; Ceburnis, D.; O'Dowd, C. D. Important Source of Marine Secondary Organic Aerosol from Biogenic Amines. *Environ. Sci. Tech.* **2008**, *42*, 9116-9121.

Fitzgerald, J. W.; Spyers-Duran, P. A. Changes in Cloud Nucleus Concentration and Cloud Droplet Size Distribution Associated with Pollution from St. Louis. *J. App. Met.* **1973**, *12*, 511-516.

Friese, E.; Ebel, A. Temperature Dependent Thermodynamic Model of the System H+-NH4 +-Na+-SO42—NO3--Cl—H2O. *J. Phys. Chem. A* **2010**, *114*, 11595-11631.

Frosch, M.; Zardini, A. A.; Platt, S. M.; Müller, L.; Reinnig, M. C.; Hoffmann, T.; Bilde, M. Thermodynamics properties and cloud droplet activation of a series of oxo-acids. *Atmos. Chem. Phys.* **2010**, *10*, 5873-5890.

Gaivoronskii, A. N.; Granzhan, V. A. Solubility of Adipic Acid in Organic Solvents and Water. *Russ. J. Appl. Chem.* **2005**, *78*, 404-408.

Gunthe, S. S.; King, S. M.; Rose, D.; Chen, Q.; Roldin, P.; Farmer, D. K.; Jimenez, J. L.; Artaxo, P.; Andreae, M. O.; Martin, S. T.; Pöschl, U. Cloud condensation nuclei in pristine tropical rainforest air of Amazonia: size-resolved measurements and modeling of atmospheric aerosol composition and CCN activity. *Atmos. Chem. Phys.* **2009**, *9*, 7551-7575.

Gysel, M.; Weingartner, E.; Baltensperger, U. Hygroscopicity of Aerosol Particles at Low Temperatures. 2. Theoretical and Experimental Hygroscopic Properties of Laboratory Generated Aerosols. *Environ. Sci. Technol.* **2002**, *36*, 63-68.

Harned, H. S.; Owen, B. B. *The Physical Chemistry of Electrolyte Solutions, 3rd Ed*; Reinhold: New York, 1958.

Hings, S. S.; Wrobel, W. C.; Cross, E. S.; Worsnop, D. R.; Davidovits, P.; Onasch, T. B. CCN activation experiments with adipic acid: effect of particle phase and adipic acid coatings on soluble and insoluble particles. *Atmos. Chem. Phys.* **2008**, *8*, 3735-3748.

Hori, M.; Ohta, S.; Murao, N.; Yamagata, S. Activation capability of water soluble organic substances as CCN. *J. Aerosol Sci.* **2003**, *34*, 419-448.

IPCC, 2007: Climate Change 2007: The Physical Science Basis. Contribution of Working Group I to the Fourth Assessment Report of the Intergovernmental Panel on Climate Change [Solomon, S., D. Qin, M. Manning, Z. Chen, M. Marquis, K.B. Averyt, M.Tignor and H.L. Miller (eds.)]. Cambridge University Press, Cambridge, United Kingdom and New York, NY, USA.

Jacobson, M. Z.; Tabazadeh, A.; Turco, R. P. Simulating equilibrium within aerosols and nonequilibrium between gases and aerosols. *J. Geophys. Res.* **1996**, *101*, 9079-9091.

Jimenez, J. L.; Canagaratna, M. R.; Donahue, N. M.; Prevot, A. S. H.; Zhang, Q.; Kroll, J. H.; DeCarlo, P. F.; Allan, J. D.; Coe, H.; Ng, N. L.; Aiken, A. C.; Docherty, K. S.; Ulbrich, I. M.; Grieshop, A. P.; Robinson, A. L.; Duplissy, J.; Smith, J. D.; Wilson, K. R.; Lanz, V. A.; Hueglin, C.; Sun, Y. L.; Tian, J.; Laaksonen, A.; Raatikainen, T.; Rautiainen, J.; Vaattovaara, P.; Ehn, M.; Kulmala, M.; Tomlinson, J. M.; Collins, D. R.; Cubison, M. J.; Dunlea, E. J.; Huffman, J. A.; Onasch, T. B.; Alfarra, M. R.; Williams, P. I.; Bower, K.; Kondo, Y.; Schneider, J.; Drewnick, F.; Borrmann, S.; Weimer, S.; Demerjian, K.; Salcedo, D.; Cottrell, L.; Griffin, R.; Takami, A.; Miyoshi, T.; Hatakeyama, S.; Shimono, A.; Sun, J. Y.; Zhang, Y. M.; Dzepina, K.; Kimmel, J. R.; Sueper, D.; Jane, J. T.; Herndon, S. C.; Trimborn, A. M.; Williams, L. R.; Wood, E. C.; Middlebrook, A. M.; Kolb, C. E.; Baltensperger, U.; Worsnop, D. R. Evolution of Organic Aerosols in the Atmosphere. *Science* **2009**, *326*, 1525-1529.

Jurányi, Z.; Gysel, M.; Weingartner, E.; Bukowiecki, N.; Kammermann, L.; Baltensperger, U. A 17 month climatology of the cloud condensation nuclei number concentration at the high alpine site Jungfraujoch. *J. Geophys. Res.* **2011**, *116*, D10204.

King, S. M.; Rosenørn, T.; Shilling, J. E.; Chen, Q.; Martin, S. T. Cloud condensation nucleus activity of secondary organic aerosol particles mixed with sulfate. *Geophys. Res. Lett.* **2007**, *34*, L24806.

Köhler, H. The nucleus in and the growth of hygroscopic droplets. *Trans. Farad. Soc.* **1936**, *32*, 1152-1161.

Koop, T.; Bookhold, J.; Shiraiwa, M.; Pöschl, U. Glass transition and phase state of organic compounds: dependency on molecular properties and implications for secondary organic aerosols in the atmosphere. *Phys. Chem. Chem. Phys.* **2011**, *13*, 19238-19255.

Kreidenweis, S. M.; Petters, M. D.; DeMott, P. J. Deliquescence-controlled activation of organic aerosols. *Geo-phys. Res. Lett.* **2006**, *33*, L06801.

Kristensson, A.; Rosenørn, T.; Bilde, M. Cloud Droplet Activation of Amino Acid Aerosol Particles. *J. Phys. Chem A* **2010**, *114*, 379-386.

Lance, S.; Nenes, A.; Medina, J.; Smith, J.N. Mapping the Operation of the DMT Continuous Flow CCN Counter. *Aer. Sci. Tech.* **2006**, *40*, 242-254.

Levin, E. J. T.; Prenni, A. J.; Petters, M. D.; Kreidenweis, S. M.; Sullivan, R. C.; Atwood, S. A.; Ortega, J.; DeMott, P. J.; Smith, J. N. An annual cycle of size-resolved aerosol

hygroscopicity at a forested site in Colorado. *J. Geophys. Res.* **2012**, *117*, D06201 1-13.

Liu, X.; Wang, J. How important is organic aerosol hygroscopicity to aerosol indirect forcing? *Environ. Res. Lett.* **2010**, *5*.

Perry, J. H. *Chemical Engineer's Handbook*; McGraw Hill Book Co.: New York, 1941; pp 1941.

Petters, M. D.; Prenni, A. J.; Kreidenweis, S. M.; DeMott, P. J.; Matsunaga, A.; Lim, Y. B.; Ziemann, P. J. Chemical aging and the hydrophobic-to-hydrophilic conversion of carbonaceous aerosol. *Geophys. Res. Lett.* **2006**, *33*, L24806.

Petters, M. D.; Kreideweis, S. M. A single parameter representation of hygroscopic growth and cloud condensation nucleus activity. *Atmos. Chem. Phys.* **2007**, *7*, 1961-1971.

Petters, M. D.; Prenni, A. J.; Kreidenweis, S. M.; DeMott, P. J. On Measuring the Critical Diameter of Cloud Condensation Nuclei Using Mobility Selected Aerosol. *Aero. Sci. Tech.* **2007**, *41*, 907-913.

Petters, M. D.; Kreidenweis, S. M.; A single parameter representation of hygroscopic growth and cloud condensation nucleus activity – Part 2: Including solubility. *Atmos. Chem. Phys.* **2008**, *8*, 6273-6279.

Petters, M. D.; Kreidenweis, S. M.; Prenni, A. J.; Sullivan, R. C.; Carrico, C. M.; Koehler, K. A.; Ziemann, P. J. Role of molecular size in cloud droplet activation. *Geophys. Res. Lett.* **2009a**, *36*, L22801.

Petters, M. D.; Parsons, M. T.; Prenni, A. J.; DeMott, P. J.; Kreidenweis, S. M.; Carrico, C. M.; Sullivan, A. P.; McMeeking, G. R.; Levin, E.; Wold, C. E.; Collett, J. L., Jr.; Moosmüller, H. Ice nuclei emissions from biomass burning. *J. Geophys. Res.* **2009b**, *114*, D07209.

Petters, M. D.; Wes, H.; Carrico, C. M.; Hallbauer, E.; Massling, A.; McMeeking, G. R.; Poulain, L.; Wu, Z.; Kreidenweis, S. M.; Stratmann, F. Towards closing the gap between hygroscopic growth and activation for secondary organic aerosol – Part 2: Theoretical approaches. *Atmos. Chem. Phys.* **2009c**, *9*, 3999-4009.

Pöschl, U. Gas-particle interactions of tropospheric aerosols: Kinetic and thermodynamics perspectives of multiphase chemical reactios, amorpohous organic substances, and the activation of cloud condensation nuclei. *Atmos. Res.* **2011**, *101*, 562-573.

Prenni, A. J.; Petters, M. D.; Kreidenweis, S. M.; DeMott, P. J.; Ziemann, P. J. Coud droplet activation of secondary organic aerosol. *J. Geophys. Res.* **2007**, *112*.

Pruppacher, H. R.; Klett, J.D. *Microphysics of Clouds and Precipitation*; Springer: New York, 1997.

Raymond, T. M.; Pandis, S. N. Cloud activation of single-component organic aerosol particles. *J Geophys. Res.* **2002**, *107*.

Roberts, G. C.; Nenes, A. A Continuous-Flow Streamwise Thermal-Gradient CCN Chamber for Atmospheric Measurements. *Aerosol Sci. Tech.* **2005**, *39*, 206-221.

Rose, D.; Gunthe, S. S.; Mikhailov, E.; Frank, G. P.; Dusek, U.; Andreae, M. O.; Pöschl, U. Calibration and measurement uncertainties of a continuous-flow cloud condensation nuclei counter (DMT-CCNC): CCN activation of ammonim sulfate and sodium chloride aerosol particles in theory and experiment. *Atmos. Chem. Phys.* **2008**, *8*, 1153-1179.

Rose, D.; Nowak, A.; Achtert, P.; Wiedensohler, A.; Hu, M.; Shao, M.; Zhang, Y.; Andreae, M. O.; Pöschl, U. Cloud condensation nuclei in polluted air and biomass burning smoke near the mega-city Guangzhou, China – Part 1: Size-resolved measurements and implications for the modeling of aerosol particle hygroscopicity and CCN activity. *Atmos. Chem. Phys.* **2010**, *10*, 3365-3383.

Rosenørn, T.; Kiss, G; Bilde, M. Cloud droplet activation of saccharides and levoglucosan particles. *Atmos. Env.* **2006**, *40*, 1794-1802.

Saltzman, E. S.; Savoie, D. L.; Zika, R. G.; Prospero, J. M. Methane Sulfonic Acid in the Marine Atmosphere. *J. Geophys. Res.* **1983**, *88*, 10897-10902.

Shiraiwa, M.; Ammann, M.; Koop, T.; Pöschl, U. Gas uptake and chemical aging of semisolid organic aerosol particles. *Proc. Nat. Acad. Sci.* **2011**, *108*, 11003-11008.

Snider, J.R.; Petters, M. D.; Wechsler, P.; Liu, P. S. K. Supersaturation in the Wyoming CCN Instrument. *J. Atmos. Ocea. Tech.* **2006**, *23*, 1323-1339.

Snider, J. R.; Wex, H.; Rose, D.; Kristensson, A.; Stratmann, F.; Hennig, T.; Henning, S.; Kiselev, A.; Bilde, M.; Burkhart, M.; Dusek, U.; Frank, G. P.; Kiendler-Scharr, A.; Mentel, T. F.; Petters, M. D.; Pöschl, U. Intercomparison of cloud condensation nuclei and hygroscopic fraction measurements: Coated soot particles investigated during LACIS Experiment in November (LExNo). *J. Geophys. Res.* **2010**, *115*, D11205 1-20.

Suda, S. R.; Petters, M. D.; Matsunaga, A.; Sullivan, R. C.; Ziemann, P. J.; Kreidenweis, S. M. Hygroscopicity frequency distributions of secondary organic aerosols. *J. Geophys. Res.* **2012**, *117*, D04207.

Topping, D. O.; McFiggans, G. Tight coupling of particle size, number and composition in

atmospheric cloud droplet activation. *Atmos. Chem. Phys.* **2012**, *12*, 3253-3260.

Twomey, S. A. Pollution and the planetary albedo. *Atmos. Env.* **1974**, *8*, 1251-1256.

VanReken, T. M.; Ng, N. L.; Flagan, R. C.; Seinfeld, J. H. Cloud condensation nucleus activation properties of biogenic secondary organic aerosol. *J. Geophys. Res.* **2005**, *110*, D07206.

Yin, S.; Ge, M. F.; Wang, W. G.; Liu, Z.; Wang, D. X. Uptake of gas-phase alkylamines by sulfuric acid. *Chinese Sci. Bull.* **2011**, *56*, 1241-1245.

Zamora, I. R.; Tabazadeh, A.; Golden, D. M.; Jacobson, M. Z. Hygroscopic growth of common organic aerosol solutes, including humic substances, as derived from water activity measurements. *J. Geophys. Res.* **2011**, *116*, D23207.

Zobrist, B.; Marcolli, C.; Pedernera, D. A.; Koop, T. Do atmospheric aerosols form glasses? *Atmos. Chem. Phys.* **2008**, *8*, 5221-5244.

Zorn, S. R.; Drewnick, F.; Schott, M.; Hoffmann, T.; Borrmann, S. Characterization of the South Atlantic marine boundary layer aerosol using an aerodyne aerosol mass spectrometer. *Atmos. Chem. Phys.* **2008**, *8*, 4711-4728.

Figures

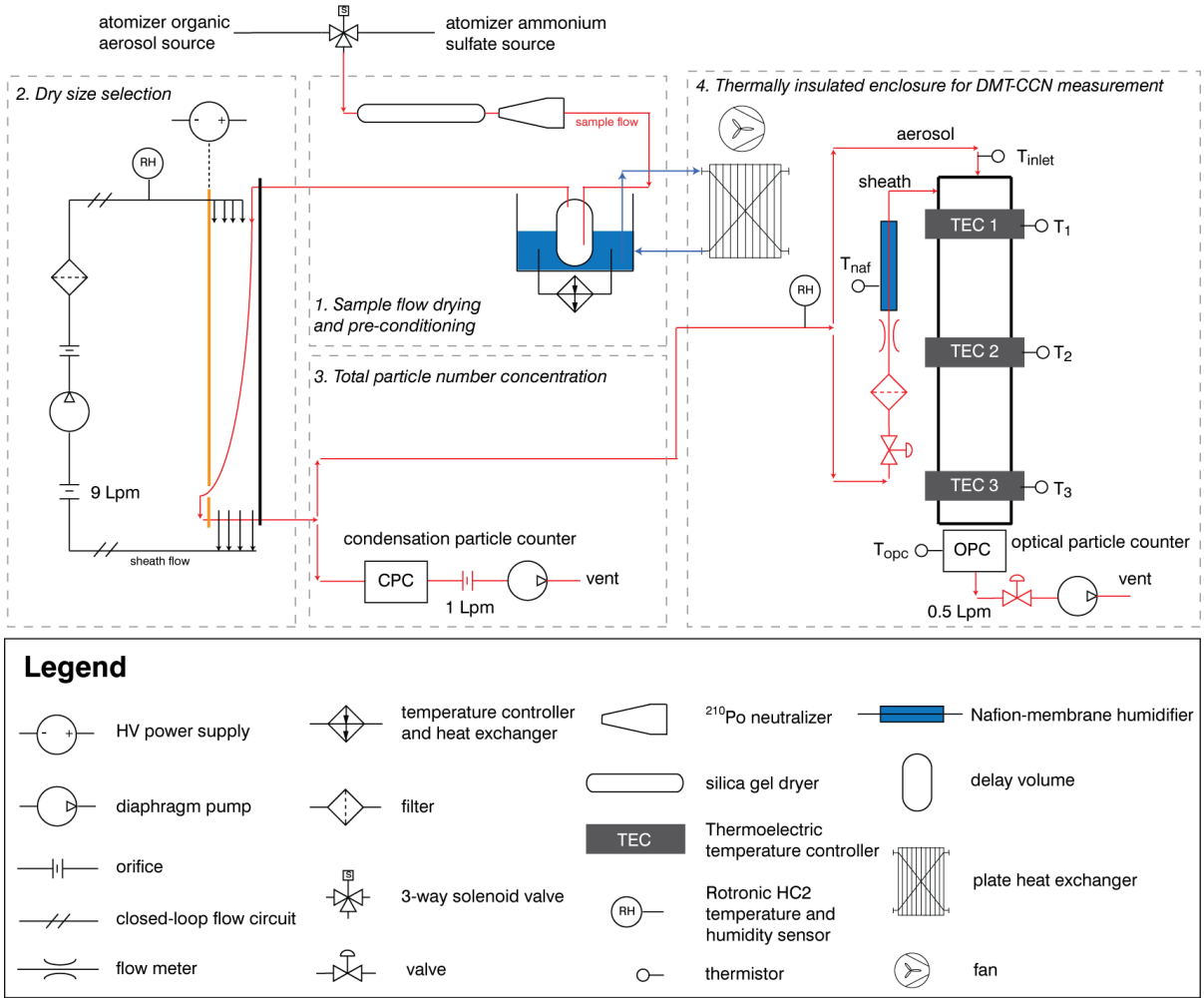

Figure 4.1. Schematic of the experimental setup for temperature-controlled size-resolved CCN measurements in the laboratory.

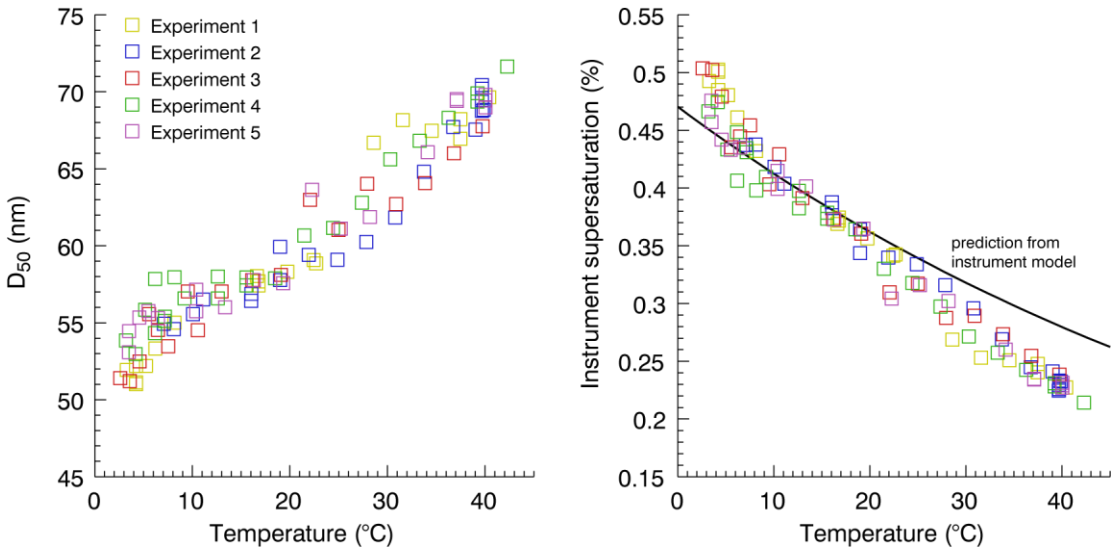

Figure 4.2. Left: activation diameters of ammonium sulfate as a function of absolute temperature from five experiments performed over a period of 7 months with instrument ΔT = 6K (identical experimental conditions). Right: computed instrument supersaturation based on ammonium sulfate calibration activation diameters, water activity from the aerosol instrument model, and temperature dependent surface tension with modeled supersaturation (black line).

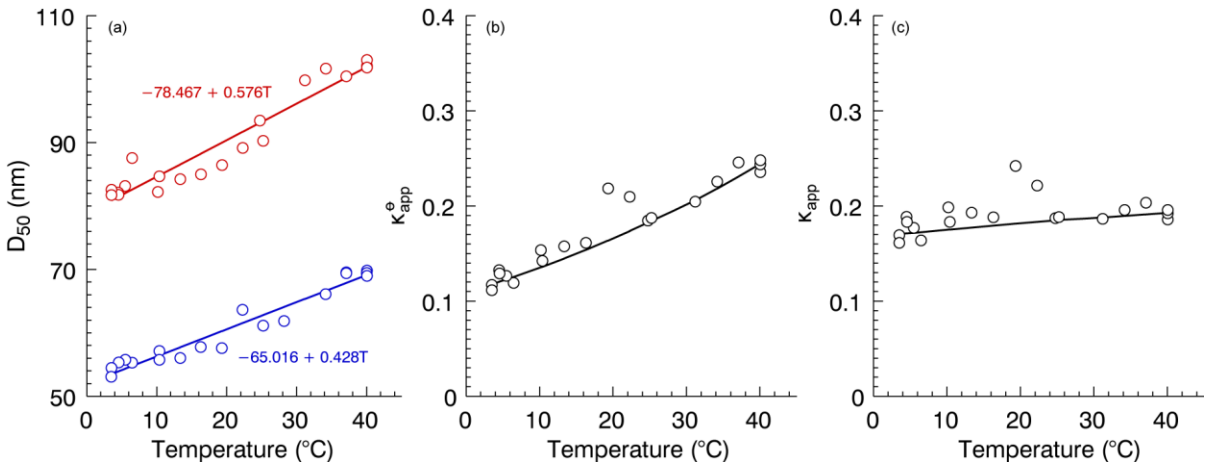

Figure 4.3. Experimental data for glucose showing (a) activation diameters for glucose (red) and ammonium sulfate (blue) with fit coefficients through the data and (b, c) κ-values versus temperature (spanning approximately 6 hours).

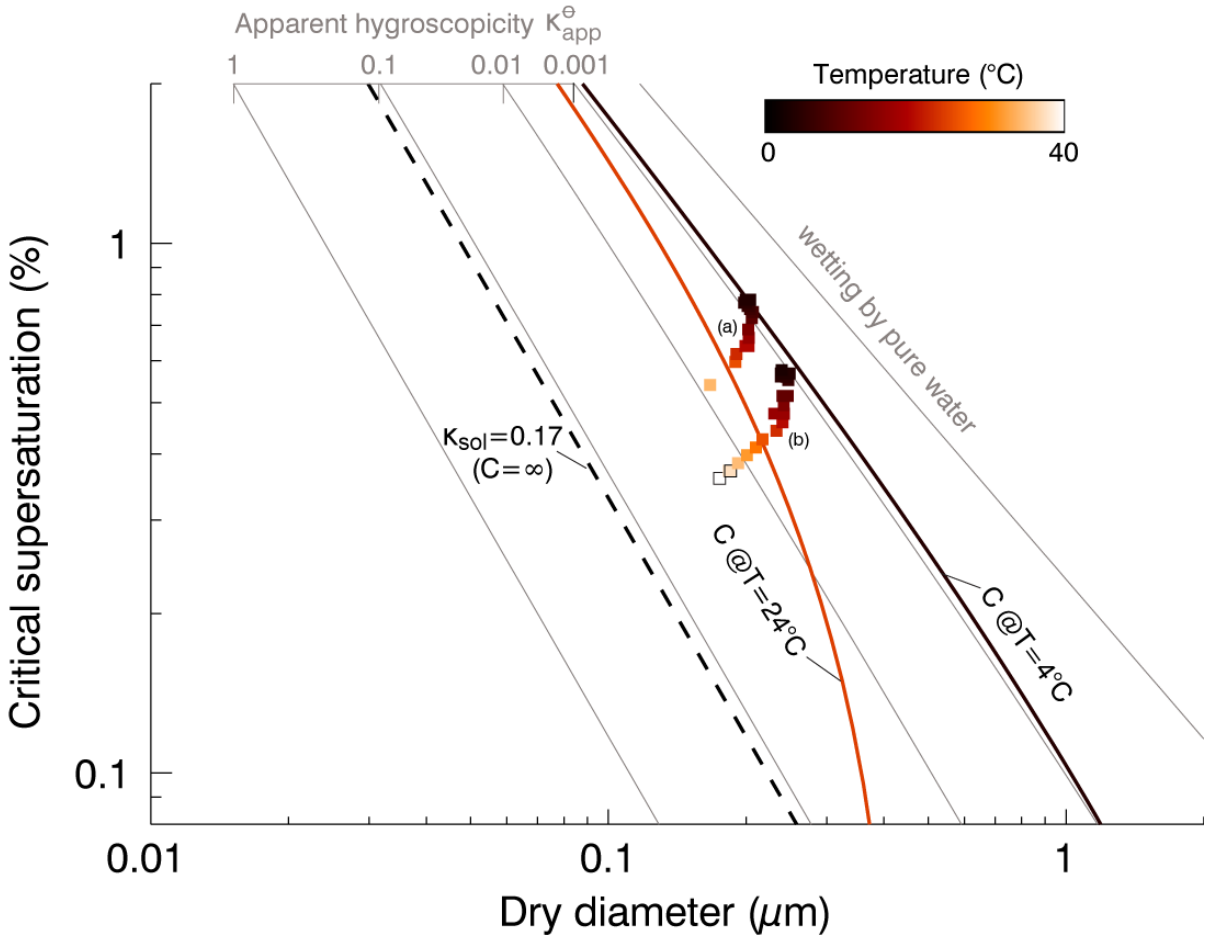

Figure 4.4. Activation data for adipic acid obtained at CCN instrument gradient ΔT = 12°C (a) and ΔT = 8°C (b). The color-coding indicates the temperature T_1. Grey grid lines show κ^{Θ}_{app}, which is computed for T = 298.15K and σ = 0.072 J m^{-2} according to Petters and Kreidenweis (2007). The dashed line shows κ_{ideal} = 0.17, which is the expected value for ideal, non-dissociating adipic acid based on molar volume without considering solubility limitations (Petters et al., 2009a). The red and black lines show theory lines for activation based on limited solubility (Petters and Kreidenweis, 2008, assuming T = 298.15K and σ = 0.072 J m^{-2}), where solubility values were selected for T = 24°C and T = 4°C given by Perry (1941).

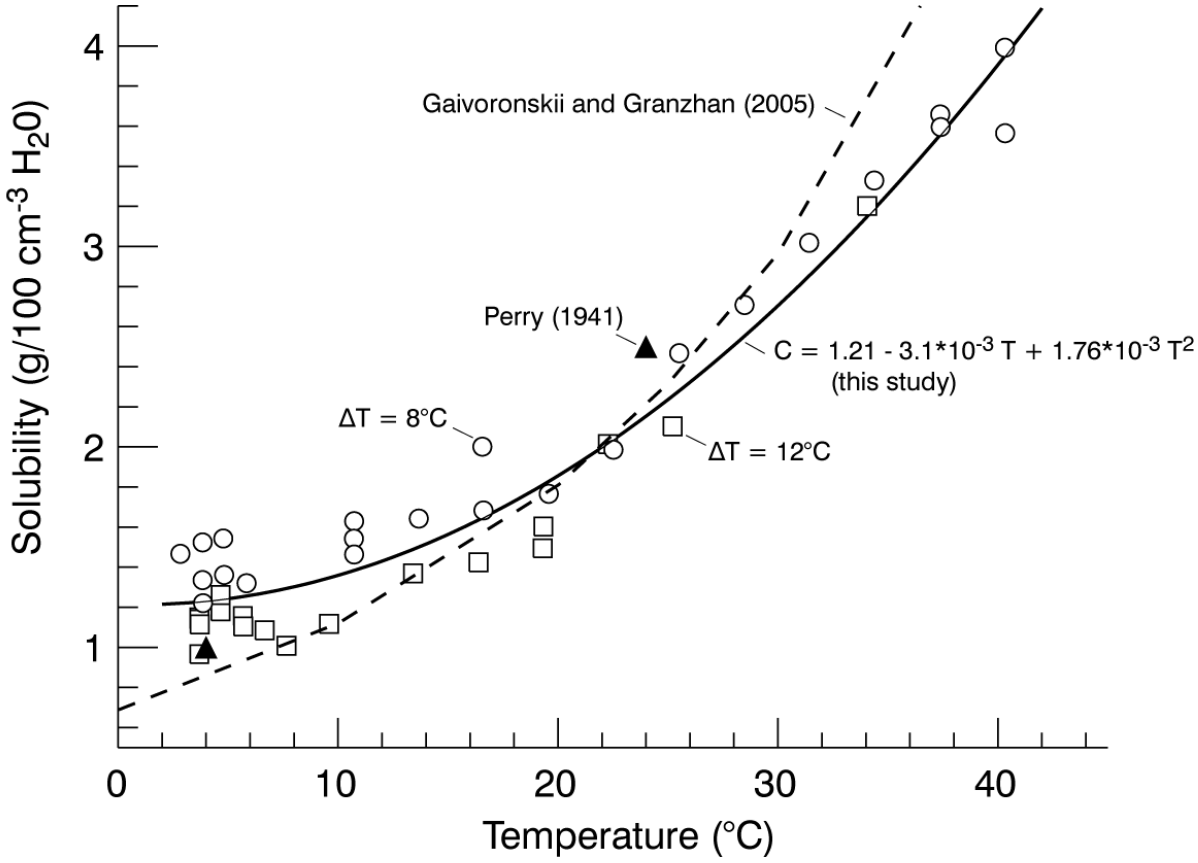

Figure 4.5. Solubility inferred from the s_c, D_d, and T data points shown in Figure 4.4. Solubility was calculated based on a dynamic model that varies temperature and surface tension as described in the text.

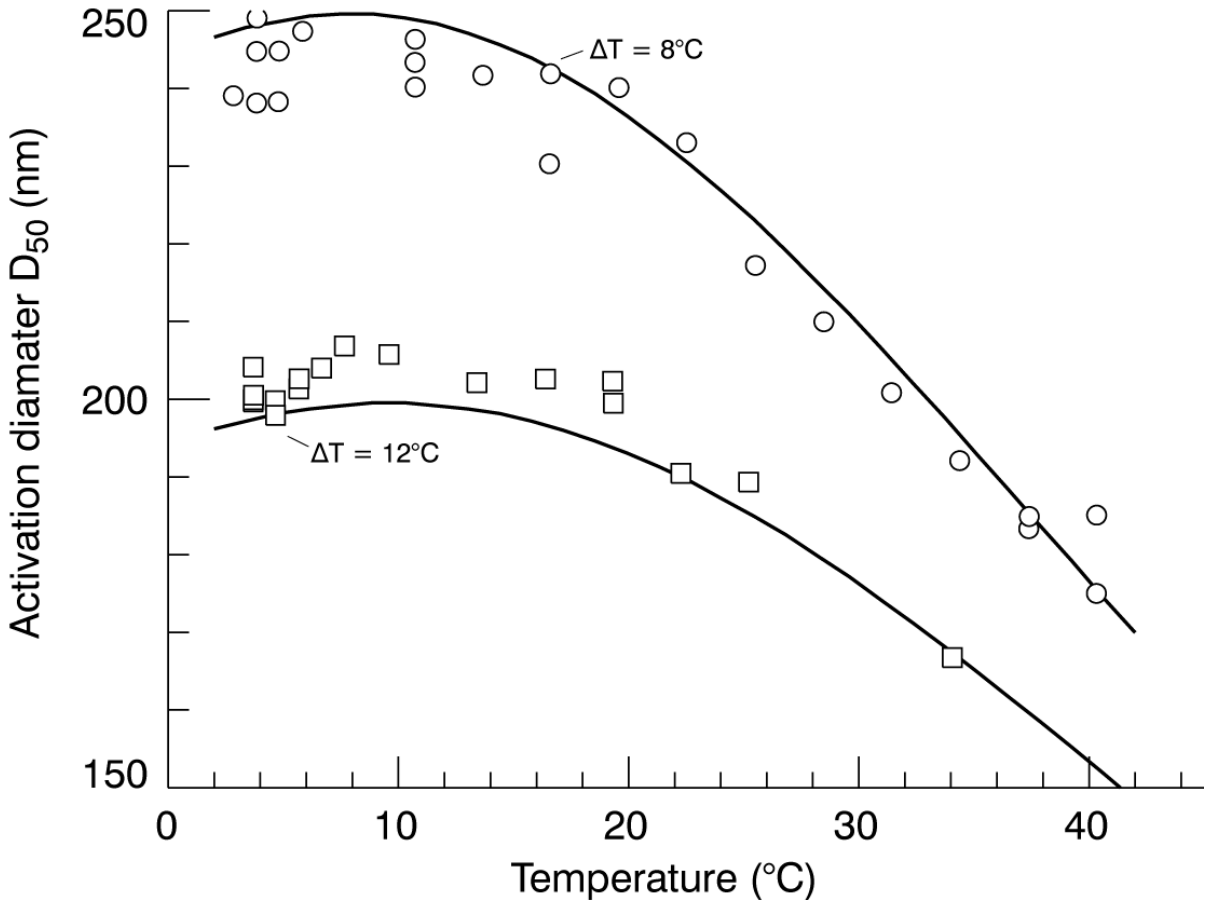

Figure 4.6. Modeled activation diameters based on the dynamic model described in the text. The relationship between solubility and temperature is taken from the polynomial fit function in Figure 4.5.

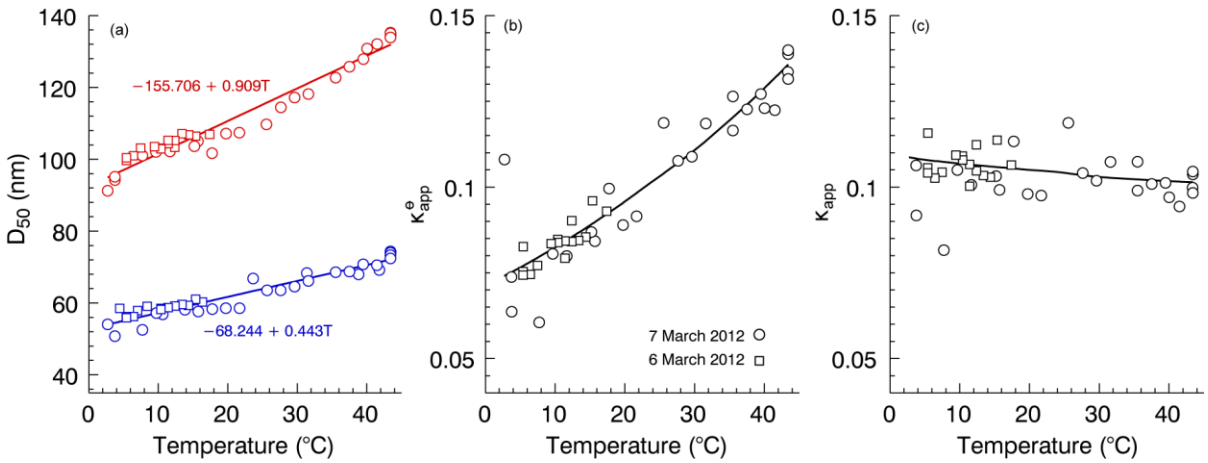

Figure 4.7. Experimental data for secondary organic aerosol generated from the ozonolysis of α-pinene showing (a) activation diameters for SOA (red) and ammonium sulfate (blue) with fit coefficients through the data and (b, c) κ values versus temperature.

Tables

Table 4.1. Equations for the various κ terms and their definitions.

κ Term	Calculation	Description
κ_{app}	$\frac{4A^3}{27D_d^3 \ln^2 S_c}$	Fitted from s_c – D_d measurements.
κ_{sol}	$\nu\phi \frac{M_w \rho_s}{M_s \rho_w}$	Calculated from chemical properties and used for aqueous solution drops; ν and ϕ are temperature dependent.
κ_{theory}	$\sum_i \epsilon_i \kappa_{sol,i} H(x_i)$ $x_i = (g^3 - 1) C_i / \epsilon_i$ $H(x_i) = \begin{cases} x_i & x_i < 1 \\ 1 & x_i \geq 1 \end{cases}$	Calculated from chemical properties for multicomponent mixtures.
κ_{ideal}	$\nu \frac{M_w \rho_s}{M_s \rho_w}$	Calculated from chemical properties and used for ideal solutions (ϕ = 1).

Table 4.2. Data for all experiments where M_w is the molecular weight, ρ is the density, C is the solubility, $\kappa_{literature}$ are published κ values, κ_{298} are values reported in this work, a is the first fit coefficient for the activation diameters, b is the second fit coefficient, ΔT is the temperature difference set in the CCN for supersaturation, $\Delta\kappa$ is the min κ minus the max κ divided by κ_{298}, and 'trend' represents if a significant trend is present (see Note 2).

compound	formula	source	purity	M_w [$g\ mole^{-1}$]	ρ [$g\ cm^{-3}$]	C [-]	$\kappa_{literature}$	run #	κ_{298}[(1)]	a	b	ΔT	$\Delta\kappa$ [%]	trend[(2)]
adipic acid	$C_6H_{10}O_4$	S-A[(3)]	99%	146.14	1.362[(a)]	0.018[b)]	variable[(c)]	1	$7.3e^{-3}$	735.772	-1.754	8	175	y
								AS[(4)]		-57.878	0.359	8		
								2	$5.1e^{-3}$	564.706	-1.081	8	131	y
								AS		-50.920	0.337	8		
								3	$4.0e^{-3}$	444.889	-0.846	12	112	y
								AS		-14.491	0.172	12		
D-glucose[(d)]	$C_6H_{12}O_6$	S-A	99.5%	180.2	1.566	0.58	0.14 – 0.20	1	0.17	-131.266	0.753	6	-19	n
								AS		-53.346	0.383	6		
								2	0.19	-78.441	0.576	6	12	n
								AS		-65.021	0.428	6		
								3	0.19	-44.81	0.451	6	35	y
								AS		-74.380	0.453	6		
L-glutamine	$C_5H_{10}N_2O_3$	S-A	99-100%	146.14	1.5326	soluble[(5)]	N/A	1	0.18	-98.220	0.631	6	1	n
								AS		-51.708	0.376	6		
								2	0.19	-90.104	0.608	6	14	n
								AS		-76.017	0.462	6		
α-ketoglutaric acid	$C_5H_6O_5$	S-A	≥99.0%	146.11	1.499	soluble[(5)]	0.27±0.05[(e)]	1	0.35	-50.890	0.416	6	33	n
								AS		-92.148	0.513	6		
								2	0.36	-33.195	0.357	6	25	y
								AS		-60.408	0.409	6		
maleic acid	$C_4H_4O_4$	FS[(6)]	99%	116.07	1.59	0.50[5)]	N/A	1	0.38	-91.491	0.550	6	11	n
								AS		-87.420	0.502	6		
								2	0.33	-77.769	0.509	6	-17	n
								AS		-32.191	0.310	6		
methanesulfonic acid (MSA)	$(CH_3)SO_3H$	S-A	≥99.5%	96.11	1.48	soluble[(5)]	N/A	1	0.46	-71.952	0.465	6	2	n
								AS		-63.522	0.422	6		
								2	0.43	-78.452	0.491	6	-22	n
								AS		-33.088	0.315	6		
								3	0.43	-55.723	0.422	6	12	n
								AS		-62.217	0.418	6		

Table 4.2. Continued.

compound	formula	source	purity	M_w [$g\ mole^{-1}$]	P [$g\ cm^{-3}$]	C [-]	$\kappa_{literature}$	run #	κ_{298} [1]	a	b	ΔT	$\Delta\kappa$	trend
methylammonium methylsulfonate[7]	$(CH_3)SO_3(CH_3)NH_3$	S-A	unknown	127.158	N/A	N/A	N/A	1	0.39	-81.062	0.497	6	-49	y
								AS		12.395	0.153	6		
								2	0.45	-110.542	0.623	6	-74	y
								AS		25.612	0.142	6		
polyethylene glycol[f]	$C_{2n}H_{4n+2}O_{n+1}$	FS	unknown	600[8]	1.13[9]	∞[10]	0.03-0.1[11]	1	$68e^{-3}$	-125.239	0.846	6	8	n
								AS		-65.265	0.424	6		
								2	$53e^{-3}$	-284.958	1.408	6	-43	y
								AS		-47.750	0.361	6		
								3	$66e^{-3}$	-228.202	1.208	6	-25	n
								AS		-65.138	0.430	6		
SOA				N/A	N/A	N/A	0.1 ± 0.04[g]	1	0.10	-91.596	0.689	6	-3	n
α-pinene	$C_{10}H_{16}$	S-A	98%					AS		-31.989	0.319	6		
ozone	O_3	T[12]	N/A					2	0.11	-149.462	0.880	6	-0	n
cyclohexane	C_6H_{12}	S-A	≥99%					AS		-73.239	0.457	6		
								3[13]	0.10	-155.706	0.909	6	-7	n
								AS		-68.244	0.443	6		

(1) Kappa values were obtained by converting $s_c - D_d$ data from our experiments using Equations 1 – 4.
(2) Is there a significant trend? "y" = yes, "n" = no. See Appendix for method.
(3) Sigma-Aldrich company
(4) Data for the ammonium sulfate aerosol run concurrently with organic.
(5) Based on MSDS information.
(6) Fisher Scientific company
(7) 1:1 molar ratio of MSA and methylamine with the expected formation of methylammonium methylsulfonate.
(8) Average molecular weight calculated from compounds ranging from approximately 570 – 630 g $mole^{-1}$.
(9) Density at 20°C.
(10) Polyethylene glycol is soluble in water, independent of solute concentration[d].
(11) Maximum range of values for PEG 1000 to PEG 400[e].
(12) Teledyne photometric ozone calibrator, model 703E
(13) Data is a combination of two separate SOA runs (6 Mar and 7 Mar 2012).

(a) Raymond and Pandis (2002)
(b) Perry et al. (1941)
(c) Hings et al. (2008)
(d) Rosenørn et al. (2006)
(e) Frosch et al. (2010)
(f) Petters et al. (2009a)
(g) Prenni et al. (2007)

5. Summary

Several single component organic compounds and a secondary organic aerosol system of α-pinene, O_3, and cyclohexane as an OH scavenger were generated into a polydisperse aerosol. These particles then underwent CCN analysis using the DMPS-CCN method, which consisted of a single DMA to produce a monodisperse aerosol, a condensation particle counter, and a DMT CCN instrument, during which temperature was decreased.

This work explored the temperature dependence of κ-values for organic aerosol proxies by introducing a cryostat temperature control feature, which cooled the CCN instrument inside an insulated box from approximately 40° to 0°C. In order to isolate how κ may be influenced by temperature, we distinguished between four different methods to calculate κ, as well as distinguishing these values at any temperature T from that value calculated at a standard reference state of 298.15K and $\sigma_{s/a} = 0.072$ J m^{-2}. Our observations show that there exists a weak dependence of water activity on temperature, a moderate dependence of solubility in water on temperature, and a strong dependence of surface tension on water. These relationships are valid for all types of clouds that activate regions of the troposphere between 0° and 40° C. Köhler theory was shown to predict the CCN activity of compounds with a weak temperature dependent water activity, as well as that of adipic acid, a sparingly soluble compound. An interesting question to be explored in future studies is the

temperature dependence of solutions where the solute depresses the surface tension, rather than using that of pure water.

Global climate models (GCMs) are expected to determine the relationships between multiple processes on spatial and temporal scales. The ability to accomplish this accurately is complicated by the fact that many of these processes are coupled and sensitive to minute error. These models are necessarily simplified in order to process all the information within. The calculation of aerosol hygroscopicity is one such simplification, as knowledge of the chemical composition goes beyond the means of these global models. We have shown that the inclusion of a more realistic temperature dependent surface tension can have meaningful impacts on the hygroscopicity trend in some cases.

The IPCC (2007) shows that the indirect effect of aerosols is the source of greatest uncertainty in determining Earth's radiative forcing. Liu and Wang (2010) use CAM to show that changing κ_{app}^{Θ} of secondary organic aerosol from 0.07 to 0.14 leads to a change in aerosol indirect forcing of 0.2 W m^{-2}. They do not include temperature dependence into the model calculations. Changes of κ_{app}^{Θ} in our calculations when considering a temperature dependence result in a comparable magnitude difference as Liu and Wang (2010); including this relationship with temperature then may be important for estimating the aerosol forcing on global climate.

APPENDIX

The following is a collection of all activation data for each experimental run (alphabetically by compound), following this format:

1. Summary Table listing information for each diameter scan during the experiment. This information includes the ending scan time (in seconds after midnight), current compound, the change in temperature inside the CCNC column (ΔT), the temperature of the enclosure (T_{box} in °C), the temperature of the CCNC at location T_1 (T_1 in °C, see Figure 4.1), the activation diameter (D_{50} in nm), the Boltzmann Parameters ($A1$ is the minimum activated fraction, $A2$ is the maximum activated fraction, and dx is the width of the Sigmoid-Boltzmann curve), and if the data was excluded due to temperature instability within the instrument or other error.
2. Activation curves for each diameter scan. These show diameter (nm) versus activated fraction (%), which gives D_{50}. Every other scan represents ammonium sulfate, or AS (consult corresponding summary table for details on scan numbers).
3. Activation diameters for ammonium sulfate and the organic versus temperature. These are denoted by the scan numbers, which are then fitted to a line. The fit line's coefficients are recorded to express the magnitude of the activation diameter trend.
4. Apparent κ at standard state (T = 298.15K and $\sigma_{s/a}$ = 0.072 J m^{-2}) and varying T versus temperature plots. These are shown separately here to highlight each scan's information. A fit line is also applied to this κ data.
5. Activation diameters versus temperature are re-plotted without scan numbers (similar to 3).

6. Apparent κ at standard state and varying T versus temperature are re-plotted together with only fit lines for better comparison between the two.

Please note that the nomenclature on these plots "apparent kappa" corresponds to the previously defined $\kappa_{app}^{\ominus}$, and "analytical kappa" corresponds to κ_{app}.

Table A.1. Adipic acid data. Each line represents one diameter scan.

						Boltzmann Parameters:			
time	compound	ΔT	T_{box}	T_{inlet}	D_{50}	$A1$	$A2$	dx	excluded
35700	adipic	8	0.00	28.60	162.17	0.0182	1.1881	3.00	yes
36120	AS	8	28.28	31.47	50.38	0.0000	0.7601	3.00	yes
36600	adipic	8	32.47	34.40	201.02	0.0163	1.2531	32.21	no
37020	AS	8	35.82	37.41	52.79	0.0000	0.7580	3.20	no
37440	adipic	8	38.30	37.39	195.68	0.0029	1.1503	25.52	no
37920	AS	8	40.16	40.34	48.38	0.0000	0.7354	3.00	no
38340	adipic	8	41.26	40.33	185.08	0.0000	1.1437	25.25	no
38760	AS	8	41.56	40.33	56.24	0.0000	0.7747	4.04	yes
39240	adipic	8	41.24	40.34	188.31	0.0000	1.1750	26.68	yes
39660	AS	8	40.58	40.33	56.24	0.0000	0.7736	3.36	yes
40080	adipic	8	39.60	40.32	180.55	0.0000	1.1060	24.72	yes
40560	AS	8	38.39	40.33	55.34	0.0000	0.7750	3.77	no
40980	adipic	8	37.12	40.33	175.00	0.0000	1.0864	20.99	no
41400	AS	8	35.99	40.34	55.64	0.0000	0.7819	3.53	no
41880	adipic	8	34.69	37.37	183.33	0.0012	1.0637	20.26	no
42300	AS	8	33.54	37.38	55.45	0.0000	0.7846	4.03	no
42720	adipic	8	32.17	37.37	184.90	0.0001	1.0740	18.19	no
43200	AS	8	30.60	34.39	57.54	0.0021	0.7982	3.00	no
43620	adipic	8	29.30	34.37	192.09	0.0026	1.0335	15.46	no
44040	AS	8	27.72	31.36	51.70	0.0000	0.7882	3.00	no
44520	adipic	8	26.27	31.44	200.83	0.0009	0.9901	16.61	no
44940	AS	8	24.79	29.11	49.78	0.0000	0.7823	3.00	no
45360	adipic	8	23.07	28.48	209.96	0.0000	0.9589	17.85	no
45840	AS	8	21.64	28.48	49.73	0.0000	0.7939	3.00	no
46260	adipic	8	20.01	25.53	217.21	0.0029	0.9425	15.75	no
46680	AS	8	18.65	25.53	49.36	0.0000	0.8023	3.00	no
47160	adipic	8	17.19	22.45	202.70	0.0099	1.0408	29.20	no
47580	AS	8	15.92	22.51	48.96	0.0000	0.8145	3.00	no
48000	adipic	8	14.75	22.53	233.01	0.0033	0.9903	19.48	no
48480	AS	8	13.48	19.56	30.00	0.3000	0.8627	40.00	yes
48900	adipic	8	12.60	19.58	240.10	0.0089	1.0027	18.48	no
49320	AS	8	11.61	19.57	48.02	0.0000	0.7714	3.00	no
49800	adipic	8	10.67	16.59	230.29	0.0261	0.8758	22.00	no
50220	AS	8	9.96	16.64	47.50	0.0000	0.7719	3.00	no
50640	adipic	8	9.25	16.61	241.87	0.0104	0.9339	17.65	no
51120	AS	8	8.40	16.62	46.57	0.0000	0.7718	3.00	no
51540	adipic	8	7.71	13.37	158.61	0.0108	0.8762	8.07	yes
51960	AS	8	7.17	13.68	47.12	0.0000	0.7722	3.00	no
52440	adipic	8	6.71	13.67	241.68	0.0108	0.9800	17.05	no
52860	AS	8	5.14	13.67	45.25	0.0018	0.7644	3.00	no
53280	adipic	8	4.12	10.57	223.25	0.0272	0.9832	29.88	no
53760	AS	8	3.54	10.72	45.16	0.0003	0.7690	3.00	no
54180	adipic	8	3.05	10.73	240.16	0.0150	0.8856	16.73	no
54600	AS	8	2.48	10.73	43.48	0.0000	0.7614	3.00	no
55080	adipic	8	2.02	10.72	243.34	0.0156	0.9533	15.52	no
55500	AS	8	1.60	10.71	43.29	0.0000	0.7510	3.00	no
55920	adipic	8	1.30	10.70	246.31	0.0160	0.9902	17.45	no
56400	AS	8	1.01	5.83	36.99	0.0000	0.7485	3.00	no
56820	adipic	8	1.09	5.85	247.34	0.0158	0.9501	16.60	no
57240	AS	8	0.75	5.84	42.70	0.0000	0.7582	3.00	no
57720	adipic	8	0.36	4.79	238.28	0.0161	1.0105	21.08	no
58140	AS	8	0.04	4.80	43.09	0.0000	0.7581	3.00	no
58560	adipic	8	-0.23	4.82	244.80	0.0198	0.9289	16.53	no
59040	AS	8	-0.50	4.81	42.34	0.0000	0.7471	3.00	no
59460	adipic	8	-0.74	3.84	249.04	0.0210	0.9820	16.40	no
59880	AS	8	-0.91	3.86	41.93	0.0000	0.7531	3.00	no
60360	adipic	8	-1.07	3.86	244.75	0.0206	0.9775	19.67	no
60780	AS	8	-1.27	3.85	41.86	0.0000	0.7574	3.00	no
61200	adipic	8	-1.43	3.85	238.11	0.0227	0.9267	18.54	no
61680	AS	8	-1.56	3.85	41.63	0.0000	0.7497	3.00	no

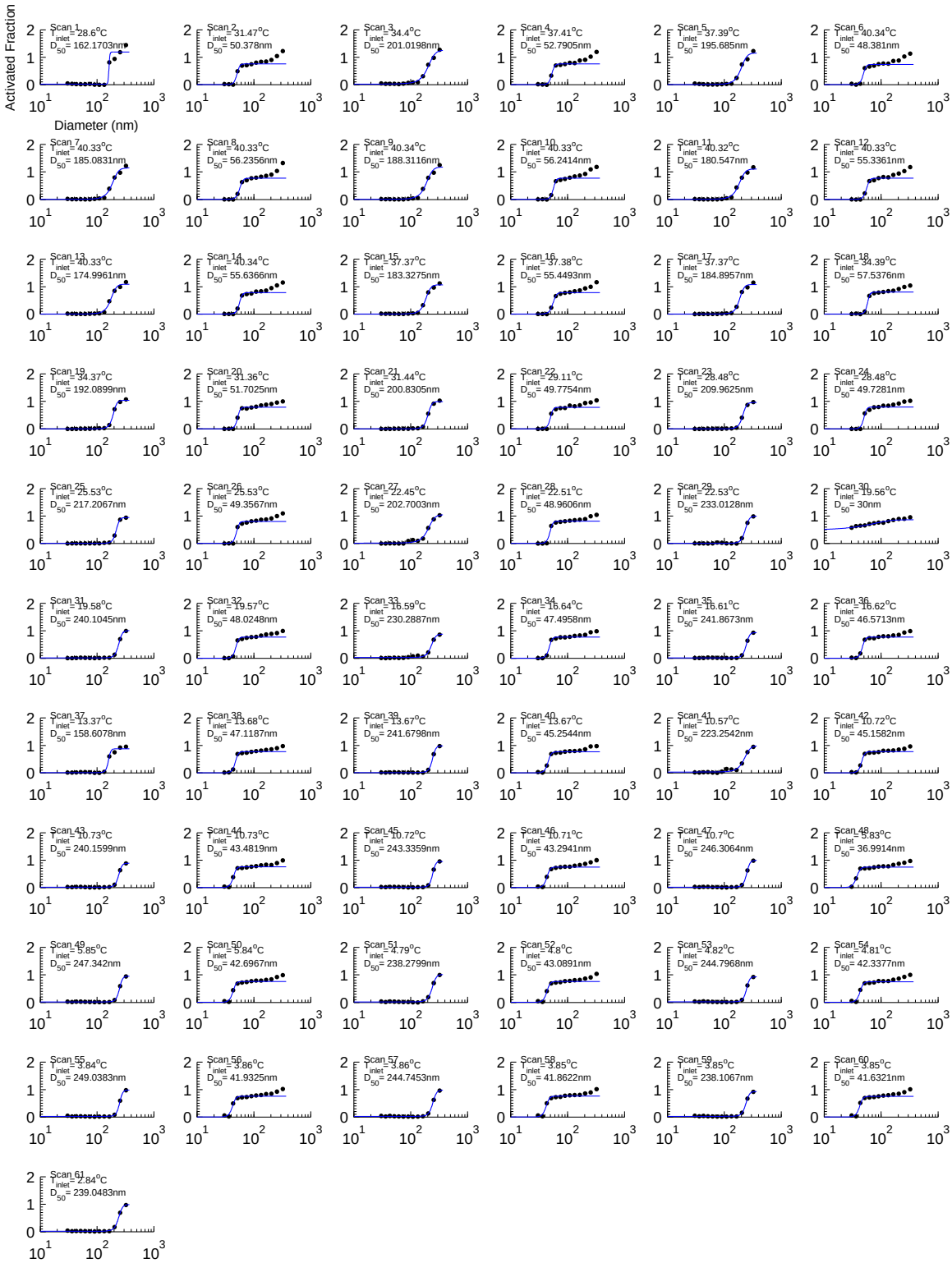

Figure A.1. Adipic acid (odd scan numbers) and $(NH_4)_2SO_4$ activation curves. The activated fractions at each diameter are fit with a Sigmoid-Boltzmann curve (blue, see Table A.1).

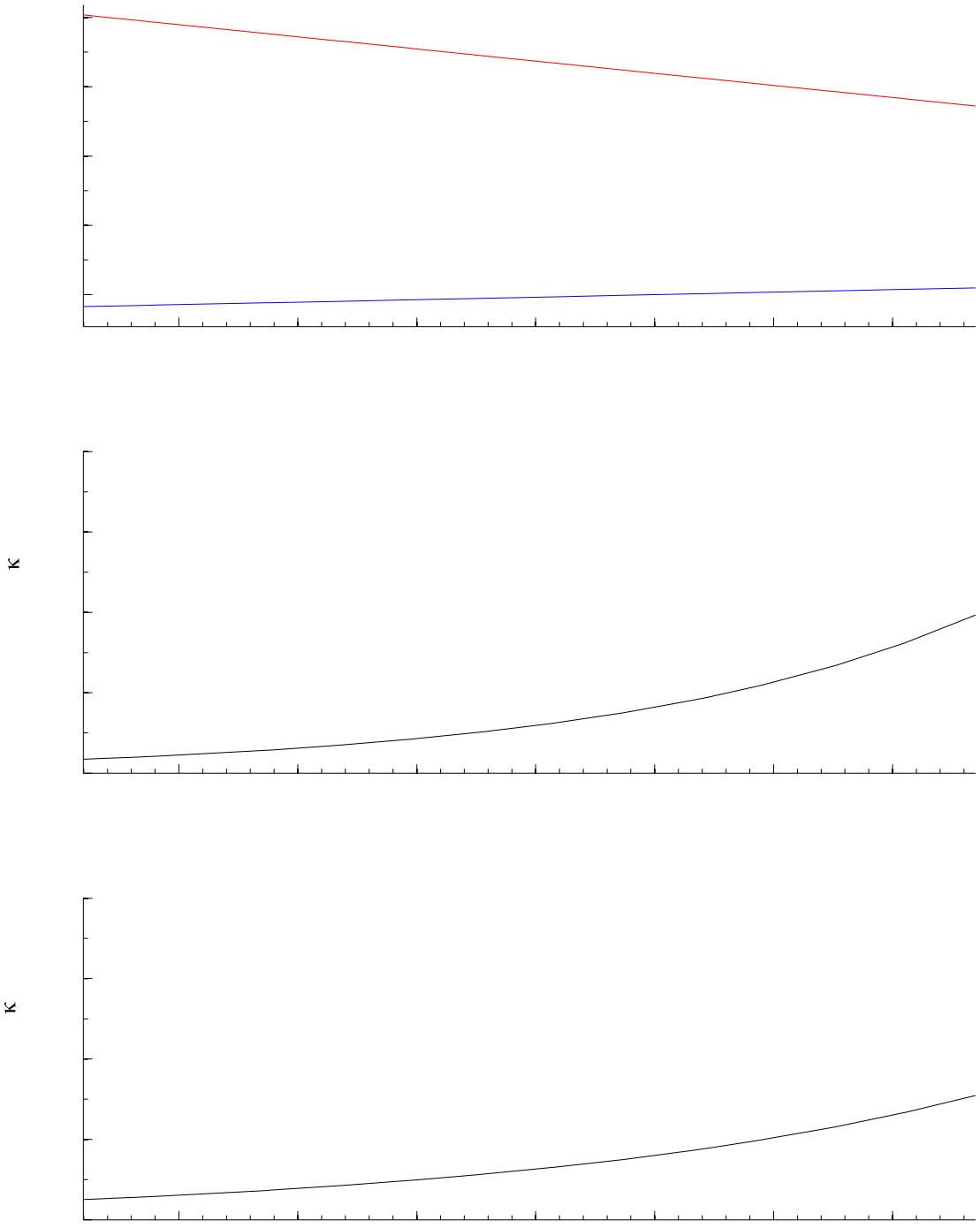

Figure A.2. Adipic acid and $(NH_4)_2SO_4$ activation diameters (top) and adipic acid κ values (center and bottom) versus temperature. Each number represents a scan from Figure A.1. Fit coefficients represent the solid line fit through the activation diameters, which then give the κ line.

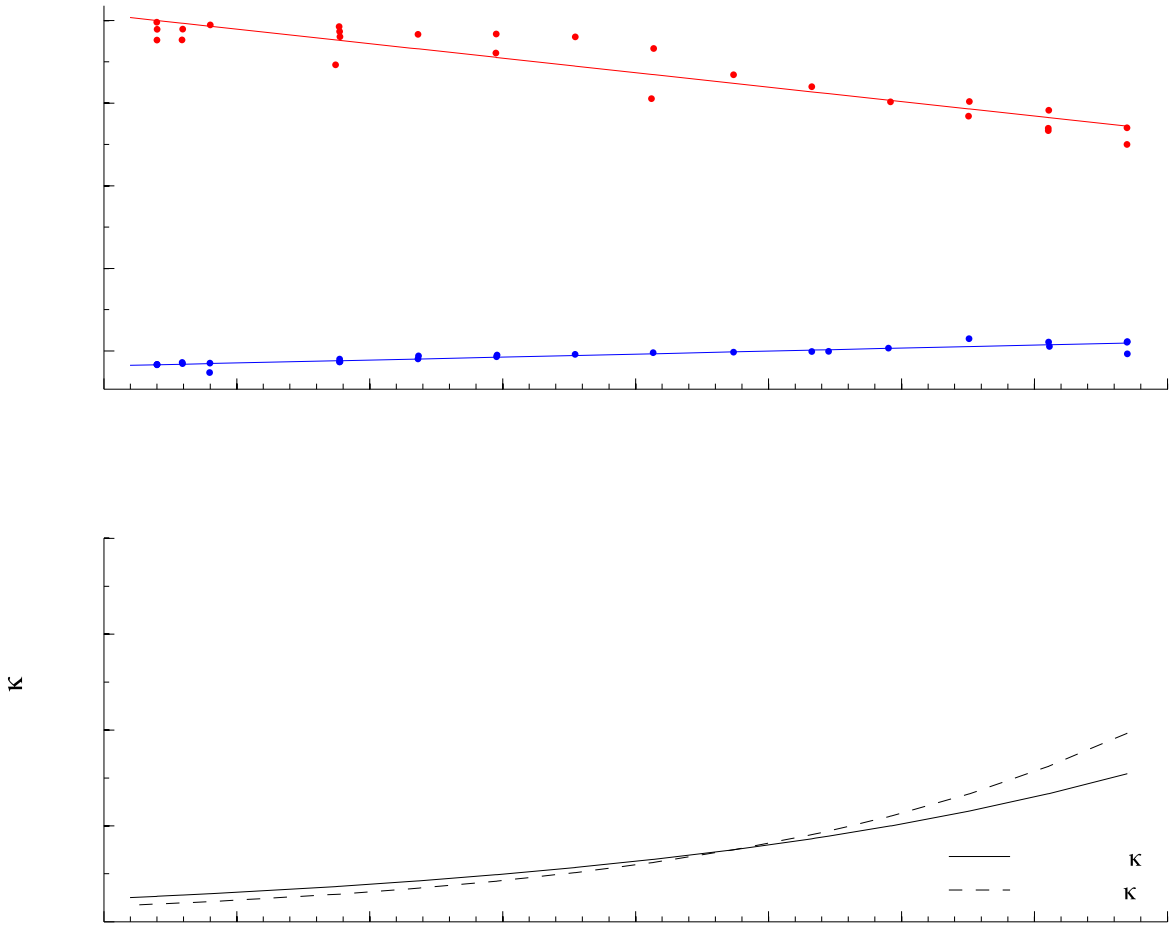

Figure A.3. Adipic acid and $(NH_4)_2SO_4$ activation diameters replotted without scan numbers (top) and κ values (bottom) plotted together.

Table A.2. Adipic acid data. Each line represents one diameter scan.

						Boltzmann Parameters:			
time	compound	ΔT	T_{box}	T_{inlet}	D_{50}	*A1*	*A2*	*dx*	excluded
35880	AS	12	0.00	39.97	167.91	0.0000	0.7533	3.02	yes
36420	adipic	12	41.32	39.99	194.53	0.0000	1.5000	33.42	yes
36840	AS	12	41.67	39.97	41.97	0.0000	0.7800	3.00	yes
37260	adipic	12	42.21	42.92	228.79	0.0000	1.3996	27.97	yes
37740	AS	12	43.00	42.90	95.47	0.0000	0.8003	6.29	yes
38160	adipic	12	43.18	42.92	234.04	0.0006	1.1380	20.33	yes
38580	AS	12	42.76	42.93	100.68	0.0014	0.8060	4.55	yes
39060	adipic	12	42.00	42.92	229.63	0.0000	1.3251	25.19	yes
39480	AS	12	40.99	42.92	76.39	0.0000	0.8211	5.41	yes
39900	adipic	12	39.79	42.92	206.34	0.0000	1.2534	24.01	yes
40380	AS	12	38.51	40.13	58.67	0.0000	0.8303	3.00	yes
40800	adipic	12	37.16	39.98	183.62	0.0000	1.4066	32.08	yes
41220	AS	12	36.02	39.97	41.56	0.0000	0.7917	3.00	yes
41700	adipic	12	34.61	36.59	140.96	0.0000	1.1968	19.81	yes
42120	AS	12	33.13	37.02	41.70	0.0000	0.7939	3.00	yes
42540	adipic	12	31.71	37.02	170.98	0.0000	1.2106	25.34	no
43020	AS	12	30.07	34.07	41.35	0.0000	0.8071	3.00	no
43440	adipic	12	28.61	34.06	179.10	0.0000	1.1859	24.58	no
43860	AS	12	26.91	31.09	30.00	0.2723	0.8594	21.46	no
44340	adipic	12	25.40	31.12	187.69	0.0000	1.2220	24.41	yes
44760	AS	12	23.71	28.13	30.00	0.0113	0.8211	6.56	yes
45180	adipic	12	22.22	28.16	186.02	0.0000	1.0988	19.03	no
45660	AS	12	20.63	25.16	38.76	0.0000	0.8333	3.00	no
46080	adipic	12	19.18	25.21	191.38	0.0004	1.1304	17.78	no
46500	AS	12	17.75	21.68	38.28	0.0000	0.8437	3.19	no
46980	adipic	12	16.38	22.27	193.62	0.0008	1.0777	15.73	no
47400	AS	12	15.22	22.26	37.56	0.0000	0.8759	3.32	no
47820	adipic	12	13.91	19.30	214.21	0.0127	1.0932	23.98	no
48300	AS	12	13.02	19.30	36.38	0.0000	0.7846	3.00	no
48720	adipic	12	11.98	19.33	206.44	0.0134	1.0818	21.08	no
49140	AS	12	11.05	16.34	30.00	0.3000	0.9332	40.00	yes
49620	adipic	12	10.41	16.39	207.49	0.0148	1.0273	20.41	no
50040	AS	12	9.69	16.37	35.40	0.0000	0.7889	3.00	no
50460	adipic	12	8.96	16.38	209.23	0.0171	1.0825	20.27	no
50940	AS	12	8.30	13.38	33.78	0.0000	0.7834	3.00	no
51360	adipic	12	7.90	13.41	203.99	0.0209	0.9445	15.25	no
51780	AS	12	6.55	10.62	36.00	0.0000	0.7901	3.00	no
52260	adipic	12	5.49	9.59	215.12	0.0155	1.0312	20.59	no
52680	AS	12	4.63	8.64	35.30	0.0000	0.7904	3.00	no
53100	adipic	12	3.92	7.65	221.29	0.0158	1.0679	22.83	no
53580	AS	12	3.32	7.66	33.74	0.0000	0.7863	3.00	no
54000	adipic	12	2.79	6.66	208.04	0.0208	0.9866	18.02	no
54420	AS	12	2.34	6.64	33.51	0.0000	0.7876	3.00	no
54900	adipic	12	1.90	5.67	204.21	0.0224	0.9946	15.48	no
55320	AS	12	1.57	5.69	33.31	0.0000	0.7821	3.00	no
55740	adipic	12	1.24	5.69	205.00	0.0246	1.0115	15.35	no
56220	AS	12	0.93	4.67	33.37	0.0000	0.7836	3.00	no
56640	adipic	12	0.71	4.65	205.39	0.0219	1.0440	19.06	no
57060	AS	12	0.50	4.67	32.65	0.0000	0.7775	3.00	no
57540	adipic	12	0.30	4.66	202.79	0.0227	1.0054	17.95	no
57960	AS	12	0.11	4.66	32.48	0.0000	0.7809	3.00	no
58380	adipic	12	-0.03	3.69	213.28	0.0232	1.1080	20.62	no
58860	AS	12	-0.12	3.71	32.65	0.0000	0.7781	3.00	no
59280	adipic	12	-0.24	3.69	202.05	0.0290	0.9856	15.11	no
59700	AS	12	-0.38	3.69	32.46	0.0000	0.7848	3.00	no
60180	adipic	12	-0.49	3.70	200.85	0.0314	0.9795	13.23	no
60600	AS	12	-0.61	3.69	32.37	0.0000	0.7810	3.00	no

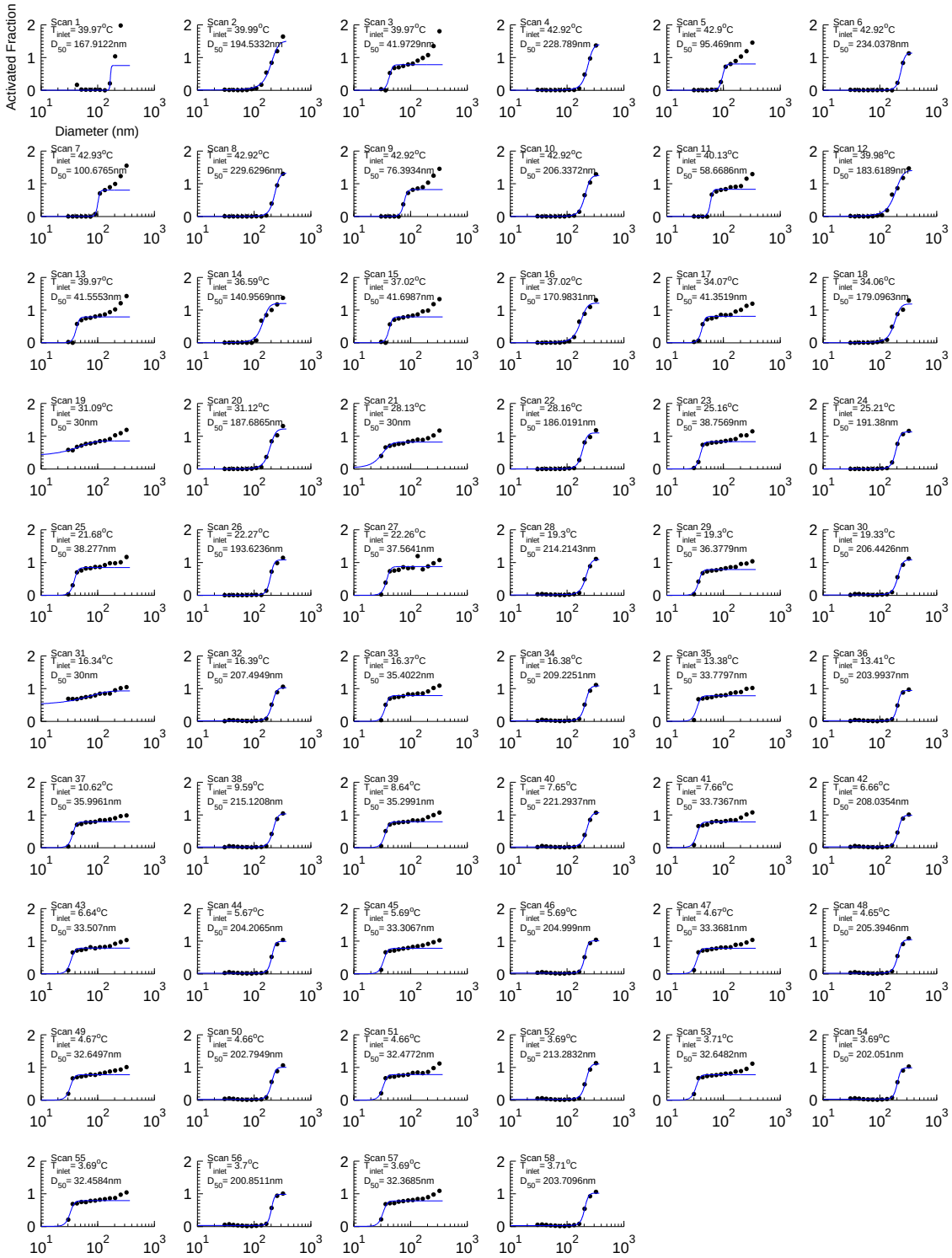

Figure A.4. Adipic acid (even scan numbers) and $(NH_4)_2SO_4$ activation curves. The activated fractions at each diameter are fit with a Sigmoid-Boltzmann curve (blue, see Table A.2).

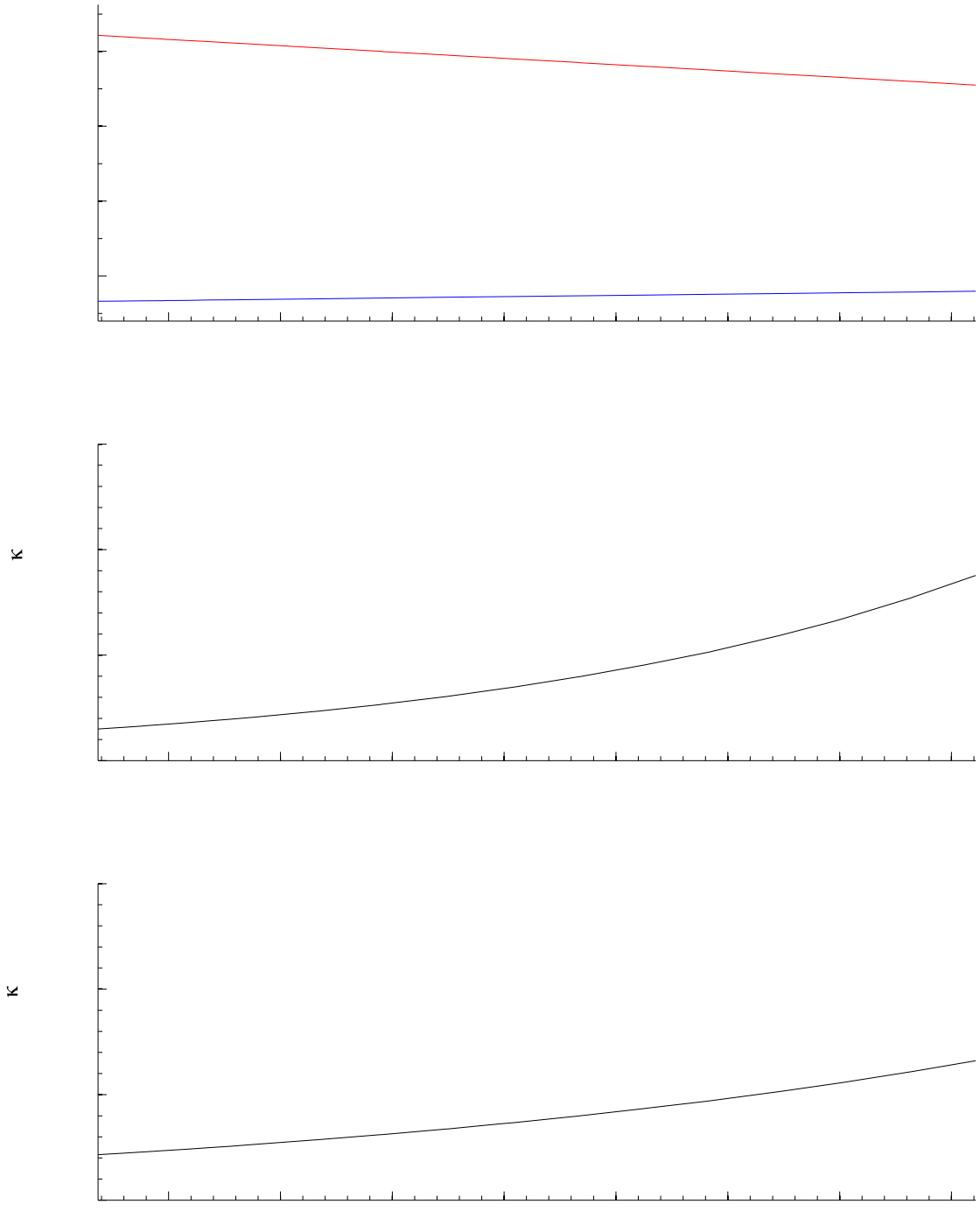

Figure A.5. Adipic acid and $(NH_4)_2SO_4$ activation diameters (top) and adipic acid κ values (center and bottom) versus temperature. Each number represents a scan from Figure A.4. Fit coefficients represent the solid line fit through the activation diameters, which then give the κ fit line.

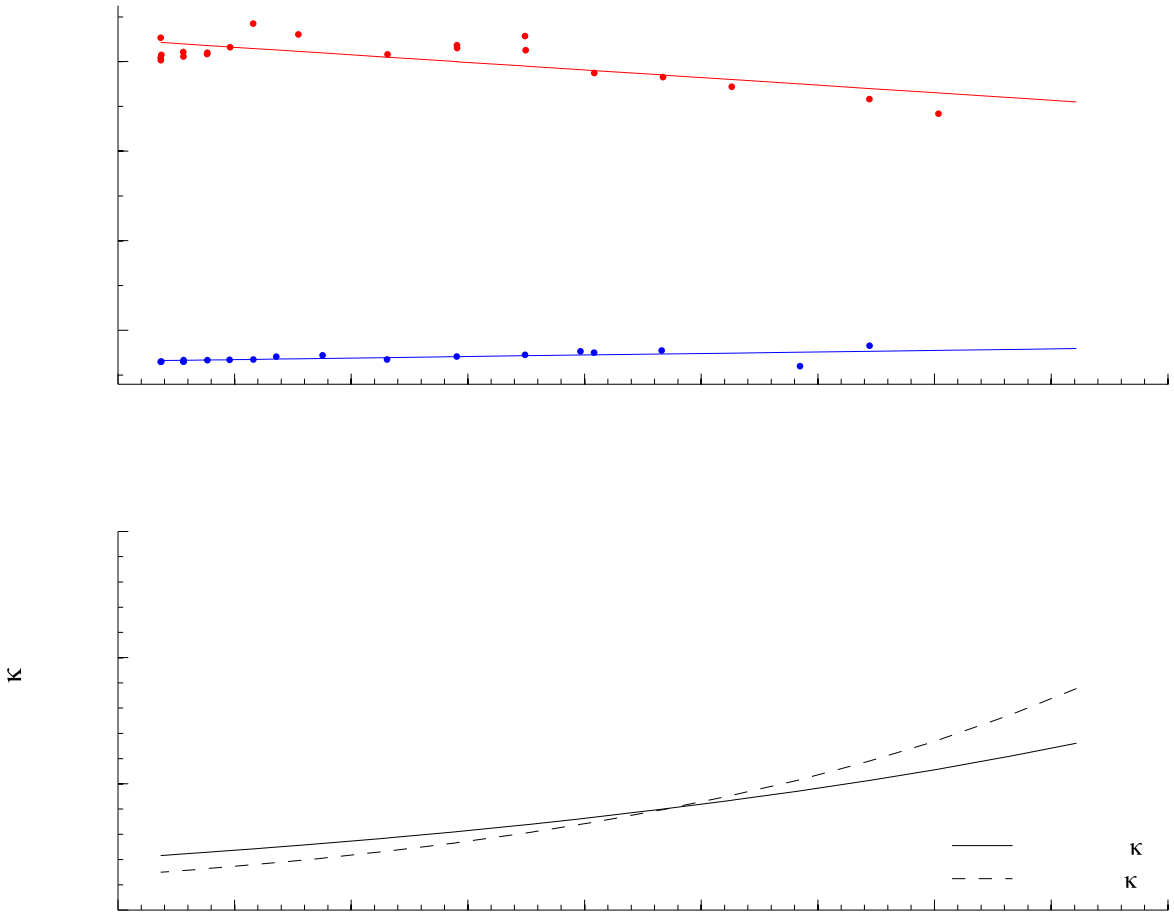

Figure A.6. Adipic acid and $(NH_4)_2SO_4$ activation diameters replotted without scan numbers (top) and κ values (bottom) plotted together.

Table A.3. Adipic acid data. Each line represents one diameter scan.

						Boltzmann Parameters:			
time	compound	ΔT	T_{box}	T_{inlet}	D_{50}	*A1*	*A2*	*dx*	excluded
34080	adipic	8	0.00	28.06	233.24	0.0000	0.9871	18.50	yes
34500	AS	8	30.89	31.07	49.05	0.0000	0.8022	3.00	yes
34980	adipic	8	34.80	37.13	211.84	0.0000	1.3286	15.13	yes
35400	AS	8	37.61	36.98	52.57	0.0000	0.8050	4.06	yes
35820	adipic	8	39.63	39.92	201.31	0.0000	1.3550	24.17	yes
36300	AS	8	40.80	39.91	57.47	0.0000	0.8176	3.00	yes
36720	adipic	8	41.15	39.91	209.17	0.0000	1.4317	25.65	yes
37140	AS	8	40.97	39.89	57.21	0.0000	0.8202	3.01	yes
37620	adipic	8	40.42	39.92	204.90	0.0000	1.3638	26.31	yes
38040	AS	8	39.59	39.91	57.16	0.0000	0.8202	3.03	yes
38460	adipic	8	38.53	39.91	212.03	0.0000	1.5000	29.64	yes
38940	AS	8	37.33	39.91	57.00	0.0000	0.8386	3.19	yes
39360	adipic	8	36.02	39.92	199.83	0.0000	1.3232	23.02	yes
39780	AS	8	34.61	36.85	47.08	0.0000	0.8112	3.00	yes
40260	adipic	8	33.30	36.98	213.74	0.0000	1.2933	26.59	yes
40680	AS	8	31.85	36.97	55.38	0.0000	0.8423	4.16	no
41100	adipic	8	30.22	33.95	223.50	0.0000	1.1999	23.33	no
41580	AS	8	28.81	33.96	51.81	0.0000	0.8283	3.27	no
42000	adipic	8	27.14	30.98	231.44	0.0002	1.1667	21.69	no
42420	AS	8	25.65	31.00	50.62	0.0000	0.8215	3.00	no
42900	adipic	8	23.99	28.01	236.47	0.0057	1.1009	22.54	no
43320	AS	8	22.51	28.07	49.86	0.0000	0.8371	3.00	no
43740	adipic	8	20.84	24.85	223.68	0.0145	1.0492	24.66	no
44220	AS	8	19.34	25.11	49.42	0.0000	0.8576	3.00	no
44640	adipic	8	17.85	21.70	177.84	0.0106	0.9927	14.48	yes
45060	AS	8	16.40	22.16	49.05	0.0000	0.8010	3.00	no
45540	adipic	8	15.18	22.16	257.00	0.0095	0.9356	13.95	no
45960	AS	8	13.87	19.19	44.09	0.0000	0.8040	5.53	yes
46380	adipic	8	12.89	19.19	262.47	0.0092	0.8709	17.06	no
46860	AS	8	11.80	19.19	48.13	0.0000	0.8114	3.00	no
47280	adipic	8	10.78	16.25	269.73	0.0110	0.8041	17.44	no
47700	AS	8	10.12	16.25	47.56	0.0000	0.8132	3.00	no
48180	adipic	8	9.27	16.23	266.85	0.0122	0.8646	17.07	no
48600	AS	8	8.51	15.06	47.28	0.0000	0.8075	3.00	no
49020	adipic	8	7.80	13.30	262.55	0.0105	0.8119	15.57	no
49500	AS	8	6.79	10.21	40.47	0.0000	0.8018	3.00	no
49920	adipic	8	5.72	9.18	259.16	0.0149	0.8674	20.36	no
50340	AS	8	4.75	8.22	46.06	0.0000	0.8074	3.01	no
50820	adipic	8	3.87	7.24	248.25	0.0123	0.9132	17.74	no
51240	AS	8	3.13	7.29	45.94	0.0000	0.8078	3.00	no
51660	adipic	8	2.45	6.28	263.65	0.0138	0.8681	15.36	no
52140	AS	8	1.87	5.26	43.67	0.0000	0.8006	3.13	no
52560	adipic	8	1.35	5.30	262.51	0.0166	0.9085	15.87	no
52980	AS	8	0.95	5.29	42.37	0.0000	0.7722	3.00	no
53460	adipic	8	0.54	4.28	262.48	0.0166	0.9051	14.41	no
53880	AS	8	0.22	4.27	42.39	0.0000	0.7917	3.00	no
54300	adipic	8	-0.11	4.29	261.13	0.0189	0.9159	16.54	no
54780	AS	8	-0.42	3.32	42.05	0.0000	0.7856	3.00	no
55200	adipic	8	-0.81	3.31	259.93	0.0203	0.9361	14.61	no
55620	AS	8	-1.13	3.31	41.95	0.0000	0.7906	3.00	no
56100	adipic	8	-1.35	3.33	260.88	0.0228	0.9851	13.90	no
56520	AS	8	-1.54	2.32	41.59	0.0000	0.7799	3.00	no

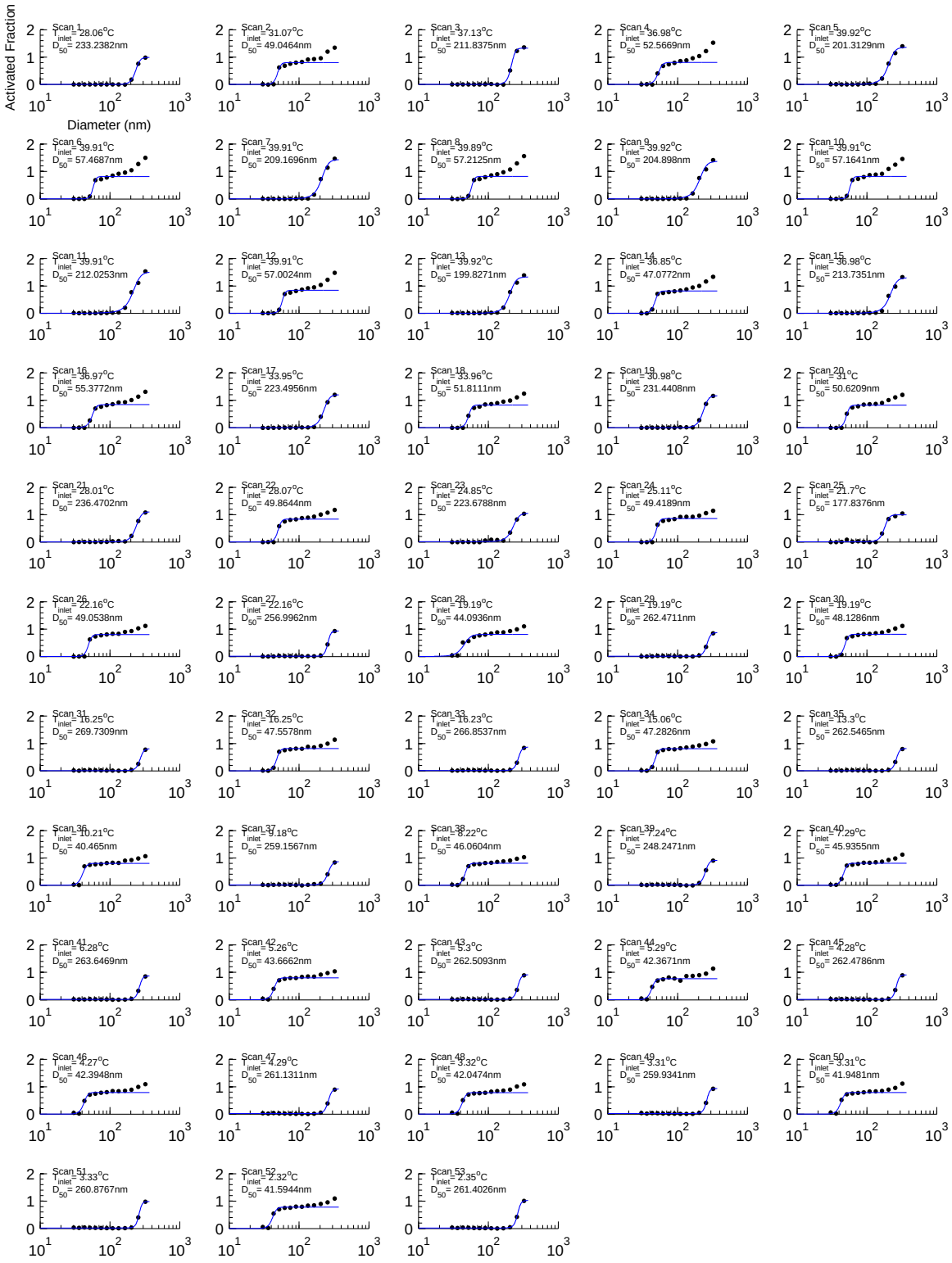

Figure A.7. Adipic acid (odd scan numbers) and $(NH_4)_2SO_4$ activation curves. The activated fractions at each diameter are fit with a Sigmoid-Boltzmann curve (blue, see Table A.3).

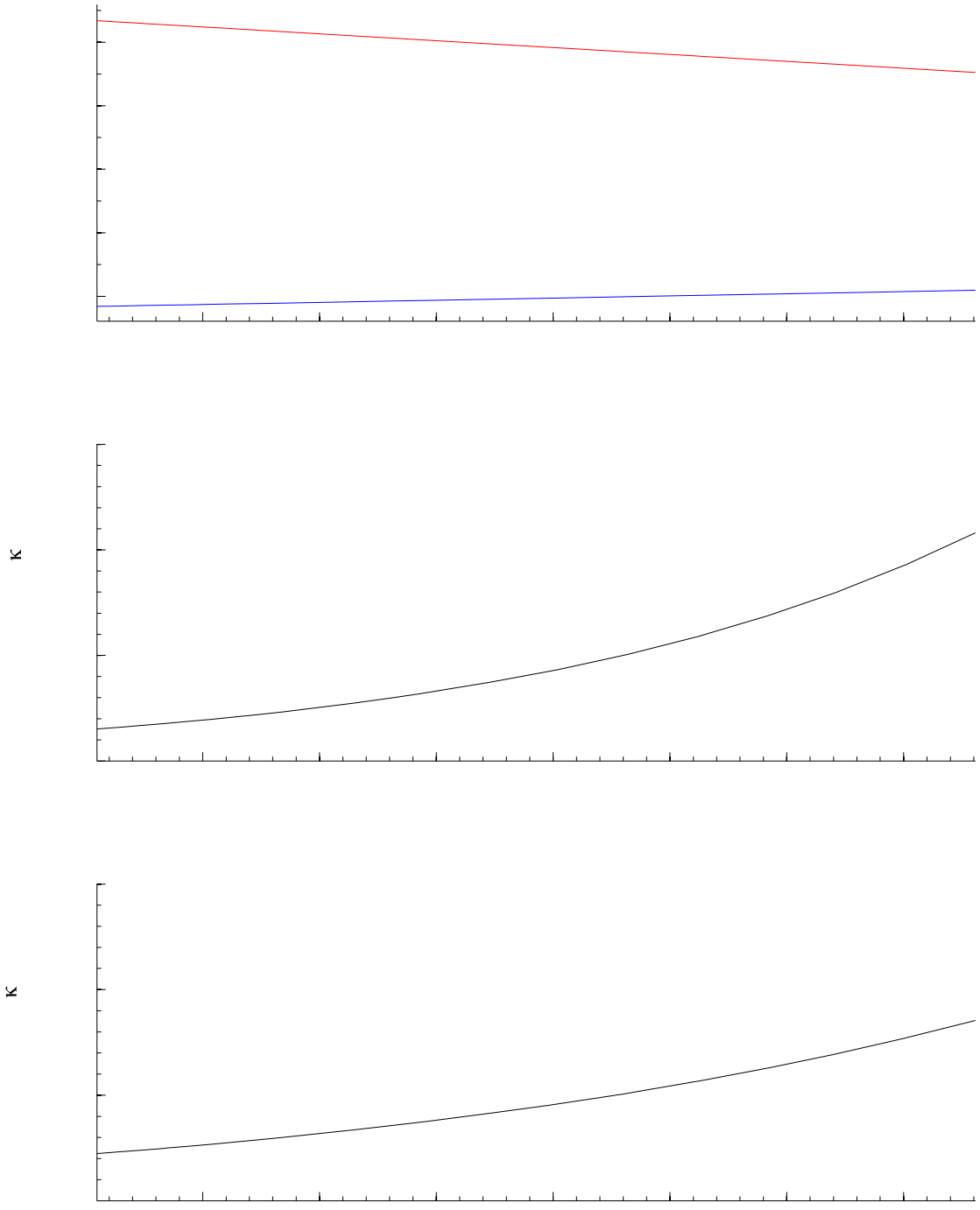

Figure A.8. Adipic acid and $(NH_4)_2SO_4$ activation diameters (top) and adipic acid κ values (center and bottom) versus temperature. Each number represents a scan from Figure A.7. Fit coefficients represent the solid line fit through the activation diameters, which then give the κ line.

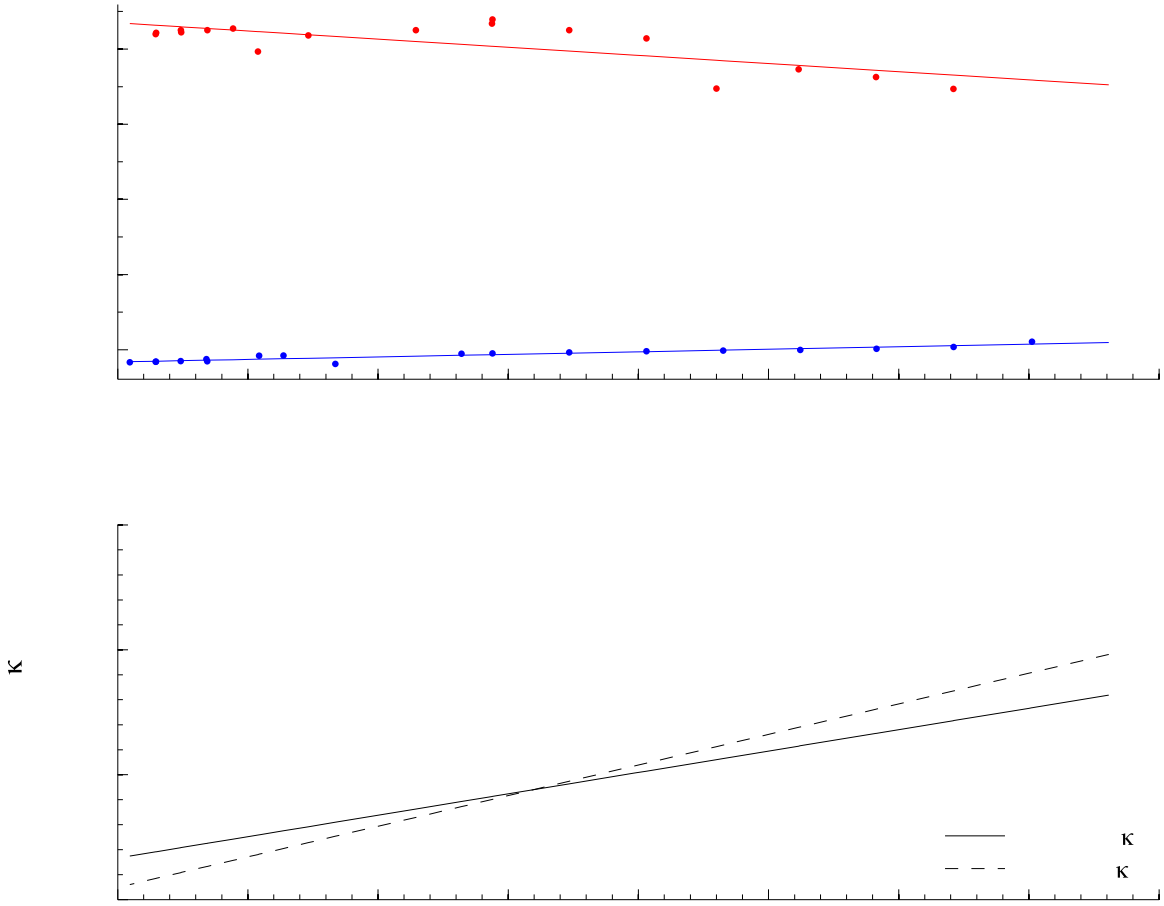

Figure A.9. Adipic acid and $(NH_4)_2SO_4$ activation diameters replotted without scan numbers (top) and κ values (bottom) plotted together.

Table A.4. Glucose data. Each line represents one diameter scan.

					Boltzmann Parameters:			
time	compound	ΔT	T_{box}[1]	T_{inlet}	D_{50}	$A1$	$A2$	dx	excluded
35220	AS	6	0.00	26.29	48.16	0.0000	0.7708	3.00	yes
35640	glucose	6	0.00	30.27	30.00	0.3000	0.9908	40.00	yes
36120	AS	6	0.00	34.26	99.18	0.0063	0.7531	4.32	yes
36540	glucose	6	0.00	36.16	30.00	0.3000	0.9859	40.00	yes
36960	AS	6	0.00	38.22	69.15	0.0000	0.7505	3.00	no
37740	glucose	6	0.00	40.11	99.15	0.0086	0.7546	4.49	no
38220	AS	6	0.00	42.15	69.44	0.0000	0.7202	3.00	no
38640	glucose	6	0.00	42.10	101.40	0.0015	0.7002	3.00	yes
39060	AS	6	0.00	42.09	70.32	0.0000	0.7264	3.00	yes
39540	glucose	6	0.00	42.09	104.57	0.0007	0.7397	3.00	yes
39960	AS	6	0.00	43.06	66.80	0.0000	0.7686	3.93	yes
40380	glucose	6	0.00	43.06	104.68	0.0056	0.8119	3.00	yes
40860	AS	6	0.00	40.25	68.68	0.0000	0.7865	3.00	yes
41280	glucose	6	0.00	40.12	104.23	0.0068	0.8137	3.00	yes
41700	AS	6	0.00	40.13	67.71	0.0008	0.7789	3.48	yes
42180	glucose	6	0.00	37.16	84.49	0.0295	0.7618	6.98	yes
42600	AS	6	0.00	37.17	66.58	0.0000	0.8011	4.50	yes
43020	glucose	6	0.00	34.16	48.77	0.0000	0.7636	3.00	yes
43500	AS	6	0.00	34.22	63.96	0.0000	0.7941	3.87	no
43920	glucose	6	0.00	31.06	82.62	0.0000	0.8184	3.00	yes
44340	AS	6	0.00	31.28	63.33	0.0000	0.8099	4.18	no
44820	glucose	6	0.00	31.26	92.16	0.0003	0.7844	3.00	no
45240	AS	6	0.00	28.25	62.85	0.0000	0.7981	4.26	no
45660	glucose	6	0.00	28.26	92.71	0.0001	0.7818	5.35	no
46140	AS	6	0.00	27.43	59.21	0.0000	0.8147	3.00	no
46560	glucose	6	0.00	25.30	69.36	0.0000	1.5000	12.85	yes
46980	AS	6	0.00	25.30	58.86	0.0000	0.8297	3.00	no
47460	glucose	6	0.00	22.39	88.59	0.0113	0.7804	4.65	no
47880	AS	6	0.00	22.37	60.62	0.0000	0.7814	3.00	no
48300	glucose	6	0.00	22.37	88.18	0.0139	0.7852	3.11	no
48780	AS	6	0.00	22.36	58.16	0.0000	0.7925	3.00	no
49200	glucose	6	0.00	19.39	91.10	0.0294	0.8260	7.63	no
49620	AS	6	0.00	19.41	58.12	0.0000	0.7978	3.00	no
50100	glucose	6	0.00	15.73	81.22	0.0580	0.8228	4.61	no
50520	AS	6	0.00	16.40	57.82	0.0000	0.7879	3.00	no
50940	glucose	6	0.00	16.38	81.91	0.0573	0.9272	6.06	no
51420	AS	6	0.00	13.10	56.38	0.0017	0.7980	3.00	no
51840	glucose	6	0.00	13.46	84.50	0.0131	0.7865	3.00	no
52260	AS	6	0.00	13.43	55.54	0.0015	0.7793	3.00	no
52740	glucose	6	0.00	13.46	83.18	0.0212	0.8053	3.00	no
53160	AS	6	0.00	13.45	54.94	0.0023	0.7880	3.35	no
53580	glucose	6	0.00	10.51	86.53	0.0220	0.7903	3.45	no
54060	AS	6	0.00	9.50	54.12	0.0012	0.7833	3.37	no
54480	glucose	6	0.00	9.53	83.03	0.0224	0.8113	3.00	no
54900	AS	6	0.00	9.54	54.64	0.0068	0.7847	3.08	no
55380	glucose	6	0.00	7.53	52.36	0.0000	0.7631	3.00	yes
55800	AS	6	0.00	7.55	54.35	0.0021	0.7703	3.80	no
56220	glucose	6	0.00	6.11	87.23	0.0349	0.7807	3.02	no
56700	AS	6	0.00	6.10	53.84	0.0020	0.7788	3.55	no
57120	glucose	6	0.00	5.08	85.93	0.0343	0.7884	3.00	no
57540	AS	6	0.00	5.08	52.22	0.0000	0.7704	3.56	no
58020	glucose	6	0.00	5.09	79.40	0.0290	0.7818	3.31	no
58440	AS	6	0.00	4.12	44.98	0.0000	0.7447	3.29	no
58860	glucose	6	0.00	4.12	80.94	0.0266	0.7987	3.34	no
59340	AS	6	0.00	4.12	52.42	0.0039	0.7701	3.19	no
59760	glucose	6	0.00	4.12	81.06	0.0266	0.8026	3.70	no
60180	AS	6	0.00	4.13	52.12	0.0000	0.7704	3.49	no
60660	glucose	6	0.00	4.12	79.59	0.0262	0.7833	3.32	no
61080	AS	6	0.00	4.13	51.91	0.0011	0.7737	3.28	no
61500	glucose	6	0.00	4.10	80.08	0.0270	0.7923	3.93	no
61980	AS	6	0.00	3.06	51.91	0.0015	0.7657	3.21	no
62400	glucose	6	0.00	3.09	80.10	0.0278	0.7982	4.00	no
62820	AS	6	0.00	3.09	50.58	0.0000	0.7630	3.00	no

[1]Sensor malfunctioned resulting in temperature error.

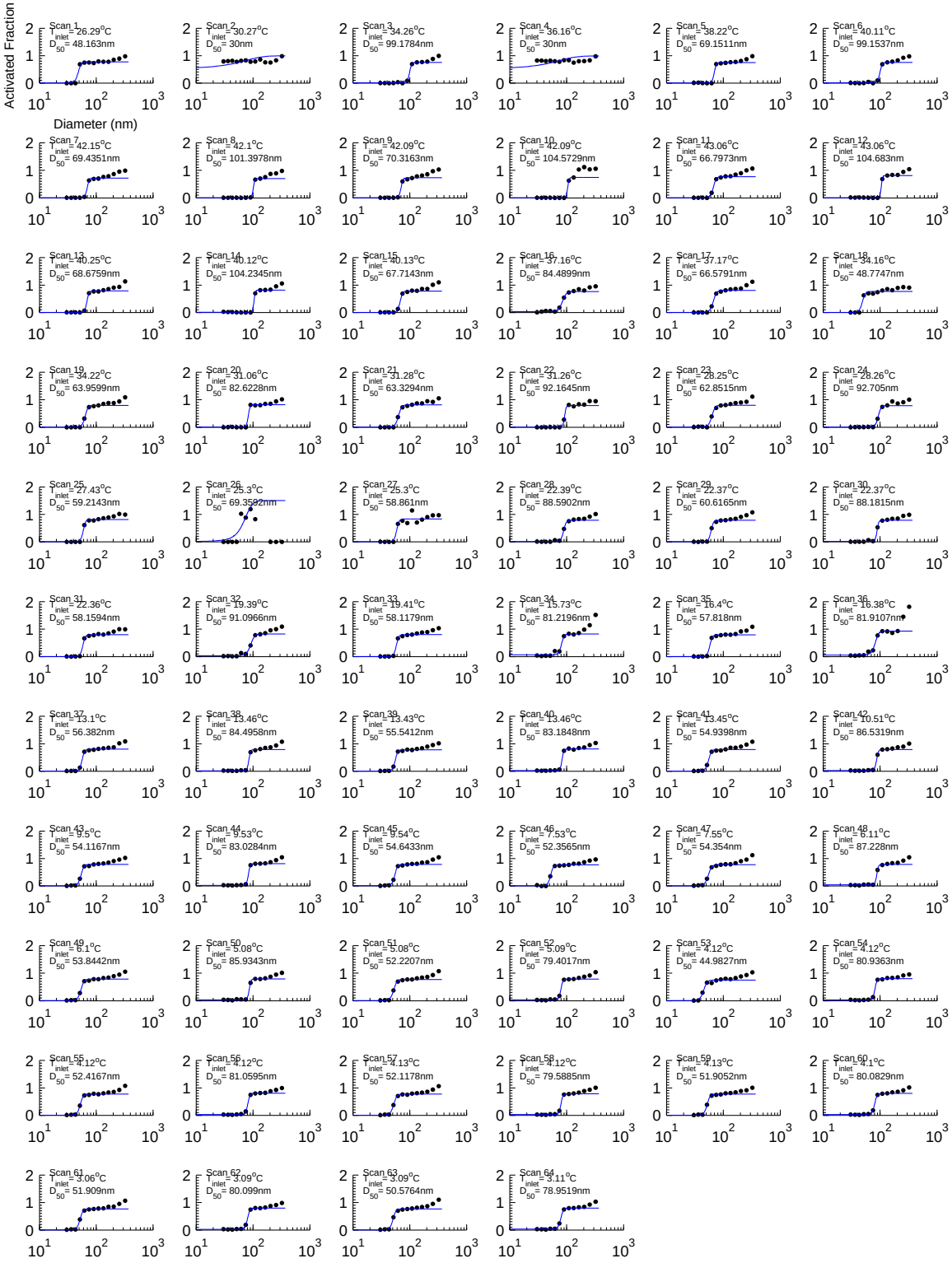

Figure A.10. Glucose (even scan numbers) and $(NH_4)_2SO_4$ activation curves. The activated fractions at each diameter are fit with a Sigmoid-Boltzmann curve (blue, see Table A.4).

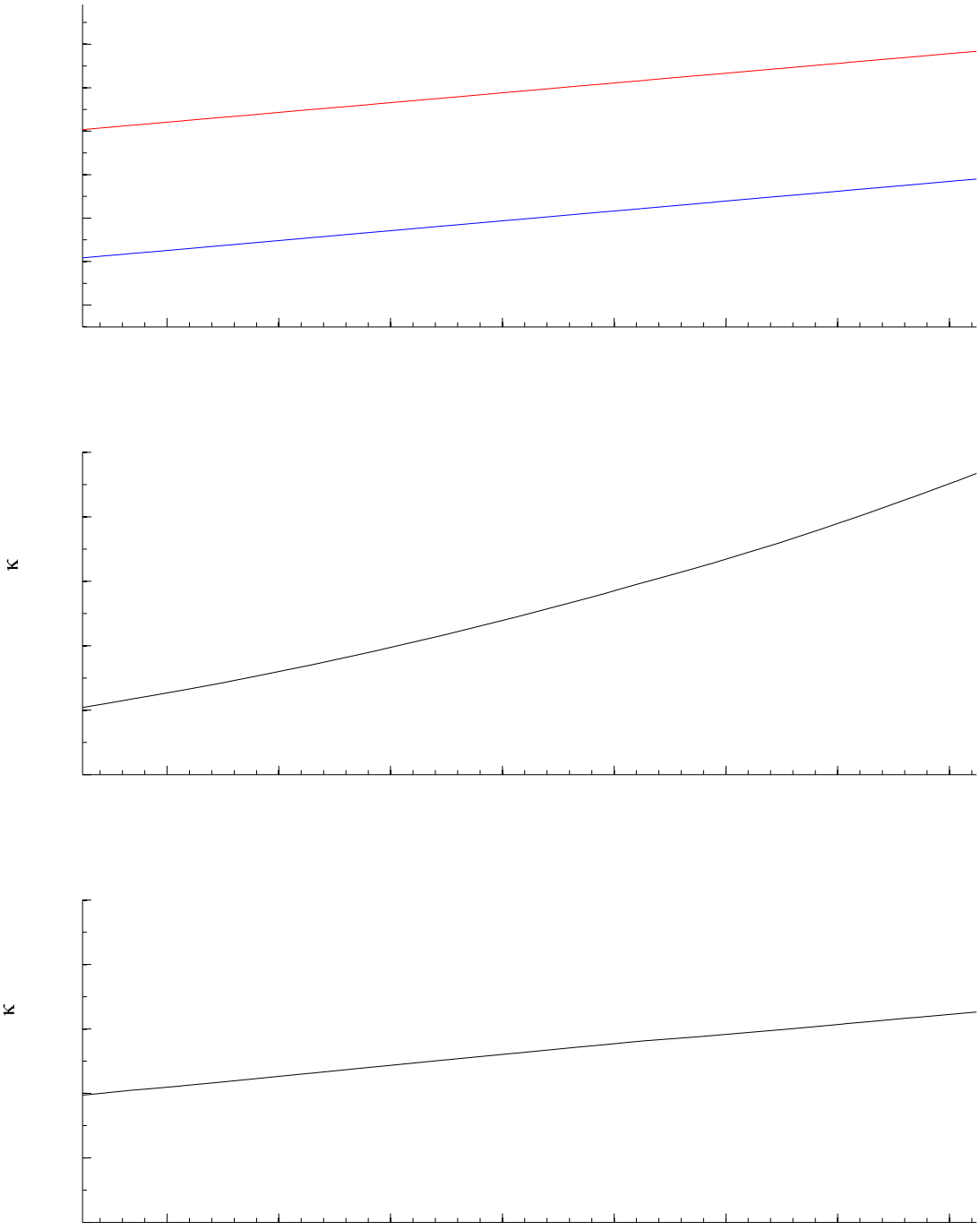

Figure A.11. Glucose and $(NH_4)_2SO_4$ activation diameters (top) and glucose κ values (center and bottom) versus temperature. Each number represents a scan from Figure A.10. Fit coefficients represent the solid line fit through the activation diameters, which then give the κ line.

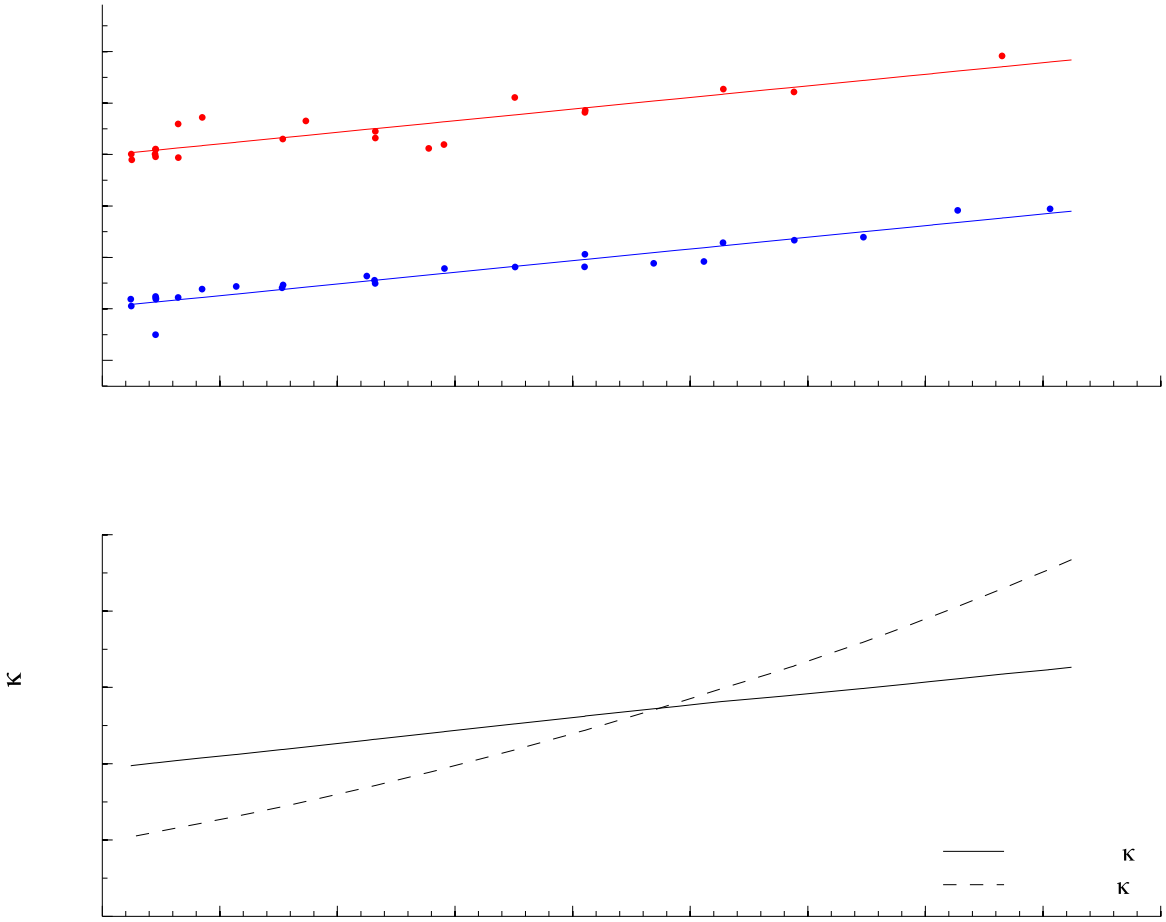

Figure A.12. Glucose and $(NH_4)_2SO_4$ activation diameters replotted without scan numbers (top) and κ values (bottom) plotted together.

Table A.5. Glucose data. Each line represents one diameter scan.

						Boltzmann Parameters:			
time	compound	ΔT	T_{box}	T_{inlet}	D_{50}	*A1*	*A2*	*dx*	excluded
34140	glucose	6	0.00	34.29	57.60	0.0009	0.8157	3.00	yes
34560	AS	6	35.79	37.29	66.65	0.0000	0.7943	4.95	yes
35040	glucose	6	37.98	37.23	102.74	0.0280	0.7847	3.00	yes
35460	AS	6	39.70	40.22	42.40	0.0000	0.7456	3.36	yes
35880	glucose	6	41.07	40.21	104.29	0.0182	0.7781	3.00	yes
36360	AS	6	42.09	43.32	70.47	0.0000	0.7858	3.00	no
36780	glucose	6	42.82	43.12	103.50	0.0185	0.7829	3.00	yes
37200	AS	6	42.91	43.13	70.58	0.0000	0.7848	3.00	yes
37680	glucose	6	42.57	43.12	105.97	0.0095	0.7925	3.00	yes
38100	AS	6	41.92	43.13	70.54	0.0000	0.7954	3.00	yes
38520	glucose	6	41.04	43.14	104.93	0.0061	0.8137	3.00	yes
39000	AS	6	39.98	43.12	70.04	0.0003	0.7979	3.00	yes
39420	glucose	6	38.79	40.14	74.01	0.0045	0.7878	3.00	yes
39840	AS	6	37.64	40.21	69.88	0.0000	0.8038	3.00	yes
40320	glucose	6	36.40	40.22	103.20	0.0012	0.8270	3.00	no
40740	AS	6	34.89	37.20	41.75	0.0000	0.7576	3.00	yes
41160	glucose	6	33.44	37.22	101.45	0.0012	0.8287	3.22	no
41640	AS	6	31.87	34.75	66.16	0.0000	0.8229	4.24	no
42060	glucose	6	30.15	34.28	102.84	0.0005	0.8344	3.05	no
42480	AS	6	28.68	34.29	64.29	0.0000	0.8252	5.33	no
42960	glucose	6	26.94	31.31	104.62	0.0079	0.8230	3.00	no
43380	AS	6	25.45	31.32	61.58	0.0000	0.8181	3.11	no
43800	glucose	6	23.71	28.36	97.55	0.0119	0.8645	8.68	no
44280	AS	6	22.22	28.37	60.26	0.0000	0.8230	3.00	no
44700	glucose	6	20.54	25.36	72.76	0.0296	0.8076	7.16	yes
45120	AS	6	19.12	25.38	59.25	0.0000	0.8216	3.00	no
45600	glucose	6	17.55	22.35	72.61	0.0000	0.8379	3.00	yes
46020	AS	6	16.21	22.43	59.05	0.0000	0.8352	3.00	no
46440	glucose	6	14.91	22.42	86.80	0.0000	0.8402	3.00	no
46920	AS	6	13.62	19.46	61.88	0.0000	0.8106	3.00	no
47340	glucose	6	12.73	19.47	86.04	0.0000	0.8561	3.00	no
47760	AS	6	11.62	19.46	57.43	0.0000	0.8476	3.00	no
48240	glucose	6	10.61	16.53	87.82	0.0000	0.8720	3.00	no
48660	AS	6	9.99	16.53	57.03	0.0000	0.8559	3.00	no
49080	glucose	6	9.16	16.51	85.79	0.0927	0.8182	3.00	no
49560	AS	6	8.31	13.44	56.94	0.0000	0.7998	3.22	no
49980	glucose	6	7.79	13.55	83.30	0.0188	0.8149	3.00	no
50400	AS	6	7.31	13.56	55.72	0.0000	0.7847	3.54	no
50880	glucose	6	6.66	13.57	82.50	0.0258	0.8077	3.00	no
51300	AS	6	6.11	13.57	54.72	0.0000	0.7899	3.07	no
51720	glucose	6	5.66	13.55	82.29	0.0339	0.8231	3.44	no
52200	AS	6	5.27	10.62	56.40	0.0000	0.7929	5.95	no
52620	glucose	6	5.16	10.63	81.85	0.0320	0.8132	3.00	no
53040	AS	6	3.83	10.60	54.58	0.0055	0.7954	3.30	no
53520	glucose	6	2.91	6.35	56.39	0.0001	0.8070	3.00	yes
53940	AS	6	2.56	6.43	54.74	0.0000	0.7921	3.57	no
54360	glucose	6	2.11	6.42	80.37	0.0433	0.8141	4.10	no
54840	AS	6	1.49	5.41	54.42	0.0064	0.7812	3.16	no
55260	glucose	6	0.99	4.42	69.24	0.0200	0.8146	3.00	yes
55680	AS	6	0.54	4.45	51.87	0.0000	0.7807	3.46	no
56160	glucose	6	0.15	4.43	78.71	0.0525	0.8150	3.97	no
56580	AS	6	-0.20	3.41	55.83	0.0158	0.7900	3.02	no
57000	glucose	6	-0.42	3.41	77.94	0.0580	0.8122	3.64	no
57480	AS	6	-0.70	3.42	50.84	0.0047	0.7824	3.00	no
57900	glucose	6	-0.94	3.42	77.55	0.0546	0.8213	4.53	no
58320	AS	6	-1.14	2.45	56.82	0.0280	0.7924	3.00	no
58800	glucose	6	-1.27	2.46	78.28	0.0584	0.8130	4.04	no
59220	AS	6	-1.47	2.47	50.35	0.0000	0.7748	3.00	no
59640	glucose	6	-1.64	2.46	77.81	0.0620	0.8098	4.00	no

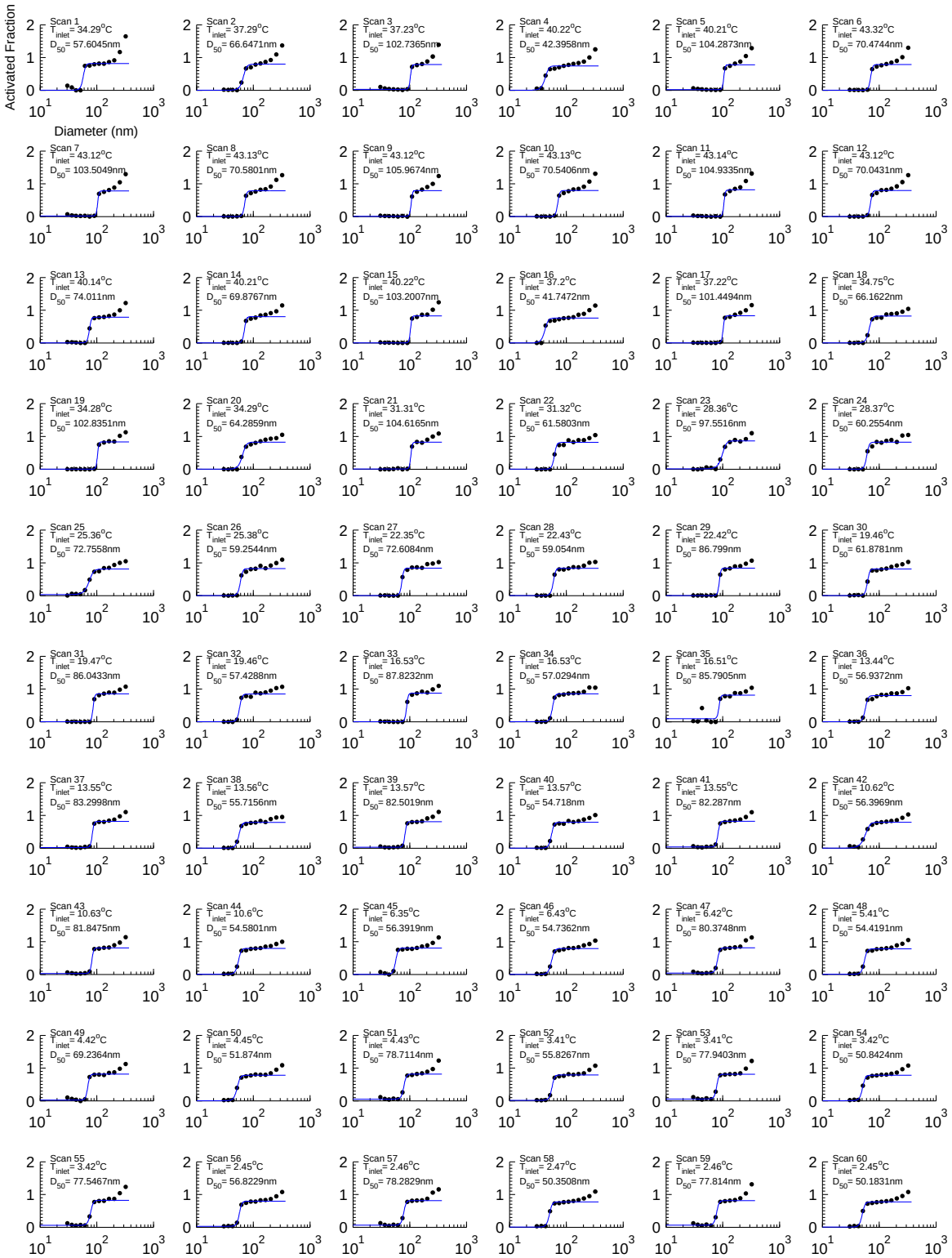

Figure A.13. Glucose (odd scan numbers) and $(NH_4)_2SO_4$ activation curves. The activated fractions at each diameters are fit with a Sigmoid-Boltzmann curve (blue, see Table A.5).

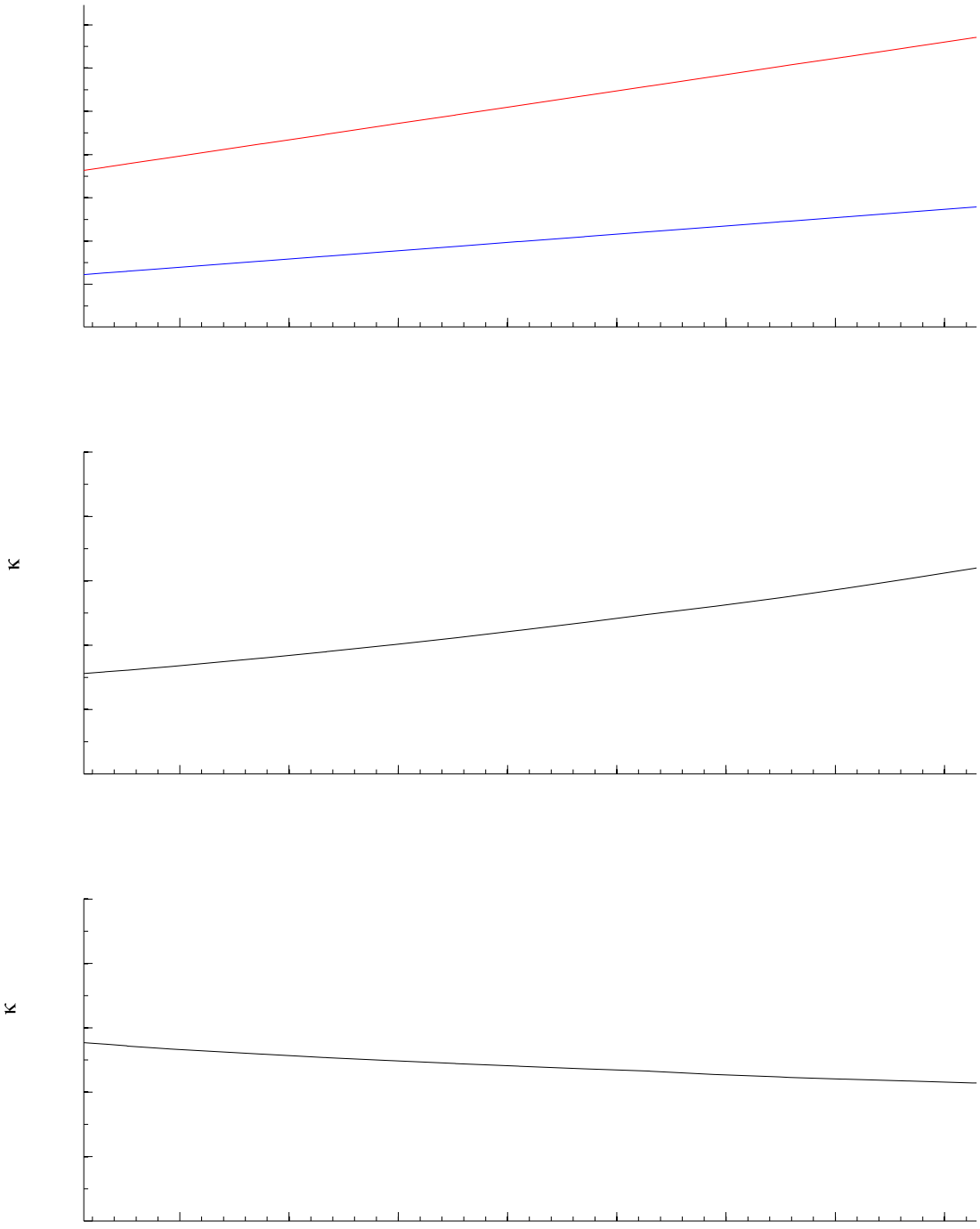

Figure A.14. Glucose and $(NH_4)_2SO_4$ activation diameters (top) and glucose κ values (center and bottom) versus temperature. Each number represents a scan from Figure A.13. Fit coefficients represent the solid line fit through the activation diameters, which then give the κ line.

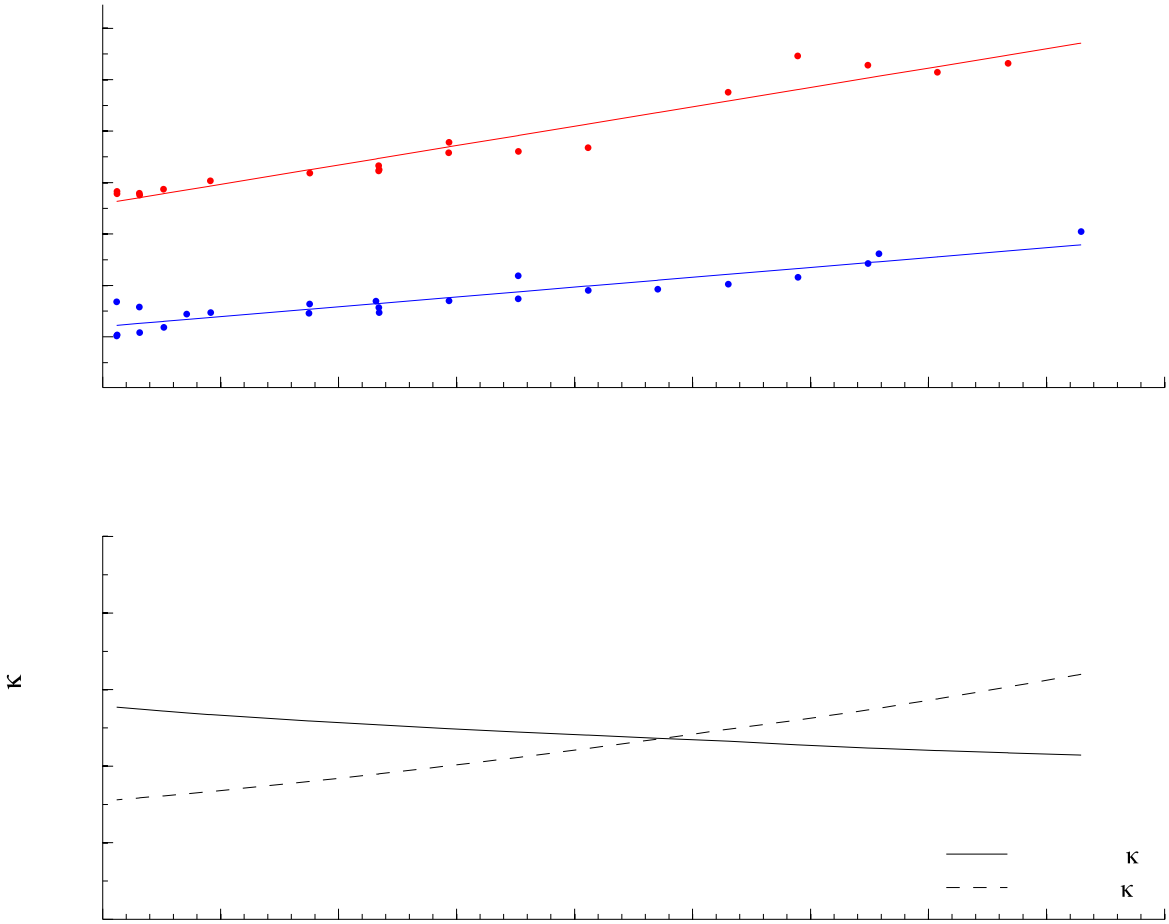

Figure A.15. Glucose and $(NH_4)_2SO_4$ activation diameters replotted without scan numbers (top) and κ values (bottom) plotted together.

Table A.6. Glucose data. Each line represents one diameter scan.

						Boltzmann Parameters:			
time	compound	ΔT	T_{box}	T_{inlet}	D_{50}	*A1*	*A2*	*dx*	excluded
37440	AS	6	0.00	22.21	30.00	0.3000	1.5000	3.00	yes
37920	glucose	6	10.00	25.27	76.51	0.0371	0.8891	3.00	yes
38340	AS	6	10.00	28.20	47.89	0.0000	0.8272	3.00	yes
38760	glucose	6	10.00	31.14	73.36	0.0589	0.8324	3.00	yes
39240	AS	6	10.00	34.10	57.61	0.0089	0.7905	3.00	yes
39660	glucose	6	11.00	37.10	87.16	0.0375	0.7993	3.00	yes
40080	AS	6	11.00	37.10	69.52	0.0000	0.7882	3.00	no
40560	glucose	6	11.00	40.06	102.05	0.0190	0.8190	3.00	no
40980	AS	6	11.00	40.04	69.80	0.0000	0.7896	3.00	no
41400	glucose	6	11.00	40.04	103.01	0.0053	0.8392	3.00	no
41880	AS	6	11.00	40.02	69.44	0.0000	0.7981	3.00	no
42300	glucose	6	11.00	40.04	101.83	0.0033	0.8169	3.00	no
42720	AS	6	11.00	40.05	68.99	0.0000	0.8135	3.00	no
43200	glucose	6	12.00	36.93	89.32	0.0062	0.8199	3.00	yes
43620	AS	6	12.00	37.10	69.40	0.0000	0.8228	3.00	no
44040	glucose	6	12.00	37.10	100.43	0.0027	0.8464	3.00	no
44520	AS	6	12.00	34.13	73.35	0.0318	0.8445	7.21	yes
44940	glucose	6	12.00	34.17	101.64	0.0042	0.8924	3.00	no
45360	AS	6	12.00	34.13	66.08	0.0015	0.8341	3.00	no
45840	glucose	6	12.00	31.18	99.80	0.0042	0.8552	3.00	no
46260	AS	6	12.00	31.18	30.00	0.3000	0.8471	40.00	yes
46680	glucose	6	12.00	28.13	49.68	0.0000	0.8153	3.00	yes
47160	AS	6	1.00	28.19	61.87	0.0000	0.8443	3.00	no
47580	glucose	6	1.00	24.76	93.45	0.0057	0.8531	4.37	no
48000	AS	6	1.00	25.21	61.12	0.0000	0.8392	3.00	no
48480	glucose	6	1.00	25.23	90.27	0.0021	0.8729	3.00	no
48900	AS	6	1.00	22.27	63.63	0.0000	0.8362	3.00	no
49320	glucose	6	1.00	22.29	89.14	0.0024	0.8507	3.00	no
49800	AS	6	1.00	19.28	40.05	0.0000	0.8335	3.00	yes
50220	glucose	6	1.00	19.33	86.45	0.0000	0.8518	3.00	no
50640	AS	6	2.00	19.32	57.57	0.0000	0.8444	3.00	no
51120	glucose	6	2.00	16.29	50.84	0.0000	0.8189	5.34	yes
51540	AS	6	2.00	16.30	57.76	0.0000	0.8388	3.00	no
51960	glucose	6	2.00	16.33	84.98	0.0000	0.8910	3.00	no
52440	AS	6	2.00	13.33	38.49	0.0000	0.8286	3.00	yes
52860	glucose	6	2.00	13.36	84.21	0.0000	0.8785	3.00	no
53280	AS	6	2.00	13.36	56.01	0.0000	0.8534	3.00	no
53760	glucose	6	2.00	10.18	82.22	0.0000	0.8881	3.00	no
54180	AS	6	3.00	10.39	57.15	0.0000	0.8491	3.00	no
54600	glucose	6	3.00	10.39	84.66	0.0033	0.8906	3.00	no
55080	AS	6	3.00	10.40	55.75	0.0000	0.8366	3.00	no
55500	glucose	6	3.00	6.48	87.56	0.0127	0.8808	3.00	no
55920	AS	6	3.00	6.48	55.30	0.0000	0.8398	3.00	no
56400	glucose	6	3.00	5.48	83.15	0.0085	0.8956	3.00	no
56820	AS	6	3.00	5.51	55.76	0.0000	0.8496	3.00	no
57240	glucose	6	3.00	4.51	82.10	0.0052	0.8711	3.00	no
57720	AS	6	4.00	4.56	55.34	0.0000	0.8360	3.00	no
58140	glucose	6	4.00	4.55	81.76	0.0041	0.8725	3.00	no
58560	AS	6	4.00	3.52	54.46	0.0000	0.8363	3.00	no
59040	glucose	6	4.00	3.53	82.54	0.0092	0.8846	3.00	no
59460	AS	6	4.00	3.50	53.08	0.0010	0.8384	3.00	no

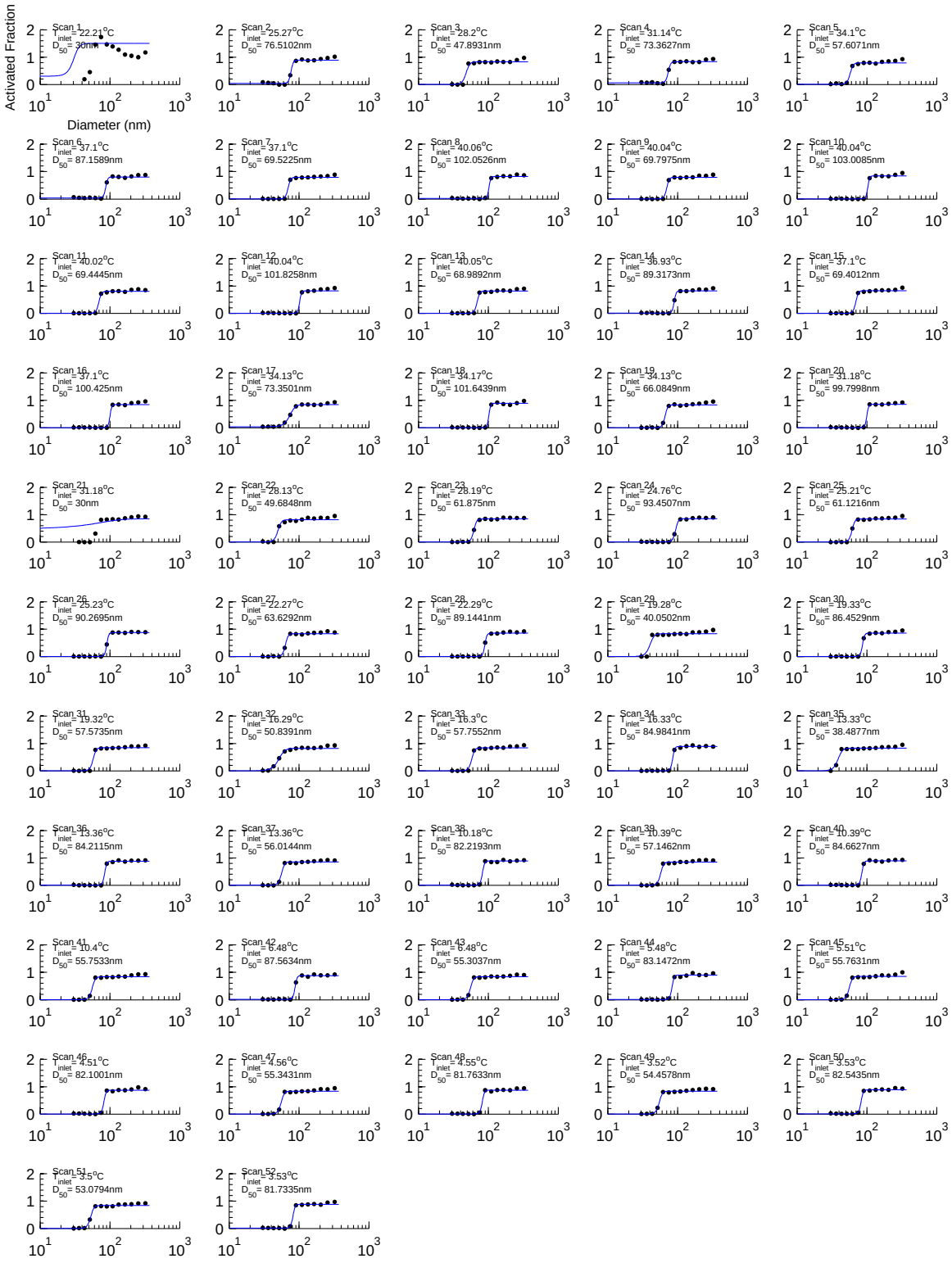

Figure A.16. Glucose (even scan numbers) and $(NH_4)_2SO_4$ activation curves. The activated fractions at each diameter fare fit with a Sigmoid-Boltzmann curve (blue, see Table A.6).

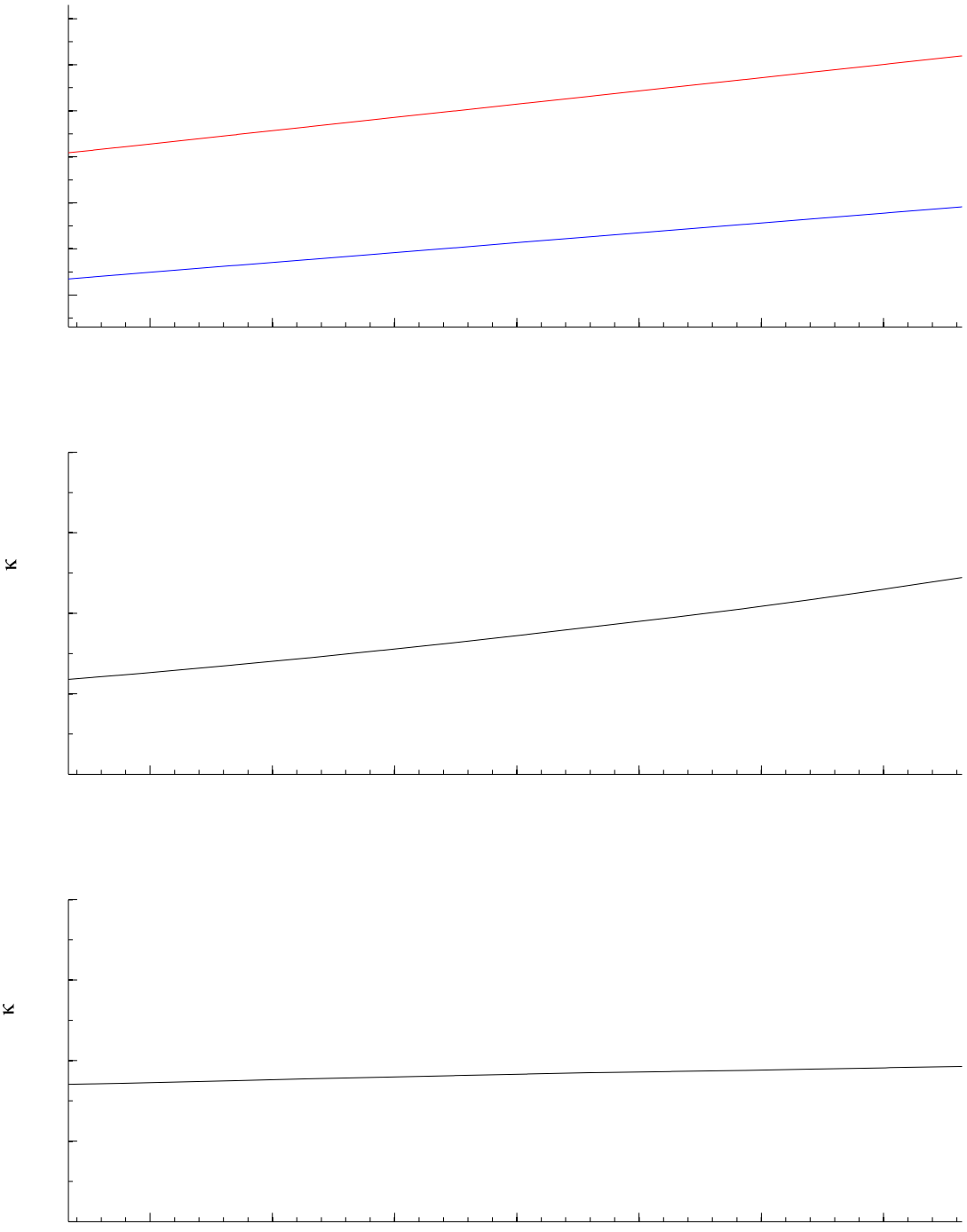

Figure A.17. Glucose and $(NH_4)_2SO_4$ activation diameters (top) and glucose κ values (center and bottom) versus temperature. Each number represents a scan from Figure A.16. Fit coefficients represent the solid line fit through the activation diameters, which then give the κ line.

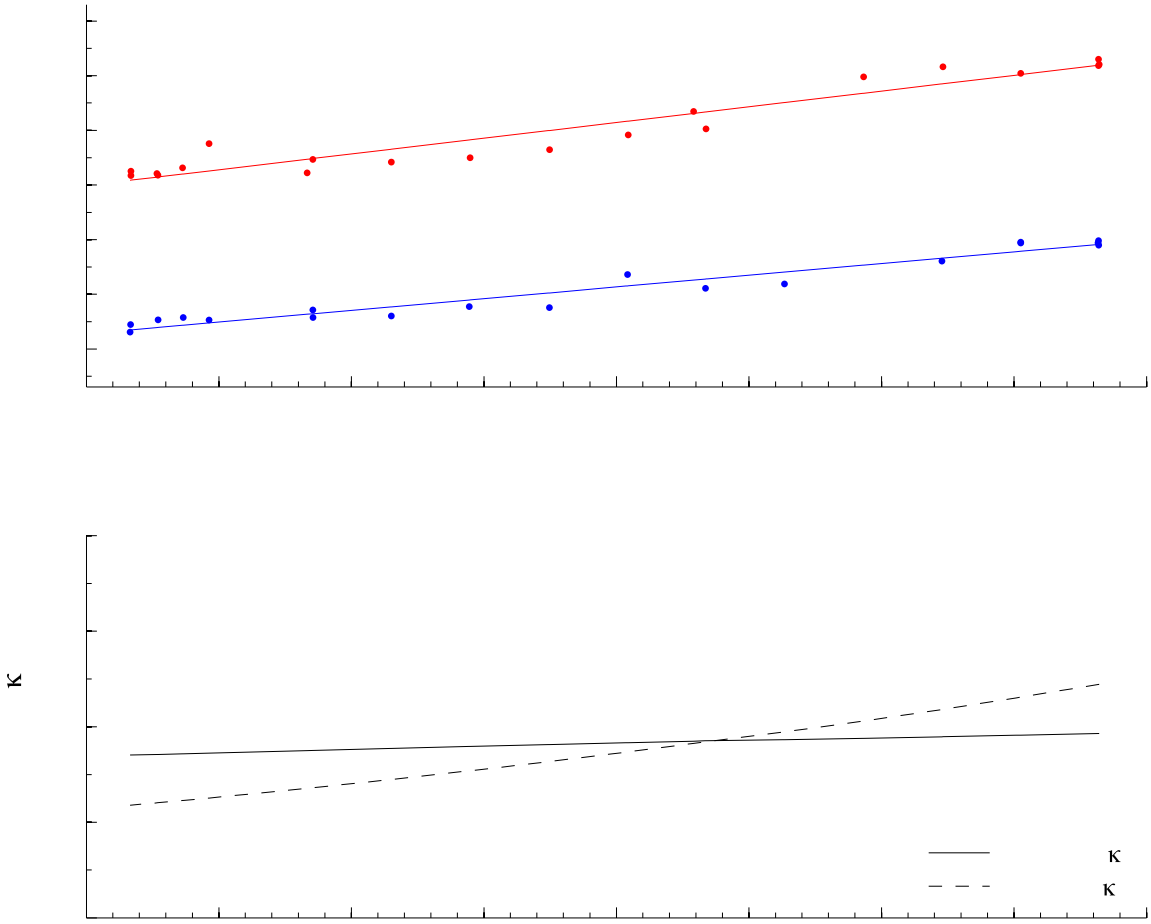

Figure A.18. Glucose and $(NH_4)_2SO_4$ activation diameters replotted without scan numbers (top) and κ values (bottom) plotted together.

Table A.7. Glutamine data. Each line represents one diameter scan.

						Boltzmann Parameters:			
time	compound	ΔT	T_{box}	T_{inlet}	D_{50}	*A1*	*A2*	*dx*	excluded
35880	glutamine	6	0.00	31.76	84.94	0.0025	0.7450	3.00	yes
36300	AS	6	31.00	34.69	67.18	0.0000	0.7832	4.81	yes
36720	glutamine	6	34.66	34.53	93.90	0.0000	0.7735	6.28	no
37200	AS	6	37.29	37.48	60.21	0.0000	0.7586	3.00	no
37620	glutamine	6	39.20	40.57	101.10	0.0038	0.8088	5.02	no
38040	AS	6	40.47	40.44	67.89	0.0013	0.7744	3.70	no
38520	glutamine	6	40.96	40.45	99.16	0.0026	0.7805	3.91	no
38940	AS	6	40.83	40.43	69.61	0.0000	0.7885	3.04	yes
39360	glutamine	6	40.31	40.43	99.09	0.0008	0.7723	3.55	yes
39840	AS	6	39.45	40.45	70.23	0.0001	0.8036	3.00	yes
40260	glutamine	6	38.37	40.46	100.59	0.0024	0.7933	3.70	yes
40680	AS	6	37.12	40.43	69.09	0.0000	0.8156	3.72	yes
41160	glutamine	6	35.76	37.24	97.85	0.0041	0.8226	3.65	yes
41580	AS	6	34.43	37.48	69.07	0.0000	0.8091	3.18	yes
42000	glutamine	6	33.56	37.48	99.78	0.0028	0.8352	5.19	no
42480	AS	6	32.36	33.85	67.47	0.0000	0.8222	4.24	no
42900	glutamine	6	31.01	34.48	98.27	0.0000	0.8014	4.41	no
43320	AS	6	29.85	34.47	65.57	0.0000	0.8122	4.55	no
43800	glutamine	6	28.37	31.47	68.53	0.0000	0.8070	3.00	yes
44220	AS	6	27.03	31.54	64.99	0.0000	0.8246	4.97	no
44640	glutamine	6	25.64	31.53	93.36	0.0000	0.8407	6.42	yes
45120	AS	6	24.06	28.58	69.14	0.0084	0.8300	3.62	yes
45540	glutamine	6	22.76	28.58	88.47	0.0042	0.8104	3.01	no
45960	AS	6	21.21	25.63	43.41	0.0000	0.8122	4.82	yes
46440	glutamine	6	19.87	25.70	88.26	0.0000	0.8181	3.00	no
46860	AS	6	18.45	25.68	59.65	0.0000	0.8359	3.00	no
47280	glutamine	6	17.09	22.73	91.90	0.0000	0.8401	6.23	no
47760	AS	6	16.10	22.74	59.15	0.0000	0.8173	3.00	no
48180	glutamine	6	14.88	19.40	86.18	0.0000	0.8422	3.00	no
48600	AS	6	13.91	19.73	58.51	0.0000	0.8325	3.00	no
49080	glutamine	6	13.14	19.74	84.97	0.0000	0.8503	3.00	no
49500	AS	6	12.24	19.73	57.75	0.0000	0.8481	3.00	no
49920	glutamine	6	11.45	16.77	87.53	0.0324	0.8334	3.00	no
50400	AS	6	11.06	16.80	57.92	0.0000	0.8484	3.00	no
50820	glutamine	6	10.39	16.78	84.46	0.0000	0.8390	3.00	no
51240	AS	6	9.77	16.78	51.61	0.0116	0.7892	3.00	no
51720	glutamine	6	9.19	16.79	82.75	0.0293	0.8212	3.41	no
52140	AS	6	8.74	13.81	30.00	0.3000	0.8924	40.00	yes
52560	glutamine	6	8.55	13.84	82.52	0.0319	0.8157	3.55	no
53040	AS	6	6.95	13.83	56.04	0.0103	0.8010	3.09	no
53460	glutamine	6	5.73	13.82	80.31	0.0348	0.8280	4.47	no
53880	AS	6	4.87	8.78	30.00	0.3000	0.8116	21.25	yes
54360	glutamine	6	4.55	8.89	81.80	0.0356	0.8071	3.71	no
54780	AS	6	4.02	7.89	54.17	0.0000	0.7971	3.55	no
55200	glutamine	6	3.40	7.92	80.79	0.0376	0.8194	3.83	no
55680	AS	6	2.79	6.90	57.32	0.0000	0.8001	3.00	no
56100	glutamine	6	2.31	6.91	78.51	0.0458	0.8218	4.93	no
56520	AS	6	1.84	5.95	56.77	0.0104	0.7988	3.00	no
57000	glutamine	6	1.46	5.93	79.17	0.0516	0.8131	4.09	no
57420	AS	6	1.14	4.89	53.43	0.0000	0.8002	3.92	no
57840	glutamine	6	0.84	4.93	75.29	0.0483	0.8014	3.24	no
58320	AS	6	0.54	4.94	51.56	0.0000	0.7876	3.48	no
58740	glutamine	6	0.28	4.91	75.73	0.0609	0.8109	3.82	no
59160	AS	6	0.05	4.94	51.17	0.0000	0.7915	3.16	no
59640	glutamine	6	-0.16	3.96	79.23	0.0499	0.8081	3.67	no
60060	AS	6	-0.31	3.97	52.17	0.0000	0.7854	3.58	no
60480	glutamine	6	-0.49	3.95	76.17	0.0514	0.8096	3.79	no
60960	AS	6	-0.67	3.96	51.94	0.0000	0.7941	3.51	no
61380	glutamine	6	-0.80	3.96	76.45	0.0415	0.8185	4.63	no

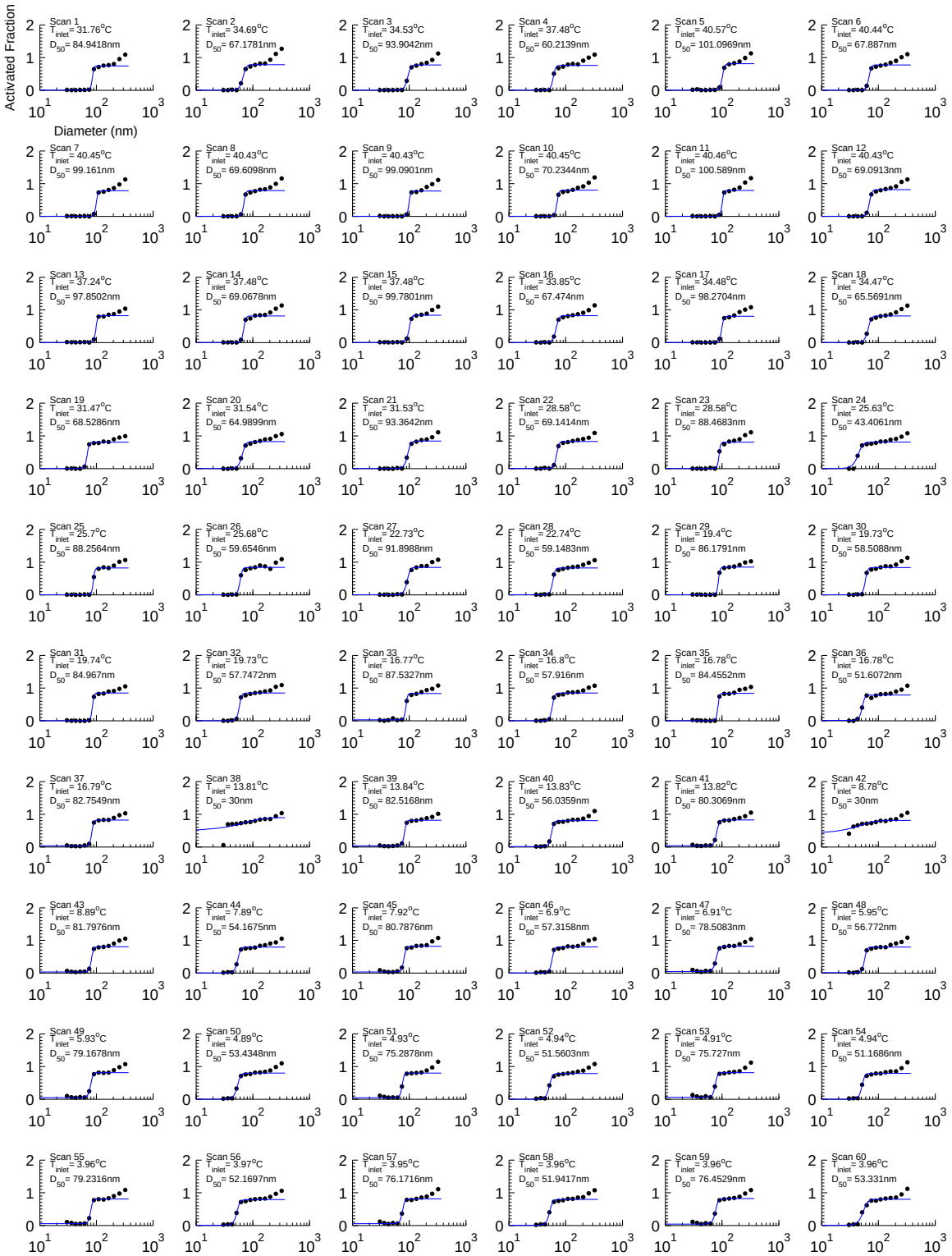

Figure A.19. Glutamine (odd scan numbers) and $(NH_4)_2SO_4$ activation curves. The activated fractions at each diameter are fit with a Sigmoid-Boltzmann curve (blue, see Table A.7).

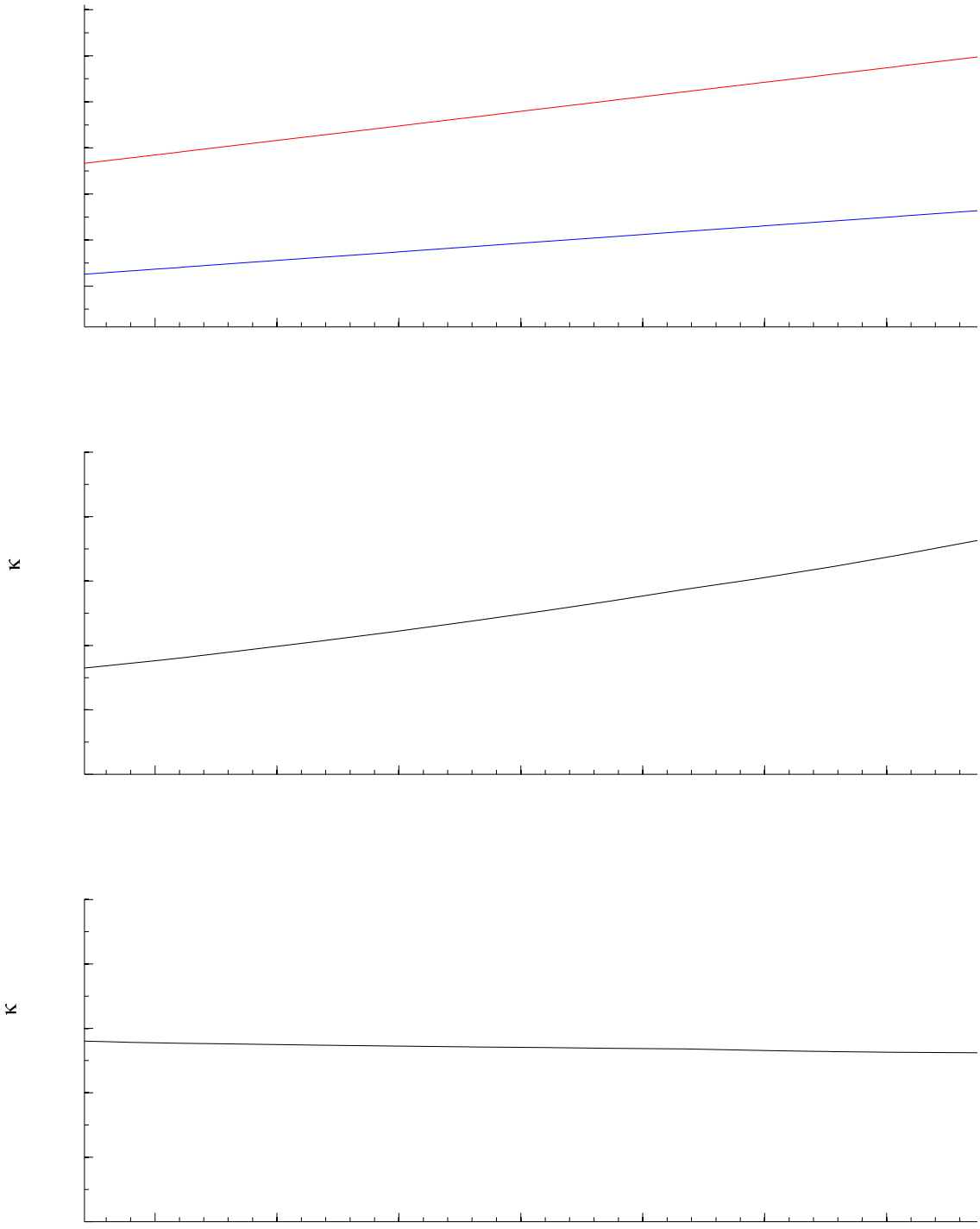

Figure A.20. Glutamine and $(NH_4)_2SO_4$ activation diameters (top) and glutamine κ values (center and bottom) versus temperature. Each number represents a scan from Figure A.19. Fit coefficients represent the solid line fit through the activation diameters, which give the κ line.

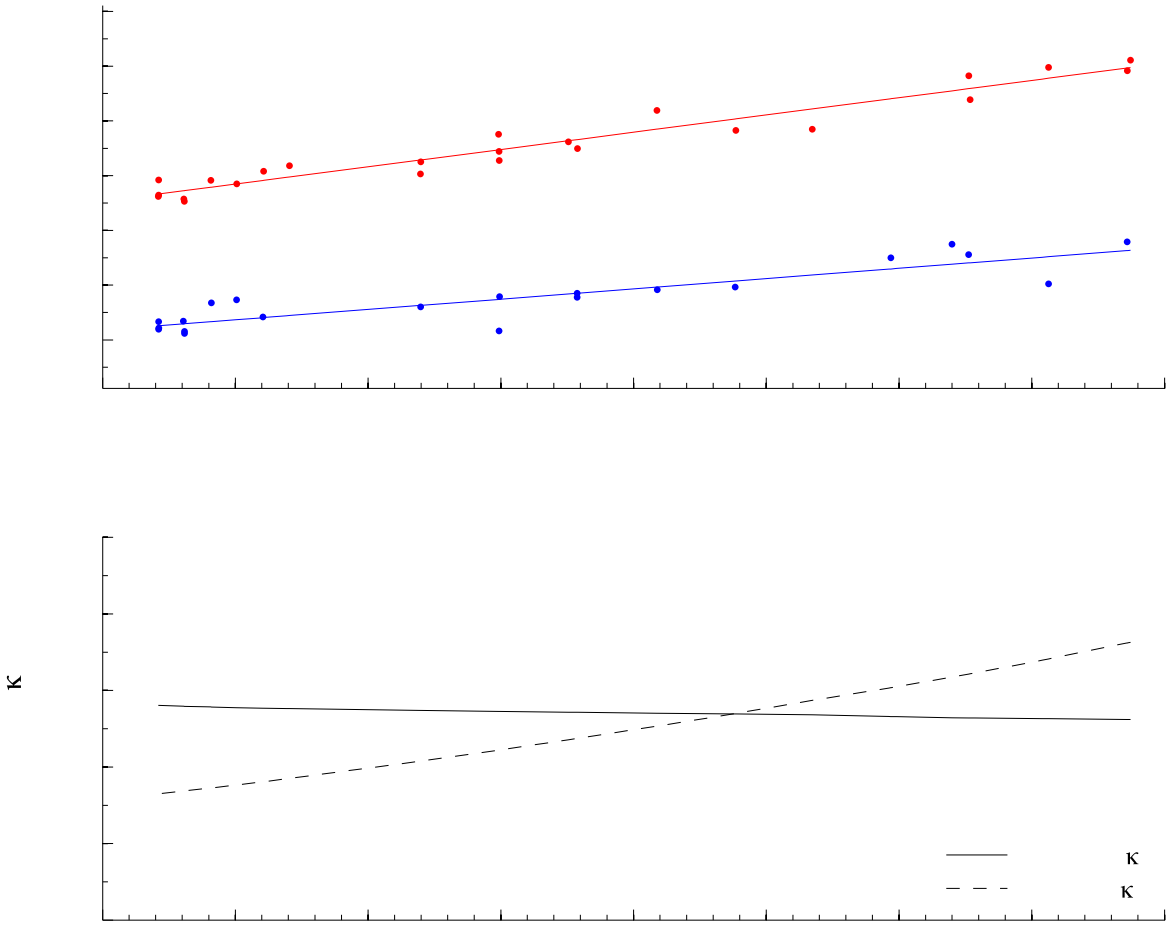

Figure A21. Glutamine and $(NH_4)_2SO_4$ activation diameters replotted without scan numbers (top) and κ values (bottom) plotted together.

Table A.8. Glutamine data. Each line represents one diameter scan.

						Boltzmann Parameters:			
time	compound	ΔT	T_{box}	T_{inlet}	D_{50}	*A1*	*A2*	*dx*	excluded
34080	glutamine	6	0.00	30.79	30.00	0.3000	1.3429	40.00	yes
34500	AS	6	32.80	33.80	30.00	0.3000	0.9721	40.00	yes
34920	glutamine	6	35.84	36.76	41.53	0.0000	0.7566	5.47	yes
35400	AS	6	38.07	39.87	68.83	0.0008	0.7802	3.35	no
35820	glutamine	6	39.76	39.70	94.54	0.0076	0.7720	4.08	yes
36240	AS	6	41.13	39.69	69.46	0.0005	0.7961	3.18	no
36720	glutamine	6	41.91	39.69	101.64	0.0040	0.7949	4.09	no
37140	AS	6	41.93	39.67	70.44	0.0003	0.8064	3.00	no
37560	glutamine	6	41.46	39.69	101.60	0.0053	0.8013	3.66	no
38040	AS	6	40.61	39.68	70.19	0.0004	0.8110	3.11	no
38460	glutamine	6	39.56	39.67	101.14	0.0056	0.8101	3.92	no
38880	AS	6	38.26	39.69	68.75	0.0002	0.8206	3.38	no
39360	glutamine	6	36.86	39.69	97.70	0.0046	0.8252	4.38	no
39780	AS	6	35.30	39.01	67.54	0.0000	0.8239	3.87	no
40200	glutamine	6	33.70	36.75	100.73	0.0019	0.8111	3.00	no
40680	AS	6	32.26	36.75	67.72	0.0000	0.8223	3.58	no
41100	glutamine	6	30.46	33.71	70.14	0.0000	0.8178	11.78	yes
41520	AS	6	28.79	33.74	64.80	0.0000	0.8245	4.58	no
42000	glutamine	6	26.97	30.76	57.03	0.0000	0.8109	3.00	yes
42420	AS	6	25.22	30.79	61.84	0.0000	0.8056	3.21	no
42840	glutamine	6	23.38	27.79	49.97	0.0000	0.8118	3.00	yes
43320	AS	6	21.70	27.84	60.24	0.0000	0.8228	3.00	no
43740	glutamine	6	19.94	24.83	56.62	0.0000	0.8339	3.00	yes
44160	AS	6	18.40	24.88	59.09	0.0000	0.8281	3.00	no
44640	glutamine	6	16.90	21.75	86.88	0.0002	0.8601	3.00	no
45060	AS	6	15.48	21.92	59.41	0.0000	0.8382	3.00	no
45480	glutamine	6	14.29	21.93	84.98	0.0000	0.8589	3.00	no
45960	AS	6	13.02	18.99	59.93	0.0000	0.8539	6.31	no
46380	glutamine	6	12.12	18.96	84.33	0.0000	0.8781	3.00	no
46800	AS	6	11.07	18.98	57.77	0.0000	0.8684	3.00	no
47280	glutamine	6	10.09	16.01	87.19	0.0132	0.8732	3.27	no
47700	AS	6	9.50	16.06	56.88	0.0000	0.8712	3.00	no
48120	glutamine	6	8.67	16.04	83.39	0.0010	0.8721	3.00	no
48600	AS	6	7.89	16.04	56.42	0.0000	0.8798	3.00	no
49020	glutamine	6	7.24	11.09	84.99	0.0289	0.8135	4.24	no
49440	AS	6	7.16	11.10	56.51	0.0000	0.7966	3.00	no
49920	glutamine	6	6.55	10.06	81.74	0.0169	0.8128	3.32	no
50340	AS	6	5.93	10.07	55.55	0.0027	0.7971	3.07	no
50760	glutamine	6	5.34	9.09	86.13	0.0216	0.8060	3.41	no
51240	AS	6	4.82	8.10	54.59	0.0009	0.7824	3.43	no
51660	glutamine	6	4.33	8.16	80.97	0.0204	0.7970	3.00	no
52140	AS	6	3.91	7.08	54.93	0.0074	0.7802	3.00	no
52560	glutamine	6	3.54	7.13	93.57	0.0097	0.8375	6.75	no
52980	AS	6	3.25	7.12	64.84	0.0000	0.9276	6.31	yes
53460	glutamine	6	2.93	6.18	97.31	0.0130	0.8414	6.64	no
53880	AS	6	2.66	6.16	67.36	0.0000	0.9625	5.56	yes
54300	glutamine	6	2.42	6.16	95.75	0.0073	0.8464	7.22	no
54780	AS	6	2.19	5.16	67.15	0.0000	0.9742	6.19	yes
55200	glutamine	6	1.99	5.19	100.22	0.0149	0.8603	5.35	no
55620	AS	6	1.81	5.20	68.24	0.0000	0.9588	5.48	yes
56100	glutamine	6	1.62	5.20	98.06	0.0182	0.8447	6.25	no
56520	AS	6	1.49	5.18	67.06	0.0000	0.9542	5.60	yes
56940	glutamine	6	1.36	5.20	98.73	0.0146	0.8766	6.61	no
57420	AS	6	1.24	5.20	67.57	0.0000	0.9669	5.95	yes
57840	glutamine	6	1.14	4.17	86.47	0.0138	0.8050	5.92	no
58260	AS	6	1.04	4.18	65.11	0.0000	0.9621	5.66	yes
58740	glutamine	6	0.04	3.21	90.93	0.0162	0.8185	5.11	no

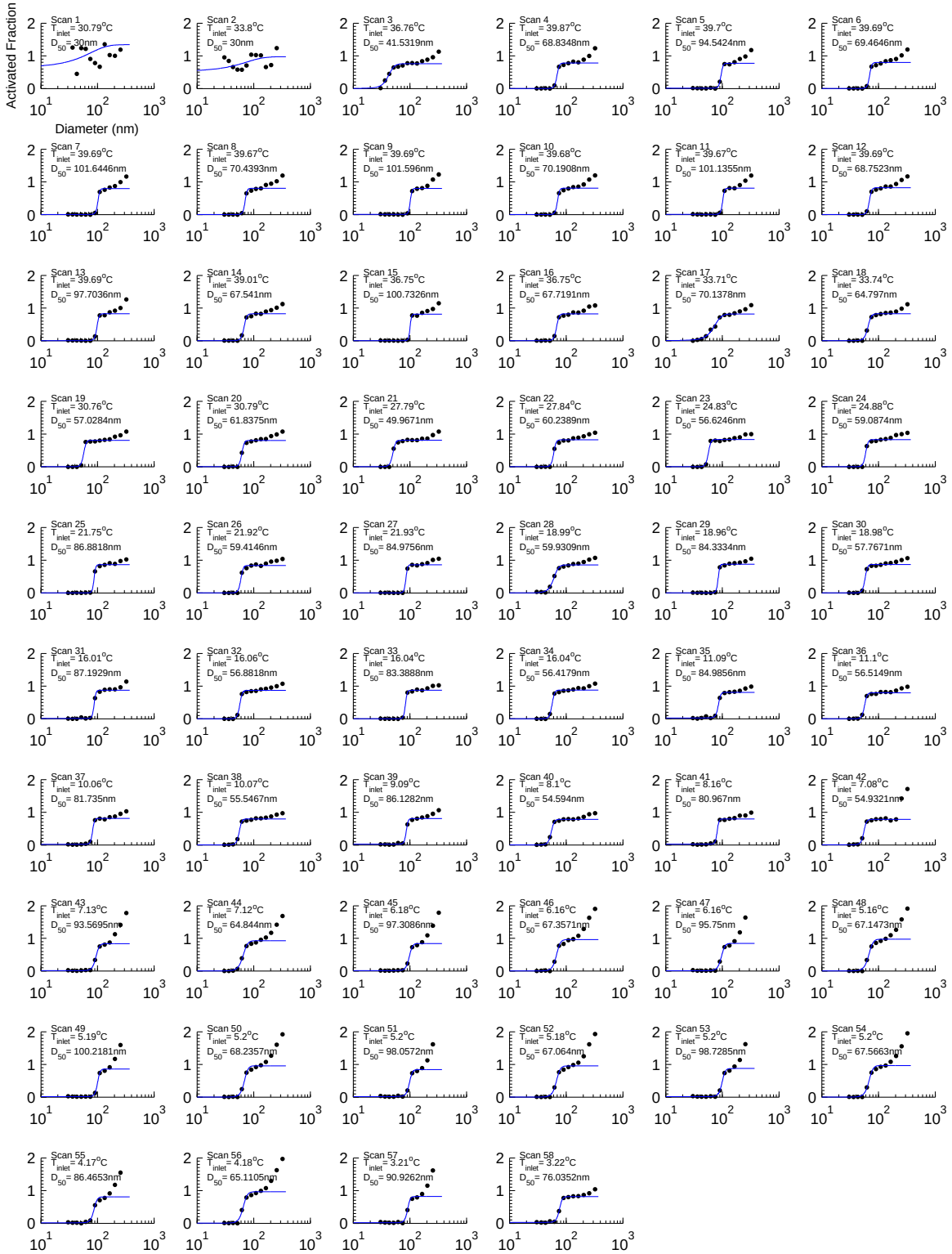

Figure A.22. Glutamine (odd scan numbers) and $(NH_4)_2SO_4$ activation curves. The activated fractions at each diameter are fit with a Sigmoid-Boltzmann curve (blue, see Table A.8).

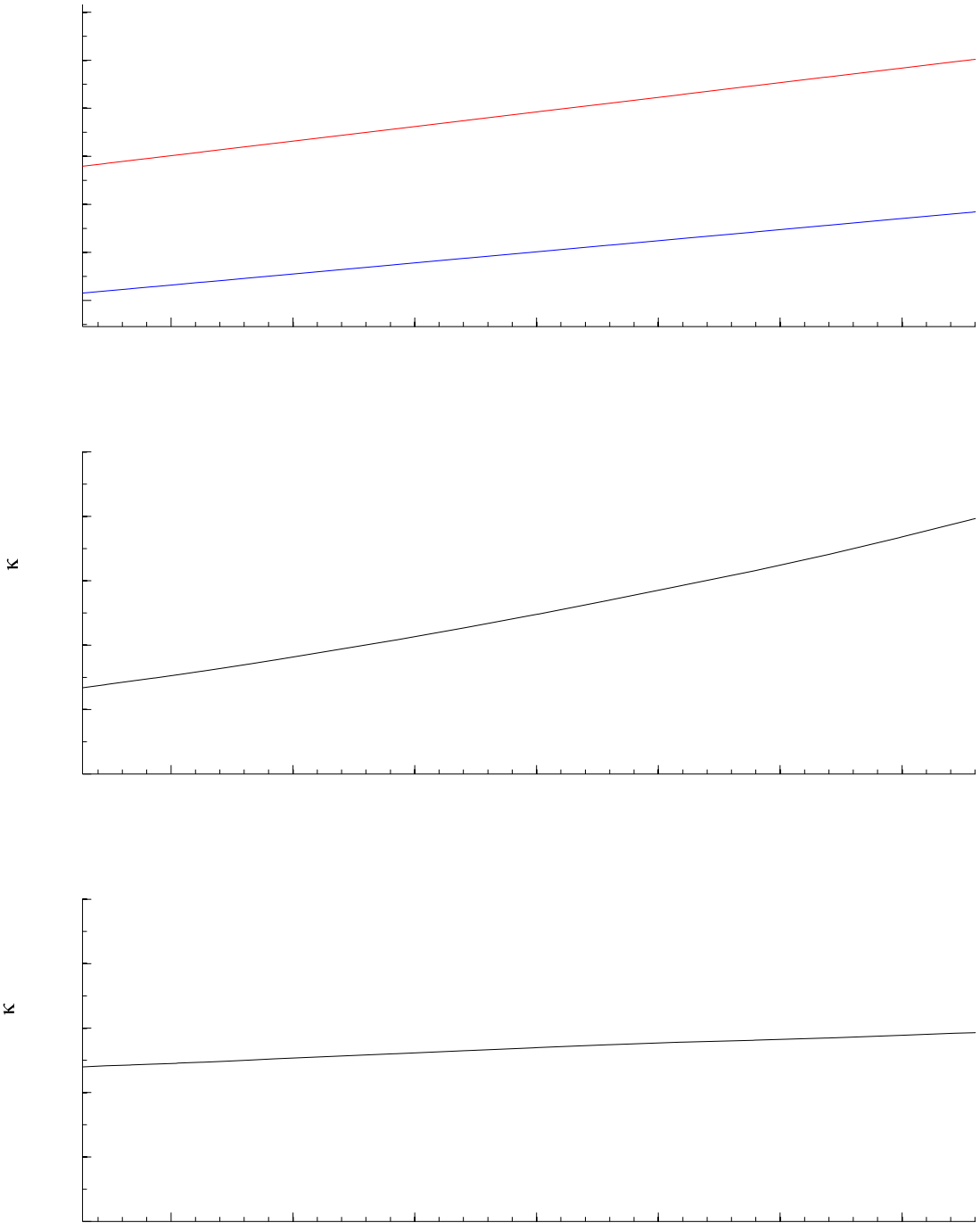

Figure A.23. Glutamine and $(NH_4)_2SO_4$ activation diameters (top) and glutamine κ values (center and bottom) versus temperature. Each number represents a scan from Figure A.22. Fit coefficients represent the solid line fit through the activation diameters, which then give the κ line.

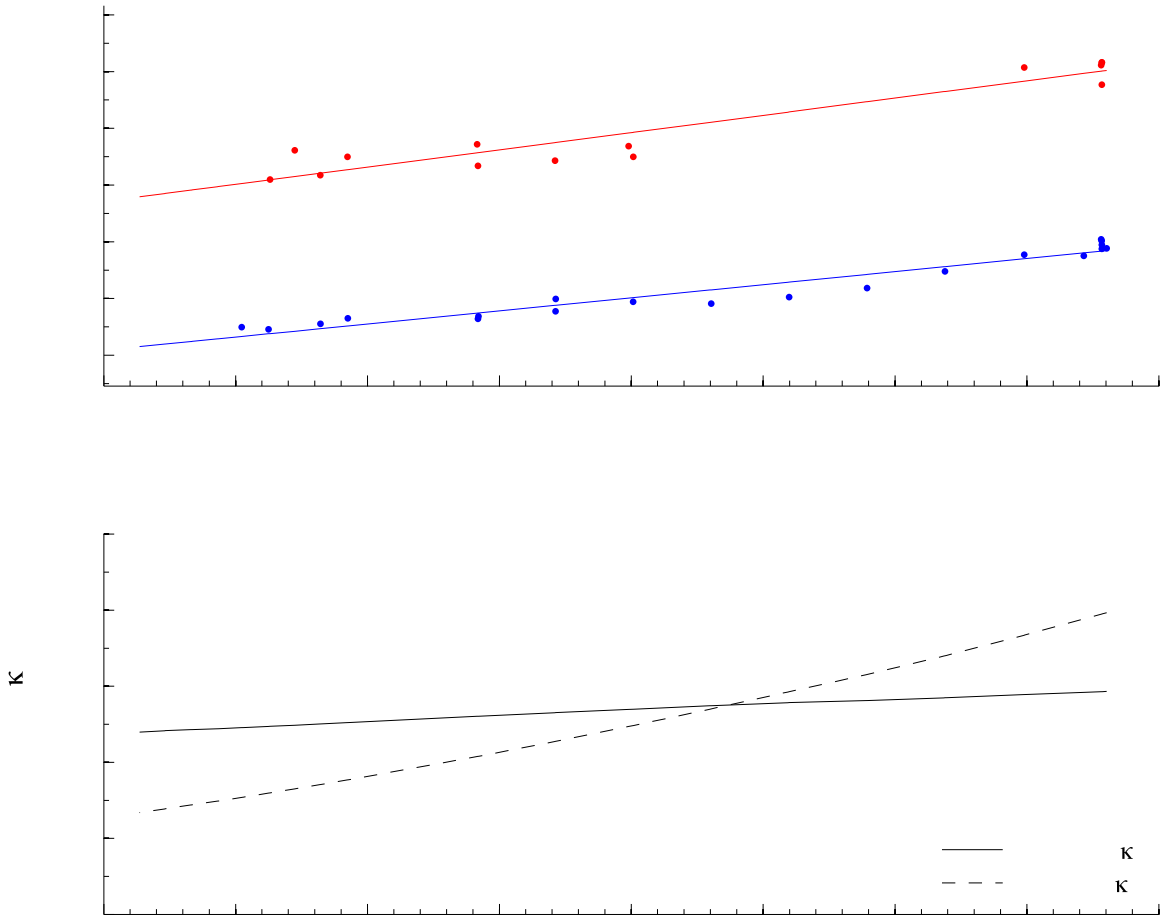

Figure A.24. Glutamine and $(NH_4)_2SO_4$ activation diameters replotted without scan numbers (top) and κ values (bottom) plotted together.

Table A.9. Ketoglutaric acid data. Each line represents one diameter scan.

						Boltzmann Parameters:			
time	compound	ΔT	T_{box}	T_{inlet}	D_{50}	*A1*	*A2*	*dx*	excluded
34860	ketoglutaric	6	0.00	33.95	74.42	0.1769	0.8955	3.00	yes
35280	AS	6	37.36	36.90	60.34	0.0000	0.7840	3.00	yes
35760	ketoglutaric	6	39.42	39.86	41.04	0.0000	0.7869	3.00	yes
36180	AS	6	40.92	39.87	68.86	0.0001	0.7987	3.61	no
36600	ketoglutaric	6	41.87	39.86	82.66	0.0015	0.7888	3.90	yes
37080	AS	6	42.10	39.84	69.75	0.0005	0.7981	3.25	yes
37500	ketoglutaric	6	41.79	39.84	83.60	0.0019	0.8058	3.75	yes
37920	AS	6	41.14	39.86	69.04	0.0004	0.8011	3.25	yes
38400	ketoglutaric	6	40.21	39.86	82.30	0.0020	0.8171	3.56	yes
38820	AS	6	39.08	39.85	68.90	0.0004	0.8055	3.29	yes
39240	ketoglutaric	6	37.82	39.85	80.95	0.0001	0.8229	4.47	yes
39720	AS	6	36.41	39.85	67.36	0.0000	0.8040	3.73	yes
40140	ketoglutaric	6	34.99	39.85	78.56	0.0000	0.8274	5.03	yes
40560	AS	6	33.44	36.91	69.65	0.0000	0.7992	3.00	no
41040	ketoglutaric	6	32.14	36.92	78.05	0.0000	0.8327	5.13	no
41460	AS	6	30.53	33.89	49.67	0.0000	0.7964	3.00	yes
41880	ketoglutaric	6	29.02	33.95	77.50	0.0000	0.8300	4.73	no
42360	AS	6	27.40	30.78	62.49	0.0000	0.8069	3.84	no
42780	ketoglutaric	6	25.73	31.00	74.63	0.0000	0.8130	3.53	no
43200	AS	6	24.21	28.29	60.48	0.0000	0.8081	3.00	no
43680	ketoglutaric	6	22.41	28.06	73.81	0.0000	0.8333	3.00	no
44100	AS	6	20.90	24.99	59.28	0.0000	0.8282	3.00	no
44520	ketoglutaric	6	19.16	25.09	73.00	0.0000	0.8585	3.00	no
45000	AS	6	18.04	25.10	58.87	0.0000	0.8465	3.00	no
45420	ketoglutaric	6	16.49	22.15	75.15	0.0000	0.8573	4.54	no
45840	AS	6	15.41	22.15	58.40	0.0000	0.8390	3.00	no
46320	ketoglutaric	6	14.41	18.57	70.13	0.0000	0.8717	3.00	no
46740	AS	6	13.29	19.21	58.83	0.0000	0.8415	3.00	no
47160	ketoglutaric	6	12.49	19.18	69.88	0.0000	0.8764	3.00	no
47640	AS	6	11.40	17.41	57.89	0.0000	0.8497	3.00	no
48060	ketoglutaric	6	10.33	16.23	70.35	0.0000	0.8807	3.00	no
48480	AS	6	9.62	16.22	57.42	0.0000	0.8621	3.00	no
48960	ketoglutaric	6	8.68	16.26	68.81	0.0018	0.8762	3.00	no
49380	AS	6	7.84	13.27	40.15	0.0000	0.8575	3.00	yes
49800	ketoglutaric	6	7.31	13.31	69.41	0.0050	0.9029	3.00	no
50280	AS	6	6.60	13.29	56.38	0.0000	0.8810	3.00	no
50700	ketoglutaric	6	5.94	13.28	68.28	0.0077	0.8931	3.21	no
51120	AS	6	5.33	13.28	55.40	0.0000	0.8948	3.33	no
51600	ketoglutaric	6	4.79	10.33	54.52	0.0176	0.8734	4.72	yes
52020	AS	6	4.44	10.35	55.05	0.0073	0.8200	3.10	no
52440	ketoglutaric	6	2.97	10.34	66.41	0.0213	0.8285	3.76	no
52920	AS	6	1.97	6.20	30.00	0.3000	0.9096	40.00	yes
53340	ketoglutaric	6	1.67	6.21	65.01	0.0203	0.8209	3.81	no

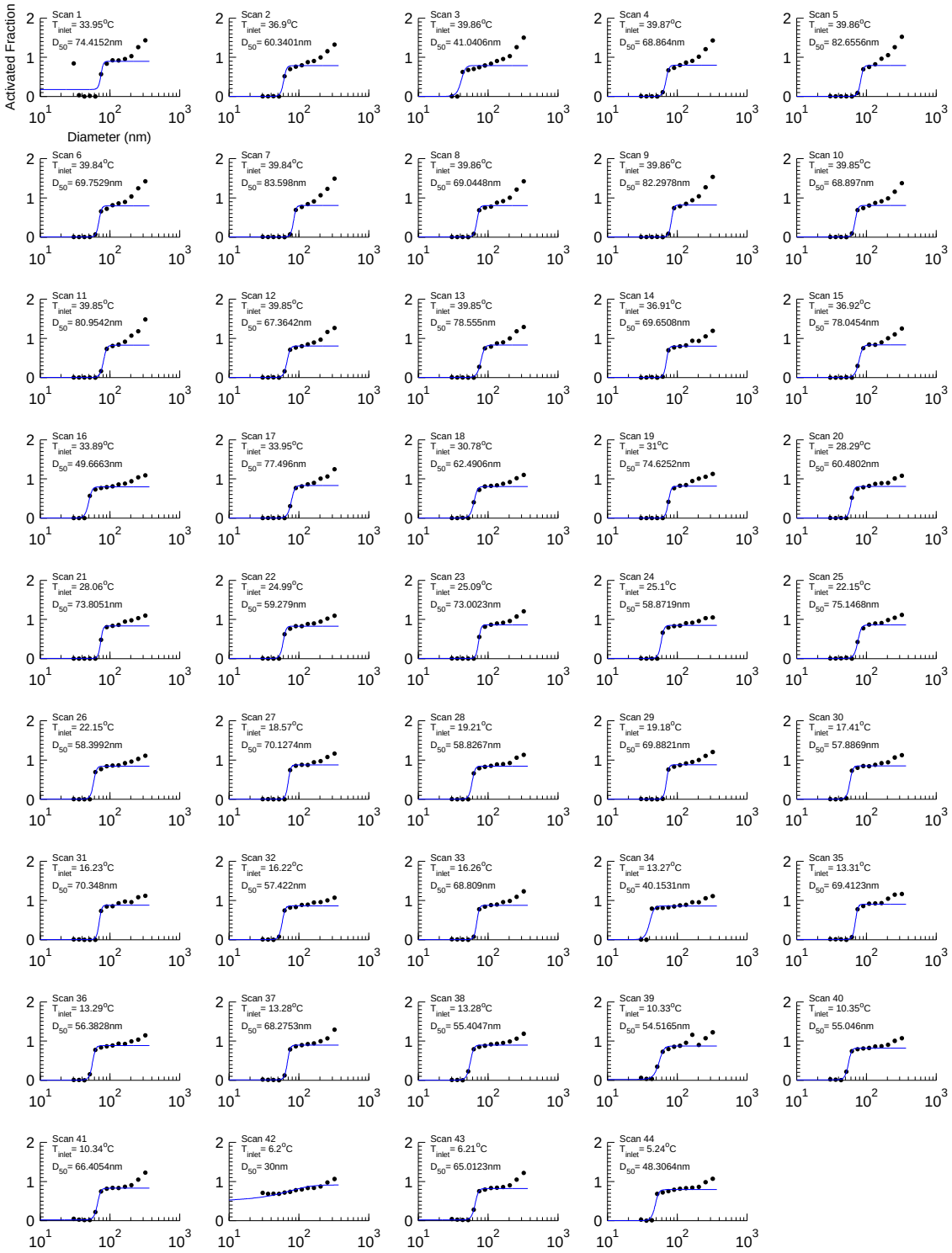

Figure A.25. Ketoglutaric acid (odd scan numbers) and $(NH_4)_2SO_4$ activation curves. The activated fractions at each diameter are fit with a Sigmoid-Boltzmann curve (blue, see Table A.9).

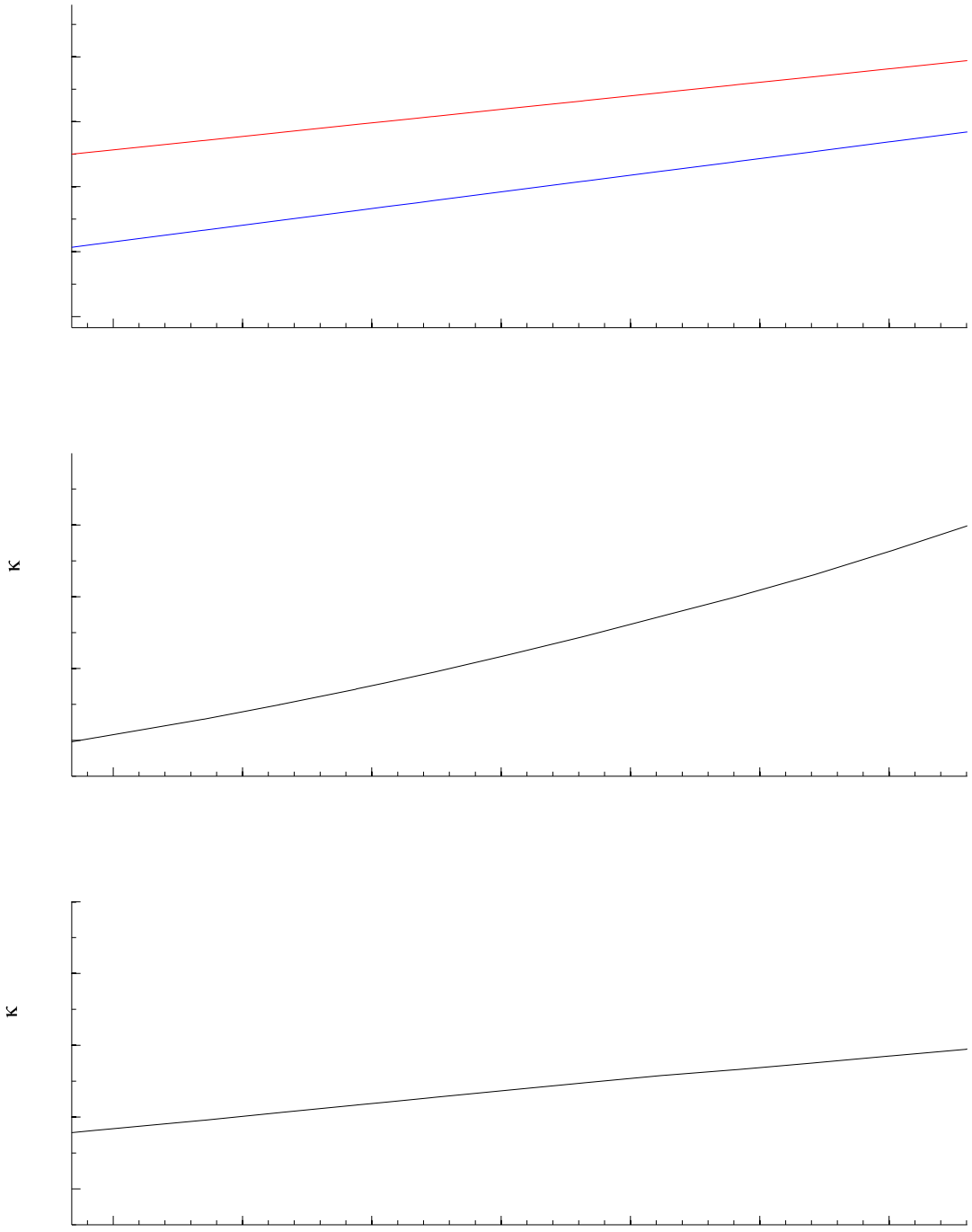

Figure A.26. Ketoglutaric acid and $(NH_4)_2SO_4$ activation diameters (top) and ketoglutaric acid κ values (center and bottom) versus temperature. Each number represents a scan from Figure A.25. Fit coefficients represent the solid line fit through the activation diameters, which then give the κ line.

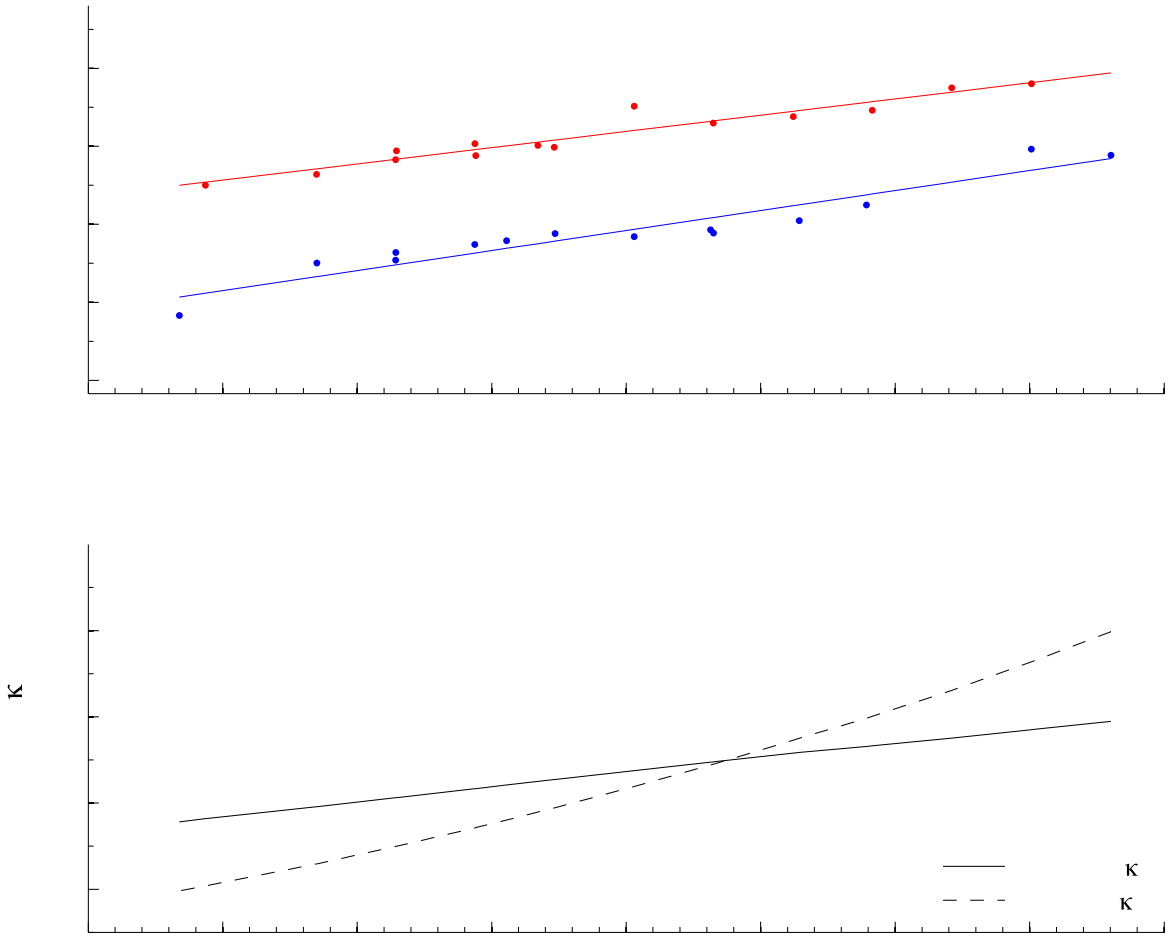

Figure A.27. Ketoglutaric acid and $(NH_4)_2SO_4$ activation diameters replotted without scan numbers (top) and κ values (bottom) plotted together.

Table A.10. Ketoglutaric acid data. Each line represents one diameter scan.

						Boltzmann Parameters:			
time	compound	ΔT	T_{box}	T_{inlet}	D_{50}	*A1*	*A2*	*dx*	excluded
35520	ketoglutaric	6	0.00	36.81	52.71	0.0000	0.7712	3.84	yes
35940	AS	6	38.82	39.87	66.40	0.0000	0.8027	4.52	yes
36420	ketoglutaric	6	40.47	39.75	81.98	0.0016	0.8305	4.71	no
36840	AS	6	41.41	39.74	67.76	0.0000	0.8062	4.23	no
37260	ketoglutaric	6	41.62	39.76	81.93	0.0002	0.8176	4.65	yes
37740	AS	6	41.32	39.75	67.29	0.0000	0.8029	4.06	yes
38160	ketoglutaric	6	40.67	39.73	81.96	0.0002	0.8188	4.69	yes
38580	AS	6	39.74	39.73	68.17	0.0000	0.8066	3.51	yes
39060	ketoglutaric	6	38.65	39.75	81.91	0.0022	0.8098	3.83	yes
39480	AS	6	37.40	39.75	67.70	0.0000	0.8185	3.97	yes
39900	ketoglutaric	6	36.04	39.75	81.96	0.0059	0.8229	3.82	yes
40380	AS	6	34.60	36.37	67.58	0.0000	0.8225	3.84	yes
40800	ketoglutaric	6	33.12	36.80	82.29	0.0018	0.8218	3.91	yes
41220	AS	6	31.82	36.80	66.00	0.0000	0.8170	4.10	no
41700	ketoglutaric	6	30.18	33.84	44.88	0.0000	0.7909	3.00	yes
42120	AS	6	28.70	33.85	64.07	0.0000	0.8196	4.42	no
42540	ketoglutaric	6	27.06	30.51	73.32	0.0000	0.8272	3.00	no
43020	AS	6	25.43	30.89	62.71	0.0000	0.8173	3.79	no
43440	ketoglutaric	6	23.88	27.42	72.94	0.0000	0.8379	3.00	no
43860	AS	6	22.11	27.93	64.03	0.0000	0.8425	4.39	no
44340	ketoglutaric	6	20.59	24.33	72.17	0.0000	0.8383	3.00	no
44760	AS	6	18.92	24.99	61.03	0.0000	0.8364	3.00	no
45180	ketoglutaric	6	17.53	24.97	70.73	0.0000	0.8688	3.00	no
45660	AS	6	15.95	22.06	62.98	0.0000	0.8418	3.37	no
46080	ketoglutaric	6	14.76	22.05	71.07	0.0000	0.8732	3.00	no
46500	AS	6	13.39	19.06	40.05	0.0000	0.8332	3.00	yes
46980	ketoglutaric	6	12.39	19.09	70.72	0.0000	0.8919	3.00	no
47400	AS	6	11.27	19.09	58.10	0.0000	0.8782	3.00	no
47820	ketoglutaric	6	10.17	16.14	70.58	0.0212	0.7899	4.44	no
48300	AS	6	9.49	16.15	57.77	0.0000	0.8155	3.00	no
48720	ketoglutaric	6	8.56	16.15	69.42	0.0000	0.8095	3.00	no
49140	AS	6	7.73	12.99	57.04	0.0000	0.8059	3.00	no
49620	ketoglutaric	6	7.14	13.20	69.76	0.0000	0.8301	3.00	no
50040	AS	6	6.53	10.56	54.52	0.0000	0.7958	5.39	no
50460	ketoglutaric	6	6.04	9.50	68.48	0.0000	0.8186	3.00	no
50940	AS	6	5.39	9.54	57.04	0.0000	0.8101	3.00	no
51360	ketoglutaric	6	4.75	8.52	70.12	0.0000	0.8228	3.00	no
51780	AS	6	4.22	7.53	53.47	0.0000	0.8039	3.79	no
52260	ketoglutaric	6	3.66	7.54	68.34	0.0018	0.8255	3.02	no
52680	AS	6	3.20	6.49	54.53	0.0000	0.8013	3.21	no
53100	ketoglutaric	6	2.54	6.54	66.60	0.0025	0.8138	3.18	no
53580	AS	6	1.17	5.58	55.56	0.0000	0.8032	3.00	no
54000	ketoglutaric	6	0.37	4.59	66.04	0.0079	0.8217	5.33	no
54420	AS	6	-0.16	4.60	52.49	0.0000	0.7932	3.56	no
54900	ketoglutaric	6	-0.62	3.57	68.02	0.0111	0.8221	4.07	no
55320	AS	6	-0.95	3.59	51.21	0.0000	0.7980	3.00	no
55740	ketoglutaric	6	-1.24	3.59	62.66	0.0000	0.8122	3.55	no
56220	AS	6	-1.48	2.62	53.16	0.0000	0.7932	6.37	yes
56640	ketoglutaric	6	-1.66	2.62	63.08	0.0000	0.7993	3.72	no

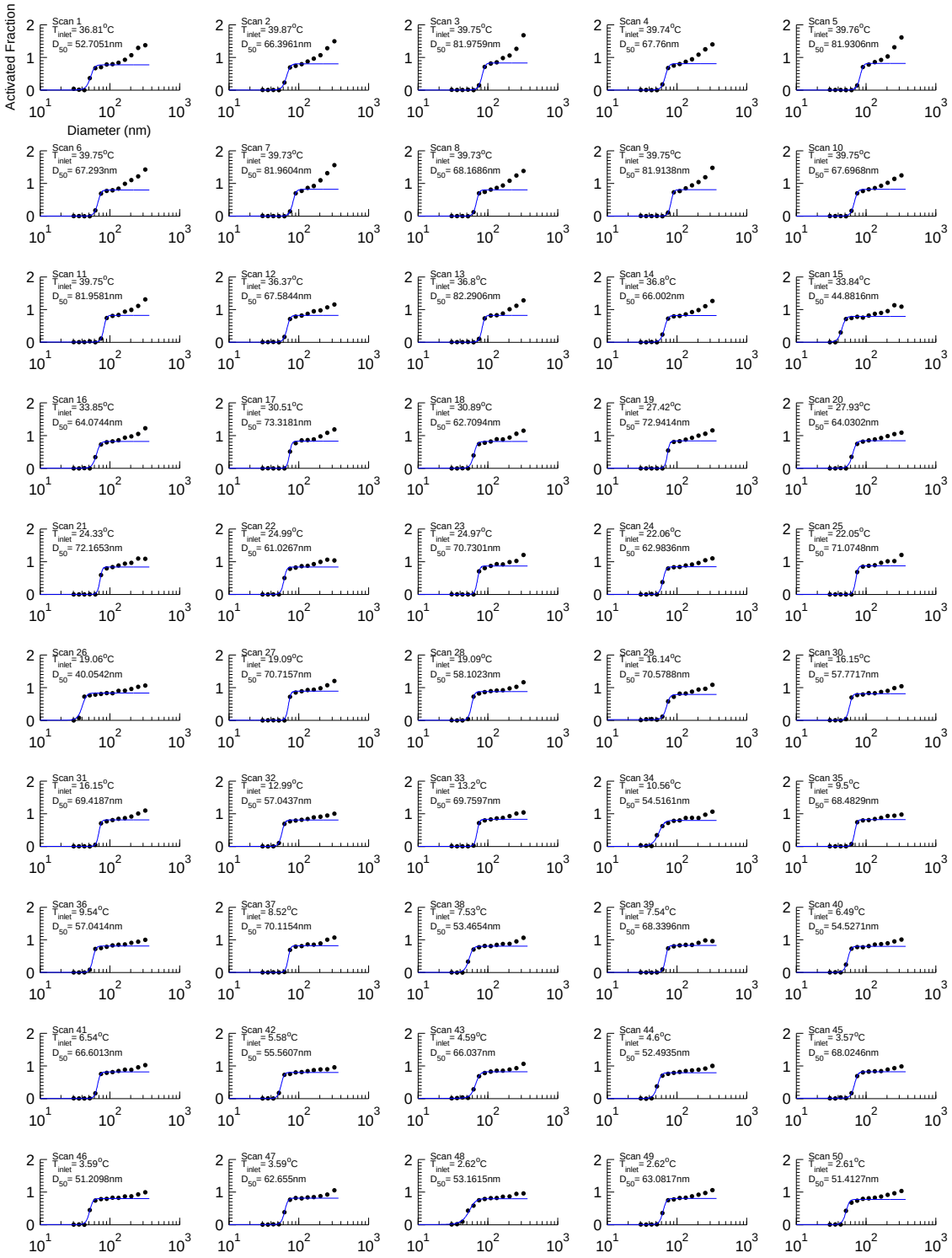

Figure A.28. Ketoglutaric acid (odd scan numbers) and $(NH_4)_2SO_4$ activation curves. The activated fractions at each diameter are fit with a Sigmoid-Boltzmann curve (blue, see Table A.10).

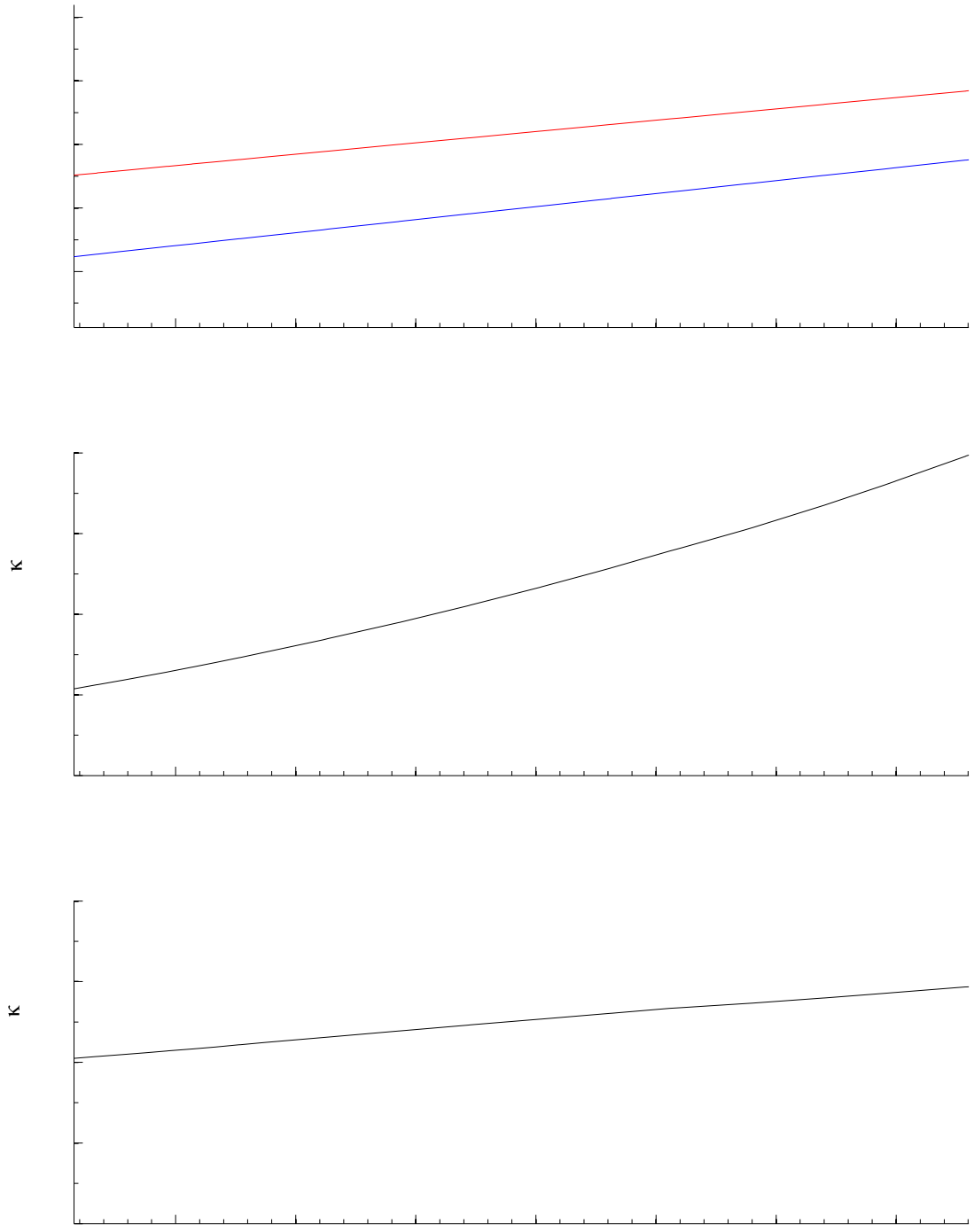

Figure A.29. Ketoglutaric acid and $(NH_4)_2SO_4$ activations diameters (top) and ketoglutaric acid κ values (center and bottom) versus temperature. Each number represents a scan from Figure A.28. Fit coefficients represent the solid line fit through the activation diameters, which then give the κ line.

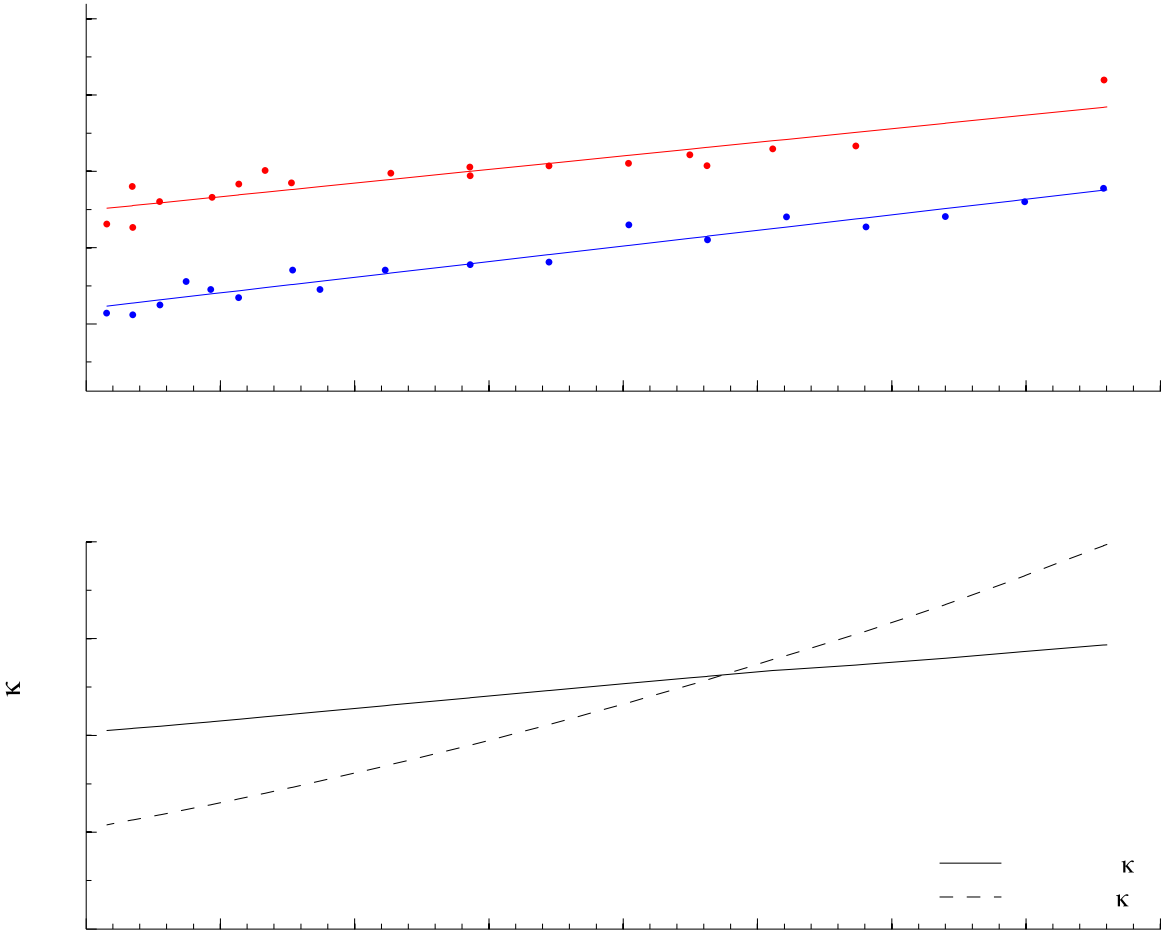

Figure A.30. Ketoglutaric acid and $(NH_4)_2SO_4$ activation diameters replotted without scan numbers (top) and κ values (bottom) plotted together.

Table A.11. Maleic acid data. Each line represents one diameter scan.

						Boltzmann Parameters:			
time	compound	ΔT	T_{box}	T_{inlet}	D_{50}	*A1*	*A2*	*dx*	excluded
36660	maleic	6	0.00	31.56	68.84	0.0000	1.0145	3.00	yes
37080	AS	6	32.62	34.56	57.90	0.0000	0.7890	3.00	yes
37500	maleic	6	35.85	37.60	79.72	0.0002	0.7507	4.16	no
37980	AS	6	38.19	37.48	66.94	0.0000	0.7630	4.27	no
38400	maleic	6	39.94	40.45	42.20	0.0000	0.7010	3.00	yes
38820	AS	6	41.16	40.43	69.64	0.0000	0.7695	3.00	no
39300	maleic	6	41.59	40.44	83.83	0.0000	0.7495	3.00	yes
39720	AS	6	41.42	40.42	69.84	0.0000	0.7758	3.00	yes
40140	maleic	6	40.79	40.43	84.70	0.0000	0.7599	3.00	yes
40620	AS	6	39.91	40.43	69.70	0.0000	0.7844	3.00	yes
41040	maleic	6	38.81	40.43	85.11	0.0000	0.7748	3.00	yes
41460	AS	6	37.75	40.44	69.50	0.0000	0.7931	3.00	yes
41940	maleic	6	36.69	40.44	84.46	0.0003	0.8079	3.00	yes
42360	AS	6	35.41	37.09	69.02	0.0000	0.7950	3.12	yes
42780	maleic	6	34.14	37.48	83.02	0.0000	0.7930	3.21	yes
43260	AS	6	32.99	37.48	68.22	0.0000	0.8067	3.54	no
43680	maleic	6	31.49	34.45	69.60	0.0000	0.8158	3.00	yes
44100	AS	6	30.10	34.54	67.47	0.0000	0.8069	3.80	no
44580	maleic	6	28.69	32.68	79.97	0.0000	0.8112	4.49	yes
45000	AS	6	27.07	31.56	68.16	0.0002	0.8056	3.25	no
45420	maleic	6	25.81	31.53	75.10	0.0000	0.8012	4.11	no
45900	AS	6	24.22	28.58	66.68	0.0099	0.8221	6.14	no
46320	maleic	6	22.86	28.59	74.25	0.0000	0.8140	3.76	no
46740	AS	6	21.29	25.62	40.59	0.0000	0.7908	3.00	yes
47220	maleic	6	19.92	25.62	71.86	0.0000	0.8198	3.00	no
47640	AS	6	18.44	22.43	59.07	0.0000	0.8148	3.00	no
48060	maleic	6	17.09	22.70	71.15	0.0000	0.8217	3.00	no
48540	AS	6	15.94	22.68	58.85	0.0000	0.8275	3.00	no
48960	maleic	6	14.67	19.72	57.62	0.0000	0.8094	10.15	yes
49380	AS	6	13.78	19.74	58.31	0.0000	0.8152	3.00	no
49860	maleic	6	12.80	19.73	69.83	0.0000	0.8478	3.00	no
50280	AS	6	11.87	16.62	58.03	0.0000	0.8388	3.00	no
50700	maleic	6	11.19	16.77	69.73	0.0000	0.8461	3.00	no
51180	AS	6	10.61	16.79	57.69	0.0000	0.8443	3.00	no
51600	maleic	6	9.89	16.78	68.93	0.0020	0.8482	3.14	no
52020	AS	6	9.30	16.78	57.43	0.0000	0.8501	3.00	no
52440	maleic	6	8.75	13.74	56.54	0.0000	0.8525	3.00	yes
52920	AS	6	8.51	13.82	59.13	0.1940	0.8624	3.00	yes
53340	maleic	6	7.34	13.85	66.61	0.0000	0.8675	3.84	no
53760	AS	6	5.92	10.18	58.95	0.0112	0.8554	3.30	yes
54240	maleic	6	5.27	9.14	65.40	0.0000	0.8635	4.04	no
54660	AS	6	4.45	8.16	55.01	0.0000	0.8675	3.49	no
55080	maleic	6	3.70	8.20	63.53	0.0000	0.8624	4.25	no
55560	AS	6	3.08	7.22	57.83	0.0000	0.8775	3.00	yes
55980	maleic	6	2.51	6.18	63.52	0.0004	0.8673	4.11	no
56400	AS	6	2.04	6.21	53.33	0.0000	0.8667	3.71	no
56880	maleic	6	1.56	6.22	60.61	0.0009	0.8586	3.00	no
57300	AS	6	1.21	5.25	56.03	0.0035	0.8727	3.31	yes
57720	maleic	6	0.88	5.25	61.74	0.0055	0.8610	3.00	no
58200	AS	6	0.53	5.25	52.20	0.0000	0.8589	3.26	no
58620	maleic	6	0.26	4.23	64.73	0.0015	0.8688	4.16	yes
59040	AS	6	0.04	4.22	51.13	0.0000	0.8616	3.00	no
59520	maleic	6	-0.23	4.23	59.78	0.0000	0.8658	3.00	no
59940	AS	6	-0.44	4.23	51.02	0.0000	0.8666	3.00	no
60360	maleic	6	-0.60	4.24	59.63	0.0001	0.8758	3.00	no
60840	AS	6	-0.76	4.23	52.19	0.0000	0.8753	3.60	no
61260	maleic	6	-0.91	3.25	66.49	0.0103	0.8857	3.75	yes

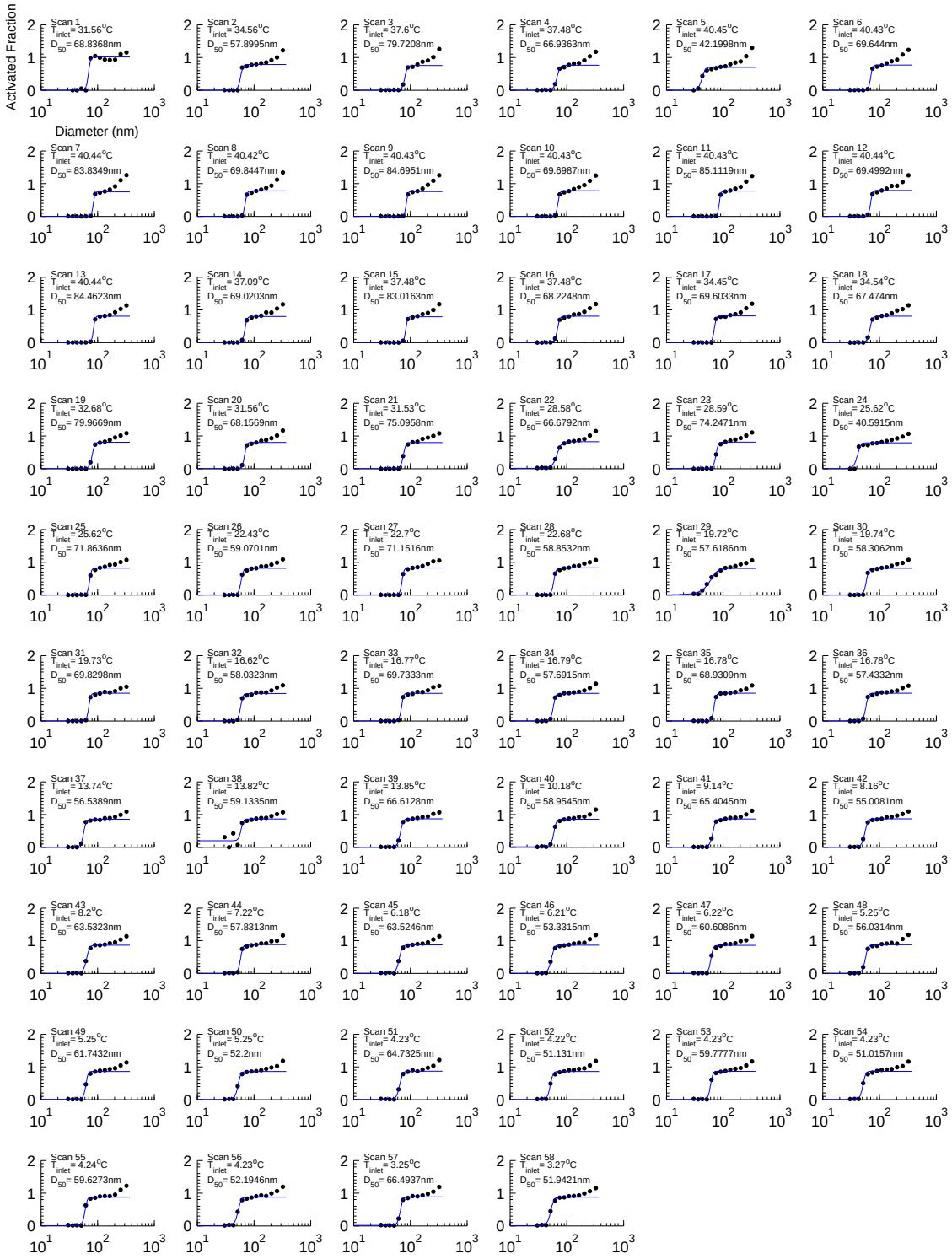

Figure A.31. Maleic acid (odd scan numbers) and $(NH_4)_2SO_4$ activation curves. The activated fractions at each diameter are fit with a Sigmoid-Boltzmann curve (blue, see Table A.11).

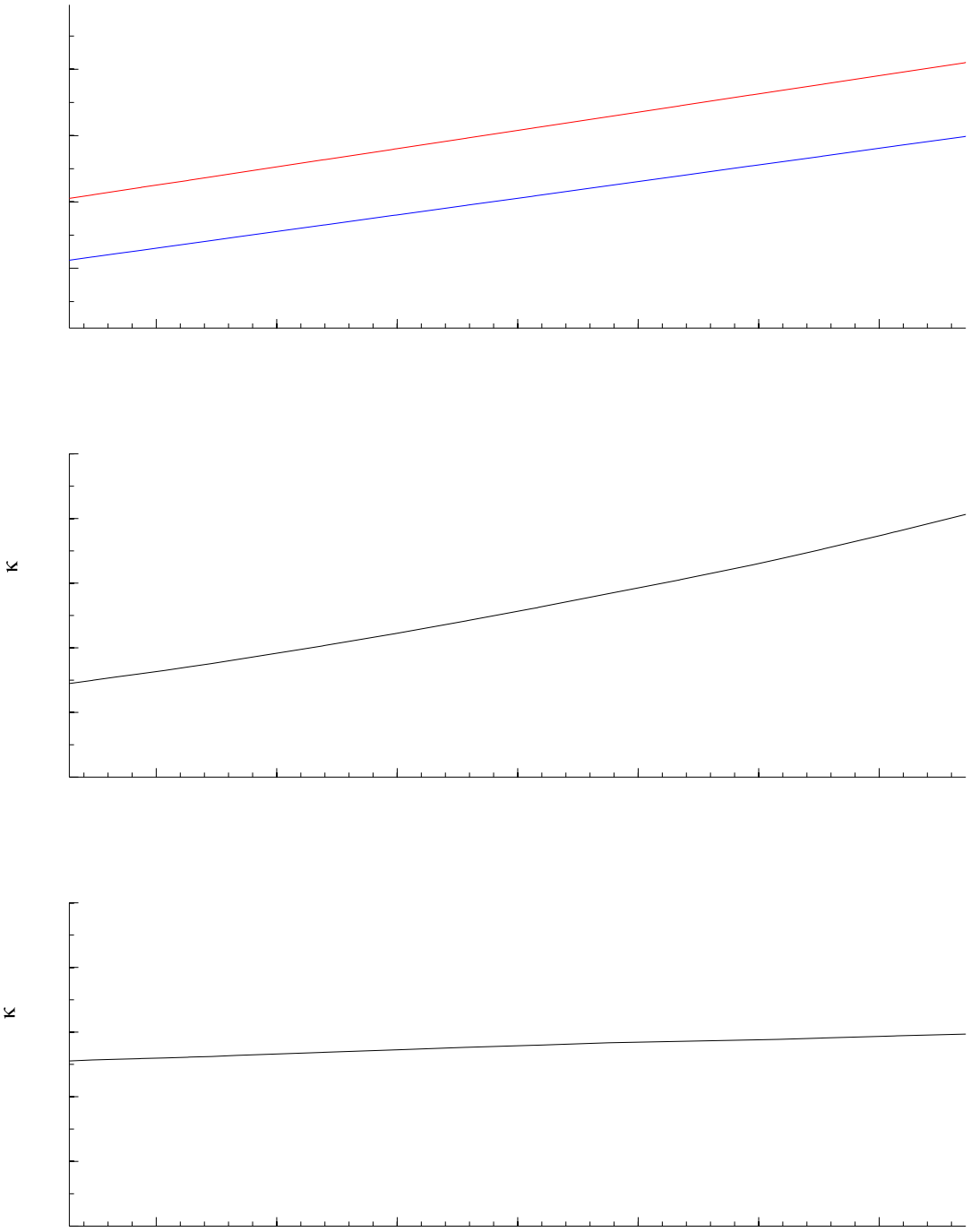

Figure A.32. Maleic acid and $(NH_4)_2SO_4$ activation diameters (top) and maleic acid κ values (center and bottom) versus temperature. Each number represents a scan from Figure A.31. Fit coefficients represent the solid line fit through the activation diameters, which then give the κ line.

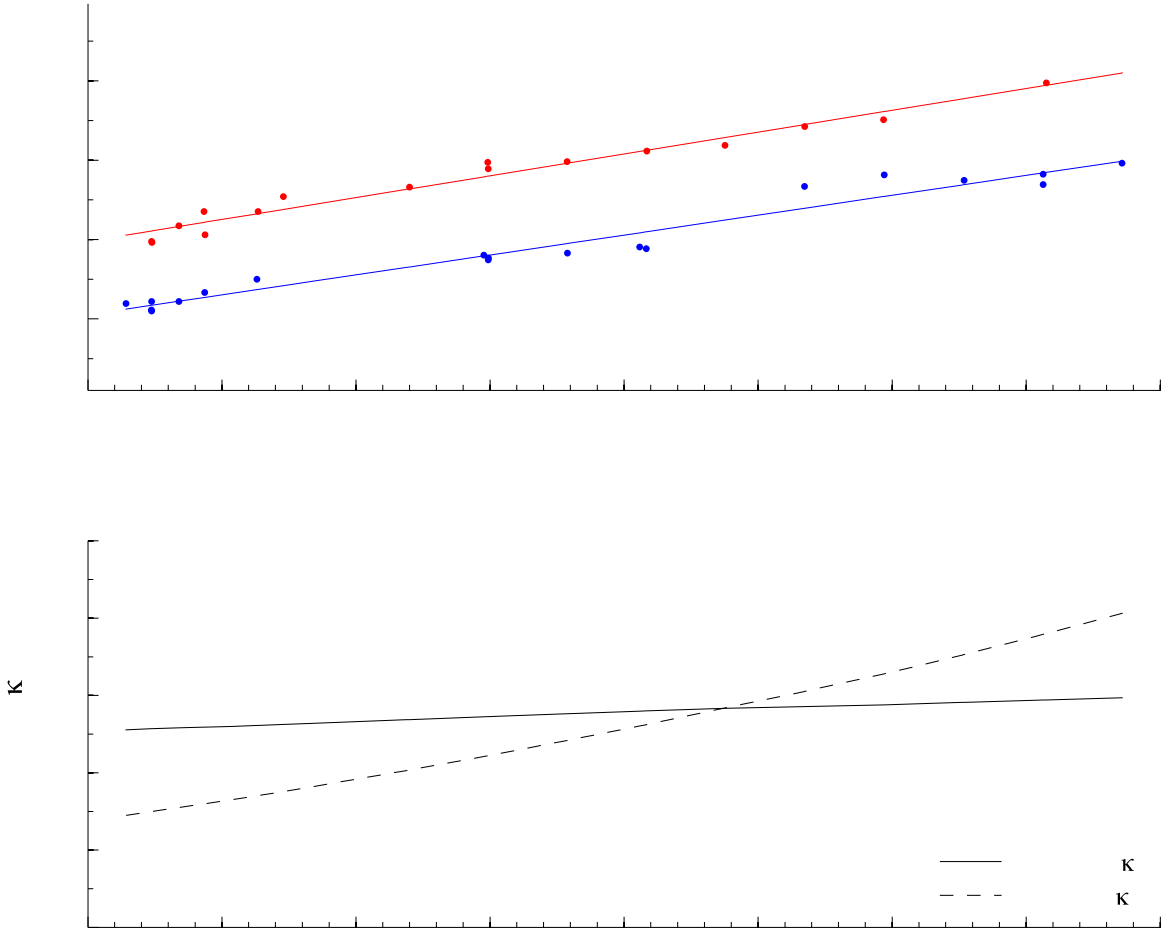

Figure A.33. Maleic acid and $(NH_4)_2SO_4$ activation diameters replotted without scan numbers (top) and κ values (bottom) plotted together.

Table A.12. Maleic acid data. Each line represents one diameter scan.

						Boltzmann Parameters:			
time	compound	ΔT	T_{box}	T_{inlet}	D_{50}	*A1*	*A2*	*dx*	excluded
35280	maleic	6	0.00	38.02	80.76	0.0086	0.8133	4.01	yes
35700	AS	6	40.84	40.97	43.12	0.0000	0.7612	3.75	yes
36180	maleic	6	41.20	40.97	83.14	0.0017	0.7804	3.41	no
36600	AS	6	40.95	40.98	69.41	0.0000	0.8045	3.57	yes
37020	maleic	6	40.34	40.96	83.80	0.0008	0.7978	3.58	yes
37500	AS	6	39.51	40.98	68.51	0.0001	0.7983	3.51	yes
37920	maleic	6	38.51	40.97	82.69	0.0010	0.7970	3.75	yes
38340	AS	6	37.32	40.97	67.88	0.0000	0.8129	4.07	yes
38820	maleic	6	36.00	37.81	81.61	0.0003	0.8167	4.58	yes
39240	AS	6	34.69	38.03	66.25	0.0000	0.8015	4.91	yes
39660	maleic	6	33.40	38.03	81.03	0.0000	0.8300	5.12	no
40140	AS	6	31.80	35.05	40.92	0.0000	0.7674	3.00	yes
40560	maleic	6	30.35	35.08	79.78	0.0000	0.8422	5.60	no
40980	AS	6	28.75	31.56	62.13	0.0000	0.7926	3.78	no
41460	maleic	6	27.08	32.13	78.18	0.0000	0.8244	4.99	no
41880	AS	6	25.55	28.79	61.44	0.0000	0.8090	3.00	no
42300	maleic	6	23.79	29.18	73.27	0.0000	0.8183	3.00	no
42780	AS	6	22.28	26.57	60.68	0.0000	0.8194	3.00	no
43200	maleic	6	20.56	26.22	73.77	0.0000	0.8335	3.12	no
43620	AS	6	19.17	26.22	59.20	0.0000	0.8232	3.00	no
44100	maleic	6	17.54	23.27	74.68	0.0000	0.8383	3.62	no
44520	AS	6	16.28	23.28	58.91	0.0000	0.8282	3.00	no
44940	maleic	6	14.83	20.25	59.87	0.0000	0.8395	7.28	yes
45420	AS	6	13.70	20.28	58.68	0.0000	0.8432	3.00	no
45840	maleic	6	12.47	20.28	69.97	0.0000	0.8570	3.00	no
46260	AS	6	11.26	17.32	59.08	0.0000	0.8397	3.00	no
46740	maleic	6	10.45	17.32	69.36	0.0000	0.8702	3.00	no
47160	AS	6	9.40	17.31	57.49	0.0000	0.8548	3.00	no
47580	maleic	6	8.50	14.35	69.71	0.0000	0.8596	3.00	no
48060	AS	6	7.93	14.35	57.55	0.0000	0.8015	3.00	no
48480	maleic	6	7.15	10.12	68.54	0.0035	0.8088	3.70	no
48900	AS	6	6.61	10.47	56.90	0.0000	0.7966	3.00	no
49380	maleic	6	5.90	9.49	63.12	0.0000	0.7980	5.86	yes
49800	AS	6	4.32	8.46	57.98	0.0001	0.7859	3.00	no
50220	maleic	6	3.22	7.50	68.68	0.0060	0.8104	3.00	no
50700	AS	6	2.36	6.48	57.28	0.0019	0.7945	3.00	no
51120	maleic	6	1.70	5.50	57.69	0.0000	0.8014	3.00	yes
51540	AS	6	1.10	5.51	54.50	0.0000	0.7877	3.74	no
52020	maleic	6	0.55	4.49	67.94	0.0157	0.7970	3.10	yes
52440	AS	6	0.12	4.49	51.41	0.0000	0.7814	3.00	no
52860	maleic	6	-0.29	3.50	56.46	0.0000	0.7873	4.19	yes
53340	AS	6	-0.62	3.52	52.52	0.0000	0.7839	3.57	no
53760	maleic	6	-0.98	3.53	61.27	0.0045	0.7975	3.00	no
54180	AS	6	-1.25	2.48	52.00	0.0000	0.7773	3.32	no
54660	maleic	6	-1.47	2.50	61.06	0.0052	0.7993	3.00	no

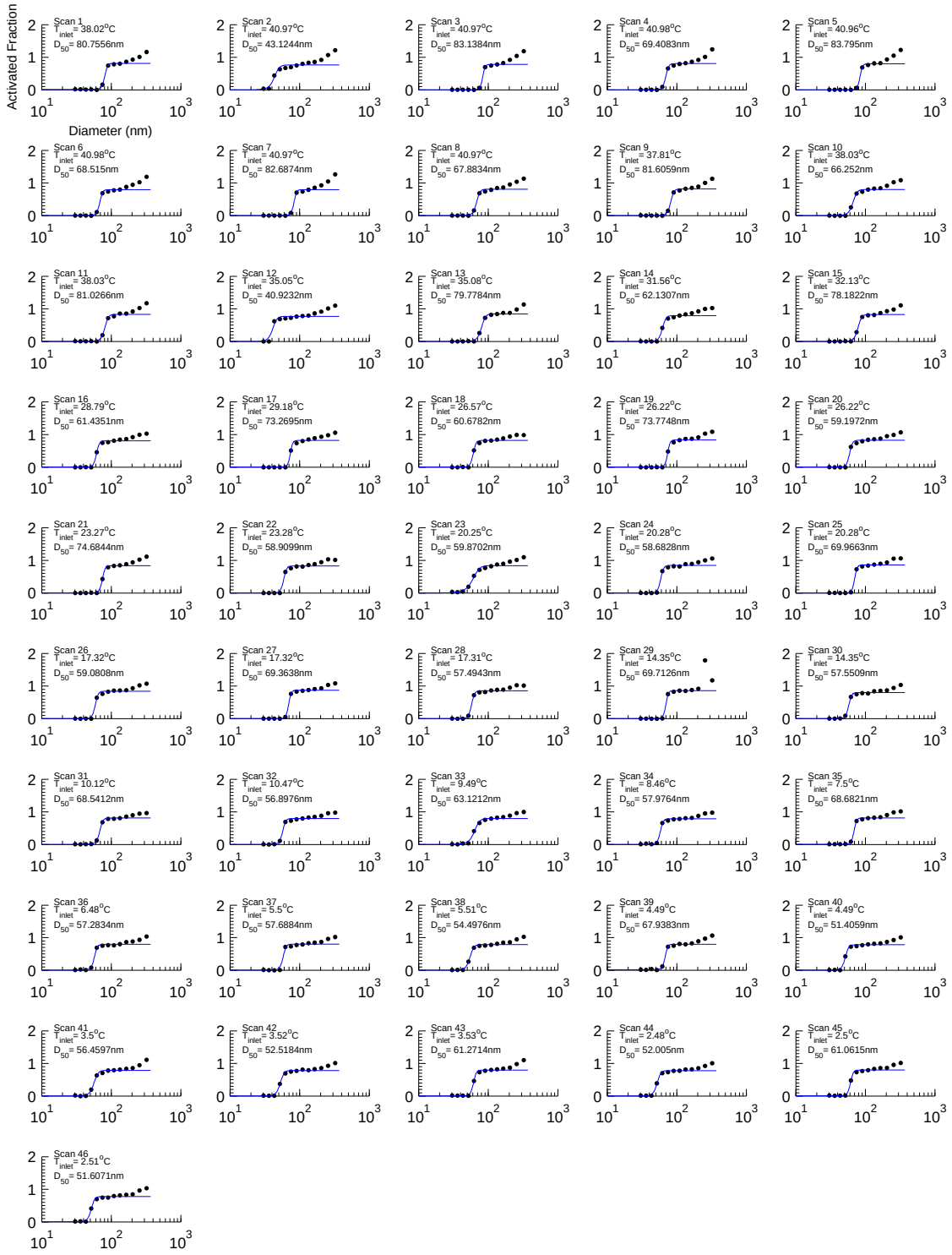

Figure A.34. Maleic acid (odd scan numbers) and $(NH_4)_2SO_4$ activation curves. The activated fractions at each diameter are fit with a Sigmoid-Boltzmann curve (blue, see Table A.12).

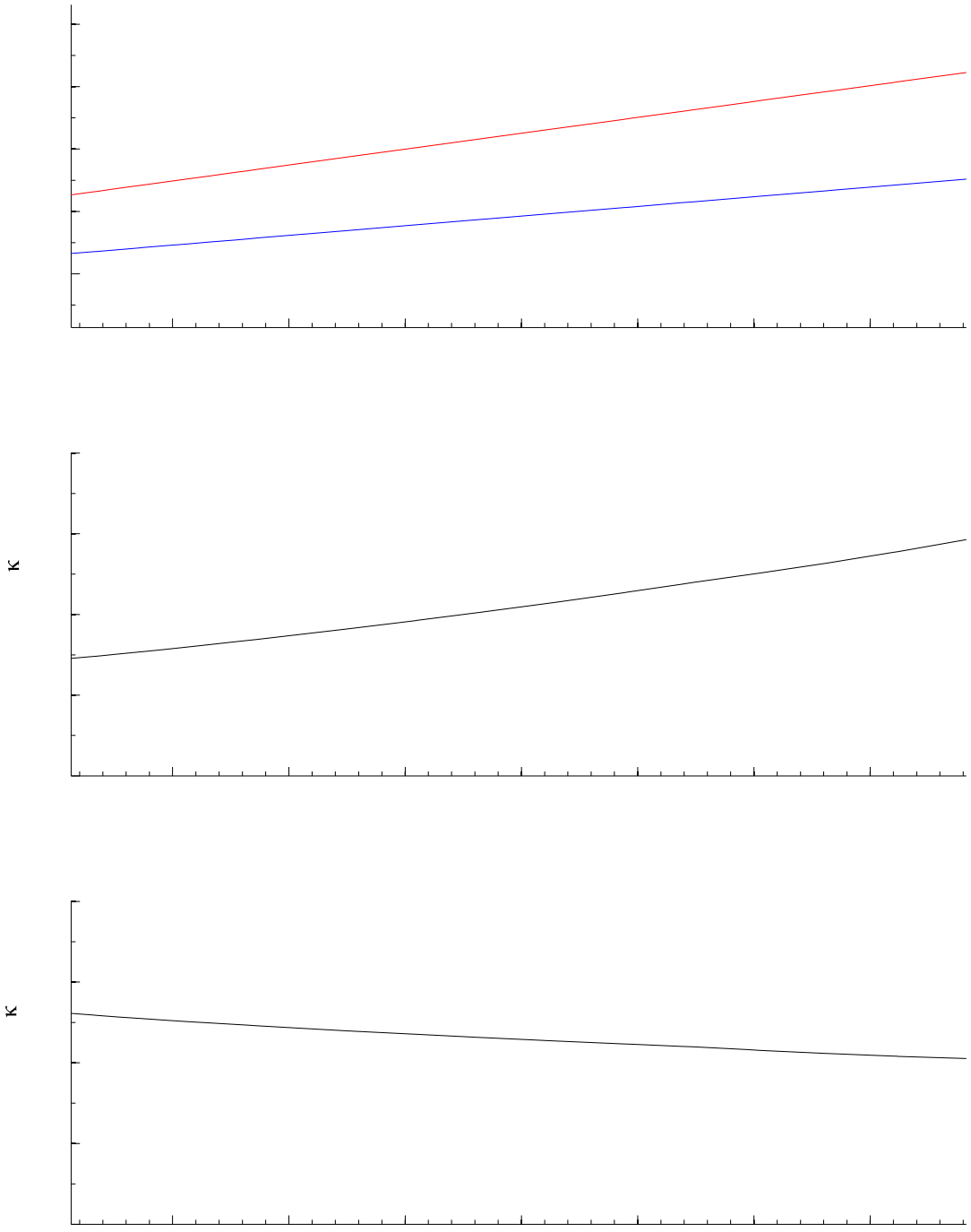

Figure A.35. Maleic acid and $(NH_4)_2SO_4$ activation diameters (top) and maleic acid κ values (center and bottom) versus temperature. Each number represents a scan from Figure A.34. Fit coefficients represent the solid line fit through the activation diameters, which then give the κ line.

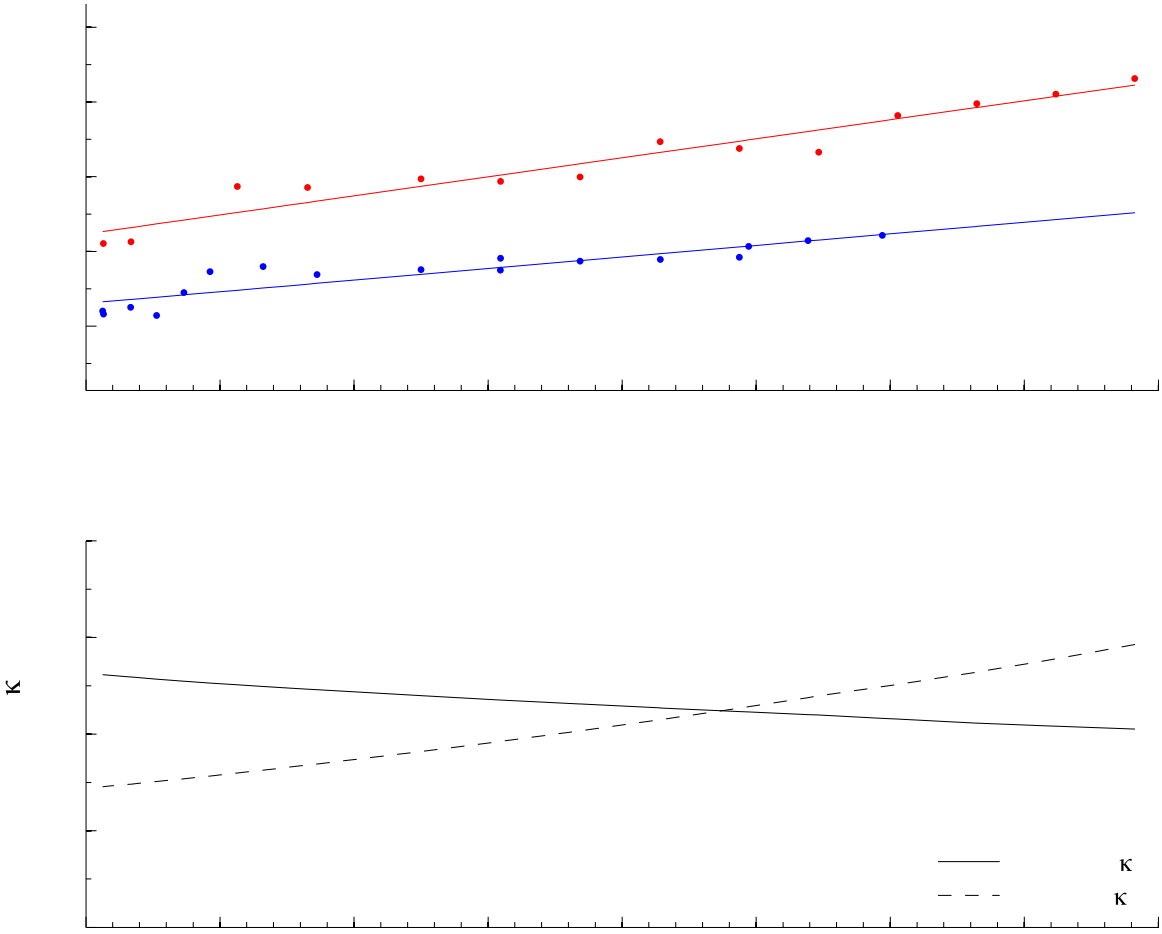

Figure A.36. Maleic acid and $(NH_4)_2SO_4$ activation diameters replotted without scan numbers (top) and κ values (bottom) plotted together.

Table A.13. Methanesulfonic acid (MSA) data. Each line represents one diameter scan.

						Boltzmann Parameters:			
time	compound	ΔT	T_{box}	T_{inlet}	D_{50}	*A1*	*A2*	*dx*	excluded
35700	MSA	6	0.00	38.26	244.07	0.0000	1.3693	3.07	yes
36180	AS	6	39.13	38.13	67.64	0.0006	0.8102	3.57	yes
36600	MSA	6	40.68	41.10	48.48	0.0000	0.7898	3.00	yes
37020	AS	6	41.44	41.09	69.22	0.0012	0.8097	3.02	no
37500	MSA	6	41.52	41.09	76.12	0.0000	0.8000	5.13	no
37920	AS	6	41.13	41.10	69.67	0.0000	0.8198	3.00	yes
38340	MSA	6	40.45	41.08	75.26	0.0000	0.7932	4.91	yes
38820	AS	6	39.49	41.10	69.24	0.0000	0.8214	3.00	yes
39240	MSA	6	38.39	41.09	73.93	0.0000	0.7913	3.00	yes
39660	AS	6	37.12	41.09	68.77	0.0000	0.8275	3.19	yes
40140	MSA	6	35.75	38.08	50.81	0.0000	0.7750	5.61	yes
40560	AS	6	34.54	38.09	67.28	0.0000	0.8284	4.00	yes
40980	MSA	6	33.10	38.10	71.39	0.0000	0.8116	3.00	no
41460	AS	6	31.43	35.12	68.98	0.0023	0.8180	3.19	no
41880	MSA	6	30.05	35.14	70.91	0.0000	0.8178	3.00	no
42300	AS	6	28.36	32.18	51.58	0.0000	0.7961	4.39	yes
42780	MSA	6	26.86	32.18	70.33	0.0000	0.8252	3.00	no
43200	AS	6	25.12	29.21	34.32	0.0000	0.7925	3.00	yes
43620	MSA	6	23.58	29.24	70.47	0.0000	0.8414	3.00	yes
44100	AS	6	21.90	26.26	40.53	0.0000	0.8273	3.00	yes
44520	MSA	6	20.34	26.30	69.75	0.0000	0.8451	3.00	yes
44940	AS	6	18.67	23.26	48.09	0.0000	0.8351	3.00	yes
45420	MSA	6	17.20	23.34	68.61	0.0000	0.8578	3.13	yes
45840	AS	6	15.65	20.23	58.56	0.0000	0.8509	3.00	no
46260	MSA	6	14.30	20.39	67.83	0.0000	0.8653	3.36	no
46740	AS	6	13.03	20.37	58.24	0.0000	0.8659	3.00	no
47160	MSA	6	11.72	17.43	70.47	0.0089	0.8705	3.22	yes
47580	AS	6	10.86	17.44	57.81	0.0000	0.8726	3.00	no
48060	MSA	6	9.79	17.43	61.35	0.0000	0.8000	3.05	no
48480	AS	6	8.79	14.47	59.38	0.0000	0.8159	3.00	no
48900	MSA	6	8.14	14.49	59.85	0.0000	0.8034	3.00	no
49380	AS	6	6.40	11.23	56.45	0.0000	0.8111	3.00	no
49800	MSA	6	5.13	11.53	60.89	0.0000	0.8031	3.00	no
50220	AS	6	4.25	11.54	56.22	0.0000	0.8098	3.45	no
50700	MSA	6	3.33	11.54	58.28	0.0000	0.8075	3.00	no
51120	AS	6	2.58	8.57	58.02	0.0000	0.8150	3.00	no
51540	MSA	6	2.16	8.58	58.31	0.0000	0.8065	3.00	no
52020	AS	6	1.48	8.59	53.58	0.0000	0.8067	3.35	no
52440	MSA	6	0.92	8.57	57.70	0.0000	0.8085	3.00	no
52860	AS	6	0.43	8.59	53.10	0.0000	0.8063	3.58	no
53340	MSA	6	0.01	3.80	59.67	0.0169	0.8036	7.04	no
53760	AS	6	-0.03	3.79	53.65	0.0000	0.8054	3.60	no
54180	MSA	6	-0.65	3.80	57.60	0.0000	0.8119	3.00	no
54660	AS	6	-1.23	2.79	53.99	0.0000	0.7965	3.13	no
55080	MSA	6	-1.69	2.78	56.88	0.0000	0.8076	3.00	no
55500	AS	6	-2.08	1.82	54.16	0.0000	0.8016	3.40	no

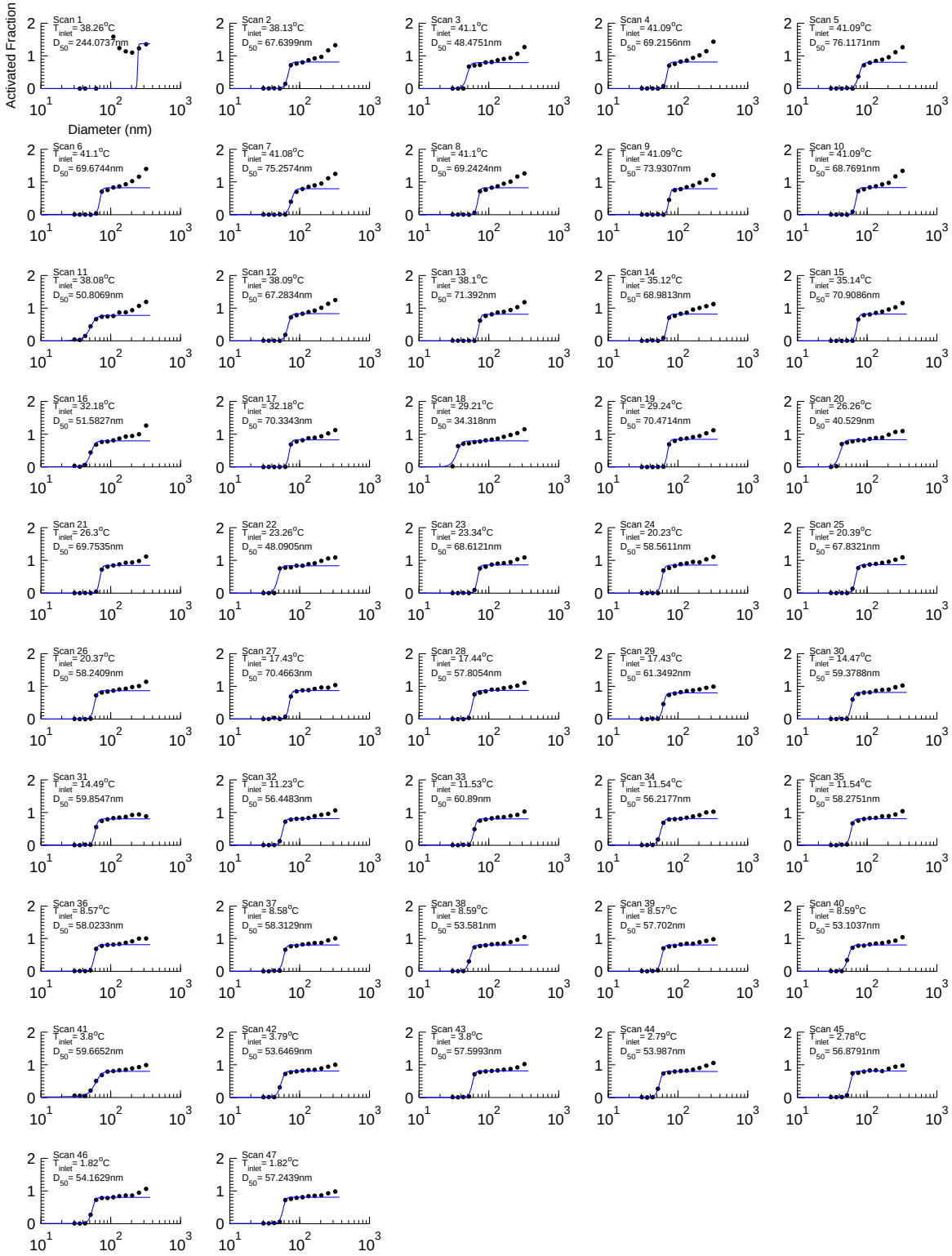

Figure A.37. MSA (odd scan numbers) and $(NH_4)_2SO_4$ activation curves. The activated fractions at each diameter are fit with a Sigmoid-Boltzmann curve (blue, see Table A.13).

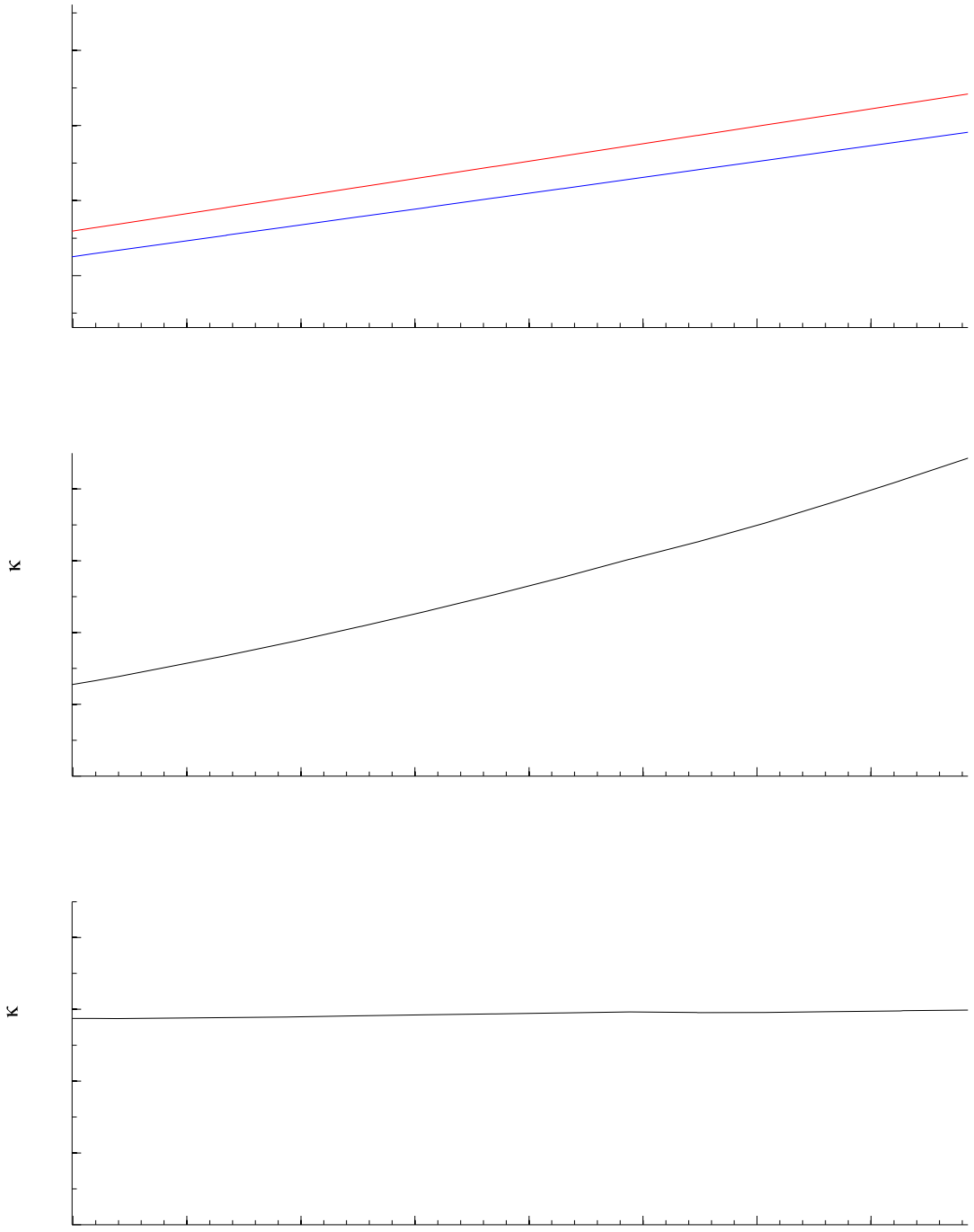

Figure A.38. MSA and $(NH_4)_2SO_4$ activation diameters (top) and MSA κ values (center and bottom) versus temperature. Each number represents a scan from Figure A.37. Fit coefficients represent the solid line fit through the activation diameters, which then give the κ line.

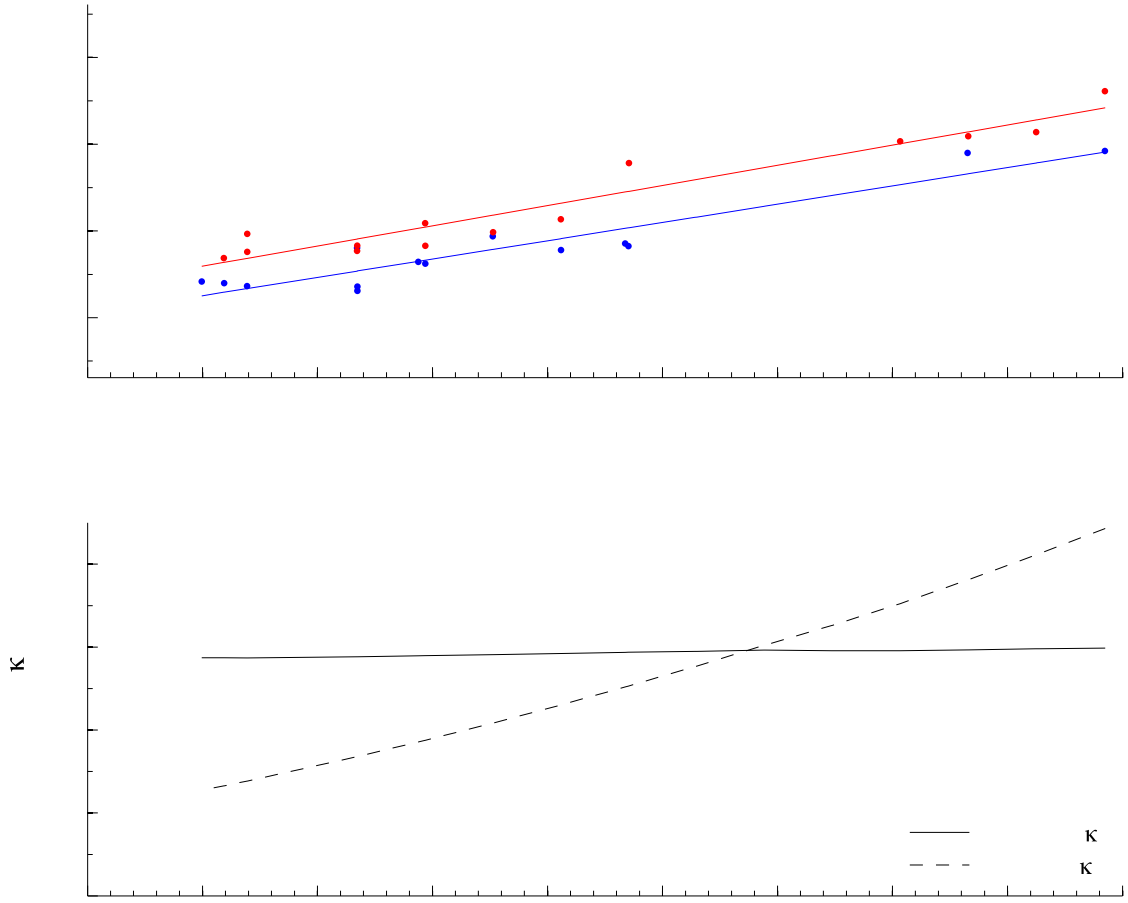

Figure A.39. MSA and $(NH_4)_2SO_4$ activation diameters replotted without scan numbers (top) and κ values (bottom) plotted together.

Table A.14. Methanesulfonic acid (MSA) data. Each line represents one diameter scan.

						Boltzmann Parameters:			
time	compound	ΔT	T_{box}	T_{inlet}	D_{50}	*A1*	*A2*	*dx*	excluded
35460	MSA	6	0.00	36.22	68.58	0.0000	0.9720	3.00	yes
35940	AS	6	36.93	36.07	62.00	0.0074	0.8089	3.39	yes
36360	MSA	6	39.06	39.00	64.43	0.0047	0.7938	4.99	yes
36780	AS	6	40.61	39.01	67.66	0.0059	0.8084	3.49	no
37260	MSA	6	41.50	41.94	34.63	0.0000	0.7625	3.00	yes
37680	AS	6	41.72	41.96	68.48	0.0015	0.8251	3.87	no
38100	MSA	6	41.42	41.96	75.09	0.0000	0.8119	4.53	yes
38580	AS	6	40.82	41.96	68.99	0.0020	0.8331	3.41	yes
39000	MSA	6	39.94	41.96	73.77	0.0000	0.8043	3.36	yes
39420	AS	6	38.83	41.93	67.72	0.0001	0.8354	3.95	yes
39900	MSA	6	37.61	38.55	73.88	0.0000	0.8129	3.11	yes
40320	AS	6	36.31	39.00	69.60	0.0000	0.8304	3.00	yes
40740	MSA	6	35.15	39.00	72.35	0.0000	0.8072	3.00	no
41220	AS	6	33.58	36.01	64.95	0.0000	0.8317	3.63	no
41640	MSA	6	32.10	36.06	71.95	0.0000	0.8173	3.00	no
42060	AS	6	30.56	33.70	63.28	0.0000	0.8316	4.13	no
42540	MSA	6	28.81	33.09	72.37	0.0000	0.8128	3.00	no
42960	AS	6	27.37	33.10	61.74	0.0000	0.8286	3.11	no
43380	MSA	6	25.60	30.15	73.10	0.0000	0.8242	3.00	no
43860	AS	6	24.09	29.98	61.00	0.0000	0.8393	3.00	no
44280	MSA	6	22.30	27.20	71.99	0.0000	0.8436	3.00	no
44700	AS	6	20.87	27.21	59.08	0.0000	0.8506	3.00	no
45180	MSA	6	19.15	24.26	71.50	0.0000	0.8537	3.00	no
45600	AS	6	17.75	24.24	58.98	0.0000	0.8599	3.00	no
46020	MSA	6	16.13	21.30	73.07	0.0130	0.8450	4.39	yes
46500	AS	6	14.83	21.31	58.87	0.0000	0.8739	3.00	no
46920	MSA	6	13.40	18.33	47.84	0.0000	0.8576	3.00	yes
47340	AS	6	12.34	18.35	58.20	0.0000	0.8216	3.00	no
47820	MSA	6	11.23	18.36	62.44	0.0000	0.7977	3.81	no
48240	AS	6	10.15	15.39	50.27	0.0000	0.7823	4.46	yes
48660	MSA	6	9.42	15.41	61.35	0.0015	0.8026	3.00	no
49140	AS	6	8.45	15.41	56.97	0.0000	0.8209	3.00	no
49560	MSA	6	7.60	12.29	60.48	0.0017	0.8145	3.00	no
49980	AS	6	6.98	12.45	57.24	0.0000	0.8237	3.00	no
50460	MSA	6	6.43	9.76	58.85	0.0168	0.8092	6.30	no
50880	AS	6	5.12	8.79	57.77	0.0000	0.8382	5.71	no
51300	MSA	6	3.69	7.78	60.74	0.0027	0.7843	3.00	no
51780	AS	6	2.60	5.85	55.76	0.0000	0.8078	3.17	no
52200	MSA	6	1.75	5.84	59.11	0.0000	0.7918	3.00	no
52620	AS	6	1.02	4.83	57.46	0.0037	0.8409	3.00	no
53040	MSA	6	0.42	3.82	57.64	0.0000	0.8177	3.00	no
53520	AS	6	-0.09	3.86	53.90	0.0000	0.8042	3.80	no
53940	MSA	6	-0.56	2.82	57.93	0.0000	0.8194	3.00	no
54360	AS	6	-0.97	2.85	51.92	0.0000	0.7881	3.00	no
54840	MSA	6	-1.32	2.84	57.16	0.0000	0.8068	3.00	no

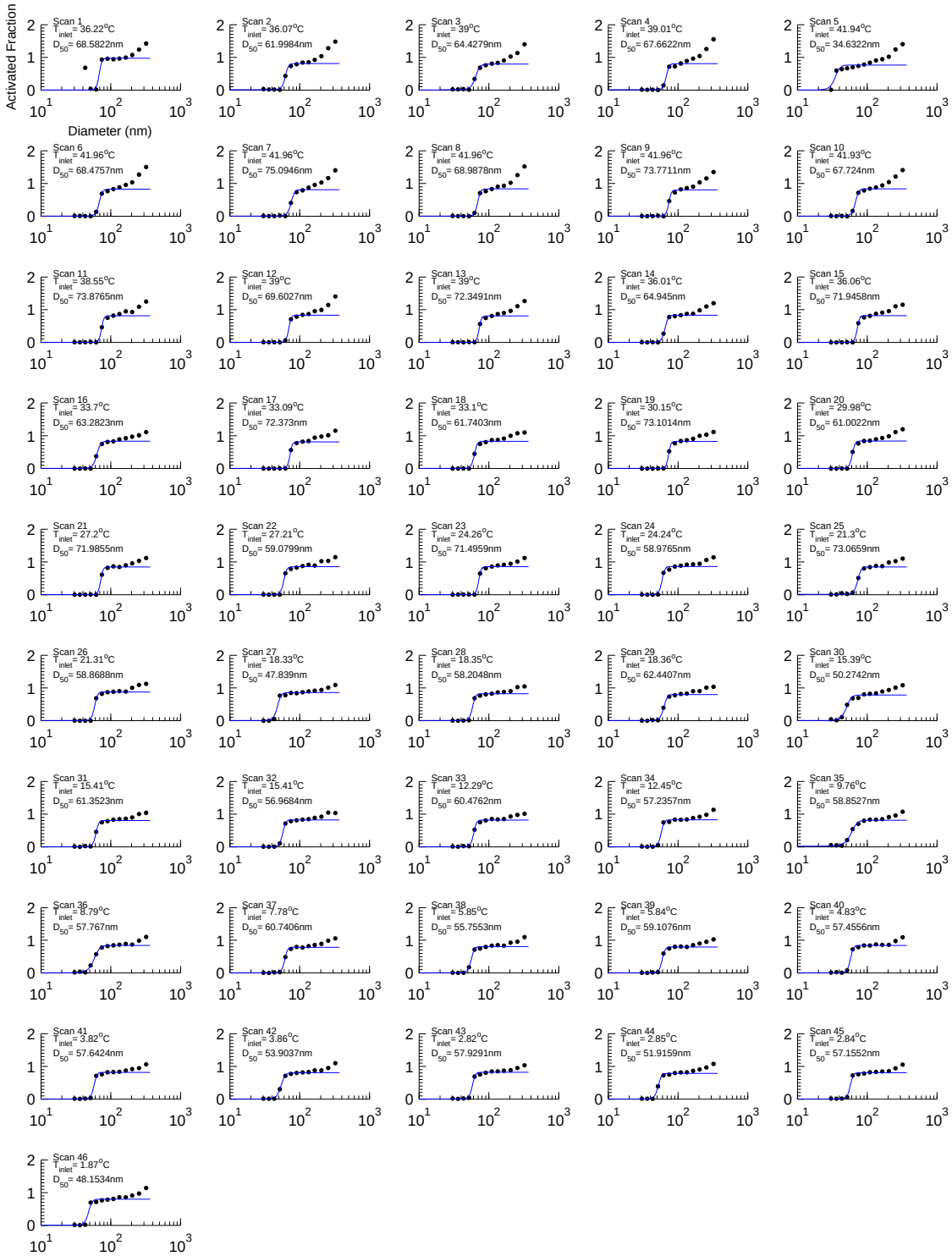

Figure A.40. MSA (odd scan numbers) and $(NH_4)_2SO_4$ activation curves. The activated fractions at each diameter are fit with a Sigmoid-Boltzmann curve (blue, see Table A.14).

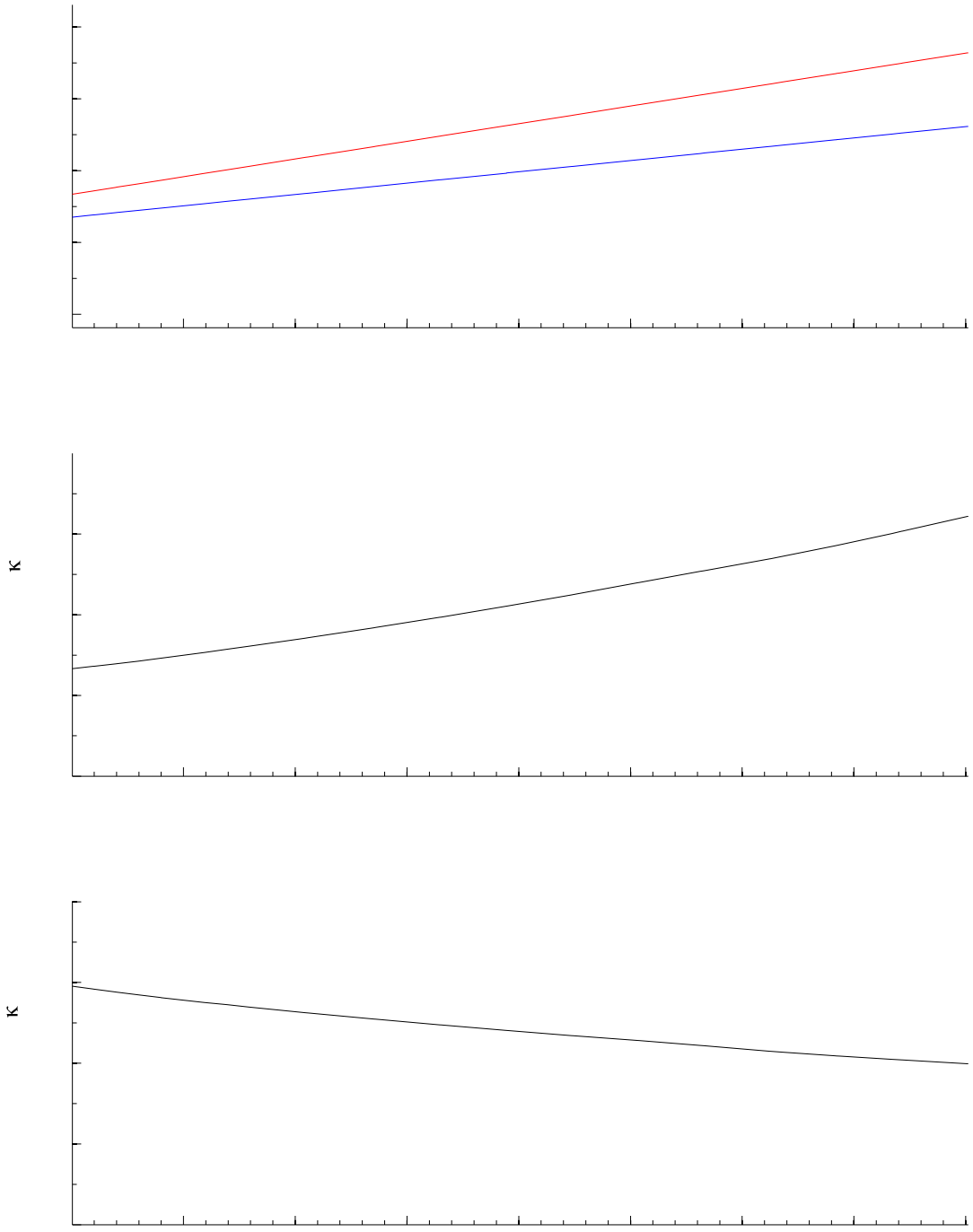

Figure A.41. MSA and $(NH_4)_2SO_4$ activation diameters (top) and MSA κ values (center and bottom) versus temperature. Each number represents a scan from Figure A.40. Fit coefficients represent the solid line fit through the activation diameters, which then give the κ line.

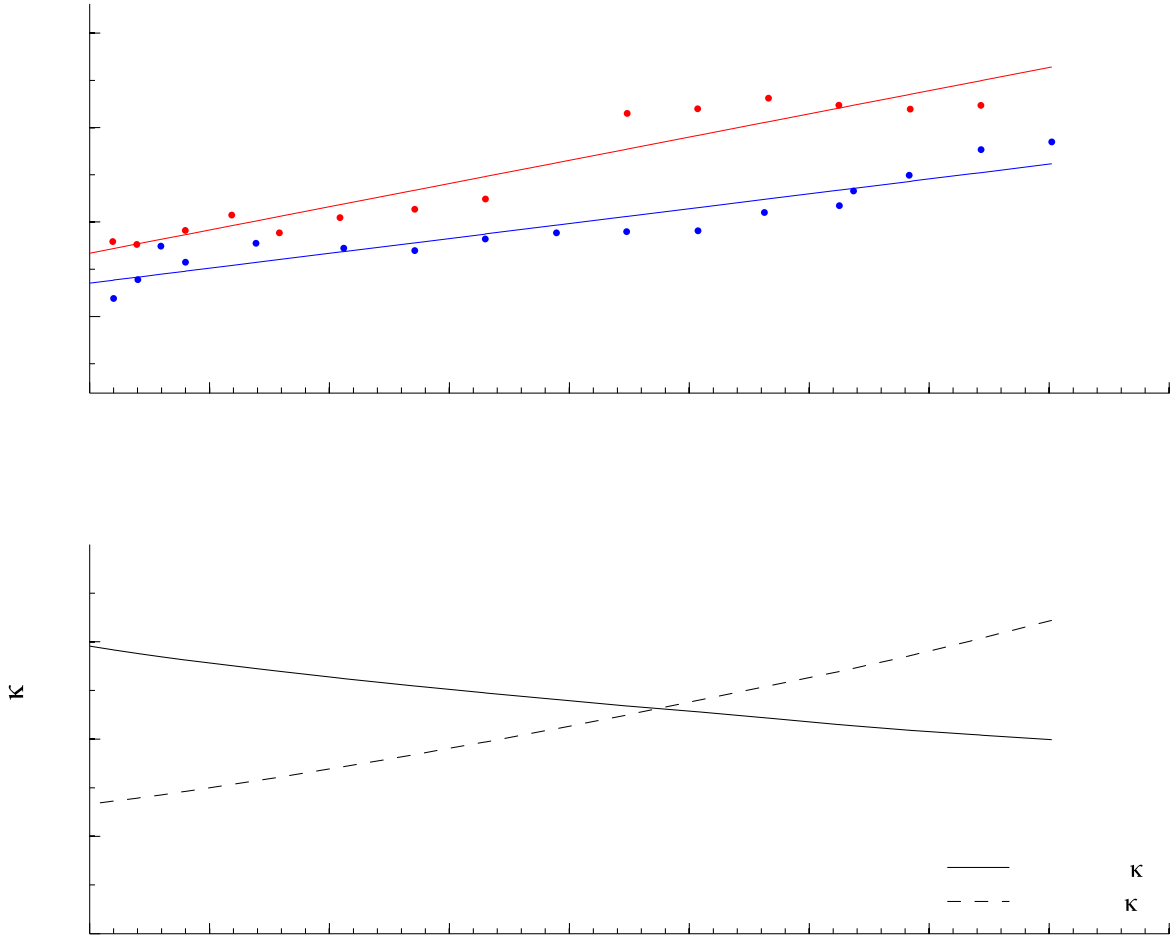

Figure A.42. MSA and $(NH_4)_2SO_4$ activation diameters replotted without scan numbers (top) and κ values (bottom) plotted together.

Table A.15. Methanesulfonic acid (MSA) data. Each line represents one diameter scan.

					Boltzmann Parameters:				
time	compound	ΔT	T_{box}	T_{inlet}	D_{50}	*A1*	*A2*	*dx*	excluded
36300	AS	6	0.00	35.88	62.74	0.0122	0.9184	3.00	yes
36780	MSA	6	0.00	38.90	74.15	0.0016	0.7702	3.00	yes
37200	AS	6	0.00	38.79	66.80	0.0061	0.7653	3.16	no
37620	MSA	6	0.00	38.78	76.28	0.0000	0.7735	4.07	no
38100	AS	6	0.00	38.79	69.25	0.0000	0.7705	3.00	no
38520	MSA	6	0.00	38.80	76.56	0.0006	0.7763	3.88	no
38940	AS	6	0.00	38.80	68.97	0.0000	0.7722	3.00	no
39420	MSA	6	0.00	38.79	76.57	0.0030	0.7857	3.25	no
39840	AS	6	0.00	38.79	68.78	0.0000	0.7749	3.00	no
40260	MSA	6	0.00	38.79	75.27	0.0024	0.7879	3.29	no
40740	AS	6	0.00	38.80	67.95	0.0024	0.7858	3.00	no
41160	MSA	6	0.00	38.81	74.29	0.0030	0.7974	3.00	no
41580	AS	6	0.00	35.85	70.12	0.0000	0.7965	3.00	no
42060	MSA	6	0.00	35.84	73.52	0.0015	0.7969	3.00	no
42480	AS	6	0.00	32.83	55.67	0.0000	0.7939	3.82	yes
42900	MSA	6	0.00	32.90	73.24	0.0007	0.8017	3.00	no
43380	AS	6	0.00	29.36	64.93	0.0019	0.8098	3.42	no
43800	MSA	6	0.00	29.88	72.70	0.0005	0.8110	3.00	no
44220	AS	6	0.00	29.89	62.42	0.0007	0.8059	3.05	no
44700	MSA	6	0.00	26.93	73.14	0.0005	0.8257	3.00	no
45120	AS	6	0.00	26.93	60.90	0.0000	0.8152	3.00	no
45540	MSA	6	0.00	23.97	76.71	0.0141	0.8383	3.81	yes
46020	AS	6	0.00	23.97	59.87	0.0000	0.8173	3.00	no
46440	MSA	6	0.00	20.99	37.51	0.0000	0.7339	3.00	yes
46860	AS	6	0.00	21.03	59.18	0.0000	0.8257	3.00	no
47340	MSA	6	0.00	21.03	68.31	0.0000	0.8471	3.00	no
47760	AS	6	0.00	18.08	61.17	0.0000	0.7986	3.70	no
48180	MSA	6	0.00	18.09	67.04	0.0018	0.8413	3.06	no
48660	AS	6	0.00	18.10	57.95	0.0000	0.8289	3.00	no
49080	MSA	6	0.00	13.13	72.57	0.2082	0.7886	3.00	yes
49500	AS	6	0.00	13.14	57.84	0.0000	0.7825	3.00	no
49980	MSA	6	0.00	11.12	66.96	0.0063	0.8004	3.20	no
50400	AS	6	0.00	10.13	58.65	0.0000	0.7969	7.90	yes
50820	MSA	6	0.00	9.17	68.22	0.0277	0.7939	3.41	no
51300	AS	6	0.00	8.13	61.07	0.0193	0.7693	3.00	yes
51720	MSA	6	0.00	7.18	66.76	0.0308	0.7946	4.25	no
52140	AS	6	0.00	6.12	55.41	0.0025	0.7700	3.00	no
52620	MSA	6	0.00	6.16	60.30	0.0009	0.7872	3.00	no
53040	AS	6	0.00	5.20	60.08	0.0258	0.7674	3.98	yes
53460	MSA	6	0.00	5.20	59.34	0.0000	0.7858	3.00	no
53940	AS	6	0.00	4.24	58.96	0.0000	0.7908	7.21	yes
54360	MSA	6	0.00	4.24	59.14	0.0000	0.7817	3.00	no
54780	AS	6	0.00	4.23	53.96	0.0048	0.7685	3.23	no
55260	MSA	6	0.00	3.22	59.93	0.0000	0.7862	3.00	no
55680	AS	6	0.00	3.21	54.08	0.0070	0.7648	3.33	no
56100	MSA	6	0.00	3.22	58.80	0.0000	0.7856	3.00	no

[1]Sensor malfunctioned resulting in temperature error.

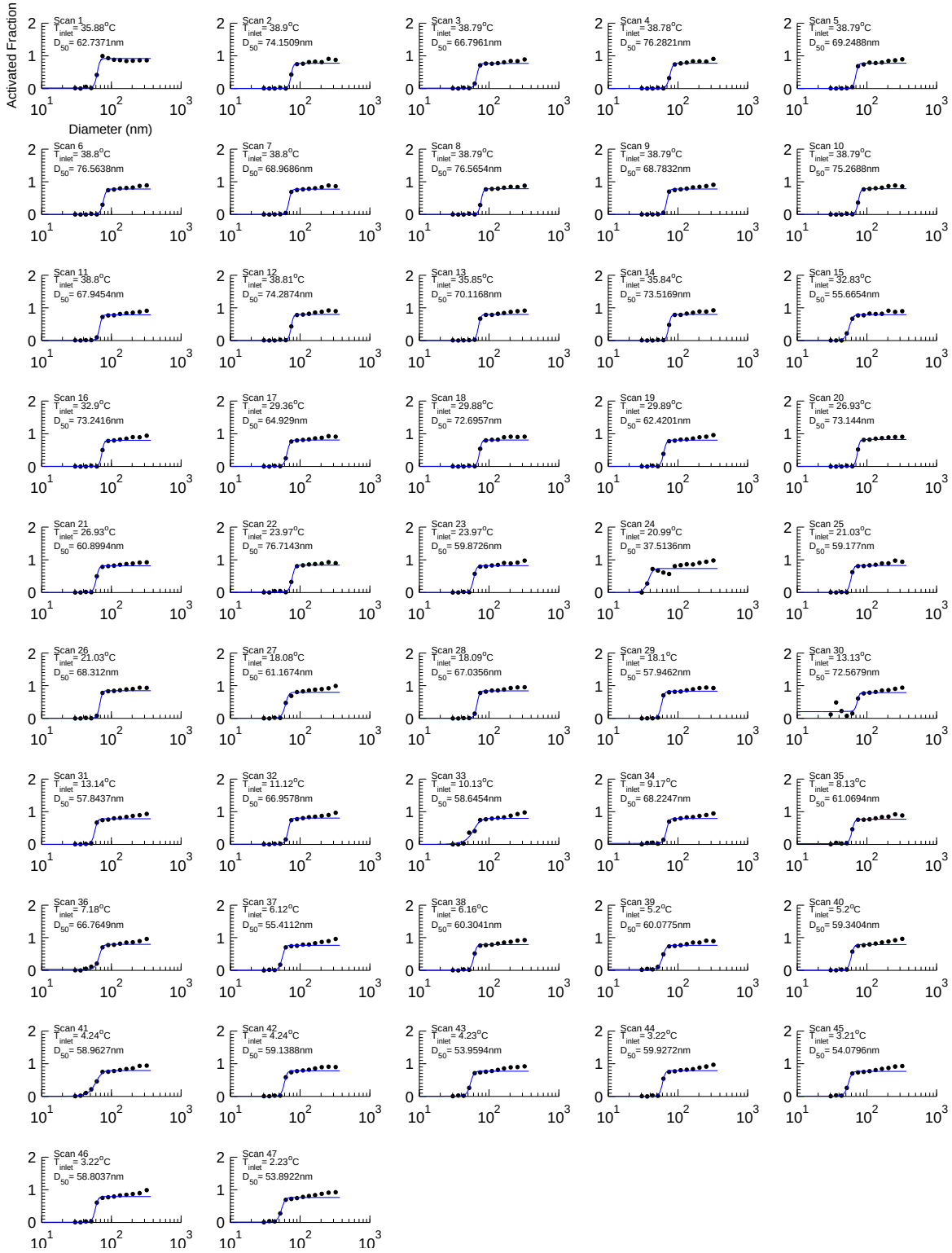

Figure A.43. MSA (even scan numbers) and $(NH_4)_2SO_4$ activation curves. The activated fractions at each diameter are fit with a Sigmoid-Boltzmann curve (blue, see Table A.15).

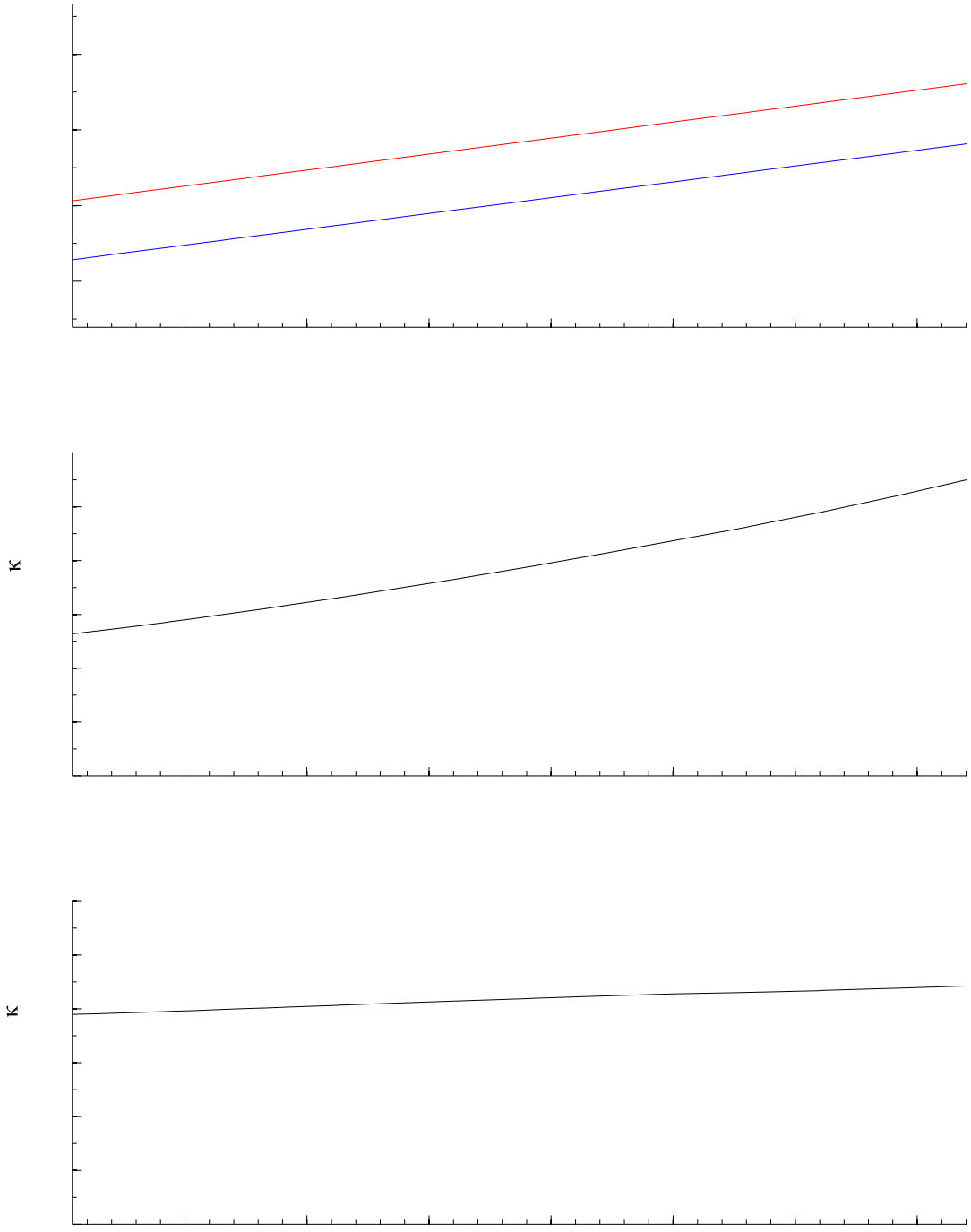

Figure A.44. MSA and $(NH_4)_2SO_4$ activation diameters (top) and MSA κ values (center and bottom) versus temperature. Each number represents a scan from Figure A.43. Fit coefficients represent the solid line fit through the activation diameters, which then give the κ line.

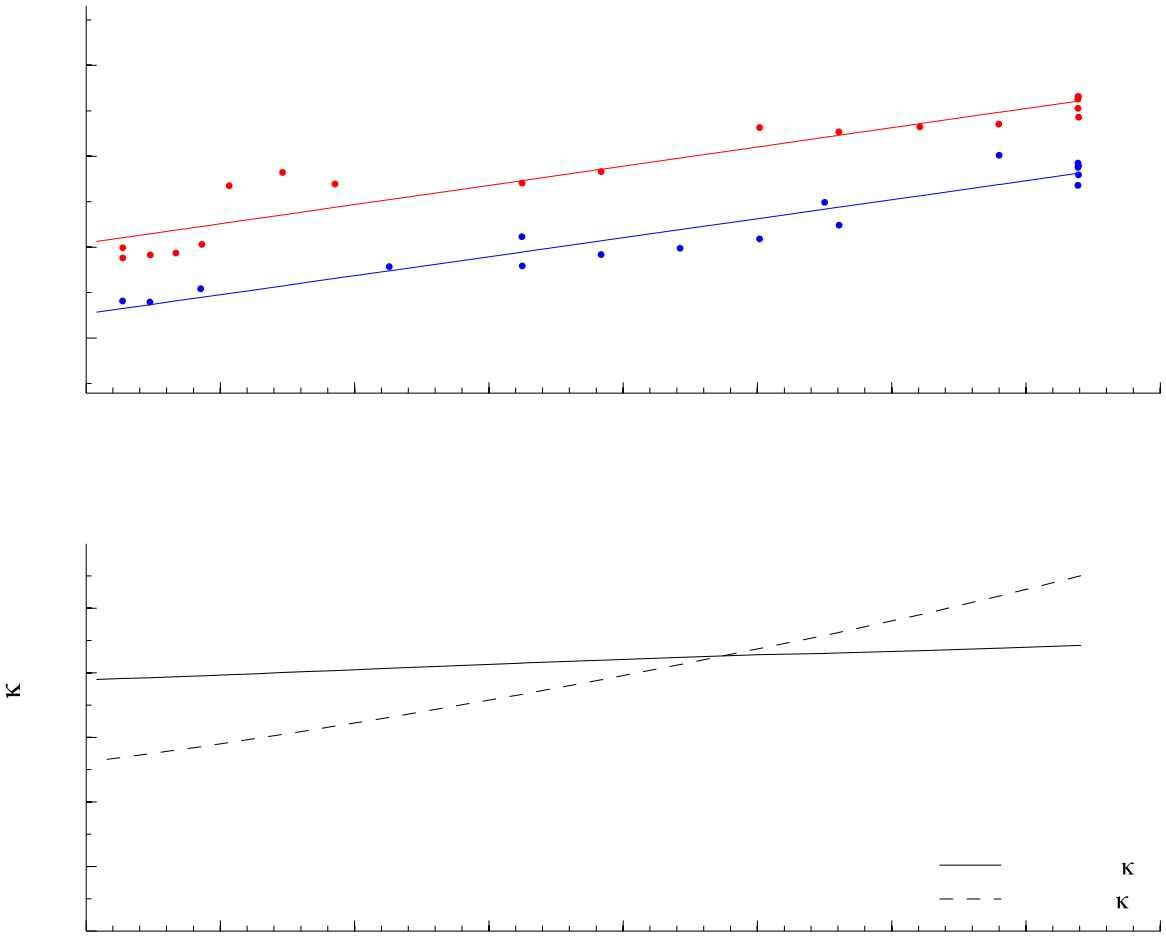

Figure A.45. MSA and $(NH_4)_2SO_4$ activation diameters replotted without scan numbers (top) and κ values (bottom) plotted together.

Table A.16. Methylammonium methylsulfonate data. Each line represents one diameter scan.

						Boltzmann Parameters:			
time	compound	ΔT	T_{box}	T_{inlet}	D_{50}	*A1*	*A2*	*dx*	excluded
36900	AS	6	0.00	39.17	30.00	0.3000	1.5000	40.00	yes
37380	MSA+MA	6	0.00	42.10	72.41	0.0071	0.7134	3.00	yes
37800	AS	6	0.00	42.13	88.55	0.0000	0.8041	3.00	yes
38220	MSA+MA	6	0.00	42.13	85.73	0.2413	0.7260	3.00	yes
38700	AS	6	0.00	42.10	65.64	0.0039	0.5877	3.00	yes
39120	MSA+MA	6	0.00	42.12	87.44	0.1013	1.0469	3.00	yes
39540	AS	6	0.00	42.12	69.18	0.0000	0.7547	3.00	yes
40020	MSA+MA	6	0.00	42.13	80.08	0.0067	0.7734	3.34	yes
40440	AS	6	0.00	42.11	68.90	0.0000	0.8005	3.00	yes
40860	MSA+MA	6	0.00	42.12	76.64	0.0106	0.7737	3.00	yes
41340	AS	6	0.00	42.11	68.15	0.0000	0.7925	3.00	yes
41760	MSA+MA	6	0.00	42.13	74.63	0.0087	0.7841	3.00	yes
42180	AS	6	0.00	39.18	68.99	0.0007	0.7869	3.00	yes
42660	MSA+MA	6	0.00	39.17	72.05	0.0047	0.7976	3.00	no
43080	AS	6	0.00	36.16	57.32	0.0000	0.8248	3.00	no
43500	MSA+MA	6	0.00	36.23	72.67	0.0072	0.8217	3.00	no
43980	AS	6	0.00	32.78	64.23	0.0064	0.8181	3.12	yes
44400	MSA+MA	6	0.00	33.21	70.43	0.0000	0.8241	3.00	no
44820	AS	6	0.00	33.22	60.89	0.0000	0.8351	3.00	no
45300	MSA+MA	6	0.00	30.26	70.40	0.0000	0.8357	3.00	no
45720	AS	6	0.00	30.29	59.51	0.0000	0.8473	3.00	no
46140	MSA+MA	6	0.00	27.31	69.76	0.0000	0.8534	3.00	no
46620	AS	6	0.00	27.33	57.52	0.0000	0.8297	3.00	no
47040	MSA+MA	6	0.00	24.37	68.88	0.0000	0.8688	3.00	no
47460	AS	6	0.00	24.35	57.89	0.0000	0.8676	3.00	no
47940	MSA+MA	6	0.00	21.41	49.43	0.0089	0.8490	3.75	yes
48360	AS	6	0.00	21.44	57.52	0.0000	0.8708	3.00	no
48780	MSA+MA	6	0.00	18.67	64.39	0.0000	0.8680	3.19	no
49260	AS	6	0.00	18.47	58.32	0.0000	0.9825	3.00	yes
49680	MSA+MA	6	0.00	18.46	60.83	0.0000	0.8705	3.00	yes
50100	AS	6	0.00	18.46	57.24	0.0000	0.8563	3.00	no
50580	MSA+MA	6	0.00	15.50	65.19	0.0051	0.8416	3.00	no
51000	AS	6	0.00	12.41	56.89	0.0000	0.8609	3.00	no
51420	MSA+MA	6	0.00	12.66	61.43	0.0000	0.8696	3.00	no
51900	AS	6	0.00	11.64	48.84	0.0000	0.8350	3.00	yes
52320	MSA+MA	6	0.00	10.67	58.20	0.0000	0.8612	3.00	no
52740	AS	6	0.00	10.67	57.27	0.0000	0.8717	3.00	yes
53220	MSA+MA	6	0.00	9.65	57.35	0.0000	0.8683	3.00	no
53640	AS	6	0.00	9.65	55.75	0.0000	0.8726	3.00	no
54060	MSA+MA	6	0.00	8.69	58.90	0.0000	0.8591	3.00	no
54540	AS	6	0.00	8.69	54.72	0.0000	0.8498	3.00	no
54960	MSA+MA	6	0.00	7.64	57.54	0.0000	0.8735	3.00	no
55380	AS	6	0.00	7.67	55.83	0.0032	0.8700	3.00	no
55860	MSA+MA	6	0.00	6.68	57.15	0.0000	0.8806	3.00	no
56280	AS	6	0.00	5.63	53.61	0.0000	0.8684	3.00	no
56700	MSA+MA	6	0.00	5.68	57.50	0.0000	0.8781	3.00	no
57180	AS	6	0.00	4.72	47.33	0.0000	0.8598	3.00	yes
57600	MSA+MA	6	0.00	4.73	57.25	0.0000	0.8741	3.00	no
58020	AS	6	0.00	3.74	46.15	0.0000	0.8566	3.00	yes
58500	MSA+MA	6	0.00	3.75	57.86	0.0000	0.8927	3.00	no
58920	AS	6	0.00	3.74	51.92	0.0000	0.8699	3.00	no

[1]Sensor malfunctioned resulting in temperature error.

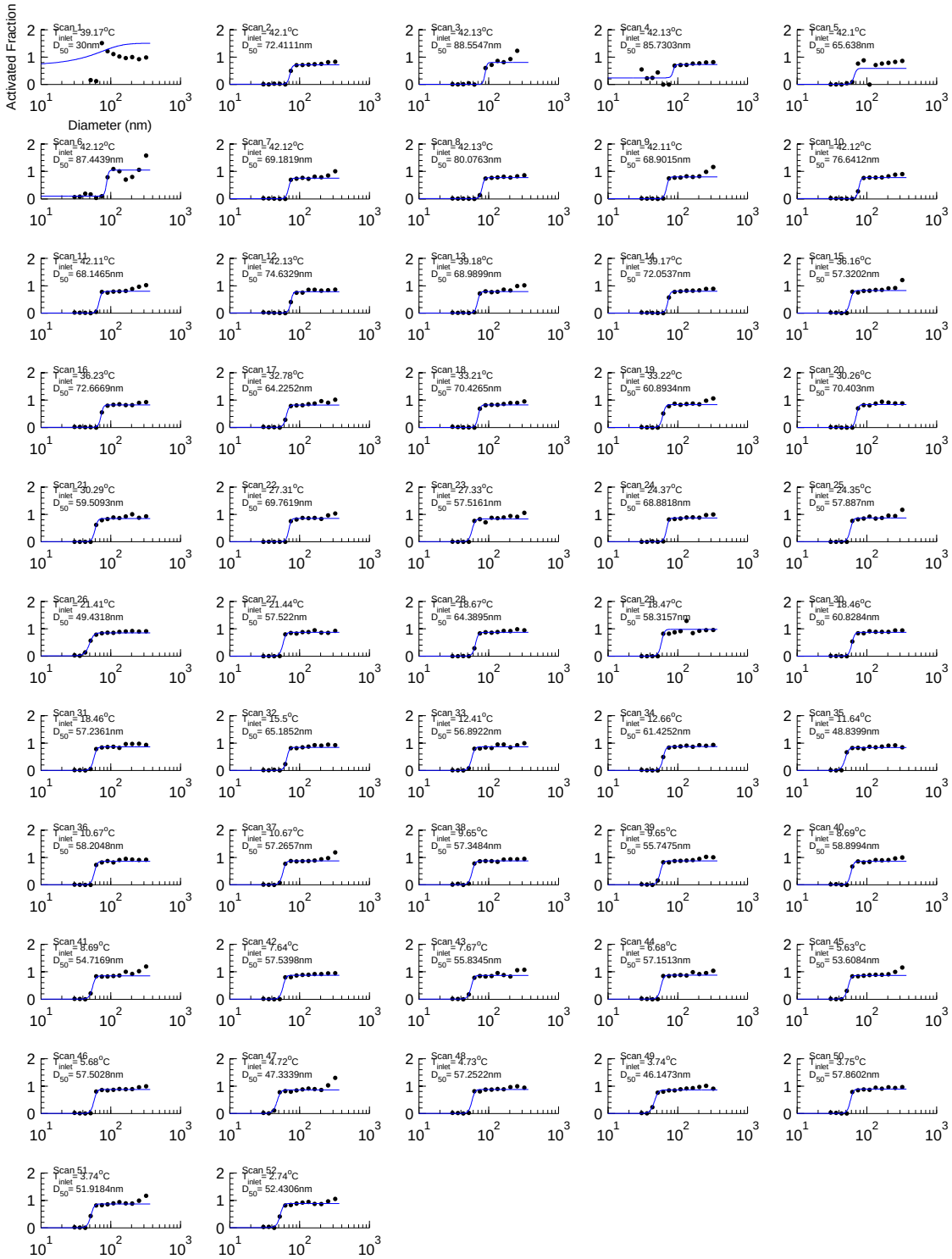

Figure A.46. Methylammonium methylsulfonate (even scan numbers) and $(NH_4)_2SO_4$ activation curves. The activated fractions at each diameter are fit with a Sigmoid-Boltzmann curve (blue, see Table A.16).

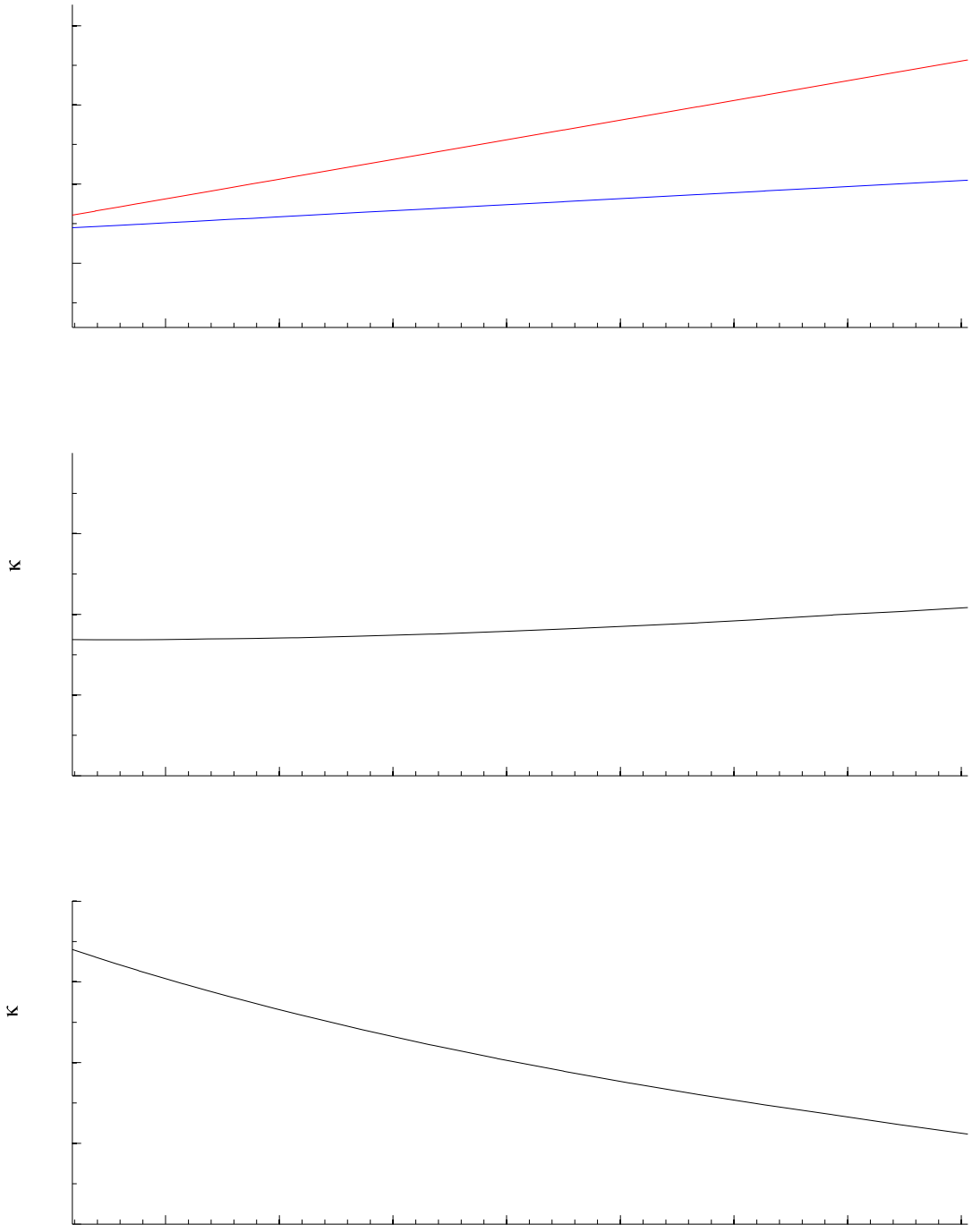

Figure A.47. Methylammonium methylsulfonate and $(NH_4)_2SO_4$ activation diameters (top) and MSA and MA κ values (center and bottom) versus temperature. Each number represents a scan from Figure A.46. Fit coefficients represent the solid line fit through the activation diameters, which then give the κ line.

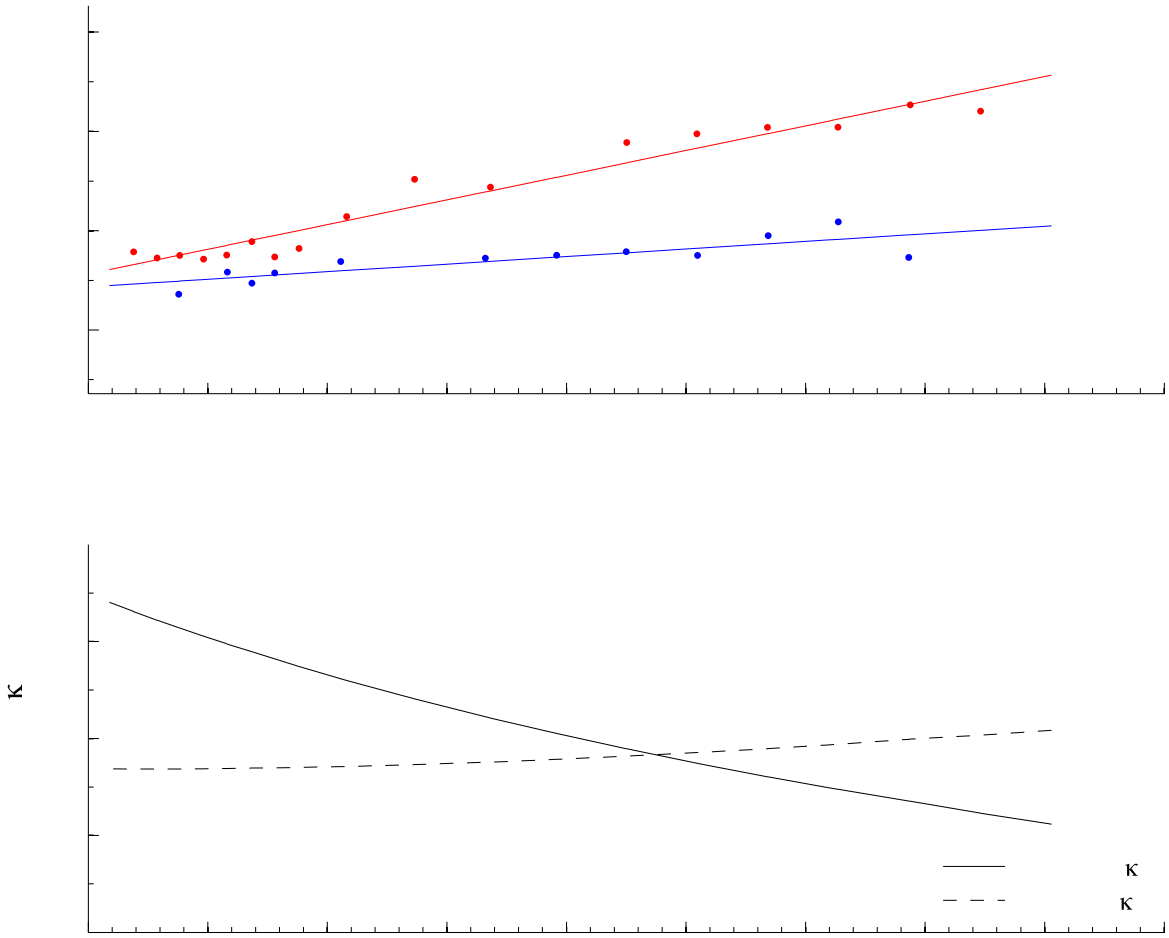

Figure A.48. Methylammonium methylsulfonate and $(NH_4)_2SO_4$ activation diameters replotted without scan numbers (top) and κ values (bottom) plotted together.

Table A.17. Methylammonium methylsulfonate data. Each line represents one diameter scan.

						Boltzmann Parameters:			
time	compound	ΔT	T_{box}	T_{inlet}	D_{50}	*A1*	*A2*	*dx*	excluded
40620	AS	6	0.00	38.34	30.00	0.3000	0.8025	17.37	yes
41040	MSA+MA	6	11.00	38.32	82.07	0.0178	0.7366	3.35	yes
41520	AS	6	11.00	41.26	56.89	0.0000	0.7910	3.00	yes
41940	MSA+MA	6	11.00	41.25	83.30	0.0166	0.7520	3.13	no
42360	AS	6	11.00	41.26	70.12	0.0000	0.7981	3.00	yes
42840	MSA+MA	6	11.00	41.27	84.73	0.0134	0.7580	3.05	yes
43260	AS	6	12.00	41.26	70.32	0.0000	0.8013	3.00	yes
43680	MSA+MA	6	12.00	41.27	84.08	0.0143	0.7453	3.06	yes
44160	AS	6	12.00	41.26	69.97	0.0000	0.7952	3.00	yes
44580	MSA+MA	6	12.00	41.27	84.13	0.0156	0.7560	3.24	yes
45000	AS	6	12.00	41.26	69.58	0.0000	0.8143	3.00	yes
45480	MSA+MA	6	12.00	41.27	83.62	0.0152	0.7533	3.13	yes
45900	AS	6	12.00	41.26	69.94	0.0000	0.8245	3.00	yes
46320	MSA+MA	6	12.00	41.27	83.69	0.0173	0.7759	3.22	yes
46800	AS	6	1.00	38.31	72.27	0.0018	0.8077	3.00	yes
47220	MSA+MA	6	1.00	38.31	83.41	0.0171	0.7819	3.65	no
47640	AS	6	1.00	38.31	69.47	0.0000	0.8356	3.00	no
48120	MSA+MA	6	1.00	35.22	85.16	0.0188	0.7445	6.21	no
48540	AS	6	1.00	35.32	69.70	0.0000	0.8223	3.00	no
48960	MSA+MA	6	1.00	35.31	80.74	0.0231	0.7837	3.86	no
49440	AS	6	1.00	31.94	69.07	0.0038	0.8307	3.09	no
49860	MSA+MA	6	1.00	32.40	83.25	0.0160	0.7954	3.91	no
50280	AS	6	1.00	32.41	70.01	0.0053	0.8394	3.24	no
50760	MSA+MA	6	2.00	28.95	78.87	0.0211	0.7818	3.89	no
51180	AS	6	2.00	29.40	69.33	0.0037	0.8317	3.41	no
51600	MSA+MA	6	2.00	29.40	75.21	0.0185	0.7964	3.61	no
52080	AS	6	2.00	26.29	66.84	0.0000	0.8563	3.65	no
52500	MSA+MA	6	2.00	26.51	76.62	0.0132	0.7974	4.47	no
52920	AS	6	2.00	26.50	67.30	0.0016	0.8429	3.00	no
53400	MSA+MA	6	2.00	23.47	72.82	0.0142	0.7835	3.67	no
53820	AS	6	2.00	23.55	67.90	0.0000	0.8464	3.00	no
54240	MSA+MA	6	3.00	23.57	72.75	0.0164	0.7912	3.00	no
54720	AS	6	3.00	20.50	68.60	0.0045	0.8491	3.43	no
55140	MSA+MA	6	3.00	20.61	74.04	0.0194	0.7860	3.00	no
55560	AS	6	3.00	20.61	66.34	0.0033	0.8435	3.00	no
56040	MSA+MA	6	3.00	17.26	71.02	0.0159	0.7935	3.00	no
56460	AS	6	3.00	17.65	67.39	0.0000	0.8512	3.00	no
56880	MSA+MA	6	3.00	17.62	70.32	0.0091	0.7788	3.00	no
57360	AS	6	3.00	17.65	65.76	0.0020	0.8564	3.61	no
57780	MSA+MA	6	4.00	12.65	85.82	0.0754	0.7883	3.00	yes
58200	AS	6	4.00	12.65	63.75	0.0007	0.8300	3.62	yes
58740	MSA+MA	6	4.00	11.69	87.81	0.0000	0.8623	3.00	yes
59160	AS	6	4.00	10.68	83.65	0.0035	1.0192	3.81	yes
59580	MSA+MA	6	4.00	9.70	89.88	0.0203	0.8426	3.00	yes
60060	AS	6	4.00	8.67	76.03	0.0000	0.9953	4.27	yes
60480	MSA+MA	6	4.00	8.68	82.83	0.0050	0.8868	3.85	yes
60900	AS	6	4.00	7.72	82.59	0.0009	1.0487	4.79	yes
61380	MSA+MA	6	5.00	7.73	81.07	0.0045	0.8775	4.32	yes
61800	AS	6	5.00	6.71	74.95	0.0000	0.9730	4.04	yes
62220	MSA+MA	6	5.00	6.70	79.74	0.0040	0.8614	4.41	yes
62700	AS	6	5.00	5.74	76.63	0.0000	1.0311	5.49	yes
63120	MSA+MA	6	5.00	5.74	80.58	0.0004	0.9033	5.32	yes
63540	AS	6	5.00	4.71	72.68	0.0000	1.0051	3.12	yes
64020	MSA+MA	6	5.00	4.78	81.01	0.0063	0.8658	4.51	yes
64440	AS	6	5.00	4.78	72.64	0.0000	0.9939	3.11	yes

[1]Sensor malfunctioned resulting in temperature error.

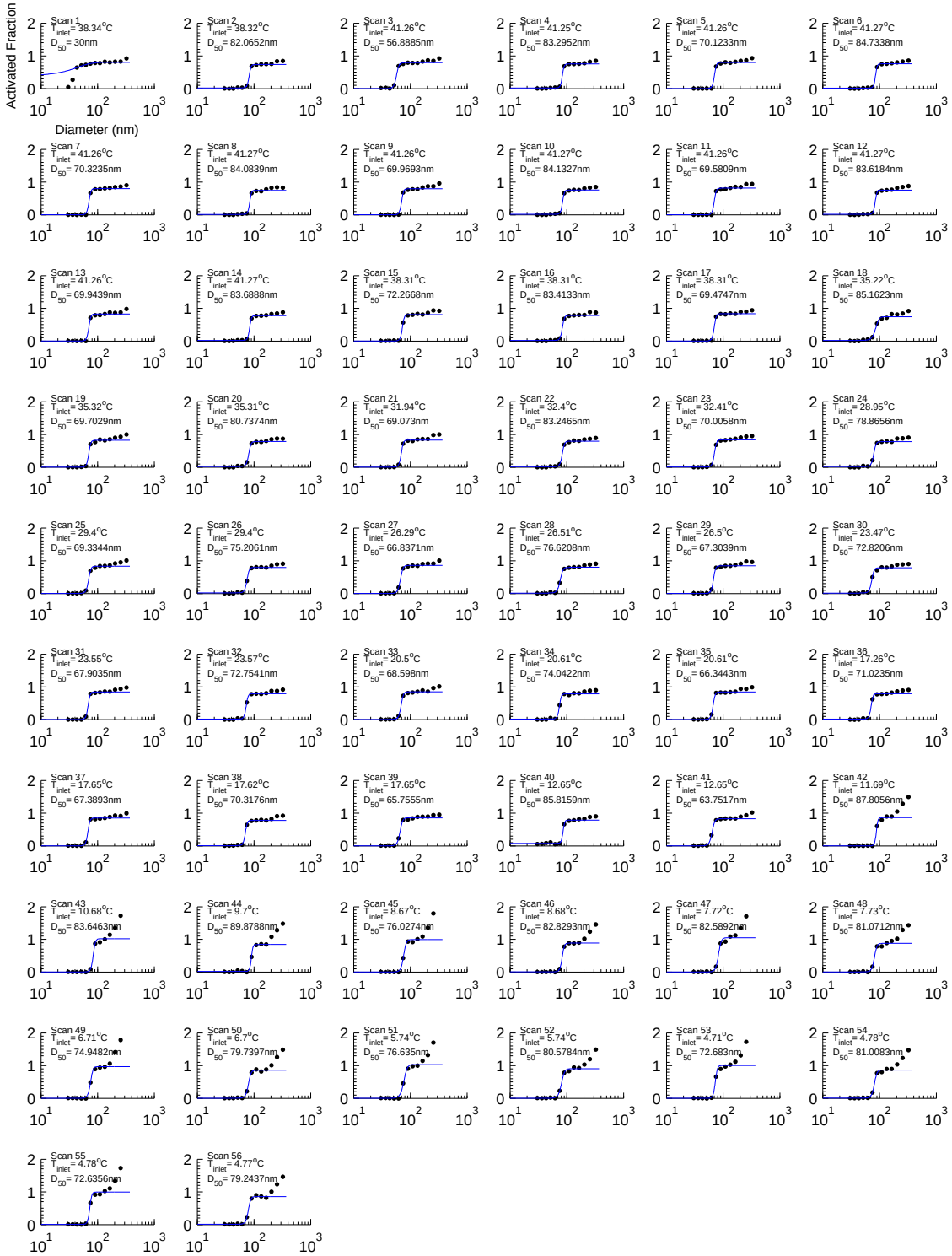

Figure A.49. Methylammonium methylsulfonate (even scan numbers) and $(NH_4)_2SO_4$ activation curves. The activated fractions at each diameter are fit with a Sigmoid-Boltzmann curve (blue, see Table A.17).

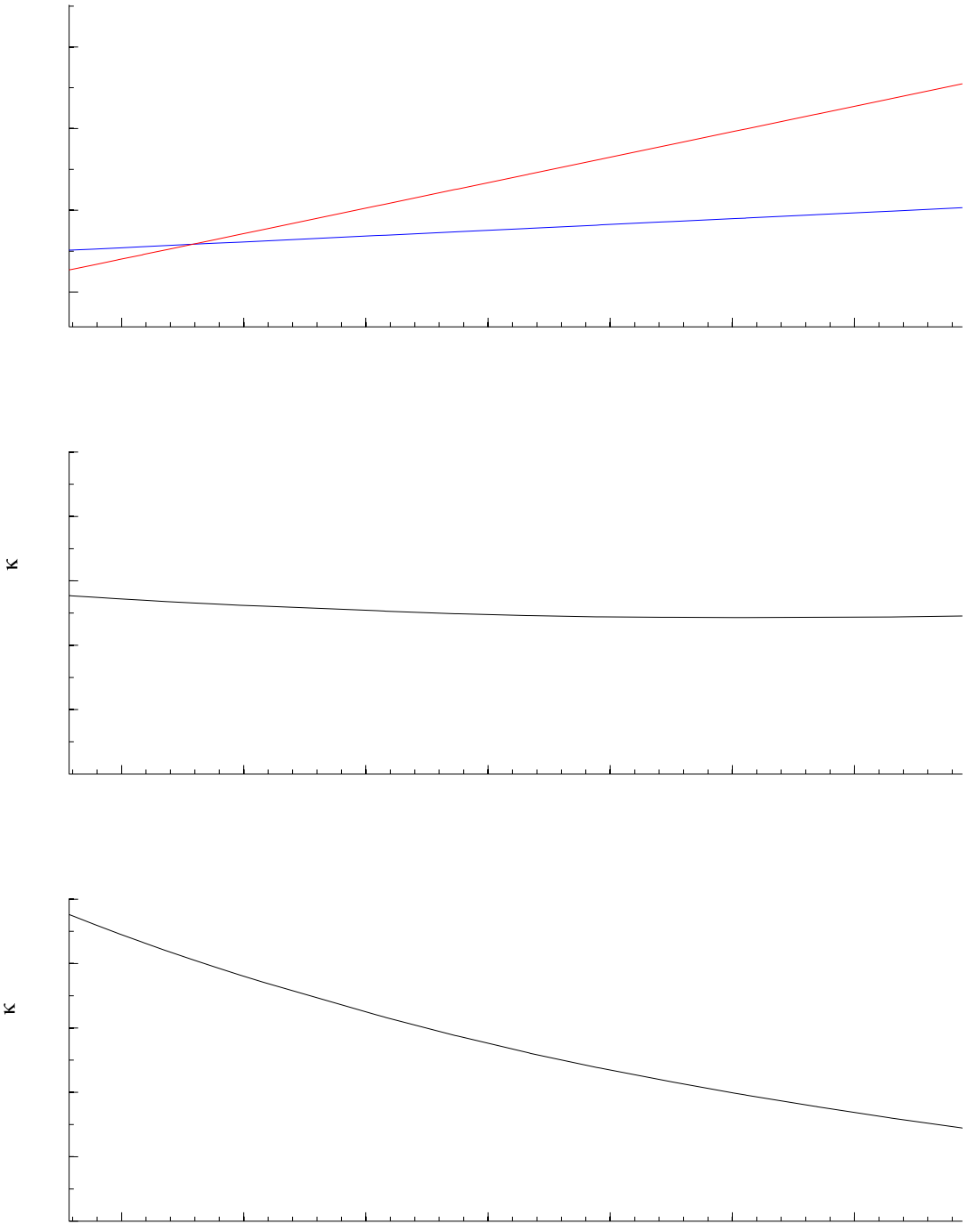

Figure A.50. Methylammonium methylsulfonate and $(NH_4)_2SO_4$ activation diameters (top) and MSA and MA κ values (center and bottom) versus temperature. Each number represents a scan from Figure A.49. Fit coefficients represent the solid line fit through the activation diameters, which then give the κ line.

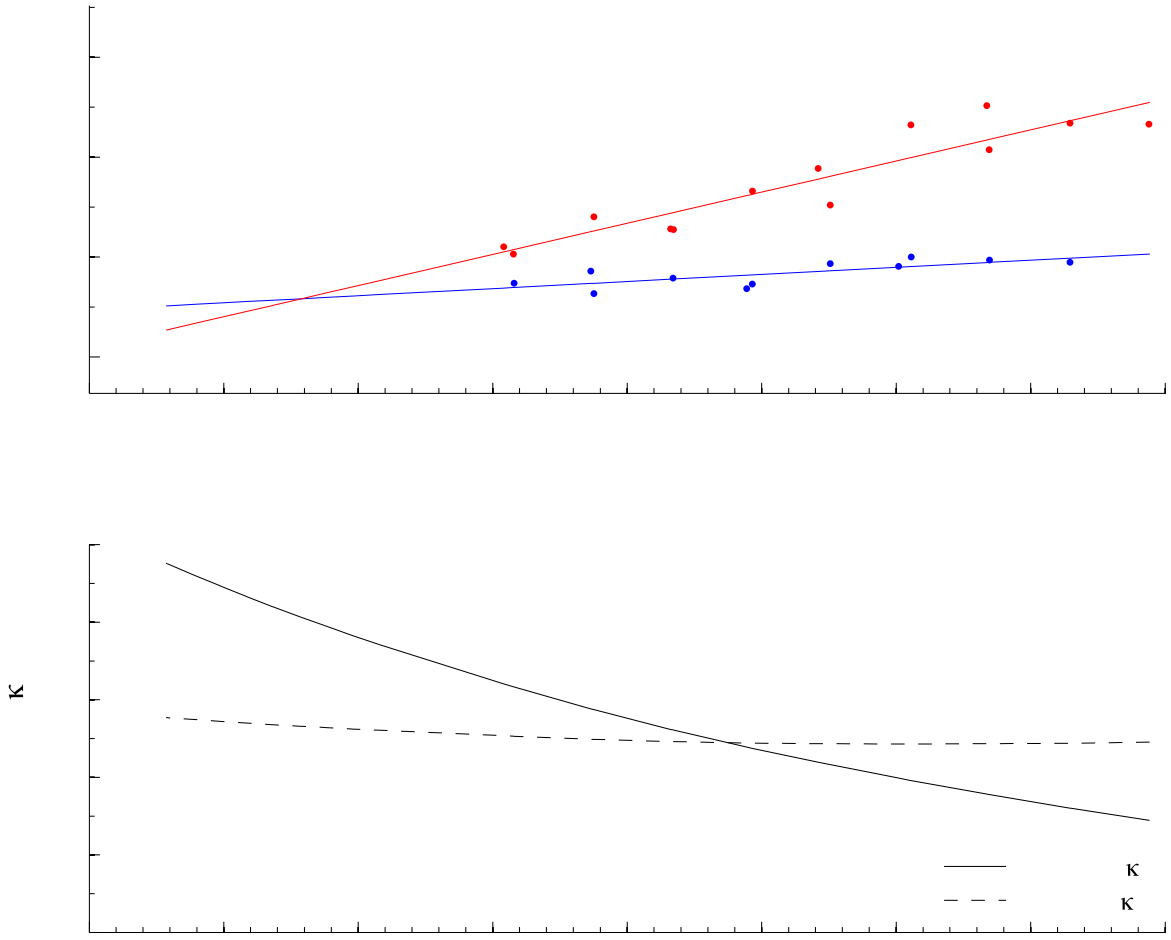

Figure A.51. Methylammonium methylsulfonate and $(NH_4)_2SO_4$ activation diameters replotted without scan numbers (top) and κ values (bottom) plotted together.

Table A.18. Polyethylene glycol (PEG) 600 data. Each line represents one diameter scan.

						Boltzmann Parameters:			
time	compound	ΔT	T_{box}	T_{inlet}	D_{50}	*A1*	*A2*	*dx*	excluded
37080	PEG600	6	0.00	30.27	89.00	0.0642	0.7843	3.00	yes
37560	AS	6	32.59	34.22	57.78	0.0000	0.7724	3.00	yes
37980	PEG600	6	35.75	36.17	83.79	0.0125	0.8082	3.00	yes
38400	AS	6	38.10	38.18	68.04	0.0000	0.8165	4.65	no
38880	PEG600	6	39.85	38.13	139.26	0.0209	0.6534	3.00	no
39300	AS	6	41.17	40.06	64.65	0.0000	0.7840	4.74	no
39720	PEG600	6	41.92	40.05	159.24	0.0180	0.9774	6.64	yes
40200	AS	6	41.98	40.04	70.03	0.0008	0.8159	3.37	yes
40620	PEG600	6	41.55	40.05	158.83	0.0168	0.9880	6.20	yes
41040	AS	6	40.78	40.07	69.52	0.0025	0.8241	3.30	yes
41520	PEG600	6	39.77	40.07	142.88	0.0160	0.7591	4.15	yes
41940	AS	6	38.58	40.06	68.99	0.0000	0.8237	3.80	yes
42360	PEG600	6	37.29	41.08	139.75	0.0145	0.7462	3.20	yes
42840	AS	6	36.25	37.90	68.77	0.0000	0.8351	3.82	yes
43260	PEG600	6	35.11	38.07	135.91	0.0063	0.7187	3.00	yes
43680	AS	6	34.12	38.09	68.30	0.0000	0.8415	3.83	no
44160	PEG600	6	32.74	35.05	136.38	0.0057	0.8057	3.00	no
44580	AS	6	31.26	35.13	68.59	0.0000	0.8300	3.55	no
45000	PEG600	6	30.08	35.13	134.30	0.0033	0.8049	5.85	no
45480	AS	6	28.60	32.15	53.33	0.0000	0.8424	14.65	yes
45900	PEG600	6	27.27	32.16	131.74	0.0010	0.8454	3.02	no
46320	AS	6	25.79	29.04	61.49	0.0000	0.8224	3.00	no
46800	PEG600	6	24.38	29.23	132.85	0.0029	0.8390	3.02	no
47220	AS	6	22.98	29.23	60.20	0.0000	0.8292	3.00	no
47640	PEG600	6	21.38	26.25	128.36	0.0000	0.8507	3.00	no
48120	AS	6	20.09	26.28	59.30	0.0000	0.8404	3.00	no
48540	PEG600	6	18.63	23.31	121.62	0.0239	0.7851	5.46	no
48960	AS	6	17.49	23.34	59.09	0.0000	0.8402	3.00	no
49440	PEG600	6	16.33	23.34	124.92	0.0007	0.9718	5.79	no
49860	AS	6	15.32	20.37	64.79	0.0000	0.8610	4.42	no
50280	PEG600	6	14.46	20.37	123.41	0.0024	0.9045	4.91	no
50760	AS	6	13.56	20.37	58.34	0.0000	0.8509	3.00	no
51180	PEG600	6	12.73	17.18	100.38	0.0013	0.8878	3.00	yes
51600	AS	6	12.15	17.41	58.25	0.0000	0.8604	3.00	no
52080	PEG600	6	11.65	17.41	119.74	0.0071	0.8966	6.48	no
52500	AS	6	10.31	17.44	57.26	0.0000	0.8696	3.00	no
52920	PEG600	6	8.94	14.41	120.48	0.0217	0.8642	7.32	no
53400	AS	6	8.16	14.43	56.41	0.0000	0.8812	3.23	no
53820	PEG600	6	7.34	14.42	109.37	0.0128	0.8490	3.00	yes
54240	AS	6	6.63	14.44	56.06	0.0000	0.9087	4.43	no
54720	PEG600	6	5.79	11.47	117.08	0.0192	0.9140	3.00	yes
58140	AS	6	5.36	6.57	75.14	0.0000	1.1601	7.77	yes
58560	PEG600	6	2.50	6.58	132.22	0.0169	0.8432	3.00	no
58980	AS	6	2.13	6.60	70.80	0.0000	1.1462	6.94	yes
59460	PEG600	6	1.75	5.53	130.36	0.0193	0.7742	3.00	no
59880	AS	6	1.42	5.57	69.53	0.0000	1.1552	6.90	no
60300	PEG600	6	1.14	5.57	130.32	0.0216	0.8445	3.00	no
60780	AS	6	0.88	5.57	65.36	0.0000	1.1225	6.89	no
61200	PEG600	6	0.62	4.55	129.06	0.0235	0.8552	3.00	no

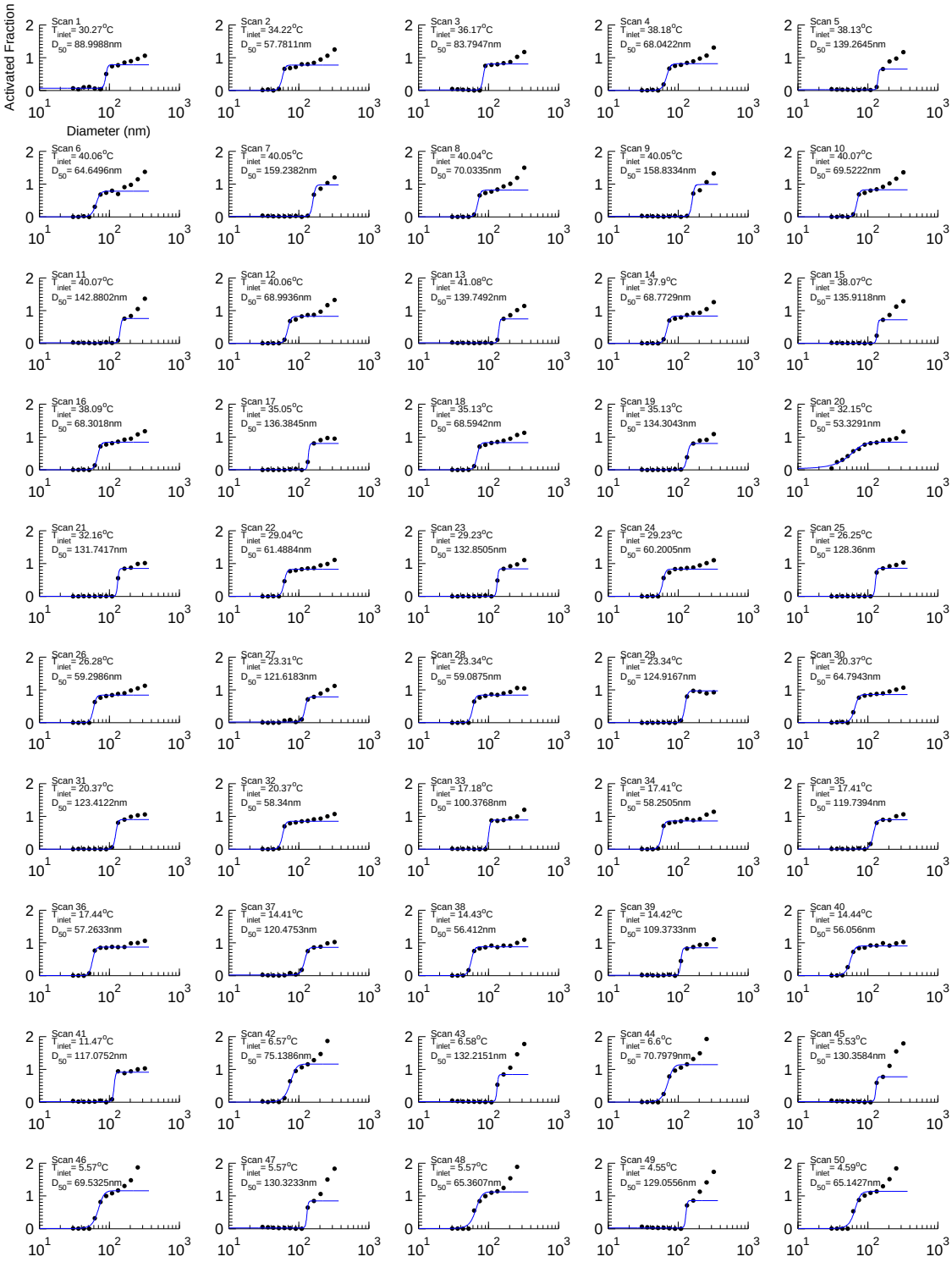

Figure A.52. PEG 600 (odd scan numbers) and $(NH_4)_2SO_4$ activation curves. The activated fractions at each diameter are fit with a Sigmoid-Boltzmann curve (blue, see Table A.18).

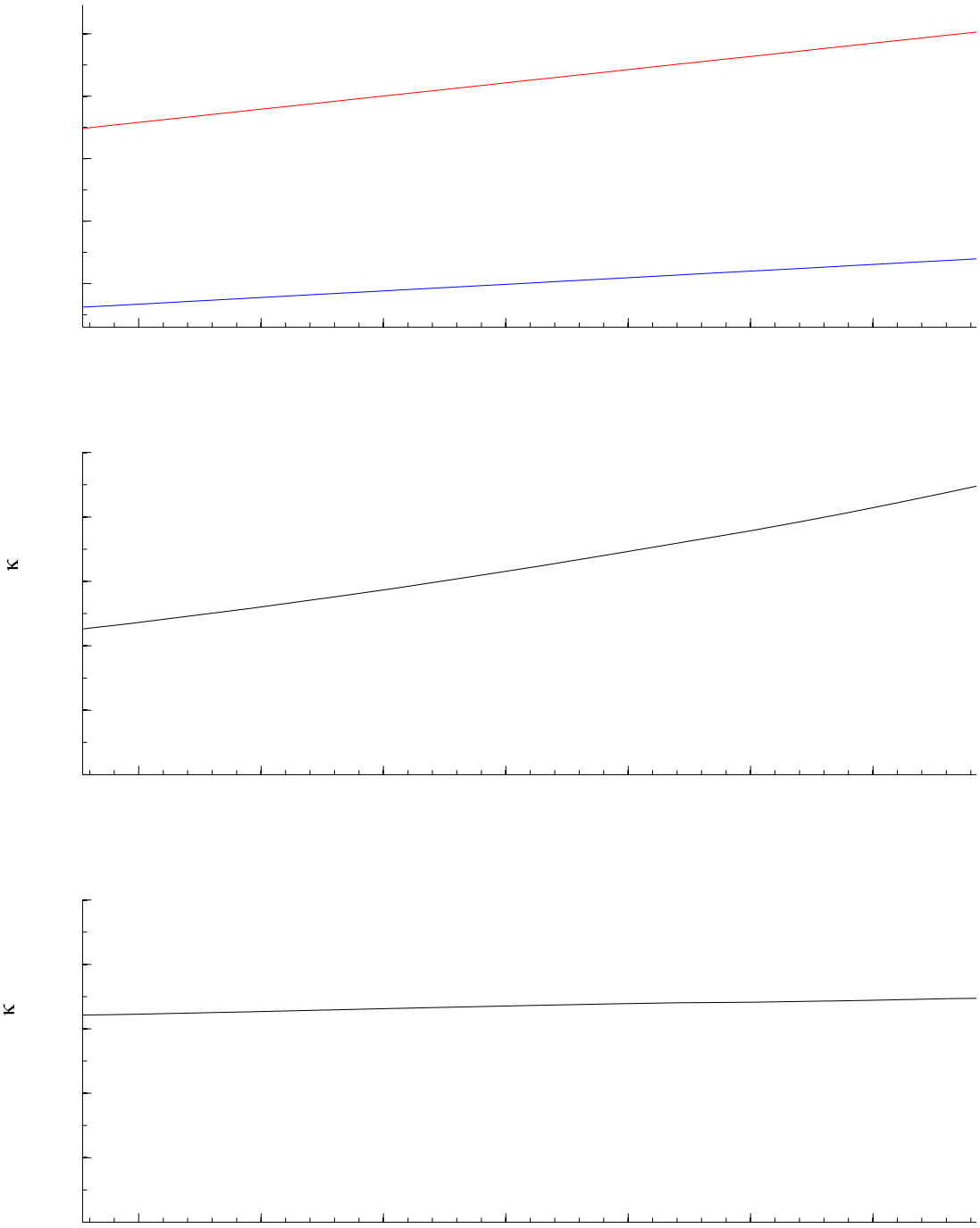

Figure A.53. PEG 600 and $(NH_4)_2SO_4$ activation diameters (top) and PEG 600 κ values (center and bottom) versus temperature. Each number represents a scan from Figure A.54. Fit coefficients represent the solid line fit through the activation diameters, which then give the κ line.

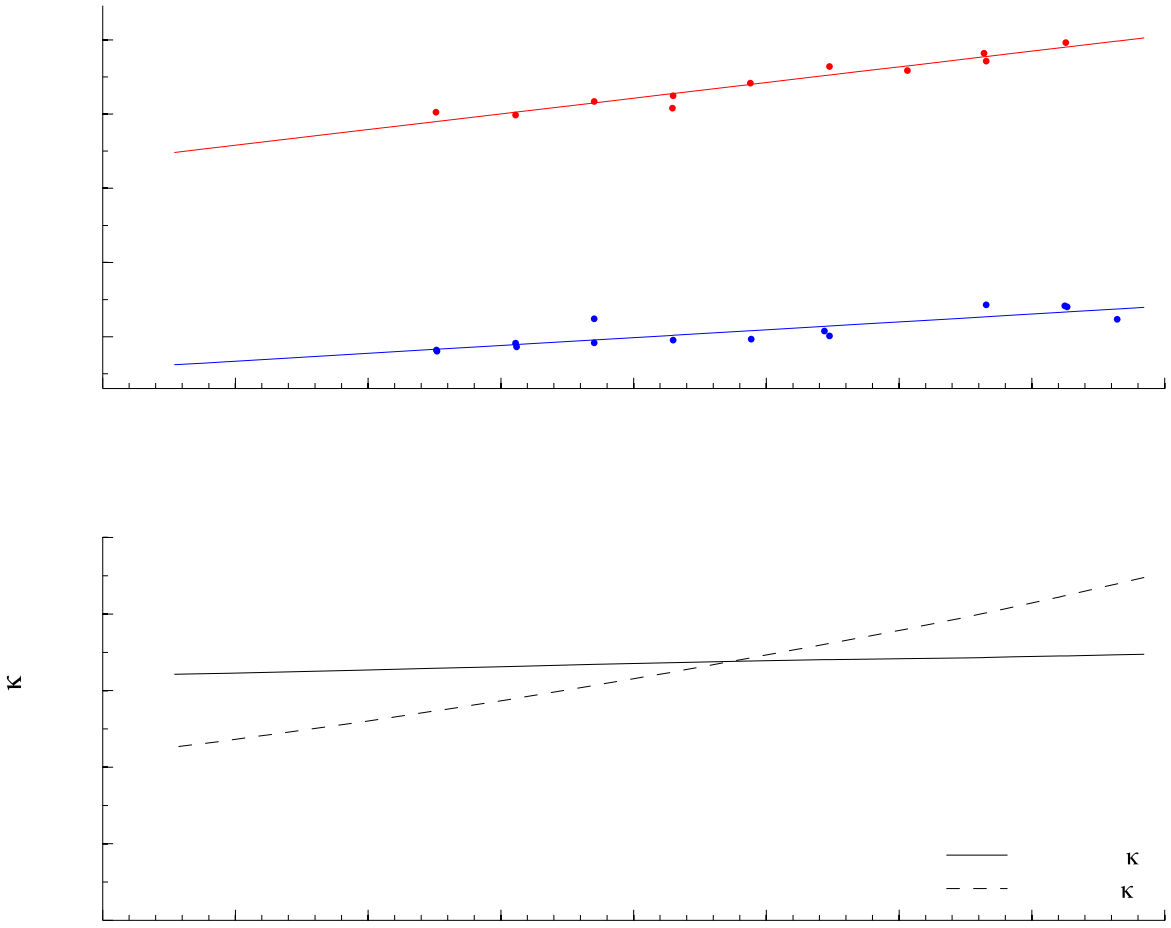

Figure A.54. PEG 600 and $(NH_4)_2SO_4$ activation diameters replotted without scan numbers (top) and κ values (bottom) plotted together.

Table A.19. Polyethylene glycol (PEG) 600 data. Each line represents one diameter scan.

						Boltzmann Parameters:			
time	compound	ΔT	T_{box}	T_{inlet}	D_{50}	*A1*	*A2*	*dx*	excluded
35100	PEG600	6	0.00	36.76	30.00	0.3000	1.5000	40.00	yes
35520	AS	6	39.02	39.73	63.78	0.0000	1.2280	5.85	yes
36300	PEG600	6	40.57	39.70	160.15	0.0105	1.0114	3.00	no
36720	AS	6	42.45	42.65	54.81	0.0000	0.9122	4.68	yes
37200	PEG600	6	43.14	42.67	160.25	0.0112	0.9501	3.06	yes
37620	AS	6	43.19	42.67	70.29	0.0000	0.9303	3.00	yes
38040	PEG600	6	42.77	42.64	159.35	0.0151	0.9652	3.00	yes
38520	AS	6	42.02	42.65	70.24	0.0000	0.9459	3.00	yes
38940	PEG600	6	41.01	42.67	159.99	0.0135	0.9826	3.01	yes
39360	AS	6	39.88	42.65	69.28	0.0000	0.9296	3.00	yes
39840	PEG600	6	38.59	42.65	157.22	0.0167	1.0363	5.14	yes
40260	AS	6	37.18	39.71	70.41	0.0000	0.9353	3.00	yes
40680	PEG600	6	35.99	39.72	152.75	0.0168	0.9981	7.54	yes
41160	AS	6	34.44	36.57	67.07	0.0000	0.9330	3.80	yes
41580	PEG600	6	32.83	36.76	147.24	0.0066	1.0068	7.71	yes
42000	AS	6	31.34	36.76	66.44	0.0000	0.9698	4.65	no
42480	PEG600	6	29.63	33.82	149.24	0.0004	1.0317	10.36	no
42900	AS	6	28.11	33.81	62.81	0.0000	0.9638	4.21	no
43320	PEG600	6	26.30	30.85	142.94	0.0003	1.0602	9.56	no
43800	AS	6	24.78	30.85	60.84	0.0000	0.9465	3.00	no
44220	PEG600	6	22.96	27.91	135.65	0.0000	0.9940	7.14	no
44640	AS	6	21.47	27.90	59.62	0.0000	0.9581	3.00	no
45120	PEG600	6	19.71	24.94	133.01	0.0036	1.0281	3.18	no
45540	AS	6	18.28	24.97	58.67	0.0000	0.9576	3.00	no
45960	PEG600	6	16.68	21.94	132.48	0.0130	1.0088	3.09	no
46440	AS	6	15.40	21.97	58.52	0.0000	0.9858	3.00	no
46860	PEG600	6	13.99	18.95	69.60	0.0000	1.0034	3.00	yes
47280	AS	6	12.85	19.00	58.43	0.0000	0.9998	3.00	no
47760	PEG600	6	11.69	18.97	121.06	0.0095	1.0423	6.75	no
48180	AS	6	10.56	16.03	38.77	0.0000	0.9639	6.65	yes
48600	PEG600	6	9.77	16.06	115.81	0.0067	1.0439	6.80	no
49080	AS	6	8.89	16.05	56.91	0.0000	0.9935	3.00	no
49500	PEG600	6	8.01	12.91	101.31	0.0271	0.9832	3.00	yes
49920	AS	6	7.33	13.11	57.56	0.0000	0.9494	3.00	no
50400	PEG600	6	6.77	13.11	118.62	0.0357	1.0157	7.50	no
50820	AS	6	6.05	13.09	56.47	0.0000	0.9500	3.00	no
51240	PEG600	6	5.49	13.09	118.54	0.0524	1.0021	6.18	no
51720	AS	6	4.93	10.12	56.39	0.0000	0.9513	3.00	no
52140	PEG600	6	4.63	10.15	117.84	0.0467	1.0065	7.30	no
52560	AS	6	4.09	10.14	54.58	0.0000	0.9392	3.36	no
53040	PEG600	6	2.62	10.16	110.96	0.0587	0.9771	4.71	no
53460	AS	6	1.73	10.14	53.14	0.0000	0.9347	3.36	no
53880	PEG600	6	1.15	7.14	117.43	0.0548	1.0010	6.86	no
54360	AS	6	0.93	7.14	51.78	0.0000	0.9266	3.00	no

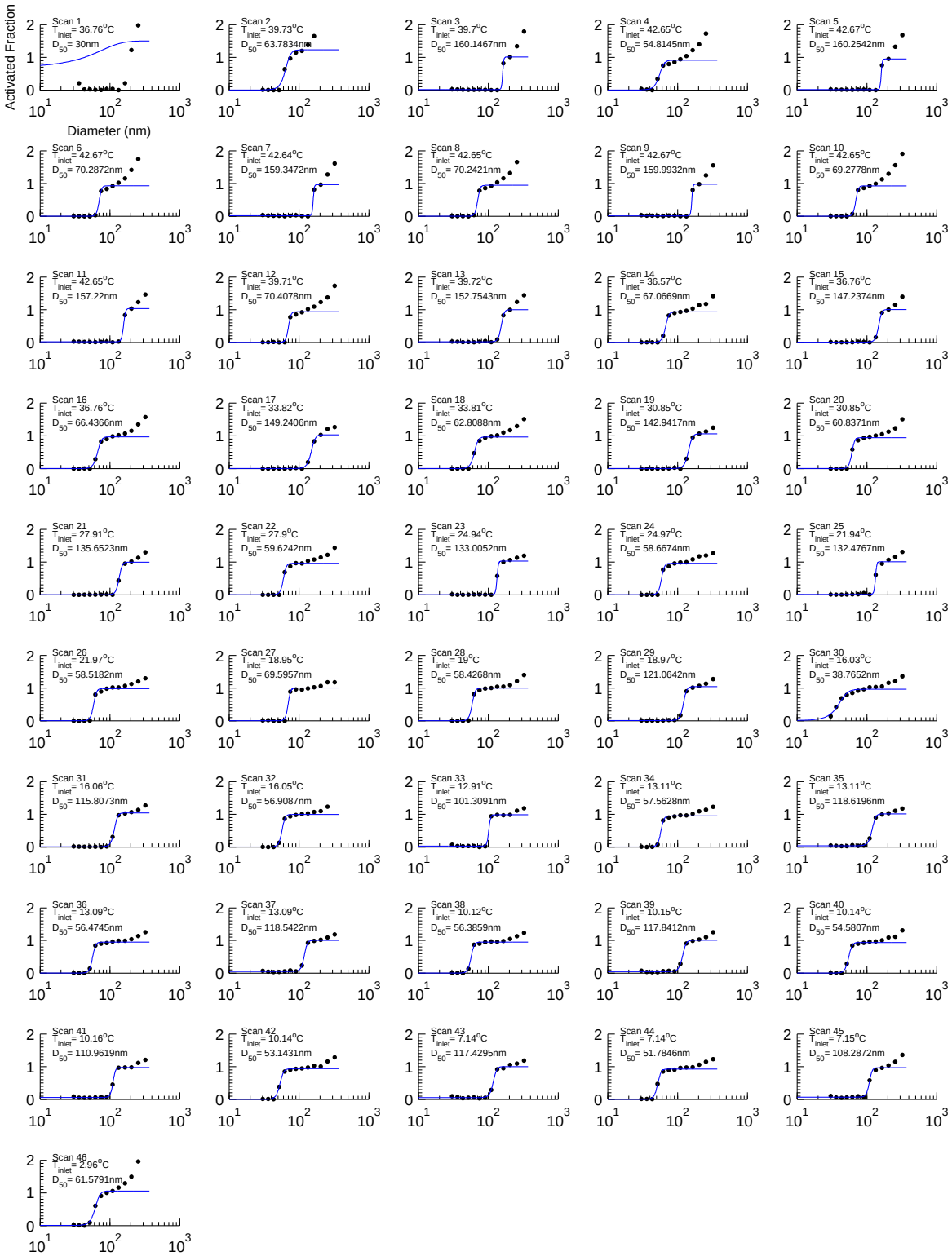

Figure A.55. PEG 600 (odd scan numbers) and $(NH_4)_2SO_4$ activation curves. The activated fractions at each diameter are fit with a Sigmoid-Boltzmann curve (blue, see Table A.19).

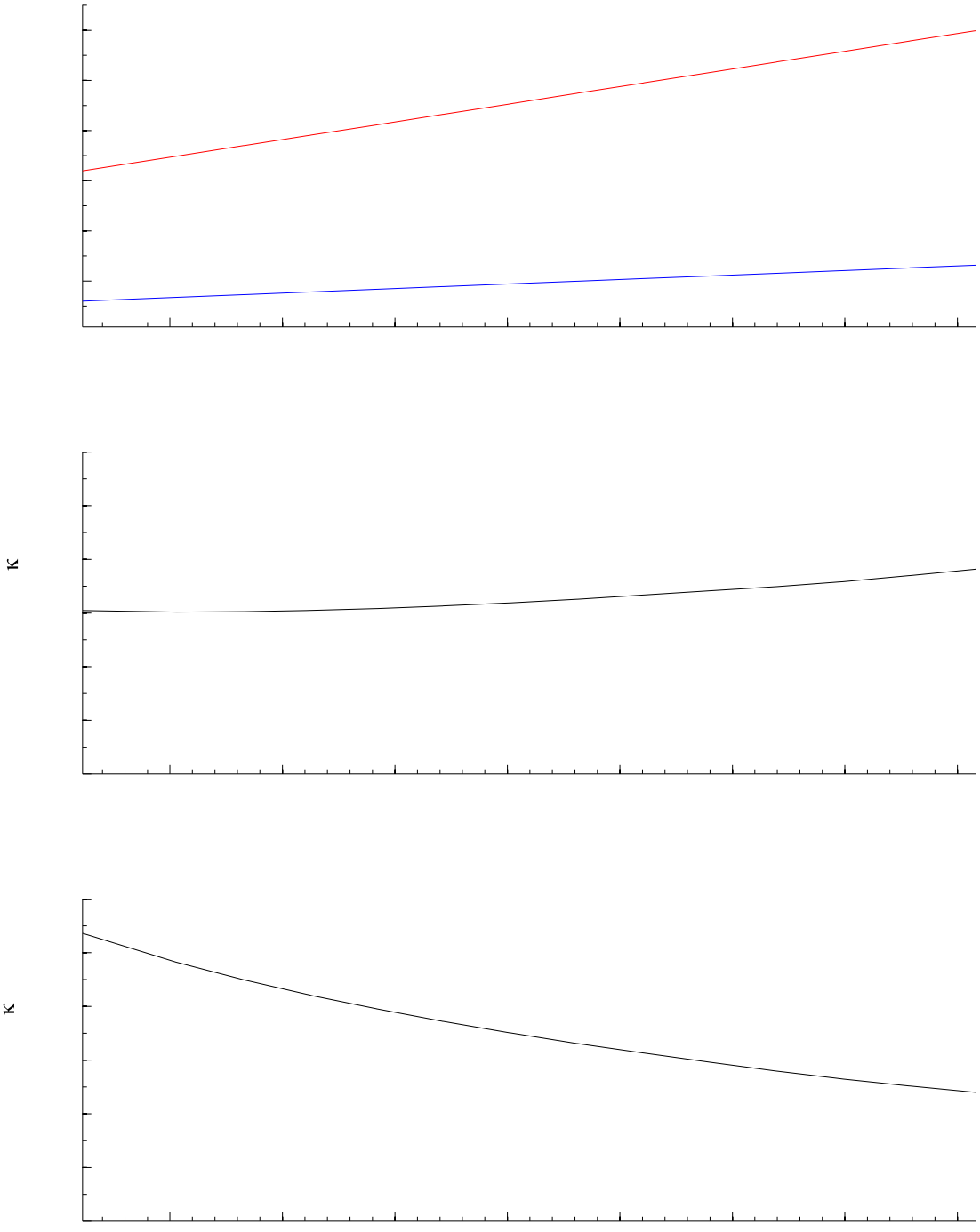

Figure A.56. PEG 600 and $(NH_4)_2SO_4$ activation diameters (top) and PEG 600 κ values (center and bottom) versus temperature. Each number represents a scan from Figure A.57. Fit coefficients represent the solid line fit through the activation diameters, which then give the κ line.

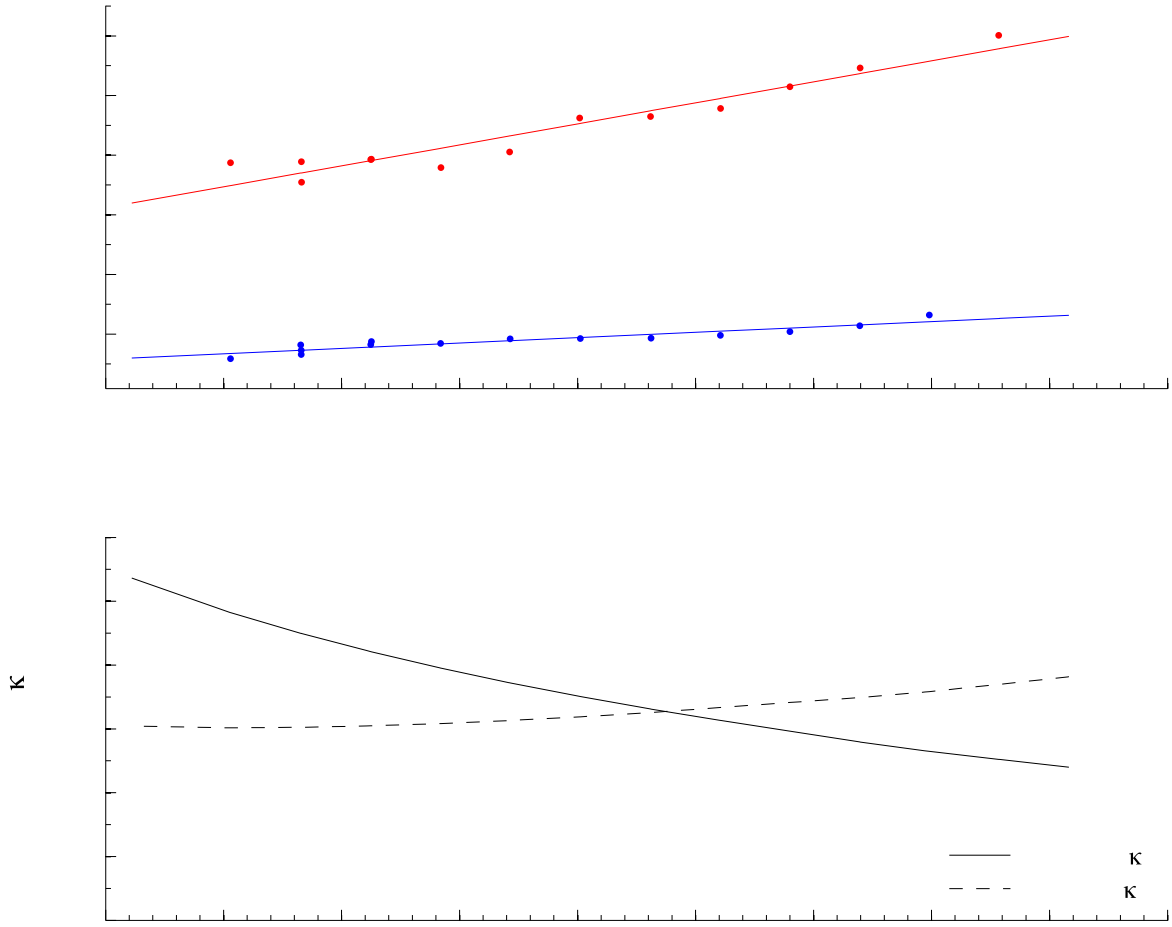

Figure A.57. PEG 600 and $(NH_4)_2SO_4$ activation diameters replotted without scan numbers (top) and κ values (bottom) plotted together.

Table A.20. Polyethylene glycol (PEG) 600 data. Each line represents one diameter scan.

						Boltzmann Parameters:			
time	compound	ΔT	T_{box}	T_{inlet}	D_{50}	*A1*	*A2*	*dx*	excluded
37020	AS	6	0.00	39.21	30.00	0.3000	1.5000	3.00	yes
37440	PEG600	6	0.00	39.23	138.98	0.0000	0.8877	3.19	yes
37860	AS	6	0.00	39.22	69.90	0.0036	0.7683	3.00	no
38340	PEG600	6	0.00	39.22	150.22	0.0045	0.8179	4.23	no
38760	AS	6	0.00	42.27	71.63	0.0011	0.7634	3.00	no
39180	PEG600	6	0.00	42.15	152.26	0.0062	0.8349	4.44	no
39660	AS	6	0.00	42.17	72.16	0.0033	0.7671	3.00	yes
40080	PEG600	6	0.00	42.17	151.06	0.0033	0.8346	3.01	yes
40500	AS	6	0.00	42.16	71.66	0.0016	0.7685	3.00	yes
40980	PEG600	6	0.00	42.17	143.05	0.0034	0.8178	3.00	yes
41400	AS	6	0.00	42.17	71.55	0.0045	0.7773	3.00	yes
41820	PEG600	6	0.00	42.16	150.88	0.0081	0.8626	4.74	yes
42300	AS	6	0.00	39.22	66.49	0.0000	0.7929	13.31	yes
42720	PEG600	6	0.00	39.24	146.90	0.0055	0.8725	5.45	yes
43140	AS	6	0.00	39.22	69.36	0.0054	0.7885	3.48	no
43620	PEG600	6	0.00	36.27	144.98	0.0052	0.8648	5.67	no
44040	AS	6	0.00	36.27	68.30	0.0064	0.7974	3.64	no
44460	PEG600	6	0.00	33.33	149.48	0.0222	0.8777	5.49	no
44940	AS	6	0.00	33.31	66.81	0.0055	0.7990	3.82	no
45360	PEG600	6	0.00	30.29	127.91	0.0467	0.8699	4.83	yes
45780	AS	6	0.00	30.29	65.62	0.0002	0.8137	4.48	no
46260	PEG600	6	0.00	27.34	95.17	0.0213	0.8680	8.98	yes
46680	AS	6	0.00	27.37	62.80	0.0000	0.8117	3.98	no
47100	PEG600	6	0.00	24.31	67.44	0.0000	0.8736	3.00	yes
47580	AS	6	0.00	24.41	61.16	0.0000	0.8067	3.00	no
48000	PEG600	6	0.00	21.23	100.20	0.0001	0.8762	3.00	yes
48420	AS	6	0.00	21.47	60.66	0.0000	0.8093	3.00	no
48900	PEG600	6	0.00	21.47	121.47	0.0027	0.8964	4.04	no
49320	AS	6	0.00	18.50	68.45	0.0619	0.8253	4.11	yes
49740	PEG600	6	0.00	18.51	121.54	0.0032	0.8931	3.87	no
50220	AS	6	0.00	18.50	57.89	0.0000	0.8286	3.00	no
50640	PEG600	6	0.00	15.53	104.60	0.0539	0.8831	6.20	yes
51060	AS	6	0.00	15.56	57.94	0.0000	0.8279	3.00	no
51540	PEG600	6	0.00	15.53	117.13	0.0045	0.8839	4.73	no
51960	AS	6	0.00	15.55	57.43	0.0000	0.8270	3.00	no
52380	PEG600	6	0.00	13.37	115.66	0.0059	0.8866	4.11	no
52860	AS	6	0.00	12.62	58.00	0.0000	0.8269	3.00	no
53280	PEG600	6	0.00	12.59	115.76	0.0057	0.8855	4.28	no
53700	AS	6	0.00	12.62	56.59	0.0000	0.8223	3.00	no
54180	PEG600	6	0.00	9.17	122.90	0.0267	0.8853	5.87	yes
54600	AS	6	0.00	9.19	56.59	0.0000	0.8230	3.00	no
55020	PEG600	6	0.00	9.18	115.69	0.0072	0.8958	6.07	no
55500	AS	6	0.00	8.17	57.96	0.0000	0.8297	3.00	no
55920	PEG600	6	0.00	8.15	111.07	0.0100	0.8785	3.80	no
56340	AS	6	0.00	7.17	55.12	0.0000	0.8229	3.23	no
56820	PEG600	6	0.00	7.18	112.83	0.0037	0.8878	5.70	no
57240	AS	6	0.00	7.18	55.40	0.0000	0.8211	3.01	no
57660	PEG600	6	0.00	7.17	110.50	0.0096	0.8866	3.11	no
58140	AS	6	0.00	6.18	57.85	0.0000	0.8210	3.00	no
58560	PEG600	6	0.00	6.16	109.12	0.0075	0.8814	5.24	no
58980	AS	6	0.00	6.17	54.32	0.0000	0.8178	3.32	no
59460	PEG600	6	0.00	6.16	107.29	0.0084	0.8832	4.84	no
59880	AS	6	0.00	5.16	55.85	0.0000	0.8193	3.00	no
60300	PEG600	6	0.00	4.17	113.71	0.0248	0.8802	6.08	no
60780	AS	6	0.00	4.17	52.96	0.0000	0.8171	3.31	no
61200	PEG600	6	0.00	3.21	118.23	0.0243	0.8966	5.99	yes

[1]Sensor malfunctioned resulting in temperature error.

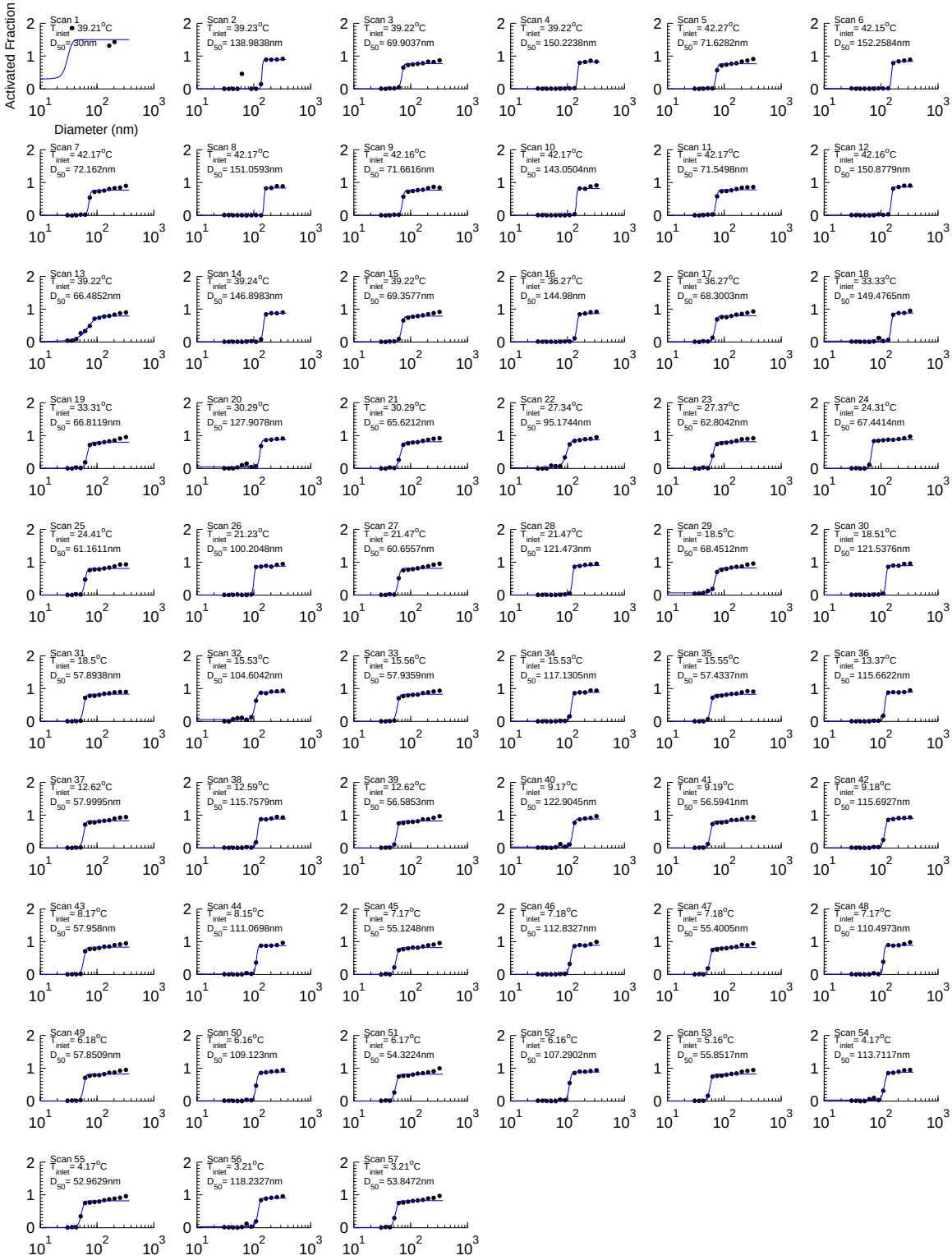

Figure A.58. PEG 600 (even scan numbers) and $(NH_4)_2SO_4$ activation curves. The activated fractions at each diameter are fit with a Sigmoid-Boltzmann curve (blue, see Table A.20).

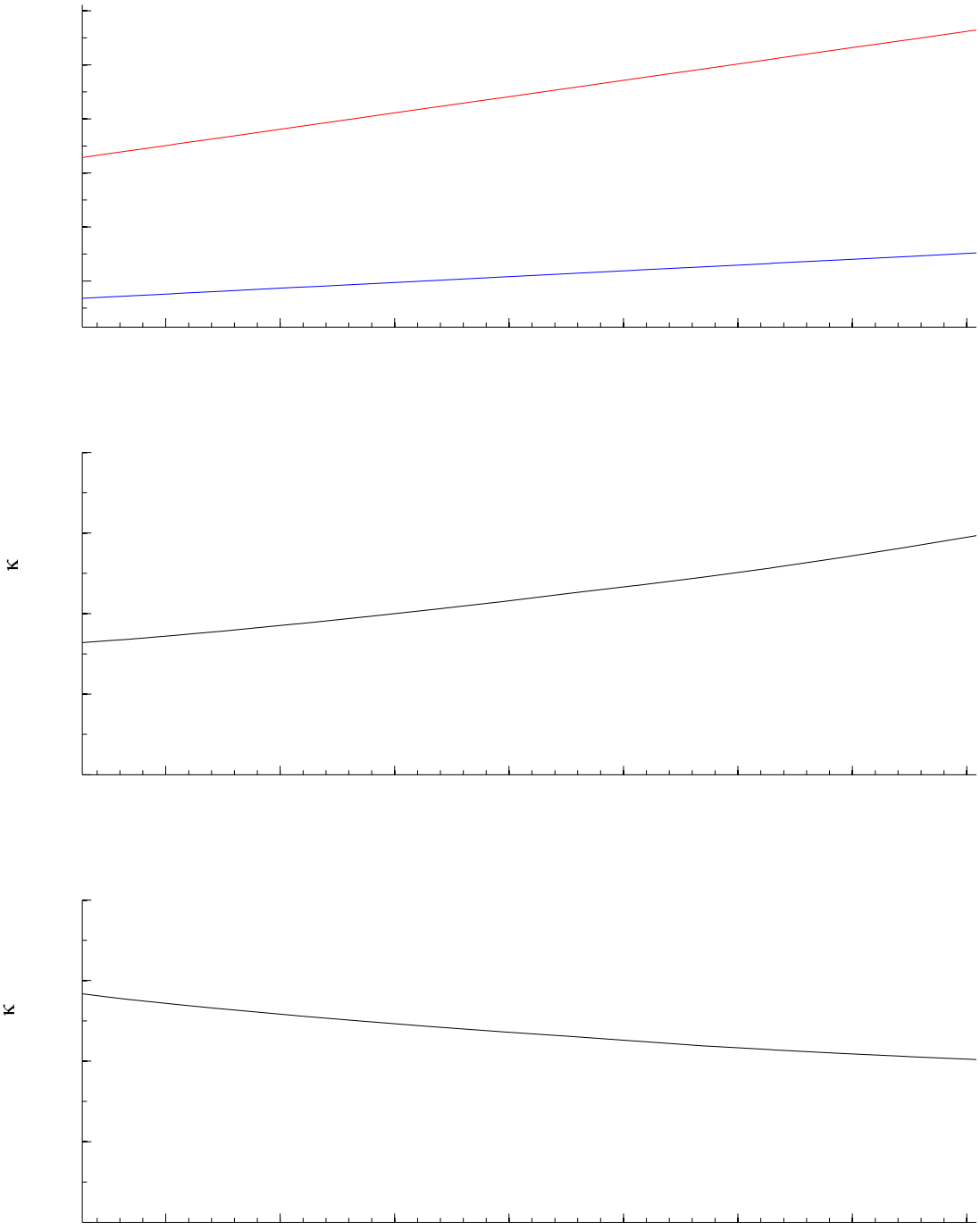

Figure A.59. PEG 600 and $(NH_4)_2SO_4$ activation diameters (top) and PEG 600 κ values (center and bottom) versus temperature. Each number represents a scan from Figure A.60. Fit coefficients represent the solid line fit through the activation diameters, which then give the κ line.

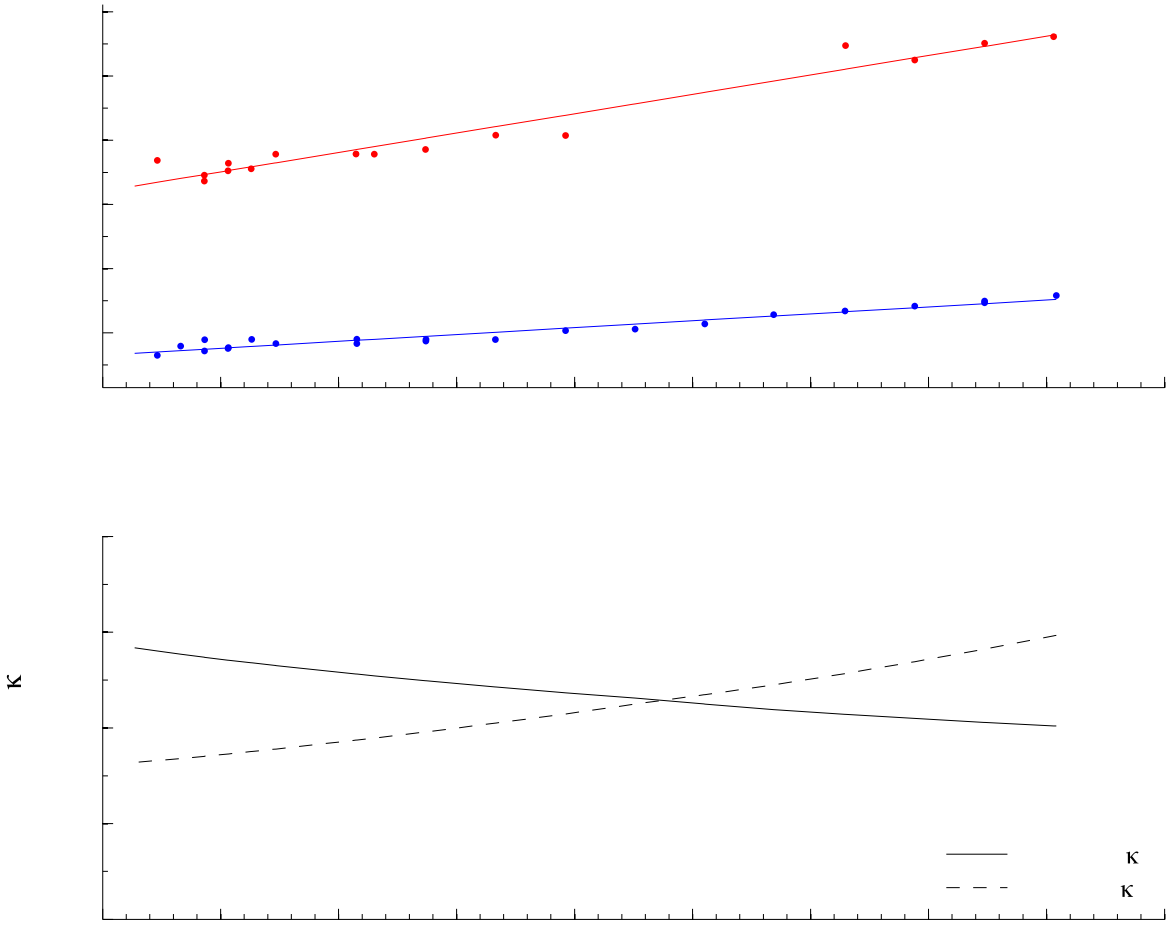

Figure A.60. PEG 600 and $(NH_4)_2SO_4$ activation diameters replotted without scan numbers (top) and κ values (bottom) plotted together.

Table A.21. Secondary organic aerosol data. Each line represents one diameter scan.

						Boltzmann Parameters:			
time	compound	ΔT	T_{box}	T_{inlet}	D_{50}	*A1*	*A2*	*dx*	excluded
52500	AS	6	0.00	17.38	71.51	0.0170	0.7691	3.00	yes
52920	SOA	6	23.61	17.38	106.90	0.0125	0.8077	3.00	yes
53400	AS	6	23.85	16.36	60.32	0.0000	0.7641	3.00	no
53820	SOA	6	24.12	15.37	106.43	0.0125	0.8232	3.00	no
54240	AS	6	24.38	15.38	61.03	0.0000	0.7715	3.00	no
54720	SOA	6	24.61	14.38	106.82	0.0263	0.8482	3.00	no
55140	AS	6	24.74	14.36	59.33	0.0000	0.7704	3.00	no
55560	SOA	6	24.88	13.40	107.07	0.0599	0.8517	3.00	no
56040	AS	6	24.92	13.41	59.56	0.0000	0.7682	3.00	no
56460	SOA	6	25.06	12.37	103.35	0.0908	0.8113	5.69	no
56880	AS	6	25.11	12.40	59.14	0.0000	0.7633	3.00	no
57360	SOA	6	25.22	12.37	105.21	0.0513	0.8241	3.75	no
57780	AS	6	25.28	11.43	64.54	0.1427	0.7688	4.04	yes
58200	SOA	6	25.43	11.43	104.38	0.0021	0.8289	4.96	no
58680	AS	6	25.49	11.43	58.74	0.0000	0.7693	3.00	no
59100	SOA	6	25.49	11.43	105.26	0.0000	0.7992	5.91	no
59520	AS	6	25.53	10.38	58.40	0.0000	0.7621	3.00	no
60000	SOA	6	25.59	10.39	103.07	0.0000	0.7765	5.59	no
60420	AS	6	25.59	10.40	58.46	0.0000	0.7663	3.00	no
60840	SOA	6	25.61	10.40	102.89	0.0000	0.7960	5.97	no
61320	AS	6	25.67	10.40	58.17	0.0000	0.7665	3.00	no
61740	SOA	6	25.66	9.43	103.49	0.0066	0.7783	5.92	no
62160	AS	6	25.70	8.41	59.08	0.0000	0.7866	3.80	no
62640	SOA	6	25.71	7.46	103.16	0.0017	0.7961	8.55	no
63060	AS	6	25.76	7.02	57.88	0.0000	0.7892	3.00	no
63480	SOA	6	25.78	6.43	100.94	0.0000	0.7879	7.52	no
63960	AS	6	25.80	6.43	56.25	0.0000	0.7886	3.00	no
64380	SOA	6	25.86	5.41	99.97	0.0000	0.7428	6.81	no
64800	AS	6	25.91	5.39	56.26	0.0000	0.7885	3.14	no
65280	SOA	6	25.89	5.41	99.67	0.0000	0.7800	7.87	no
65700	AS	6	25.98	5.41	55.85	0.0000	0.7901	3.00	no
66120	SOA	6	25.98	5.42	100.43	0.0000	0.7981	9.27	no
66600	AS	6	25.99	4.45	58.51	0.0000	0.7918	3.00	no

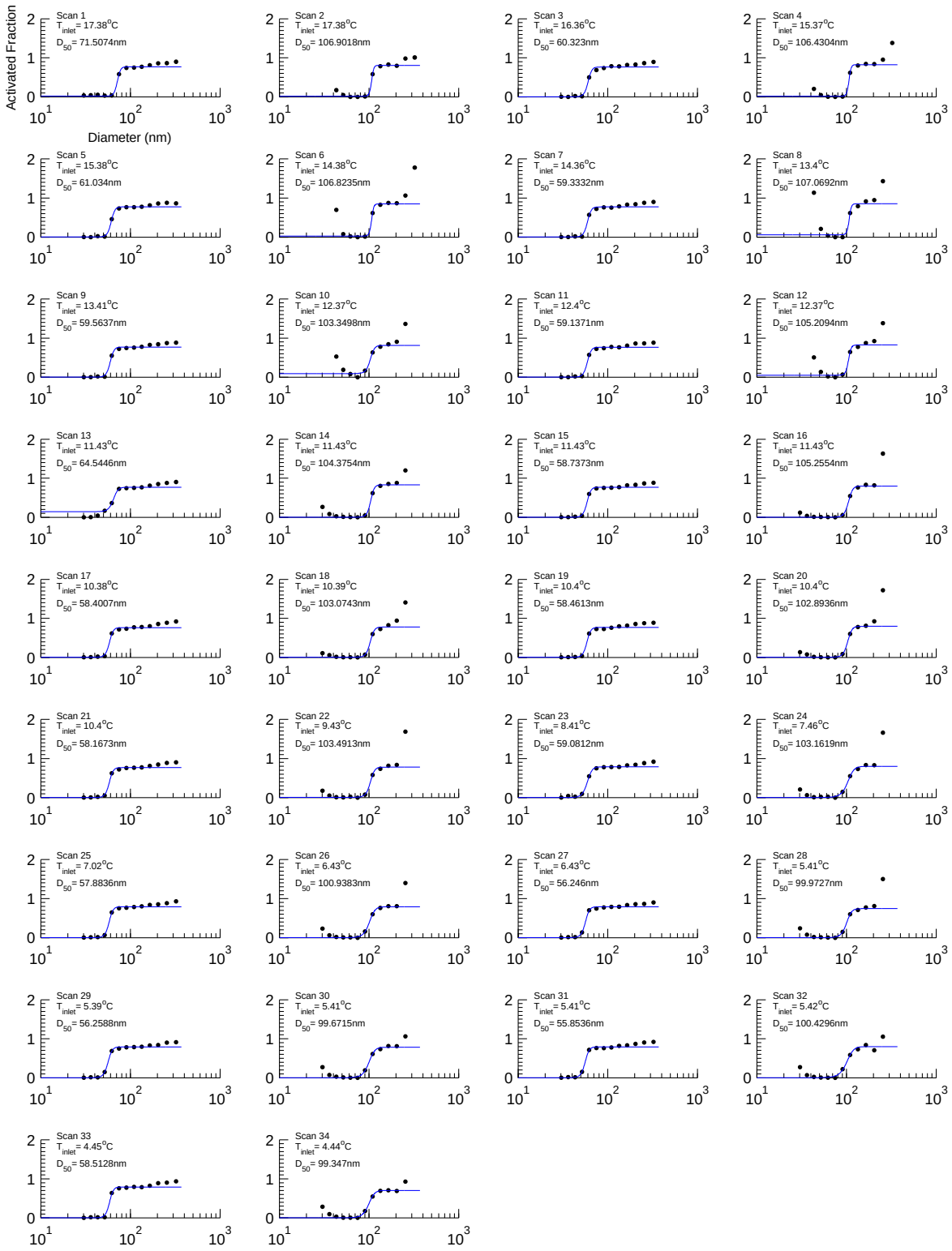

Figure A.61. SOA (odd scan numbers) and $(NH_4)_2SO_4$ activation curves. The activated fractions at each diameter are fit with a Sigmoid-Boltzmann curve (blue, see Table A.23).

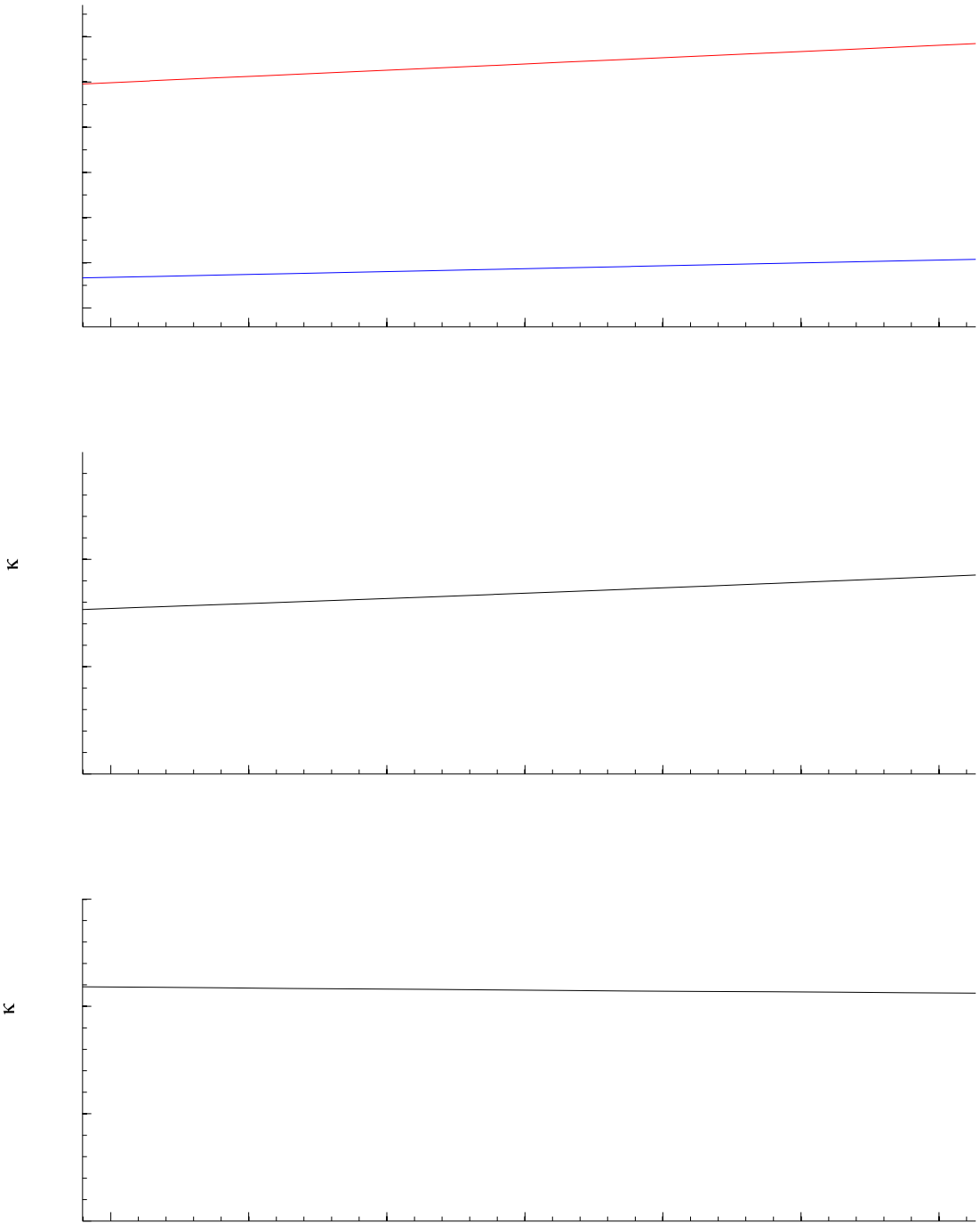

Figure A.62. SOA and $(NH_4)_2SO_4$ activation diameters (top) and SOA κ values (center and bottom) versus temperature. Each number represents a scan from Figure A.69. Fit coefficients represent the solid line fit through the activation diameters, which then give the κ line.

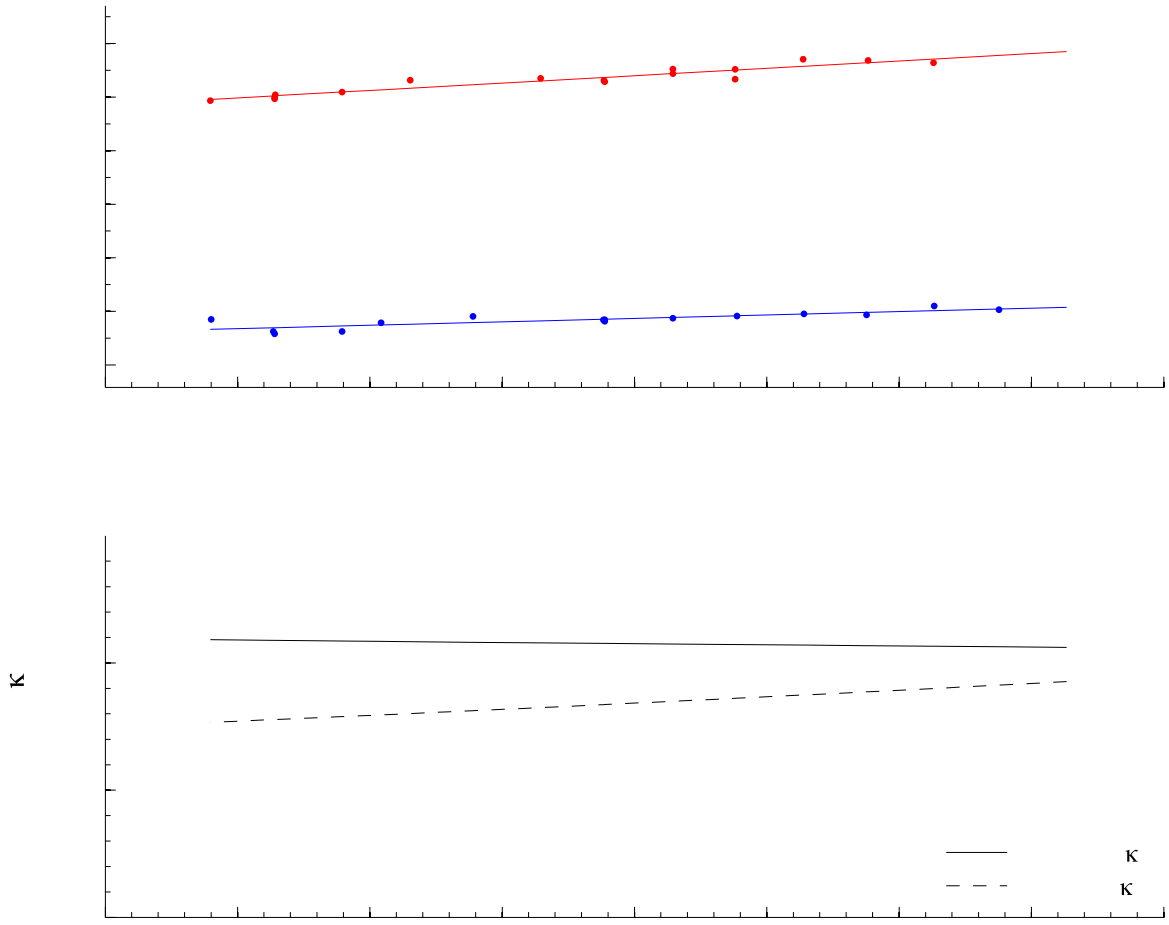

Figure A.63. SOA and $(NH_4)_2SO_4$ activation diameters replotted without scan numbers (top) and κ values (bottom) plotted together.

Table A.22. Secondary organic aerosol data. Each line represents one diameter scan.

						Boltzmann Parameters:			
time	compound	ΔT	T_{box}	T_{inlet}	D_{50}	$A1$	$A2$	dx	excluded	
34920	SOA	6	0.00	37.15	101.07	0.0000	0.8222	3.00	yes	
35400	AS	6	9.00	38.83	67.93	0.0000	0.7917	3.00	yes	
35820	SOA	6	9.00	41.90	103.96	0.0000	0.8105	3.00	yes	
36240	AS	6	10.00	41.81	69.18	0.0000	0.7862	3.00	no	
36720	SOA	6	10.00	41.80	104.95	0.0001	0.8146	3.00	yes	
37140	AS	6	10.00	43.42	57.63	0.0000	0.7816	3.00	yes	
37560	SOA	6	10.00	43.43	134.85	0.0010	0.6073	3.07	yes	
38040	AS	6	10.00	43.43	74.19	0.0000	0.7798	3.07	yes	
38460	SOA	6	10.00	43.41	135.19	0.0013	0.5951	3.00	yes	
38880	AS	6	10.00	43.42	74.35	0.0008	0.7733	3.00	yes	
39360	SOA	6	10.00	43.42	134.12	0.0005	0.5581	3.11	yes	
39780	AS	6	11.00	43.41	73.96	0.0000	0.7795	3.00	yes	
40200	SOA	6	11.00	43.40	135.04	0.0010	0.6320	3.01	yes	
40680	AS	6	11.00	43.42	73.34	0.0000	0.7822	3.00	yes	
41100	SOA	6	11.00	43.41	133.88	0.0011	0.6539	3.02	yes	
41520	AS	6	11.00	43.42	72.38	0.0000	0.7920	3.00	yes	
42000	SOA	6	11.00	41.50	132.03	0.0009	0.8273	3.02	yes	
42420	AS	6	11.00	41.48	70.52	0.0000	0.7958	3.00	yes	
42840	SOA	6	11.00	40.04	130.69	0.0011	0.8367	4.06	no	
43320	AS	6	12.00	39.49	70.73	0.0000	0.7918	3.00	no	
43740	SOA	6	12.00	39.51	127.77	0.0015	0.8368	4.61	no	
44160	AS	6	12.00	37.49	37.85	0.0003	0.7970	12.28	yes	
44640	SOA	6	12.00	37.52	125.66	0.0006	0.8568	6.28	no	
45060	AS	6	12.00	37.51	68.78	0.0000	0.8056	3.00	no	
45480	SOA	6	12.00	35.51	122.68	0.0006	0.8411	5.42	no	
45960	AS	6	12.00	35.52	68.59	0.0000	0.8169	3.00	no	
47160	AS	6	1.00	31.37	68.34	0.0000	0.8232	3.00	no	
47640	SOA	6	1.00	31.61	118.18	0.0000	0.8252	6.74	no	
48060	AS	6	1.00	31.61	66.17	0.0000	0.8156	3.02	no	
48480	SOA	6	1.00	29.62	117.20	0.0000	0.8780	8.61	no	
48960	AS	6	1.00	29.62	64.54	0.0000	0.8041	3.03	no	
49380	SOA	6	1.00	27.63	114.47	0.0000	0.8842	10.87	no	
49800	AS	6	1.00	27.62	63.50	0.0000	0.8124	3.56	no	
50280	SOA	6	1.00	25.56	109.70	0.0001	0.8322	3.00	no	
50700	AS	6	2.00	25.66	63.54	0.0000	0.8121	3.17	no	
51120	SOA	6	2.00	25.64	108.73	0.0000	0.8281	4.27	no	
51600	AS	6	2.00	23.66	66.63	0.0000	0.8225	3.13	no	
52020	SOA	6	2.00	23.67	107.96	0.0000	0.8334	3.70	no	
52440	AS	6	2.00	21.63	30.00	0.3000	0.8107	13.25	yes	
52920	SOA	6	2.00	21.68	107.40	0.0000	0.8367	3.08	no	
53340	AS	6	2.00	21.69	58.54	0.0000	0.8071	3.00	no	
53760	SOA	6	2.00	19.74	107.17	0.0000	0.8093	3.00	no	
54240	AS	6	3.00	19.73	58.51	0.0000	0.8097	3.00	no	
54660	SOA	6	3.00	17.74	101.69	0.0000	0.8224	10.92	no	
55080	AS	6	3.00	17.76	58.31	0.0000	0.8192	3.00	no	
55560	SOA	6	3.00	15.69	105.01	0.0000	0.8040	4.60	no	
55980	AS	6	3.00	15.77	57.67	0.0000	0.7901	3.00	no	
56400	SOA	6	3.00	15.20	103.61	0.0000	0.8083	5.66	no	
56880	AS	6	3.00	13.83	58.11	0.0000	0.8061	3.00	no	
57300	SOA	6	3.00	11.66	102.18	0.0007	0.8153	7.77	no	
57720	AS	6	4.00	10.65	56.82	0.0000	0.8007	3.00	no	
58200	SOA	6	4.00	9.67	102.03	0.0000	0.7718	6.41	no	
58620	AS	6	4.00	9.72	57.18	0.0000	0.7753	3.00	no	
59040	SOA	6	4.00	8.68	101.74	0.0000	0.7620	6.82	no	
59520	AS	6	4.00	7.71	59.28	0.2993	0.7784	8.72	yes	
59940	SOA	6	4.00	7.71	101.01	0.0000	0.6968	7.11	no	
60360	AS	6	4.00	6.69	57.93	0.0000	0.6536	3.10	no	
60840	SOA	6	4.00	5.69	108.04	0.0000	0.2273	9.93	yes	
61260	AS	6	5.00	5.74	109.24	0.0234	0.5176	40.00	yes	
61680	SOA	6	5.00	5.75	156.12	0.0000	0.2000	39.97	yes	
62160	AS	6	5.00	4.71	60.12	0.0000	0.2314	4.02	yes	
62580	SOA	6	5.00	4.72	147.73	0.0000	0.2000	39.40	yes	
63000	AS	6	5.00	4.72	127.80	0.0243	0.2008	40.00	yes	
63480	SOA	6	5.00	3.74	220.71	0.0022	0.2038	39.99	yes	
63900	AS	6	5.00	3.74	197.34	0.0045	0.2002	36.01	yes	
64320	SOA	6	5.00	3.74	258.61	0.0022	0.2000	37.59	yes	
64800	AS	6	6.00	3.75	79.96	0.0000	0.7969	9.82	yes	
65220	SOA	6	6.00	3.76	94.03	0.0000	0.6568	7.89	no	
65640	AS	6	6.00	3.74	50.36	0.0031	0.7525	3.38	no	
66120	SOA	6	6.00	3.74	94.96	0.0000	0.6958	8.55	no	
66540	AS	6	6.00	2.72	54.09	0.0000	0.7556	3.57	no	

[1] Sensor malfunctioned resulting in temperature error.
[2] Atomizers switched – ammonium sulfate was scanned twice in a row here.

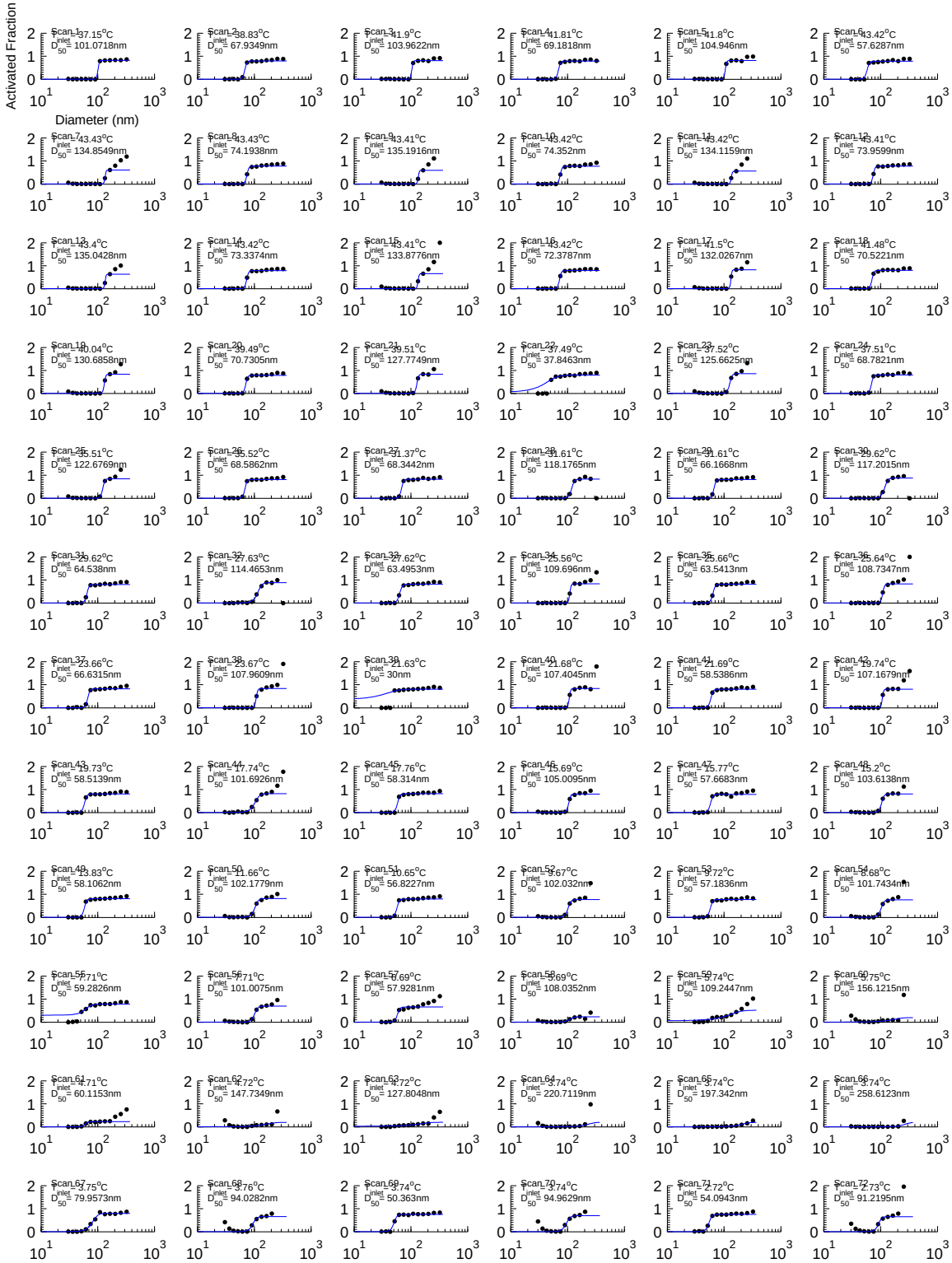

Figure A.64. SOA (odd scan numbers) and $(NH_4)_2SO_4$ activation curves. The activated fractions at each diameter are fit with a Sigmoid-Boltzmann curve (blue, see Table A.24).

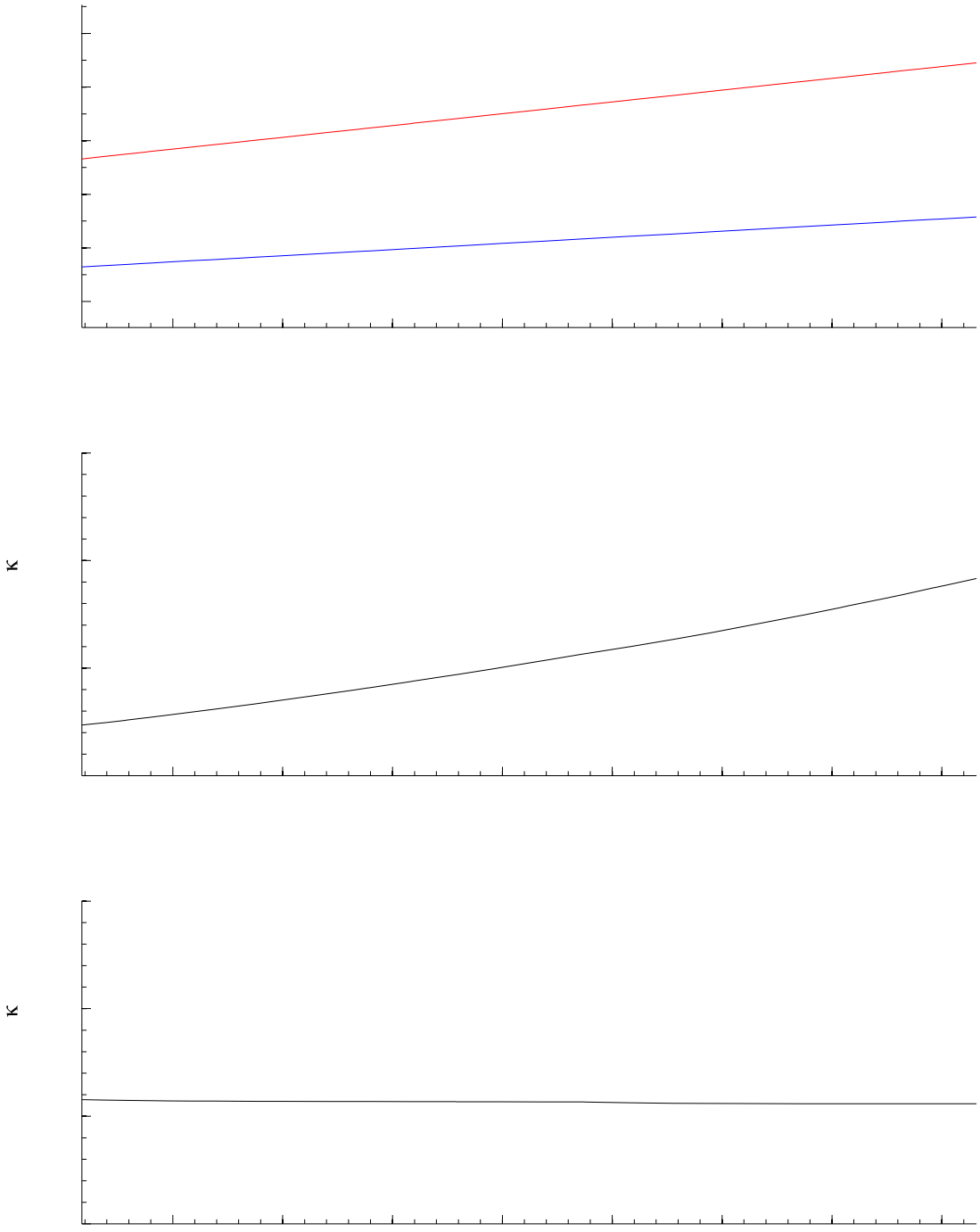

Figure A.65. SOA and $(NH_4)_2SO_4$ activation diameters (top) and SOA κ values (center and bottom) versus temperature. Each number represents a scan from Figure A.72. Fit coefficients represent the solid line fit through the activation diameters, which then give the κ line.

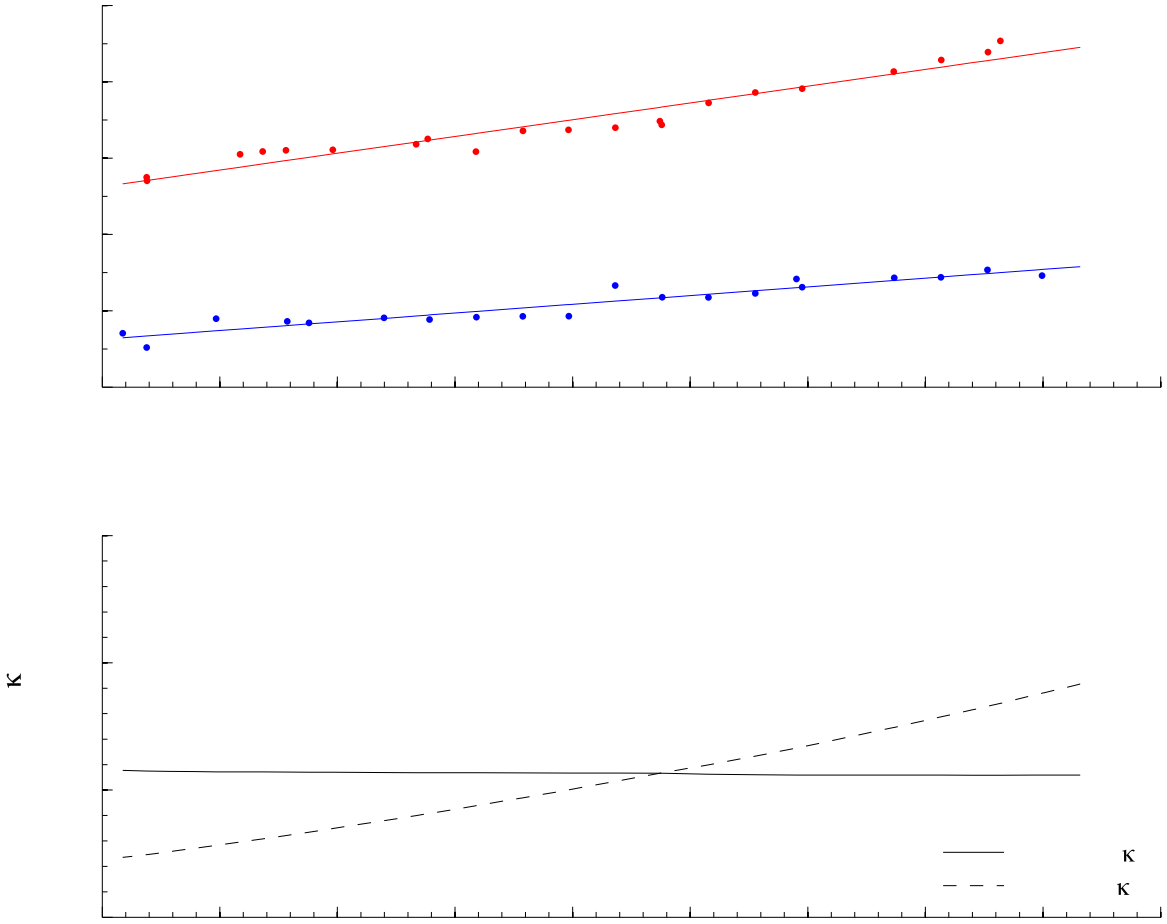

Figure A.66. SOA and $(NH_4)_2SO_4$ activation diameters replotted without scan numbers (top) and κ values (bottom) plotted together.

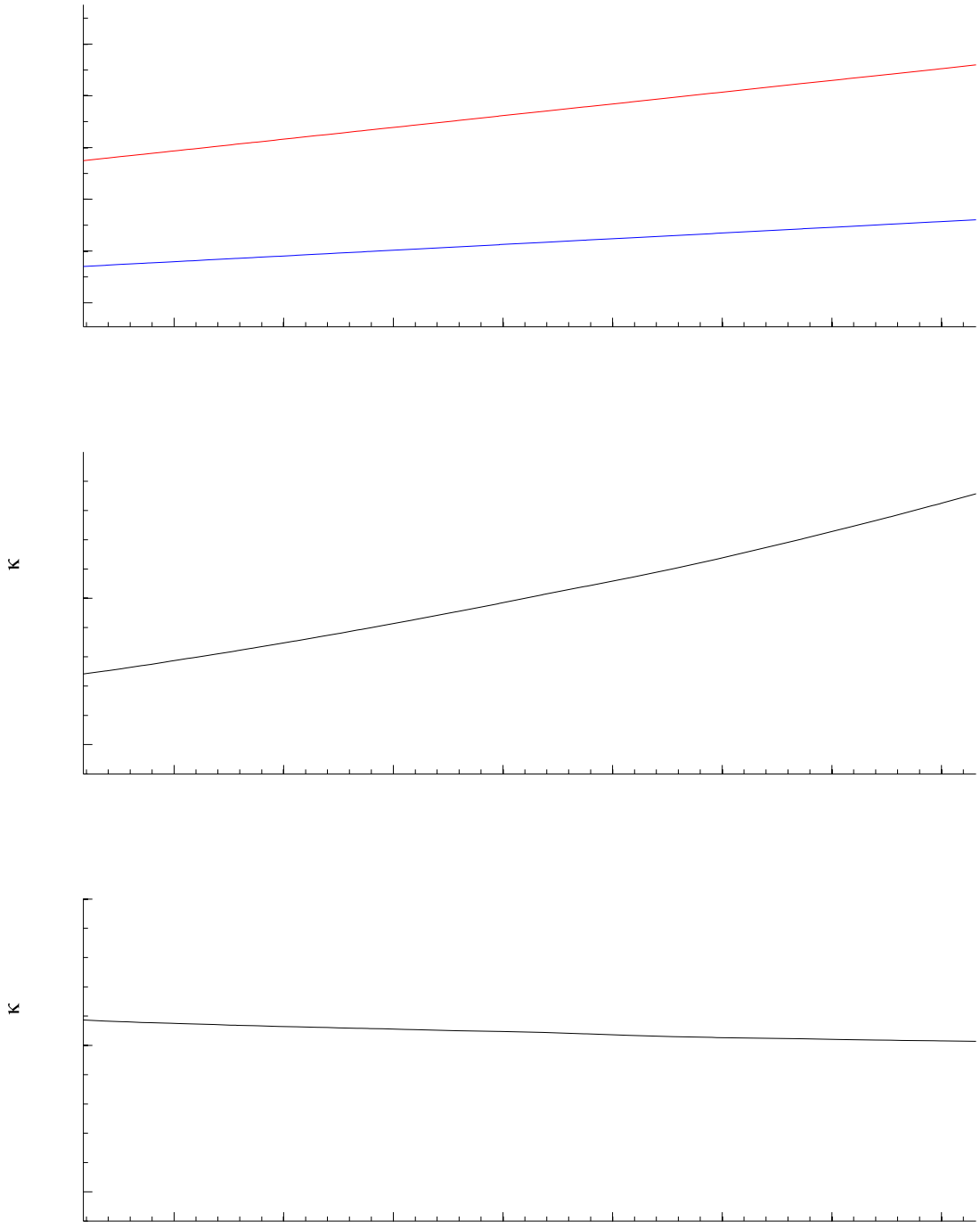

Figure A67. SOA from 6 March 2012 and 7 March 2012 combined and $(NH_4)_2SO_4$ activation diameters (top) and SOA κ values (center and bottom) versus temperature. Fit coefficients represent the solid line fit through the activation diameters, which then give the κ line.

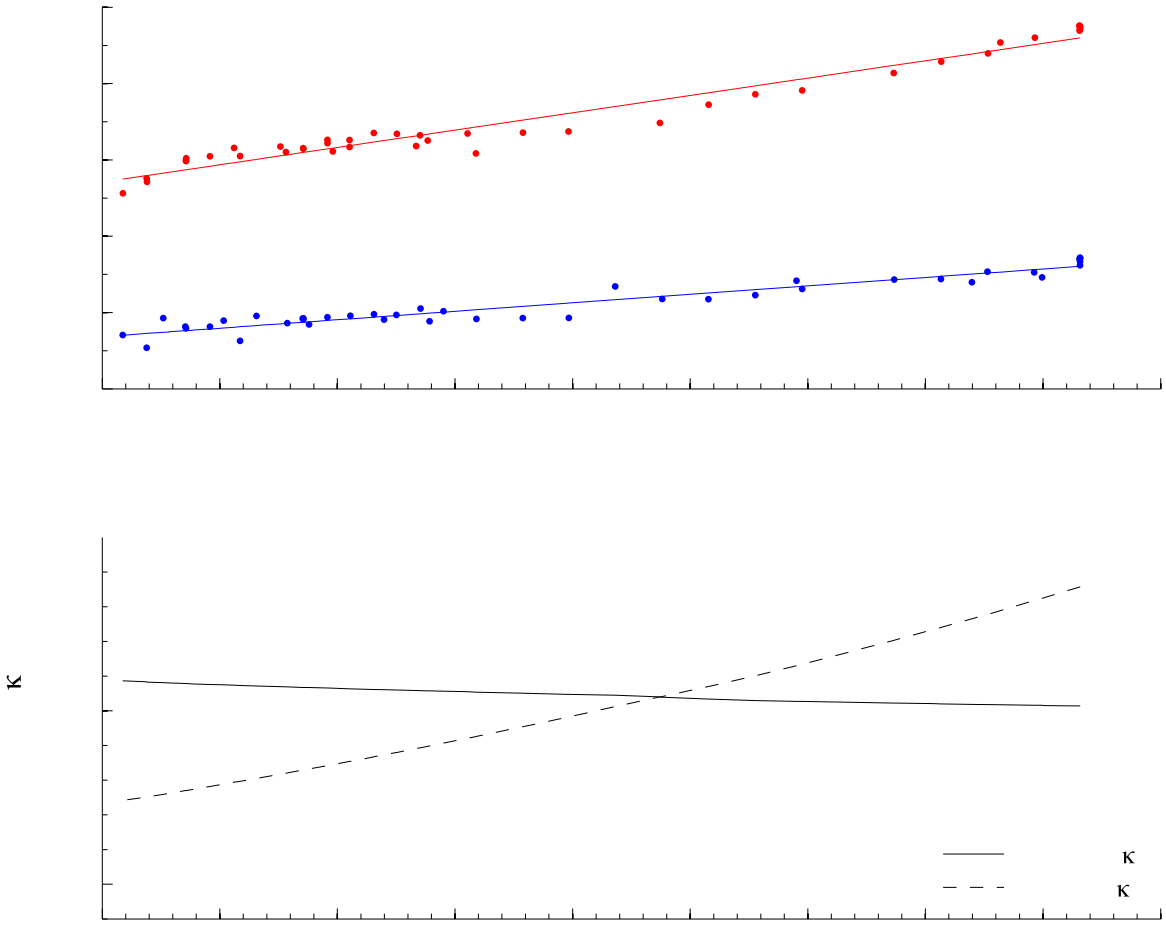

Figure A.68. SOA from 6 March 2012 and 7 March 2012 combined and $(NH_4)_2SO_4$ activation diameters replotted without scan numbers (top) and κ values (bottom) plotted together.